

**INVESTIGATIONS OF THE NATURAL  
PRODUCT ANTIBIOTIC THIOSTREPTON  
FROM *STREPTOMYCES AZUREUS* AND  
ASSOCIATED MECHANISMS OF RESISTANCE**

**by**

**Cullen Lucan Myers**

A thesis  
presented to the University of Waterloo  
in fulfillment of the  
thesis requirement for the degree of  
Doctor of Philosophy  
in  
Chemistry

Waterloo, Ontario, Canada, 2013

## **AUTHOR'S DECLARATION**

I hereby declare that I am the sole author of this thesis. This is a true copy of the thesis, including any required final revisions, as accepted by my examiners.

I understand that my thesis may be made electronically available to the public.

## ABSTRACT

The persistence and propagation of bacterial antibiotic resistance presents significant challenges to the treatment of drug resistant bacteria with current antimicrobial chemotherapies, while a dearth in replacements for these drugs persists. The thiopeptide family of antibiotics may represent a potential source for new drugs and thiostrepton, the prototypical member of this antibiotic class, is the primary subject under study in this thesis.

Using a facile semi-synthetic approach novel, regioselectively-modified thiostrepton derivatives with improved aqueous solubility were prepared. *In vivo* assessments found these derivatives to retain significant antibacterial ability which was determined by cell free assays to be due to the inhibition of protein synthesis. Moreover, structure-function studies for these derivatives highlighted structural elements of the thiostrepton molecule that are important for antibacterial activity.

Organisms that produce thiostrepton become insensitive to the antibiotic by producing a resistance enzyme that transfers a methyl group from the co-factor *S*-adenosyl-L-methionine (AdoMet) to an adenosine residue at the thiostrepton binding site on 23S rRNA, thus preventing binding of the antibiotic. Extensive site-directed mutagenesis was performed on this enzyme to generate point mutations at key active site residues. Ensuing biochemical assays and co-factor binding studies on these variants identified amino acid residues in the active site that are essential to the formation of the AdoMet binding pocket

and provided direct evidence for the involvement of an active site arginine in the catalytic mechanism of the enzyme.

Certain bacteria that produce neither thiostrepton nor the resistance methyltransferase express the thiostrepton binding proteins TIP-AL and TIP-AS, that irreversibly bind to the antibiotic, thereby conferring resistance by sequestration. Here, it was found that the point mutation of the previously identified reactive amino acid in TIP-AS did not affect covalent binding to the antibiotic, which was immediately suggestive of a specific, high affinity non-covalent interaction. This was confirmed in binding studies using chemically synthesized thiostrepton derivatives. These studies further revealed structural features from thiostrepton important in this non-covalent interaction. Together, these results indicate that thiostrepton binding by TIP-AS begins with a specific non-covalent interaction, which is necessary to properly orient the thiostrepton molecule for covalent binding to the protein.

Finally, the synthesis of a novel AdoMet analogue is reported. The methyl group of AdoMet was successfully replaced with a trifluoromethyl ketone moiety, however, the hydrated form (geminal diol) of this compound was found to predominate in solution. Nevertheless, the transfer of this trifluoroketone/ trifluoropropane diol group was demonstrated with the thiopurine methyltransferase.

## ACKNOWLEDGEMENTS

My sincerest thanks are expressed to my supervisor Professor John Honek, for his steady tutelage, guidance and support throughout my doctoral studies. I am deeply grateful for his fostering the growth of my self-confidence as a researcher, by encouraging open discussions about ideas and his unfailing way of steering me in a right direction without belittlement and always ensuring that I was learning in the process.

I also wish to thank the members of my committee, Drs. Dieckman, Guillemette and Wettig for their constructive advice which helped to advance my project.

My gratitude extends to the many members of the Honek Laboratory over the years that provided their friendship and support, foremost among whom is Dr. Pei Hang, who began the work on this project. I am immensely grateful for her spending the time to train me (in spite of being in the process of preparing her own doctoral thesis). I would also especially like to thank Drs. Zhengding Su, Uthiawan Suttisansanee and Betsey Daub for sharing scientific expertise and advice that was tremendously helpful at many different stages of my studies. Thanks are also owed Joshua Yuen, Jesse Harris and Jacky Yeung, who assisted in the synthesis of thiostrepton analogues and in studies of thiostrepton resistance proteins.

I am deeply grateful to the Department of Chemistry at the University of Waterloo for wonderful technical support that was vital to the success and understanding of many aspects of this project. In particular, I would like to thank Dr. Richard Smith for mass spectrometry training, invaluable advice and suggestions; Jan Venne for NMR training and assistance with two-dimensional NMR experiments; and Valarie Goodfellow and the Dmitrienko group for allowing me access to their HPLC equipment. I am additionally grateful to all the administrative and support staff of the Department of Chemistry. As well, I greatly appreciate the gracious assistance of Marcie Chaudet and the Rose group (Department of Biology) with X-ray crystallography.

Finally, I would like to express my deepest and heartfelt gratitude to my family for their unwavering support, love and understanding, which has been a great source of motivation and inspiration throughout my studies. Thank you, all of you, for your encouragement during my times of despair.

*For Mama & Janine*

## TABLE OF CONTENTS

<b>LIST OF TABLES .....</b>	<b>xiii</b>
<b>LIST OF FIGURES .....</b>	<b>xv</b>
<b>LIST OF ABBREVIATIONS .....</b>	<b>xix</b>
<b>CHAPTER 1: INTRODUCTION .....</b>	<b>1</b>
1.1. Antibiotic action and mechanisms of resistance .....	2
1.1.1. Target sites and modes of action for common antibiotics .....	4
1.1.1.1. Cell wall synthesis and cell membrane disruption .....	4
1.1.1.1.1. <i>Inhibitors of peptidoglycan synthesis</i> .....	4
1.1.1.1.2. <i>Bacterial cell membrane</i> .....	5
1.1.1.2. Ribosome targeting antibiotics .....	5
1.1.1.3. Antibiotics targeting DNA synthesis and replication .....	10
1.1.2. Mechanisms of antibiotic resistance.....	11
1.1.2.1. Drug efflux .....	11
1.1.2.2. Antibiotic modification .....	12
1.1.2.3. Target site modification.....	13
1.1.2.4. Molecular neutralization.....	13
1.1.3. Emergence and transfer of antibiotic resistance .....	14
1.1.4. Antibiotic development .....	17
1.2. Thiostrepton and the thiopeptide family of antibiotics .....	18
1.2.1. Structure and physical properties .....	18
1.2.2. Total synthesis and biosynthesis of thiostrepton .....	21
1.2.3. Biological properties of thiostrepton .....	26
1.2.3.1. Antibacterial activity .....	26
1.2.3.2. Additional biological properties of thiostrepton.....	30
1.3. Thiostrepton resistance .....	31
1.3.1. Resistance in thiostrepton producing organisms .....	31
1.3.1.1. RNA methylation and antibiotic resistance .....	34
1.3.1.2. AdoMet dependent methyltransferases .....	36
1.3.1.3. Mechanism of transmethylation .....	37
1.3.1.4. AdoMet-dependent methyltransferases as tools .....	39
1.3.2. Resistance in organisms that do not produce thiostrepton.....	43
1.3.2.1. Thiostrepton resistant mutants.....	43
1.3.2.2. Thiostrepton binding proteins .....	45

1.4. Research objectives.....	47
-------------------------------	----

## **CHAPTER 2: SYNTHESIS AND BIOLOGICAL ACTIVITY OF**

### **THIOSTREPTON ANALOGUES**

2.1. Preface .....	49
2.2. Materials and methods .....	51
2.2.1. Chemicals and reagents.....	51
2.2.2. Equipment .....	52
2.2.2.1. Chromatography.....	52
2.2.2.2. Mass spectrometry.....	52
2.2.2.3. Luminescence.....	52
2.2.2.4. Nuclear magnetic resonance.....	52
2.2.3. General methods.....	53
2.2.3.1. Synthesis of thiostrepton analogues .....	53
2.2.3.2. Computational determination of the solubility properties for thiostrepton and its derivatives.....	56
2.2.3.3. Inhibition of bacterial growth.....	56
2.2.3.4. <i>In vitro</i> inhibition of protein synthesis .....	57
2.2.3.5. Reaction of thiostrepton with ionic copper.....	57
2.3. Results and discussion .....	58
2.3.1. Synthesis of thiostrepton derivatives.....	57
2.3.2. Purification & characterization of thiostrepton derivatives.....	59
2.3.2.1. Optimization of purification conditions .....	58
2.3.2.2. Physical characterization of the thiostrepton-MENSA derivative.....	61
2.3.2.3. Modification of thiostrepton by bulky, polar thiols.....	65
2.3.2.4. Aqueous solubility of thiostrepton derivatives.....	67
2.3.3. Biological activity of various thiostrepton derivatives.....	69
2.3.4. Thiostrepton-copper interactions.....	75
2.4. Conclusions, perspectives and future work.....	82

## **CHAPTER 3: DETERMINANTS OF ADOMET BINDING AND METHYL GROUP TRANSFER FOR THIOSTREPTON RESISTANCE**

### **METHYLTRANSFERASE**

3.1. Preface .....	84
3.2. Materials and methods .....	85



3.2.1. Chemicals and reagents .....	85
3.2.1.1. PCR and DNA manipulation .....	85
3.2.1.2. Media .....	86
3.2.1.3. Enzyme substrates .....	86
3.2.2. Equipment .....	87
3.2.2.1. Incubators .....	87
3.2.2.2. Centrifugation .....	87
3.2.2.3. Cell disruption .....	87
3.2.2.4. Chromatography .....	87
3.2.2.5. Spectrophotometry .....	88
3.2.2.6. Fluorescence spectroscopy .....	88
3.2.2.7. Isothermal titration calorimetry .....	89
3.2.2.8. Mass spectrometry .....	89
3.2.2.9. Polymerase chain reaction .....	89
3.2.3. General methods .....	89
3.2.3.1. Electrophoresis .....	89
3.2.3.2. Protein mass spectrometry .....	90
3.2.3.3. Protein quantification .....	91
3.2.3.4. DNA manipulation .....	91
3.2.3.5. Site directed mutagenesis of TSR .....	91
3.2.3.6. Expression, purification and characterization of TSR mutants .....	95
3.2.3.6.1. <i>Size exclusion chromatography</i> .....	98
3.2.3.7. RNA methylation by TSR .....	98
3.2.3.8. Isothermal titration calorimetry .....	99
3.3. Results and discussion .....	101
3.3.1. Development of the coupled fluorometric assay .....	101
3.3.2. Effect of point mutations on TSR activity .....	103
3.3.3. Enzyme kinetics of AdoMet for TSR mutants .....	108
3.3.4. AdoMet binding in point mutants of TSR .....	113
3.4. Conclusions, perspectives and future work .....	120

## **CHAPTER 4: SYNTHESIS OF A NOVEL ADOMET ANALOGUE AND ITS EVALUATION AS AN ADOMET METHYLTRANSFERASE CO- SUBSTRATE**

4.1. Preface .....	123
4.2. Materials and methods .....	125

4.2.1. Chemicals and reagents.....	125
4.2.2. Equipment .....	125
4.2.2.1. Chromatography.....	125
4.2.2.2. Spectrophotometry .....	125
4.2.2.3. Mass spectrometry.....	126
4.2.2.4. Gas chromatography .....	126
4.2.2.5. Nuclear magnetic resonance.....	126
4.2.3. General methods.....	127
4.2.3.1. Synthesis of 3-iodo-1,1,1-trifluoroprop-2-one .....	127
4.2.3.2. Synthesis of S-adenosyl-S-(1,1,1-trifluoropropan-2-one)-L-methionine (4.1).....	127
4.2.3.3. Synthesis of the thiopurine methyltransferase product standard (1,1,1trifluoro-3-[(4-nitrophenyl)thio]propane-2-one) (4.3) .....	129
4.2.3.4. TMPT activity assay.....	129
4.2.3.5. Competition assays.....	131
4.3. Results and discussion .....	131
4.3.1. Synthesis of S-adenosyl-S-(1,1,1-trifluoropropan-2-one)-L-methionine (4.1) .....	131
4.3.2. Optimization of the reaction conditions for the synthesis of 4.1 .....	135
4.3.2.1. General conditions.....	135
4.3.2.2. Silver salts .....	136
4.3.2.3. Synthesis of 3-iodo-1,1,1-trifluoroprop-2-one (4.3) and its reaction with AdoHcy .....	137
4.3.2.4. Attempted synthesis of activated trifluoromethyl ketones .....	140
4.3.3. Evaluation of the trifluoropropane-2,2-diol AdoMet derivative (4.2) as a potential Mtase co-substrate.....	141
4.3.3.1. Thiopurine methyltransferase activity with 4.2 .....	141
4.4. Conclusions, perspectives and future work.....	149

## **CHAPTER 5: MOLECULAR INTERACTIONS BETWEEN THIOSTREPTON AND THE TIPAS RESISTANCE PROTEIN FROM *STREPTOMYCES***

### ***LIVIDANS***

5.1. Preface .....	154
5.2. Materials and methods .....	155
5.2.1. Chemicals and reagents.....	155
5.2.2. Equipment .....	155

5.2.2.1. Protein chromatography .....	155
5.2.2.2. Flash chromatography .....	156
5.2.2.3. Fractionation of peptide digests using high performance liquid chromatography .....	156
5.2.2.4. Mass spectrometry.....	156
5.2.2.5. Circular dichroism.....	157
5.2.2.6. Fluorescence spectroscopy .....	157
5.2.2.7. Nuclear magnetic resonance.....	157
5.2.2.8. Isothermal titration calorimetry .....	157
5.2.2.9. Polymerase chain reaction.....	157
5.2.3. General methods.....	158
5.2.3.1. DNA manipulation .....	158
5.2.3.2. Electrophoresis .....	158
5.2.3.3. Protein characterization.....	158
5.2.3.4. Expression, purification and characterization of TIP proteins .....	158
5.2.3.5. Ion exchange chromatography .....	162
5.2.3.6. Reaction of TIP proteins with thiostrepton.....	163
5.2.3.7. Cyanogen bromide digestion of TIP proteins & protein-thiostrepton complexes.....	163
5.2.3.8. Synthesis of thiostrepton derivatives .....	164
5.2.3.8.1. <i>Truncated derivatives</i> .....	164
5.2.3.8.2. <i>Michael adducts</i> .....	166
5.2.3.9. Fluorescence quenching of TIPAS.....	167
5.2.3.10. Isothermal titration calorimetry.....	167
5.2.3.11. Molecular modeling .....	168
5.3. Results and discussion .....	169
5.3.1. Modeling the TIPAS-thiostrepton interaction .....	169
5.3.2. Interaction of TIPAS and its variants with thiostrepton .....	172
5.3.3. Mapping the site of covalent addition of thiostrepton by point mutation studies on TIPAS.....	175
5.3.4. Qualitative evaluation of the non-covalent binding of thiostrepton to TIPAS .....	180
5.3.5. Non-covalent binding affinity of thiostrepton to TIPAS.....	183
5.3.6. X-ray crystallography of TIPAS & the TIPAS-thiostrepton complex.....	188
5.4. Conclusions, perspectives and future work.....	191

<b>REFERENCES</b> .....	194
-------------------------	-----

## **APPENDICES**

Appendix 1: NMR spectra for thiostrepton derivatives.....	224
Appendix 2: Cell free assays of inhibition of protein translation by thiostrepton and its derivatives.....	229
Appendix 3: Crystal data and structure refinement for the copper complex.....	230
Appendix 4: ITC supplement – curve fitting and data processing.....	232
Appendix 5: Fluorometric enzyme assay supplement & enzyme kinetics for AdoMet.....	238
Appendix 6: Comparison of TSR and NHR.....	245
Appendix 7: Confirmation of mutant identity.....	246
Appendix 8: Additives used in screens for TIPAS crystallization.....	253

## LIST OF TABLES

### **CHAPTER 2: SYNTHESIS AND BIOLOGICAL ACTIVITY OF THIOSTREPTON ANALOGUES**

Table 2.1: Theoretical solubility of Thiostrepton and Michael adducts .....	68
Table 2.2: Antibacterial activity of thiostrepton analogues .....	69

### **CHAPTER 3: DETERMINANTS OF AdoMet BINDING AND METHYL GROUP TRANSFER FOR THIOSTREPTON RESISTANCE METHYLTRANSFERASE**

Table 3.1: PCR primers for site directed mutagenesis of TSR .....	93
Table 3.2: Experimental conditions for PCR reactions to generate full length TSR genes ..	93
Table 3.3: Kinetic parameters for enzyme catalyzed RNA methylation by TSR and its variants .....	110
Table 3.4: Parameters for AdoMet binding to TSR and its variants .....	113

### **CHAPTER 4: SYNTHESIS OF A NOVEL AdoMet ANALOGUE AND ITS EVALUATION AS AN AdoMet METHYLTRANSFERASE CO-SUBSTRATE**

Table 4.1: Energy of transfer (kJ/mol) for various groups to nucleophilic acceptors.....	147
--	-----

### **CHAPTER 5: MOLECULAR INTERACTIONS BETWEEN THIOSTREPTON AND THE TIPAS RESISTANCE PROTEIN FROM STREPTOMYCES LIVIDANS**

Table 5.1: PCR primers used for TIPS protein expression and point mutant generation .....	161
Table 5.2: PCR conditions for amplification of the coding sequence for TIPAS and TIPAS <sub>t</sub> from <i>S. lividans</i> genomic DNA .....	161
Table 5.3: PCR conditions to generate full length TIPAS mutant genes.....	162
Table 5.4: ESI-MS characterization of CNBr digestion products.....	178

### **APPENDIX 3**

Table A3.1: Atomic coordinates ( $\times 10^4$ ) and equivalent isotropic displacement parameters ( $\text{\AA}^2 \times 10^3$ ) for $\text{C}_{24}\text{H}_{26}\text{O}_6\text{Cu}$ .....	230
Table A3.2: Hydrogen coordinates ( $\times 10^4$ ) and equivalent isotropic displacement parameters ( $\text{\AA}^2 \times 10^3$ ) for $\text{C}_{24}\text{H}_{26}\text{O}_6\text{Cu}$ .....	230
Table A3.2: Bond lengths [ $\text{\AA}$ ] and angles [ $^\circ$ ] for Copper complex .....	231

### **APPENDIX 4**

Table A4.1: Parameters of AdoMet binding to TSR .....	234
Table A4.2: Parameters for AdoMet binding to TSR mutants.....	235
Table A4.3: Parameters for the binding of thiostrepton analogues to TIP-AS (or its C214A variant).....	236

### **APPENDIX 5**

Table A5.1: AdoHcy standard curve .....	241
Table A5.2: Sample calculations for the conversion of ( $\Delta\text{RFU}/\text{second}$ ) to ( $\Delta[\text{AdoHcy}]/\text{second}$ ) .....	243
Table A5.3: Raw data used for the generation of Michaelis-Menten plots and the determination of enzyme kinetic parameters .....	244

### **APPENDIX 8**

Table A8.1: Additive screen reagents.....	253
---	-----

## LIST OF FIGURES

### CHAPTER 1: INTRODUCTION

Figure 1.1: Structural diversity of antibiotics .....	3
Figure 1.2: Binding sites of antibiotics on the bacterial ribosome.....	6
Figure 1.3: Antibiotic and the elongation cycle of protein translation .....	10
Figure 1.4: Structures of the thiopeptide antibiotics.....	19
Figure 1.5: Thiostrepton .....	21
Figure 1.6: Proposed formation of mature thiostrepton.....	24
Figure 1.7: The binding of thiostrepton to the bacterial ribosome.....	28
Figure 1.8: The TSR-AdoMet complex.....	33
Figure 1.9: The interaction of RNA with TSR .....	34
Figure 1.10: Topological diagram of the SPOUT methyltransferases (Class IV).....	37
Figure 1.11: General mechanism for methyltransferase catalysis .....	38
Figure 1.12: Postulated mechanism of RlmN .....	39
Figure 1.13: Riboadenosyl transfer from AdoMet analogues.....	41
Figure 1.14: Mtase catalyzed transfer of extended alkyl chains .....	42

### CHAPTER 2: SYNTHESIS AND BIOLOGICAL ACTIVITY OF

#### THIOSTREPTON ANALOGUES

Figure 2.1: Mechanism for Michael addition of thiols to DHA.....	51
Scheme 2.1: Synthesis of Michael adducts of thiostrepton .....	59
Figure 2.2: Optimization of the HPLC purification of thiostrepton-MENSA derivatives....	60
Figure 2.3: Proton NMR of the MENSA derivative of thiostrepton.....	61
Figure 2.4: Proton COSY spectrum of thiostrepton.....	62
Figure 2.5: Proton TOCSY spectrum of thiostrepton .....	63
Figure 2.6: TOCSY spectra of thiostrepton-MENSA derivatives .....	64
Figure 2.7: Configurations of the MENSA appendage in the thiostrepton derivatives .....	65
Figure 2.8: Structures of 2-thio- $\beta$ -D-glucose and captopril.....	66
Figure 2.9: Purification and characterization of the thiostrepton-captopril derivative .....	67
Figure 2.10: Relative (aqueous) solubility of Michael adducts .....	68
Figure 2.11: Effect of thiostrepton and its derivatives on <i>in vitro</i> protein synthesis .....	71
Figure 2.12: Space-filling structures of the polar thiols used to modify thioistrepton.....	73
Figure 2.13: Importance of the thiostrepton tail in ribosome binding .....	75
Figure 2.14: Effect of copper on UV absorbance of thiostrepton .....	76

Figure 2.15: Interaction of thiostrepton with organic copper complexes .....	78
Figure 2.16: Ketones used to aid thiostrepton-copper complexation.....	79
Figure 2.17: UV-absorbance spectra for thiostrepton in complex with copper and ketones	81

### **CHAPTER 3: DETERMINANTS OF AdoMet BINDING AND METHYL GROUP TRANSFER FOR THIOSTREPTON-RESISTANCE**

#### **METHYLTRANSFERASE**

Figure 3.1: Potentially relevant amino acid residues in the TSR active site.....	85
Figure 3.2: Schematic of the pET28a plasmid bearing the TSR gene .....	92
Figure 3.3: Site directed mutagenesis of TSR .....	93
Figure 3.4: Overexpression and purification of TSR and its variants in <i>E. coli</i> .....	97
Figure 3.5. Optimization of ITC experiments for investigation of the binding of AdoMet to TSR .....	100
Figure 3.6: Development of the coupled fluorometric assay for TSR .....	102
Figure 3.7: Relative activity of point mutants of TSR.....	103
Figure 3.8: Hydrogen bonding between AdoMet and R135 and R165.....	105
Figure 3.9: Orientation of S246 in the active sites of (A) the nosiheptide resistance methyltransferase and (B) TSR .....	106
Figure 3.10: Orientation of K221 and E220 with respect to AdoMet in the CTD of TSR ...	107
Figure 3.11: Michaelis-Menten plots for TSR and its variants with AdoMet.....	109
Figure 3.12: The importance of K221 in the AdoMet binding pocket.....	111
Figure 3.13: Possible role of E220 in RNA binding.....	112
Figure 3.14: Measurement of AdoMet binding to point mutants of TSR by isothermal titration calorimetry.....	114
Figure 3.15: Importance of N129/ Helix 6 for the AdoMet binding site .....	116
Figure 3.16: Size exclusion chromatography of TSR and its N129D variant.....	117
Figure 3.17: Circular dichroism spectra for TSR and its N129 variant .....	119

### **CHAPTER 4: SYNTHESIS OF A NOVEL AdoMet ANALOGUE AND EVALUATION AS AN AdoMet METHYLTRANSFERASE CO-SUBSTRATE**

Figure 4.1: Mechanism for the formation of S-adenosyl-L-(1,1,1-trifluoropropan-2-one)-L-methionine .....	131
Figure 4.2: Purification of the fluoro-ketoAdoMet analogue .....	133
Figure 4.3: NMR characterization of the fluoro-ketoAdoMet analogue.....	134



Scheme 4.1: Optimized conditions for the synthesis of trifluoromethyl ketone derivatives of AdoMet.....	137
Figure 4.4: Attempted synthesis of 3-iodo-1,1,1-trifluoroprop-2-one using conventional Finkelstein conditions.....	139
Scheme 4.2: Synthesis of 3-iodo-1,1,1-trifluoropropan-2-one .....	139
Figure 4.5: Analysis of the products from the reaction of 3-bromo-1,1,1-trifluoroprop-2-one with KI in methanol.....	139
Figure 4.6: Adaptation of the TPMT activity assay to 96-well microplate format .....	141
Figure 4.7: TPMT catalyzed transfer of the trifluoroketone group to 4-nitrobenzenethiol...	142
Figure 4.8: Modification of 4-nitrobenzenethiol by TPMT monitored by the coupled fluorescence assay .....	144
Figure 4.9: Dependence of TPMT activity on enzyme concentration .....	145
Figure 4.10: Effect of 4.2 on TPMT-catalyzed methylation of 4-nitrobenzenethiol .....	149
Figure 4.11: Attachment of reporter molecules to trifluoroketone modified Mtase substrates .....	151

## CHAPTER 5: MOLECULAR INTERACTIONS BETWEEN THIOSTREPTON AND THE TIPAS RESISTANCE PROTEIN FROM *STREPTOMYCES*

### *LIVIDANS*

Figure 5.1: Proposed thiostrepton binding site .....	169
Figure 5.2: Modeling TIPAS-thiostrepton binding.....	171
Figure 5.3: The binding of thiostrepton to TIPAS .....	171
Figure 5.4: Purification and characterization of TIP-thiostrepton complexes .....	173
Figure 5.5: Deconvoluted mass spectra of thiostrepton complexes with TIPAS mutants ....	175
Figure 5.6: Cyanogen bromide cleavage sited in TIPAS.....	176
Figure 5.7: Analysis of the cleavage products from cyanogens bromide digestion of thiostrepton complexes with TIPAS mutants .....	178
Figure 5.8: Confirmation of conversion of cysteine to cysteic acid during CNBr digestion	179
Figure 5.9: Fluorescent residues in TIPAS.....	180
Figure 5.10: Structures of truncated thiostrepton derivatives .....	181
Figure 5.11: Efect of thiostrepton binding on TIPAS fluorescence .....	182
Figure 5.12: TIPAS reaction with <b>5.1</b> .....	183
Figure 5.13: Structures of Michael derivatives of thiostrepton.....	185
Figure 5.14: Site of thiol Michael addition in <b>5.4</b> .....	185
Figure 5.15: Isothermal titration calorimetry of TIPAS with thiostrepton derivatives .....	187
Figure 5.16: Schematic of an individual well from a 96-well sitting drop plate.....	188

Figure 5.17: High throughput screening for crystal growth conditions for TIPAS .....	189
Figure 5.18: Optimized conditions for crystal growth of TIPAS and the TIPAS-thiostrepton complex .....	190

## APPENDIX 1

Figure A1.1: Full proton spectra for thiostrepton and its Michael adducts used in antibacterial testing .....	224
Figure A1.2: Full COSY (top panel) and TOCSY (bottom panel) spectra for thiostrepton .....	225
Figure A1.3: Full TOCSY spectra for Michael adducts of thiostrepton with MENSA .....	226
Figure A1.4: Full TOCSY spectra for Michael adducts of thiostrepton with captopril .....	227
Figure A1.5: Full proton spectra for thiostrepton derivatives used in binding studies with TIPAS .....	228

## APPENDIX 2

Figure A2.1: Optimization of the assay for the inhibition of <i>in vitro</i> translation.....	229
---	-----

## APPENDIX 5

Figure A5.1: General approaches to non-radiometric assays of Mtase activity.....	239
Figure A5.2: Principle of the fluorometric Mtase assay from the Cayman Chemical Company .....	240
Figure A5.3: Linear dependence of $\Delta$ RFU/ second on [AdoHcy] .....	241
Figure A5.4: Dependence of initial rate of the K221 variant on [AdoMet].....	242

## APPENDIX 6

Figure A6.1: Sequence alignment of NHR (nosiheptide resistance methyltransferase) and TSR (thiostrepton resistance emthyltransferase) .....	245
Figure A6.2: A) Stereoview of superimposed structures for TSR (green) and the nosiheptide resistance methyltransferase (purple). (B) Superimposed structures of AdoMet, as positioned in the binding pockets of the individual subunits of TSR (white) and the nosiheptide resistance methyltransferase (magenta).....	245

## LIST OF ABBREVIATIONS

AdoMet	S-adenosyl-L-methionine
AgOTs	silver p-toluenesulfonate
AgOTf	silver trifluoromethanesulfonate
BSA	bovine serum albumin
CD	circular dichroism
COSY	COrelation SpectrometrY
CNBr	cyanogen bromide
CTD	C-terminal domain
ddH <sub>2</sub> O	doubly distilled water
DHA	dehydroalanine
DHB	dehydrobutyrine
DMF	dimethylformamide
DMSO	dimethyl sulfoxide
dNTP	dinucleotide triphosphate
DTT	dithiothreitol
EDTA	ethylenediaminetetraacetic acid
EF	elongation factor
ESI-MS	electrospray ionization mass spectrometry
FOXMI	forkhead box M1
GC/MS	gas chromatography/ mass spectrometry
GTP	guanosine triphosphate
GTPase	guanosine triphosphate hydrolysis
HPLC	high performance liquid chromatography
H-TSR	histagged TSR

IC <sub>50</sub>	concentration at 50% inhibition
IPTG	isopropyl β-D-1-thiogalactopyranoside
ITC	isothermal titration calorimetry
K <sub>cat</sub>	catalytic efficiency/ turnovers/ second
K <sub>d</sub>	dissociation constant
K <sub>m</sub>	substrate concentration at half the maximum velocity
LogP	octanol/ water partition coefficient
MENSA	2-mercaptoethanesulfonic acid
m.p.	melting point
mTAN	adenosylhomocysteine nucleosidase
Mtase	methyltransferase
M <sub>w</sub>	molecular weight in Daltons/ g/ mol
NHR	nosiheptide resistance methyltransferase
NTD	N-terminal domain
PCR	polymerase chain reaction
PDB	Protein Database
pKa	acid dissociation constant
QTOF	quadrupole time of flight
R <sub>f</sub>	relative mobility in thin layer chromatography
rRNA	ribosomal ribonucleic acid
tRNA	transfer ribonucleic acid
SDS	sodium dodecyl sulfate
SPOUT	<i>SpoU</i> – <i>TrmD</i>
Tris	tris (hydroxymethyl) aminoethane
TFA	trifluoroacetic acid

TOCSY	TOTal Correlation Spectrometry
TPMT	thiopurine-S-methyltransferase
TSR	23S rRNA 2'-O-methyltransferase
$V_{\max}$	maximum velocity for enzyme activity

## CHAPTER 1: INTRODUCTION

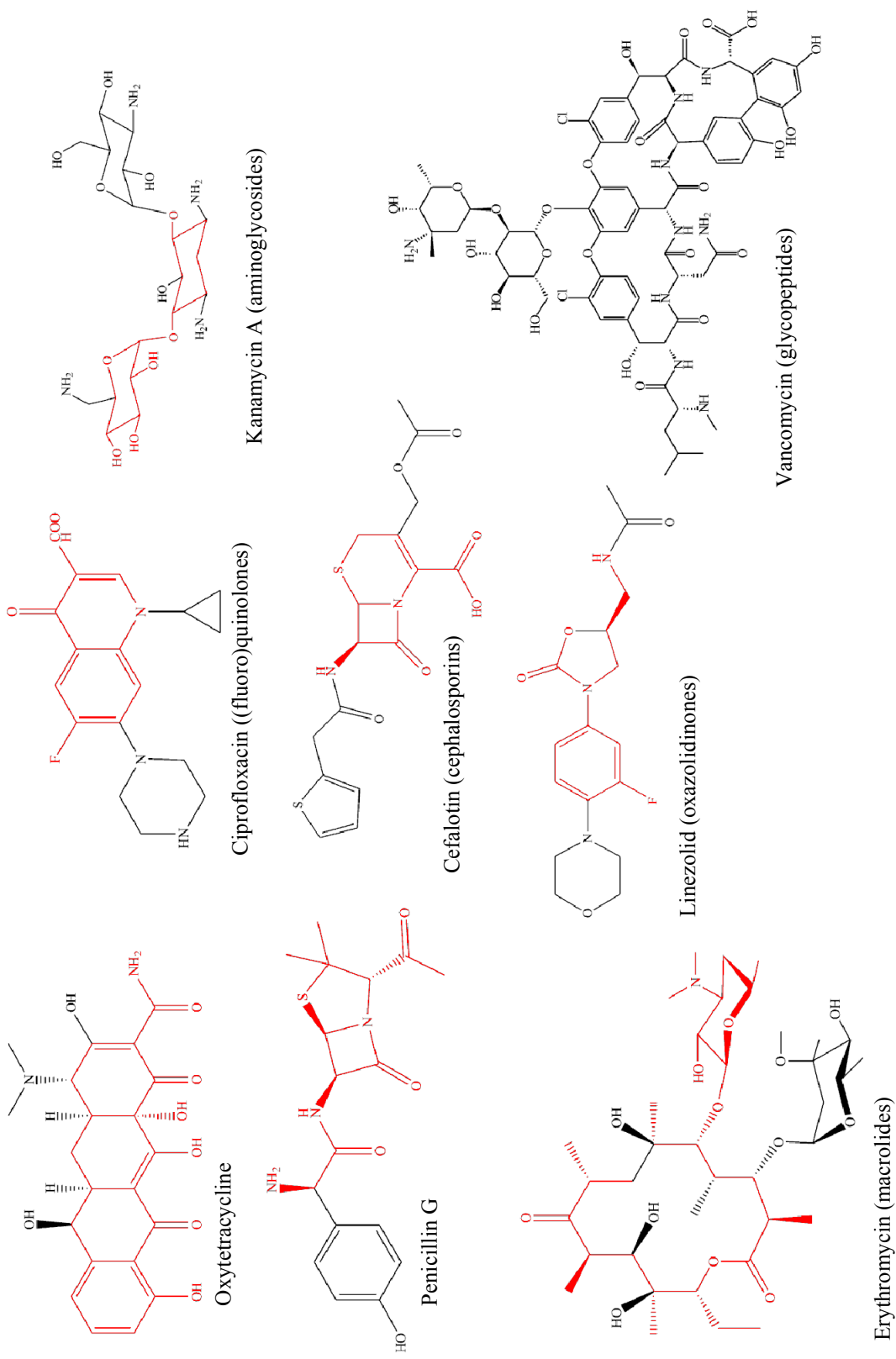
---

Antibiotics have been successfully used in the treatment of bacterial infections for the last seven decades, undeniably bringing about profound improvements in human health. However, upsurging bacterial antibiotic resistance has become an immense source of concern and frustration to biomedical researchers and clinical health care providers. Antibiotics are secondary metabolites whose functions may well extend beyond the inhibition of bacterial growth (1, 2). While some debate exists over the evolutionary origins and functions of antibiotics, it is clear that the antibiotic producing phenotype provides a fitness advantage to antibiotic producers and thus has been passed down through natural selection. The evolution of antibiotic resistance is by necessity linked to that of the antibiotic production, as the organisms producing these toxic compounds would require mechanisms to prevent their self-destruction.

The first recorded clinical case of antibiotic resistance was that observed against penicillin, within two years of its discovery in the mid-1940s (3, 4). Since then, nosocomial resistance has been observed, on average, within months to a few years after the clinical introduction of an antibiotic (4). This emergence and the persistence of resistant strains is a direct consequence of the selective pressure arising from the overuse and misuse of these drugs. Thus far, incidences of infection have been generally contained, yet the possibility of widespread, uncontrollable outbreak remains.

## **1.1. Antibiotic action and mechanisms of resistance**

Antibiotics exert bacteriocidal or bacteriostatic effect on bacteria through inhibitory or destructive effects on essential bacterial cellular processes and/ or organelles. Many structurally diverse classes of these compounds (Figure 1.1) exist and the mode of action for numerous antibiotics as well as associated resistance mechanisms has been determined. As these topics have been extensively researched and thoroughly reviewed, a cursory overview will be presented in the following sections (**1.1.1** and **1.1.2**).



**Figure 1.1. Structural diversity of antibiotics.** Representatives from various antibiotic classes are shown. The core scaffold is colored red.



## **1.1.1. Target sites and modes of action for common antibiotics**

### **1.1.1.1. Cell wall synthesis and cell membrane disruption**

#### *1.1.1.1.1. Inhibitors of peptidoglycan synthesis*

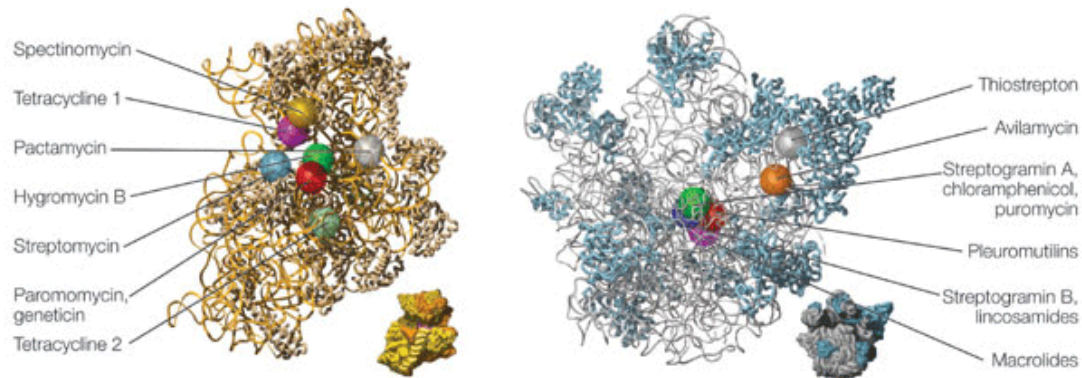
Modern clinical use of antibiotics for the treatment of bacterial infections began with penicillin in the 1940s, the progenitor of the  $\beta$ -lactam antibiotics (cephalosporins, monobactams, carbapenems). These compounds feature a reactive four-membered ring that serves as the key structure in the disruption of cell wall synthesis. The integrity of bacterial cell walls is maintained by a peptidoglycan network formed from cross-linked adjacent polymers of repeating N-acetylmuramic acid and N-acetylglucosamine units. It is believed that the beta-lactam drugs structurally mimic the peptide substrate (D-alanine-D-alanine) of the transpeptidases that catalyze this cross-linking, thus covalently inhibiting these enzymes (5). Glycopeptides, including vancomycin and teicoplanin, are another group of antibiotics that target cell wall biosynthesis. In the case of vancomycin, the antibiotic selectively binds (through hydrogen bonding) the terminal D-alanyl-D-alanine on the peptide precursors of peptidoglycan biosynthesis, which prevents their transglycosylase-mediated incorporation into peptidoglycan (6). Peptidoglycan synthesis is a complex, multistage process and the antibiotic targets of this process are not restricted to the transglycosylase enzymes, as seen with additional glycopeptides and other classes of antibiotics, including some lantibiotics (7–11).

#### *1.1.1.1.2. Bacterial cell membrane*

Antibiotics that affect the cell membrane (type A lantibiotics, daptomycin) include cationic bacteriocins that are able to interact with the negatively charged lipid moieties on the outer surfaces of bacterial cells (12). Membrane association by these molecules is believed to promote the self-uptake that leads to the formation of membrane permeabilizing pores. The mechanism of pore formation is unclear but likely varies between molecules and several models have been postulated to explain this process (13). Nevertheless, membrane permeabilization has been found to impact small molecule transport and energy transduction process across the membrane, while facilitating internalization of the cationic peptide, with bactericidal consequences to the cell (13, 14).

#### **1.1.1.2. Ribosome targeting antibiotics**

Protein synthesis is an essential cellular process that is a target of several antibiotics (Figure 1.2). As well, the eukaryotic process is sufficiently different from that occurring in bacteria (15), making this an attractive drug target and accordingly, antibiotics that interfere with protein synthesis are well represented in the clinic. Antibiotics inhibiting virtually all stages of protein translation have been discovered, however, the processes of the elongation cycle are most targeted.



**Figure 1.2. Binding sites of antibiotics on the bacterial ribosome.** The 30S ribosomal subunit is shown on the left and the 50S ribosomal subunit is shown on the right. The antibiotic-binding sites were initially determined by biochemical and genetic techniques; subsequently, many sites were revealed in greater detail by X-ray crystallography. At the overlapping sites, antibiotic binding is usually mutually exclusive (for example, for macrolide, lincosamide and streptogramin B compounds), however, streptogramin A and B compounds bind synergistically at adjacent sites. Subunit models are based on the *Thermus thermophilus* 70S ribosome structure. In this figure, for clarity, part of the r-protein L9 has been omitted. Ribosomal RNAs are shown in yellow and grey and r-proteins in bronze and blue. Reprinted by permission from Macmillan Publishers Ltd: [Nature Reviews Microbiology]. Poehlsgaard and Douthwaite, 2005. *The Bacterial Ribosome as a target for Antibiotics*. *Nature Reviews Microbiology*. 3, 870 – 881. Copyright (2005)

The elongation cycle of protein synthesis commences with the decoding stage, which follows after initiation. The P Site is occupied with a peptidyl-tRNA and the A Site displays the codon for the next aminoacyl tRNA (aatRNA) encoded by the sequence (16). Tetracyclines act at this stage by binding to the A Site which prevents accommodation of the incoming aatRNA (17). The binding of aatRNA at the A Site is facilitated by elongation factor Tu (EF-Tu), which forms a ternary complex with aatRNA and GTP (18). Subsequent GTP hydrolysis allows the requisite conformational change in EF-Tu for its dissociation (16). Hence, inhibition of these EF-Tu mediated activities could also prevent A Site occupation, as seen with the kirromycins (prevent the

dissociation of EF-Tu), pulvomycin (prevent the formation of the aaRNA-EF.Tu-GTP complex) and ribotoxins (impede the binding of the aaRNA-EF.Tu-GTP complex) (17).

Aminoglycosides (streptomycin, kanamycin) utilize a different approach to interfere with A Site processes. These polycationic molecules promote self uptake into the bacterial cells through interactions with the negatively charged lipopolysaccharides in the bacterial membrane (similar to membrane targeting antibiotics discussed above) and their inherent positive charge also directs them to the negatively charged rRNA in the 30S subunit of the bacterial ribosome where they bind to specific bases at the A-site (19). This binding induces structural rearrangements in these bases that are critical to the fidelity of translation and the consequent misreading leads to the incorporation of incorrect amino acids and the synthesis of useless translational products which are ultimately detrimental to the cell (20). As well, aminoglycoside binding at the A Site can interfere with translocation of tRNA from the A Site to the P Site (21).

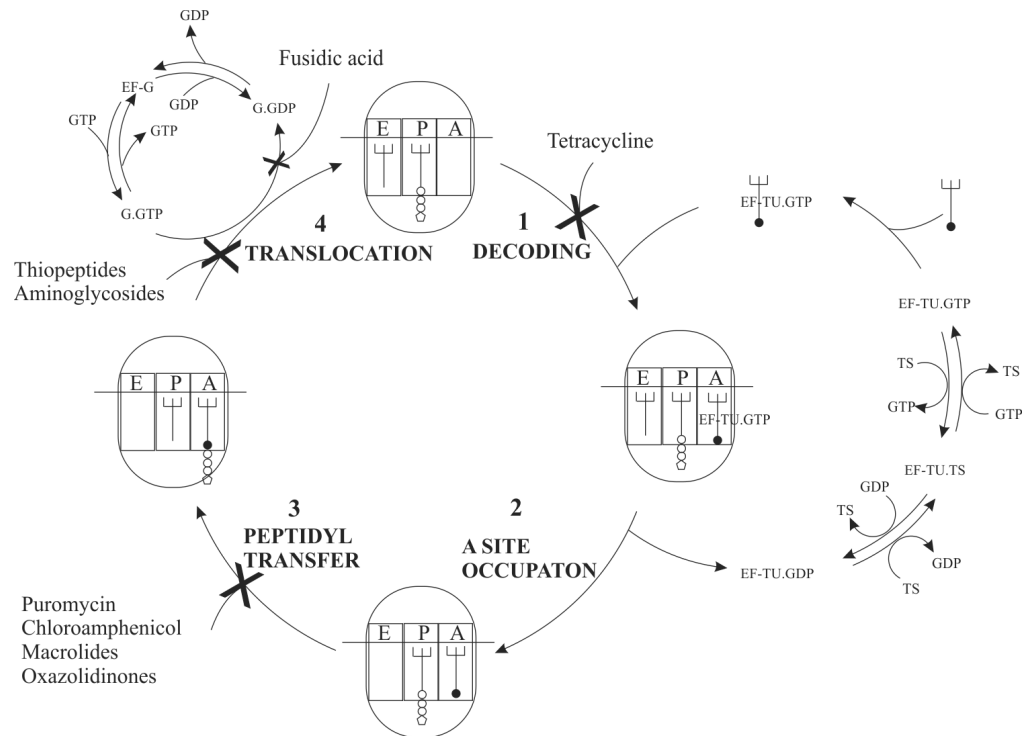
The peptidyl transfer reaction occurs between the peptidyl-tRNA that occupies the P Site and the aaRNA at the A Site after A Site occupation. In this RNA catalyzed reaction, the amino group of the A Site tRNA attacks the carbonyl group at the ester linking the peptide moiety to tRNA in the P Site peptidyl tRNA (22, 23). The end result is the formation of a peptide bond between the aaRNA at the A Site and the peptidyl residue formerly associated with the P-site peptidyl tRNA (16, 24). Antibiotics that inhibit this stage of the elongation typically do so by outcompeting the native substrates of the peptidyl

transferase reaction or by preventing the progression of the immature peptide as it is being synthesized. Puromycin and blasticidin resemble the 3'-end of aa-tRNA, and the former is incorporated into the growing polypeptide chain, forming an ester linkage to the ribose of tRNA that cannot be cleaved by the ribosome (17). Chloroamphenicol and the lincosamides have overlapping binding sites at the peptidyl transferase centre and these antibiotics act by disrupting tRNA binding at the A Site (25, 26). Likewise, streptogramin A and oxazolidinone binding at the peptidyl transferase center hinders tRNA binding at the A and P Sites (27, 28).

After peptidyl transfer, deacylated tRNA is transferred from the P Site to the E Site and peptidyl-tRNA is transferred from the A Site to the P Site in a translocation process that makes the A Site available for the next incoming aa-tRNA that is encoded by the sequence. As this cycle repeats, the nascent peptide is threaded through the exit tunnel as it grows in length until a stop codon is reached (16). The polyketide macrolide antibiotics bind the 50S ribosomal subunit at the exit tunnel near the peptidyl transferase center, thereby reducing the diameter of this passageway and obstructing the exit path for the nascent peptide chain (29, 30). The binding site of streptogramin B antibiotics at the peptidyl transferase center overlaps with that of the macrolides, also leading to inhibition of the nascent chain progression (26).

Translocation is linked to directional mRNA movement in a concerted process that preserves the reading frame while lengthening the peptide one residue at a time (18). This process takes advantage of their differential binding

affinities that tRNA species have for the respective binding sites (aatRNA for the A-site, peptidyl tRNA for the P-site and deacylated tRNA for the E-site), but is also directly aided by elongation factor G (EF-G) and GTP hydrolysis, which mediate structural rearrangements in the ribosome that allow complimentary tRNA and mRNA movement (18, 31, 32). Fusidic acid is a classic translocational inhibitor and binds at the GTPase center, effectively stalling the ribosome by stabilizing the EF-G.GDP complex on the ribosome. Conversely, viomycin and spectinomycin operate at the other end of the EF-G cycle by interfering with EF-G.GTP binding. The binding of thiopeptide antibiotics at the GTPase center also disrupts GTP-dependent activities (17). Thiostrepton, the archetypal member of this antibiotic family, is the central focus of study in this thesis and the details of its mode of action and that of other thiopeptides will be elaborated in following sections. The elongation cycle of protein translation and the points of antibiotic action are summarized in Figure 1.3.



**Figure. 1.3. Antibiotics and the elongation cycle of protein translation.** (1) Decoding: The A Site on the ribosome is available for the next aatRNA encoded by the mRNA sequence. (2) A Site occupation: aatRNA binds at the A Site, aided by EF-Tu. (3) Petidyl transfer: A peptide bond forms between the amino acid from the aatRNA and the peptidyl moiety from the peptidyl tRNA that is at the P Site, lengthening the peptide chain by one residue. (4). Concerted movement of the ribosome with respect to mRNA by one codon, aided by EF-G, leaving deactivated tRNA in the E Site and the A Site free for and incoming aatRNA. The points of action of various antibiotics are indicated. (Adapted from (17))

### 1.1.1.3. Antibiotics targeting DNA synthesis and replication

Quinolone antibiotics were discovered in the early 1960s and became widely used in the clinic from the mid-1980s (33). Their observed bactericidal ability was initially limited to Gram-negative species but later extended to Gram-positive species as well as to *Mycobacterium tuberculosis*, through fluorine derivatization, giving rise to the fluoroquinolones which also possess an improved pharmacokinetic profile (34, 35).

Quinolones and fluoroquinolones are broad spectrum antibiotics that impede DNA replication by targeting DNA gyrase and topoisomerase IV. DNA gyrase acts to relieve the positive supercoiling and torsional stress ahead of the transcriptional complex. Quinolone binding induces conformational changes in the enzyme that stabilize the DNA-DNA gyrase complex, thus stalling the replication fork (36). DNA replication is arrested by quinolone binding to topoisomerase IV through the prevention of the decatenation of daughter DNA strands that is performed by this enzyme (37).

### **1.1.2. Mechanisms of antibiotic resistance**

The diversity in the ways by which antibiotics act is matched by an assortment of ways in which bacteria are able to avoid the effects of these drugs. These generally fall within four general mechanisms: efflux, antibiotic modification, target site modification and drug neutralization.

#### **1.1.2.1. Drug efflux**

Antibiotics must accumulate inside the bacterial cell at sufficiently high concentrations to be effective. This accumulation is prevented by the actions of membrane spanning protein systems that actively transport drug molecules out of the cell. Drug efflux was first reported as a cause of tetracycline insensitivity (38), but these systems are now known to confer resistance to a broad range of antibiotics. They have also been the subject of extensive study, particularly those systems of the resistance-nodulation-cell division-class (RND) (39). Members of the RND class, such as the Arc-AB-TolC and MexAB-OprM



systems in *E. coli* and *P. aeruginosa*, respectively, feature a tripartate system of an outer membrane pore and a transmembrane pump linked by a bridging protein (40). Efflux proteins are not necessarily expressed in direct response to antibiotic presence, but rather appear to be integrated into bacterial cellular stress response (41). However, the chemical cues that activate the regulatory elements for the transcription of the genes encoding these proteins remain poorly described (41)

#### **1.1.2.2. Antibiotic modification**

Antibiotic modifications that result in the direct destruction of the drug molecule were first described in  $\beta$ -lactamase catalyzed hydrolytic lactam ring opening of penicillin that renders the antibiotic inactive (42). The substrate specificity of these enzymes has been expanded by evolution, giving rise to the extended spectrum  $\beta$ -lactamases (ESBL) and metallo- $\beta$ -lactamases that cause resistance to later generations of  $\beta$ -lactam antibiotics (cephalosporins, carbapenems) (43, 44). In addition, scaffold opening in some macrolides and streptogramins leads to deactivation of these drugs (39). Antibiotic modifications causing resistance can also take the form of enzyme modification by the additional of functional groups that hinder the interaction of the antibiotic with its target site. Such is the result of adenylation, phosphorylation or acetylation of aminoglycosides by resistance enzymes that leads to their diminished affinity for the bacterial ribosome (21).

### **1.1.2.3. Target site modification**

Analogous to the antibiotic addition of chemical groups to the antibiotic molecule, antibiotic binding may be prevented by modifications at the antibiotic target site. Such target site modifications are particularly important as a mechanism of resistance among ribosome targeting antibiotics. Examples include the specific adenine methylations on 23S rRNA by Erm methyltransferases that averts the binding of macrolide antibiotics to the bacterial ribosome; the prevention of ribosomal binding by avilamycin due to the methylation of guanosine or uridine by AviRa and AviRb; and the methylation of purine nucleotides on 16S rRNA that results in resistance to certain aminoglycosides (21, 29, 45, 46). Methylation of rRNA is also an important form of resistance to thiopeptides antibiotics, which will be later discussed specifically with respect to thiostrepton and from the broader context of methylation as a resistance mechanism.

### **1.1.2.4. Molecular neutralization**

Molecular neutralization encompasses bacterial strategies that indirectly accomplish antibiotic deactivation. Such is the case for vancomycin resistance that results from alterations to the content of the peptidoglycan during its synthesis. Organisms exhibiting this form of resistance express enzymes that synthesize a depsipeptide mimic that replaces the normal acyl-D-alanyl-D-alanine in peptidoglycan construction, and another that degrades the D-Ala-D-Ala (39). Vancomycin binding is dependent on interactions with D-Ala-D-Ala, which do not occur with the ester linkage in the depsipeptide, thus rendering the

organism resistant (39). A second example is thiopeptide resistance in non-producing *Streptomyces*. In the presence of certain thiopeptides, these species upregulate the expression of so called TIP proteins, which irreversibly bind the antibiotics, thereby preventing binding at their target sites (47, 48). Antibiotic binding and sequestration is also the mechanism of bleomycin and mitomycin resistance (49–52).

### **1.1.3. Emergence and transfer of antibiotic resistance**

Antibiotic resistance genes are believed to have originated from a primordial gene pool that favored resistance as a means of forestalling cellular death in antibiotic producers and these genes subsequently evolved into the resistome in parallel with the antibiotic producing phenotype (2, 53). This spawned innate bacterial antibiotic resistance, where the organisms inherently possess the genetic information that encodes resistance. Broadly speaking, this refers to any genes that enable the bacteria to elicit a resistance response, such as non-specific efflux pumps that bestow multidrug resistance, stress response proteins or antibiotic binding proteins but also include genes encoding resistance to a specific antibiotic or class of antibiotics.

On the other hand, resistance genes may be acquired through genetic mutations or horizontal gene transfer, establishing resistance in a previously sensitive species. Mutations have been associated with resistance to antibiotics in many classes, but are likely not to be the predominating natural means by which resistance is acquired. Nevertheless, the contribution of this mechanism cannot be discounted. The broad spectrum resistance exhibited by multi-drug

resistant tuberculosis is mediated by mutations and provides an excellent example of resistance emerging through spontaneous mutation (54, 55), as well as the mutational resistance that frequently develops against synthetic antibiotics (28, 56–58). In addition, mutations can affect how resistance genes are expressed and undoubtedly contribute to their evolution, which may be of particular relevance to the emergence of resistance against newly introduced antibiotics (59). It is also believed that a general “housing keeping” gene product is duplicated and modified to provide resistance to externally present antibacterial agents.

Once established in the genome of a bacterial species, resistance genes become susceptible to horizontal gene transfer (HGT) to other species. Bacteria can accomplish HGT by conjugation (conjugative plasmids or transposons), transformation (recombination) or transduction (bacteriophages), but conjugative plasmid mediated transmission is foremost among these for the transfer of resistance genes. These resistance plasmids can be transmittable between a narrow set of similar species, or more worryingly, between a large number of different species and genera, as well as between Gram-negative and Gram-positive organisms. The frequency with which such conjugative transfer occurs nature may not be empirically measurable, yet it is believed to happen to a far greater extent than that shown under laboratory conditions and plasmid mediated resistance has been identified to occur against most clinically relevant antibiotics.

It is not uncommon to find several resistance genes on a single plasmid, which results from integration of mobile resistance genes. Integrons are the capture systems for such genes, which are found on mobile genetic elements referred to as cassettes (60–62). They can be found on plasmids or within transposons that are on plasmids and basic integron structure consists of an *intI* gene that encodes an integrase and a recombination site, *attI*, where gene cassettes are inserted under the control of a promoter (63–66). Gene cassettes are simple DNA segments consisting of a single (promoterless) gene, followed by a recombination site (*attC*) and the integrase gene that catalyzes recombination between *attI* and *attC* (60, 64). This arrangement can allow for the insertion of multiple cassettes under the control of this single strong promoter. Over 100 such cassettes, representing all major classes of antibiotics, have been discovered (62, 67).

The presence of resistance genes in nature has provoked discussions on their origins and additional functions, but ultimately, the emergence, propagation and maintenance of antibiotic resistance genes are subject to natural selection. The selective pressure imposed by the widespread use of antibiotics has unquestionably been the thrust behind the surge in resistance seen in recent times. Moreover, retro-analyses suggest that modern day resistance and resistance gene dissemination are relatively recent phenomena, the progression of which coincided with increasing antibiotic use (67, 68). This prompted notions that removal of selective pressure (widespread antibiotic use) would eventually lead to the reversal of resistance due to the biological cost of

maintaining a resistant phenotype (69, 70), however, many instances where bacteria are able to compensate for this cost are known (67, 69).

#### **1.1.4. Antibiotic development**

The overview of antibiotic modes of action and resistance mechanisms in the preceding sections serve to illustrate that in spite of the myriad ways by which antibiotics are able to exert their toxic effects on the bacterial cell, bacteria continue to demonstrate flexibility and versatility in avoiding the effects of these drugs. This problem of antibiotic resistance cannot be overstated as resistance has been reported to occur against all antibiotics in current clinical use, in addition to those drugs that have yet to reach the clinic and underscores the need for novel, antibacterial chemotherapies.

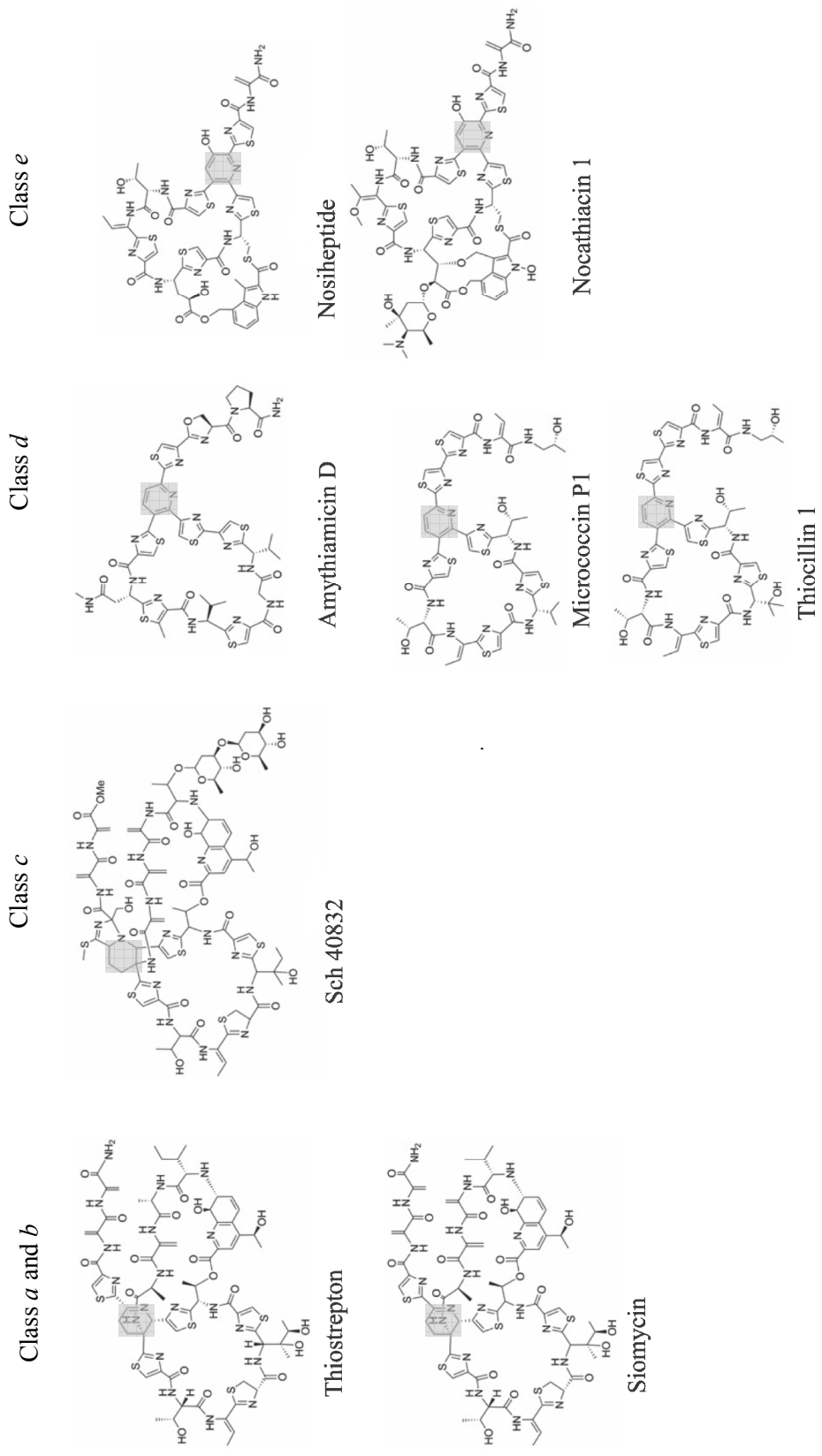
Natural products have historically served as a fruitful source of antibiotics. The reservoir was seemingly exhausted by the 1960s, with the major classes of antibiotics being discovered ( $\beta$ -lactams, aminoglycosides, tetracyclines, macrolides, glycopeptides). This was followed by what is referred to by many as an “innovation gap”, where no new antibiotic classes were introduced until the discovery of the oxazolidinones in the early 2000s. Even so, the emergence of resistance and the characterization of associated molecular mechanisms spurred a period of antibiotic development during this time and these natural products as scaffolds for drug development by semi-synthetic approaches. More recent approaches to the discovery of new antibiotic classes have sought to identify new antibiotic targets through genomic screening and application of combinatorial chemistry towards drug development. As well,

biosynthetic engineering is being explored as a means for antibiotic production and derivatization (71–74). These methodologies, however, are in their nascent stages and have realized little success beyond proof of principle. Concurrent with these efforts, the search for new antibiotic classes among natural products continues. New organisms are being considered as potential sources and while some species do show promise in this regard, an untapped pool of potential “novel” drugs may yet exist among families that have already been discovered. The thiopeptide family of antibiotics, of which thiostrepton is the prototypical member, is one such group under reconsideration.

## **1.2. Thiostrepton and the thiopeptide family of antibiotics**

### **1.2.1. Structure and physical properties**

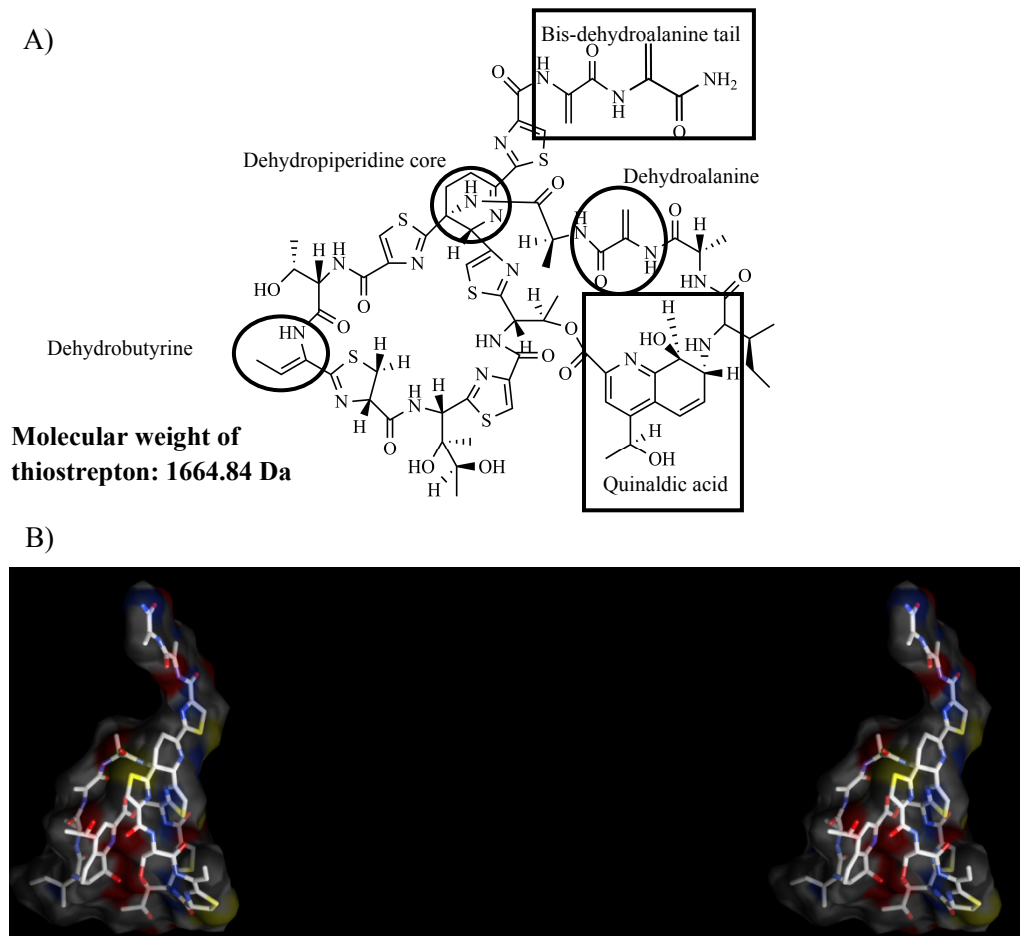
Thiopeptide antibiotics are sulfur rich, naturally occurring peptides that are produced by actinomycetes, particularly of the *Streptomyces* genus. These compounds typically feature a macrocyclic arrangement of modified amino acids and heterocycles and as a family, display extremely poor aqueous solubility. More than 80 members are included within this antibiotic family which are divided into 5 classes according to the oxidation state of their central heterocyclic domain and further subdivided into 29 families based on structural homology (Figure 1.4) (75, 76).



**Figure 1.4. Structures of the thiopeptide antibiotics.** Representatives from each of the five classes of thiopeptides are shown. Note the differences in the structure of the piperidine core (boxed in gray) and the macrocycle structure between class members: Class a and b: delhydropiperidine (or piperidine); Class c: dihydroimidazopiperidine; Class d: 2,3,6-trisubstituted pyrimidine; Class e: 2,3,5,6-tetrasubstituted pyrimidine (Thiopeptide structures were obtained from the *ThioFinder* website (77))



Thiostrepton is considered to be the parent compound of the thiopeptide antibiotics and was discovered as an antibacterial secondary metabolite produced by *Streptomyces azureus* in the mid-1950s (78, 79) and later, also by and *Streptomyces laurentii* (80). The molecular structure of the antibiotic was deduced from chemical degradation studies, where its various components (modified amino acids, heterocycles) were identified (Figure 1.5A) (81). Physical evidence of the macrocyclic arrangement of these moieties was first suggested in the early crystallographic work of Anderson *et al.* (82) and later confirmed by the solution of NMR derived structures of thiostrepton (83) and most recently, by the solution of the crystal structure of thiostrepton (84), all of which portray a globular-type conformation of the thiostrepton macrocycles, from which extends a tail region that was later found to be flexible in solution (Figure 1.5B) (85). Thiostrepton is assigned to the *a* series of thiopeptides, a class typified by their central dehydropiperidine and bis-macrocyclic peptide backbone that features a quinaldic acid residue (75). The central dehydropiperidine that acts as a lynchpin that connects the two macrocycles, which contain modified amino acids, thiazoles and the quinaldic acid residue, to the bis-dehydroalanine tail.



**Figure 1.5. Thiostrepton.** (A) Important structural features of the thiostrepton molecule. (B) Stereo-view of thiostrepton (PDB: 1E9W)

### 1.2.2. Total synthesis and biosynthesis of thiostrepton

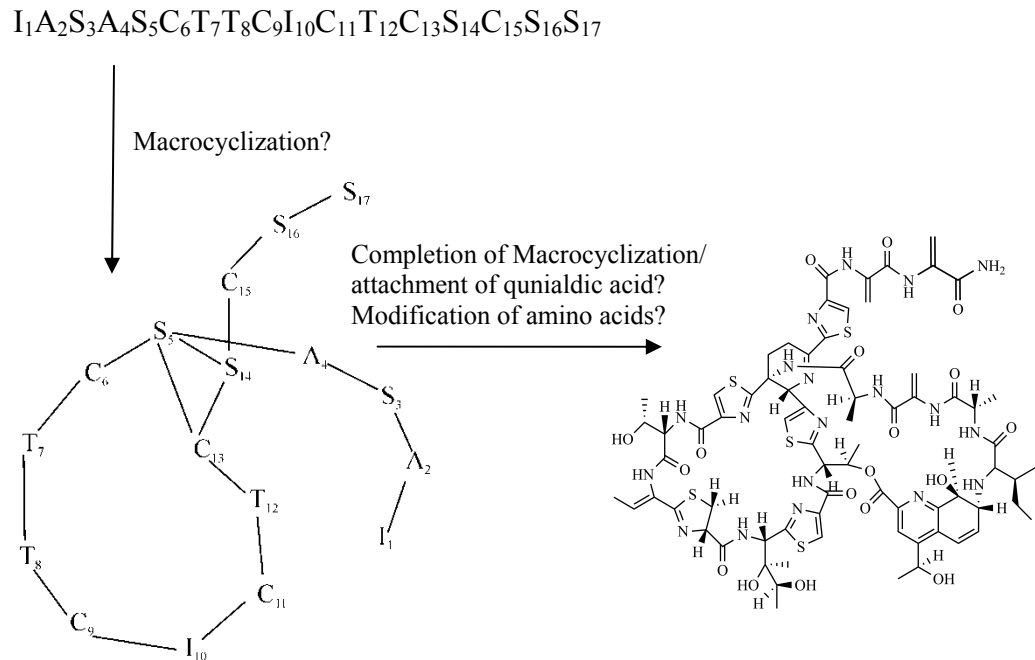
The complexity of thiostrepton and the thiopeptides in general, adds a substantial amount of difficulty to their total syntheses, yet such syntheses frequently provide insights into the biosynthesis of natural products such as these. Retrosynthetic analyses outlined chemical routes to the various heterocycles and modified amino acids that form the building blocks of thiostrepton (and other thiopeptides), yet pragmatically obtaining these proved to be a synthetic challenge. Nevertheless, through tremendous efforts, total

syntheses of thiopeptides were achieved, with promothiacin and amythiamycin D being the first compounds being synthesized (86–88). Both compounds present simpler structures than thiostrepton, each possessing a single macrocycle composed primarily of thiazoles (Figure 1.4). Thiostrepton eventually succumbed to total synthesis through the remarkable efforts of Nicolaou and co-workers (89, 90). These researchers divided thiostrepton into 4 fragments, corresponding to each of the macrocycles, the bis-dehydroalanine tail and the central dehydropiperidine core, which were subsequently assembled into the intact thiostrepton molecule (89, 91). The preparation of these fragments was not trivial, particularly the dehydropiperidine core, which was obtained through an elegant cascade sequence (92). A detailed description of the approaches is beyond the scope of this thesis and the reader is directed to reference (93) for an excellent review. At the time of writing, total and partial synthesis for a number of additional thiopeptides has been reported (94–99).

Insights into thiostrepton biosynthesis have been intertwined with efforts at its total synthesis, with each contributing towards the greater understanding of the other. The exploration of thiostrepton biosynthesis was initially performed by feeding isotopically labeled precursor amino acids to cultures of *Streptomyces* (*S. azureus*, *S. laurentii*), then monitoring the incorporation of these isotopic labels in the thiostrepton that was produced. These experiments revealed that the dehydroalanine and dehydrobutyrine residues derived from threonine and serine, the thiostreptine moiety from isoleucine and cyclodehydrations involving cysteine and serine or threonine gave rise to

thiazoles and oxazoles respectively (100). More complicated descriptions were suggested for the formation of the dehydropiperidine core and the quinaldic acid residue. Although quinaldic acid was demonstrated to derive from methionine and tryptophan, arrival at quinaldic acid requires indole ring breakage then expansion, followed by the installation of the hydroxyl and amine groups which may include (NADPH dependent) reduction and concluding with esterification/epoxidation, then epoxide ring opening (101–103). Serine and cysteine were identified as the progenitors of the dehydropiperidine moiety, which was proposed to occur from a hetero-Diels-Alder cycloaddition similar to that suggested for the formation of the pyridine core in micrococcin (104). Both mechanisms were somewhat synthetically validated on course to total thiostrepton synthesis (92, 105).

An important observation from these early investigations was that all the carbon atoms present in thiostrepton originated from a conventional amino acids. When considered in light of practical demonstrations of chemical syntheses of thiostrepton fragments, this hinted at the possibility that thiostrepton biogenesis commences with its initial synthesis as a linear peptide of the sequence that is subsequently subjected to the host of post translational modifications that results in the macrocyclic, highly modified thiostrepton molecule (Figure 1.6).



**Figure 1.6. Proposed formation of mature thiostrepton.** Schematic depiction of the cyclization of the thiostrepton from a linear prepeptide predicted from isotopic labeling studies. According to this model, the attachment of the quinaldic acid residue is one of the last steps in the formation of mature thiostrepton.

However, it was still unclear whether biogenesis was ribosomally directed or the result of non-ribosomal enzymatic processes. Also unknown was the sequence in the events leading to macrocyclyzation, amino acid modification, the formation of the dehydropiperidine core and the attachment quinaldic. These were clarified by the recent discovery of the gene cluster responsible for thiostrepton biosynthesis, which unequivocally confirm the hypothesis of ribosomal synthesis (106).

Whole genome scanning of *S. laurentii*, identified a gene encoding a thiostrepton precursor consisting of a leader peptide, followed by sequence

identical to that predicted for a thiostrepton prepeptide. The deletion of this gene completely abolished thiostrepton production. The region surrounding this gene included 21 potential open reading frames that were deduced to encode putative enzymes responsible for post translational modifications of thiostrepton precursor, including the dehydratases that would render dehydroalanine (DHA) and dehydrobutyryne (DHB) residues from serine and threonine, the dehydrogenases that would enable the cyclodehydration of cysteine with the peptide backbone to generate thiazoles and the putative enzymes responsible for the terminal amidation of thiostrepton and dihydroxylation of I10 (106). Amidation at the C-terminus of thiostrepton has been since shown to result from the deesterification-amidation of a methyl ester thiostrepton intermediate and is accomplished by two enzymes encoded in the gene cluster (107).

Almost concurrently, similar results showing thiostrepton to be the result of post-translational modifications to a ribosomally encoded precursor peptide were obtained independently by Liao *et al.* (108). These researchers further identified putative genes for enzymes that accomplish the cycloaddition reaction that produces the dehydropiperidine core and demonstrated their requirement in thiostrepton production through deletion studies. In addition, open reading frames for enzymes carrying out all the necessary chemical steps in quinaldic acid biosynthesis were identified. This expanded upon the work by Kelly *et al.*(106), in which a putative methyltransferase that sequentially resembled members of the radical SAM family (SAM = S-adenosyl-L-methionine) was identified, along with a putative aminotransferase were identified and together,

these enzymes could accomplish early steps in the biosynthesis of quinaldic acid from tryptophan as proposed by Mocek (101). Most recently, Duan and coworkers assigned unambiguous functions to these putative enzymes by monitoring thiostrepton production in *S. laurentii* strains engineered to be deficient in specific genes from the cluster, after they were fed an intermediate that would occur during the proposed mechanism for quinaldic acid biosynthesis (109). These results were largely consistent with earlier mechanisms and implicated a radical SAM enzyme in the initial methylation of the indole from tryptophan.

Continued research will undoubtedly seek to describe the attachment of quinaldic acid to the thiostrepton macrocycle, as current evidence indicates that this residue is formed separately from the rest of the molecule. As well, the mechanisms of macrocyclization and detachment of the structural peptide remain to be elucidated. Parallel investigations on the biosynthetic pathways of related thiopeptides have revealed the common theme in thiopeptide biosynthesis thus far: ribosomal synthesis as a precursor, followed by extensive post translational modifications by a host of enzymes included within the same gene cluster (110–115).

### **1.2.3. Biological properties of thiostrepton**

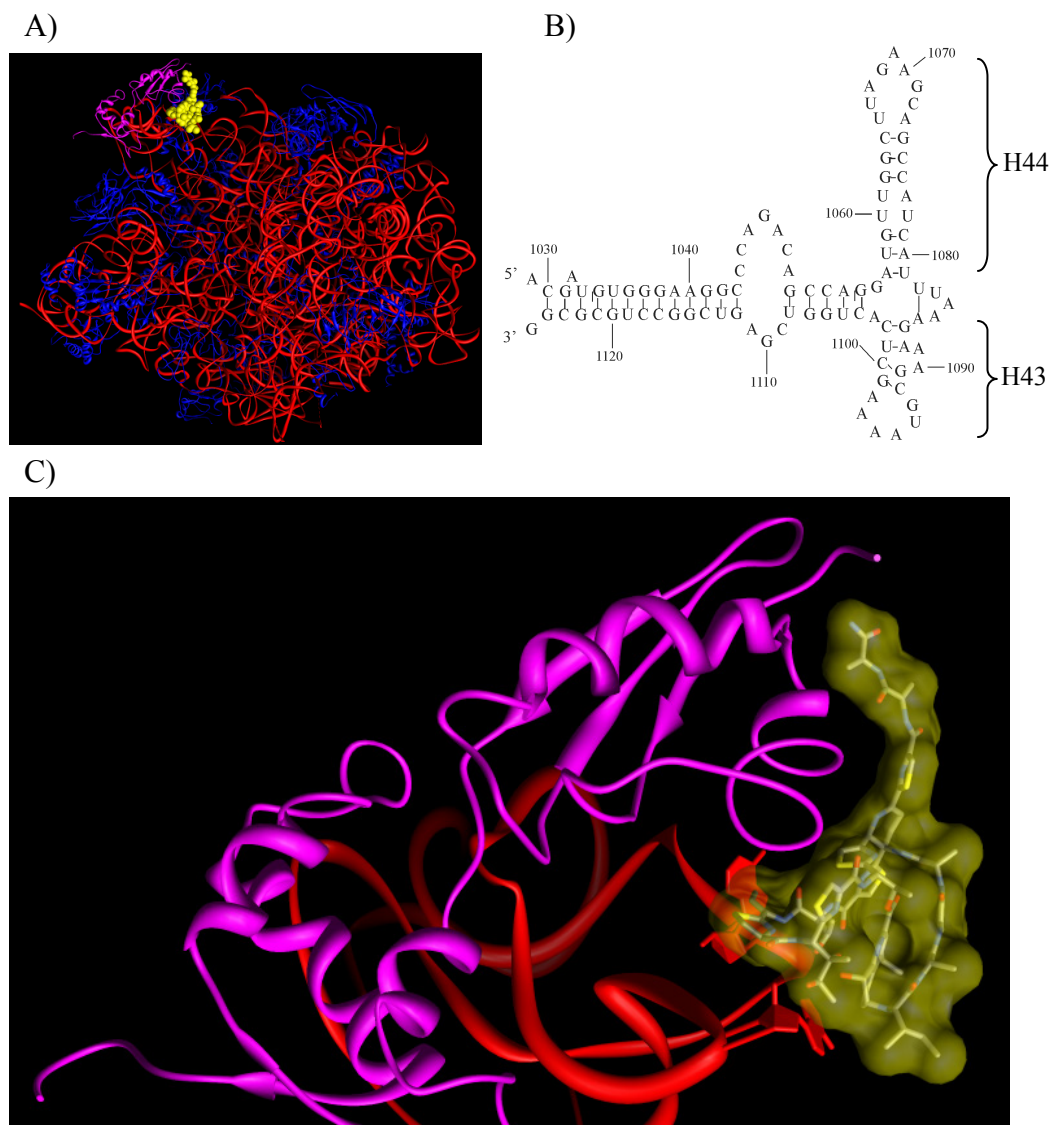
#### **1.2.3.1. Antibacterial activity**

Upon its discovery, thiostrepton was found to exhibit potent bactericidal effects against Gram-positive bacteria (116). Species of the Gram-negative

genera are insensitive to the antibiotic, which is most likely the result of its inability to penetrate the Gram-negative cell wall, since the functions of isolated Gram-negative ribosomes are indeed inhibited by thiostrepton (*117, 118*). The bacterial ribosome is the organelle targeted by thiostrepton, where the antibiotic impedes the elongation cycle during protein translation, ultimately leading to cell death.

The thiostrepton binding site has been mapped to the GTPase center on the 50S subunit of bacterial ribosomes, where a high affinity interaction occurs with 23S rRNA (Figure 1.7A) (*117, 119, 120*). This interaction occurs with rRNA on cell-free ribosomes from either Gram-positive or Gram-negative species, and involves a 58 nucleotide region that includes H43 and H44 from domain II of 23S rRNA and is critically dependent on thiostrepton interactions with A1067 and A1095 (Figure 1.7B, 1.7C) (*120, 121*). This region of 23S rRNA is also the binding site for ribosomal protein L11 (*122–124*) and this protein enhances the affinity of the thiostrepton-binding interaction through cooperative interactions mediated by its N-terminal domain (*118, 125–130*). This effect appears to be contingent on a key proline residue that is conserved among bacteria and the absence of this residue in the equivalent eukaryotic protein presumably accounts for the insensitivity of eukaryotic ribosomes to thiostrepton (*131–133*).





**Figure 1.7. The binding of thiostrepton to the bacterial ribosome.** (A) Thiostrepton binding site on the 50S subunit of the ribosome from *Deinococcus radiodurans* (PDB: 3CF5). The figure is colored as follows: thiostrepton – yellow; rRNA – red; ribosomal proteins (except L11) – blue; L11 - magenta. (B) Secondary structure of the thiostrepton binding motif from 23S rRNA. (C) Magnified view of thiostrepton binding to the ribosome showing the interaction between the thiostrepton macrocycles and A1067 and A1095 from rRNA, and the bis-DHA tail with the NTD from L11.

The GTPase center of the bacterial ribosome oversees the hydrolysis of GTP, which is coupled to the decoding and elongation stages of protein translation with the involvement of elongation factors EF-Tu and EF-G respectively (18). Thiostrepton binding at the GTPase center induces conformational changes in this region of the ribosome that leads to the inhibition of these processes. Although thiostrepton primarily affects the elongation cycle of protein translation, the antibiotic has been reported to inhibit tRNA delivery during decoding, A Site occupation as well as translation termination (134, 135). This may not be surprising given the GTP-dependent nature of these processes (18).

With respect to the elongation cycle, there was early disagreement on whether the antibiotic acted by preventing the dissociation or association of EF-G from the ribosomal complex, as evidence in support of both scenarios was presented (136, 137). Subsequent work has placed emphasis on the latter as the predominant mechanism of drug action, with the involvement of ribosomal protein L11, which was shown to be important for the structural integrity of the ribosome (122) and for conformational changes requisite for EF-G dependent translocation (138–141). Taken together, the sum of available biochemical and structural evidence implies that the enhancement of thiostrepton binding affinity caused by L11 imposes conformational restrictions on the protein that impede EF-G binding to the rRNA, which consequently halts protein synthesis (127, 130, 131, 142–145).

### 1.2.3.2. Additional biological properties of thiostrepton

Thiostrepton is known to be toxic to the malaria parasite *Plasmodium falciparum*, which was attributed to binding of the drug to ribosomal RNA in the apicoplast of the parasite and the resultant inhibition of protein synthesis by this organelle (146–150). This was reminiscent of the mode of action of thiostrepton in bacteria, however, the immediate cell death brought about in *Plasmodium* by thiostrepton was contrary to the effects of other apicoplast-targeting drugs (151, 152). Some clarity of this apparent anomaly was offered in recent studies that presented evidence suggesting that the rRNA of the apicoplast is a secondary drug target and the immediate killing effect of thiostrepton primarily results from its inhibition of protein translation by the proteasome (153, 154) or by thiostrepton-induced alteration in gene expression profiles (155).

Anti-cancer properties for thiostrepton were first reported by Nicolaou (156) and subsequently found to result from the selective induction of apoptosis in cancer cells, in response to thiostrepton mediated down regulation of the expression of transcription factor forkhead box M1 (FOXM1) and accordingly, the inhibition of the activities of its downstream targets (157–161). Interestingly, inhibitors of FOXM1 were also shown to inhibit proteasome activity (162), which is consistent with the descriptions of the anti-plasmodial effect of thiostrepton discussed above. Most recent evidence has found that thiostrepton directly interacts with FOXM1, thereby hindering its binding to genomic targets (163). Such a mechanism would account for the observed

reduction in the activities of downstream FOXM1 targets, but does not completely discount transcriptional inhibition of FOXM1 by thiostrepton.

Finally, thiostrepton is reportedly a potent inhibitor of the growth of *Mycobacterium tuberculosis*, the predominant causative agent of tuberculosis (164, 165). However, the mechanism by which this is accomplished remains to be described.

### **1.3. Thiostrepton resistance**

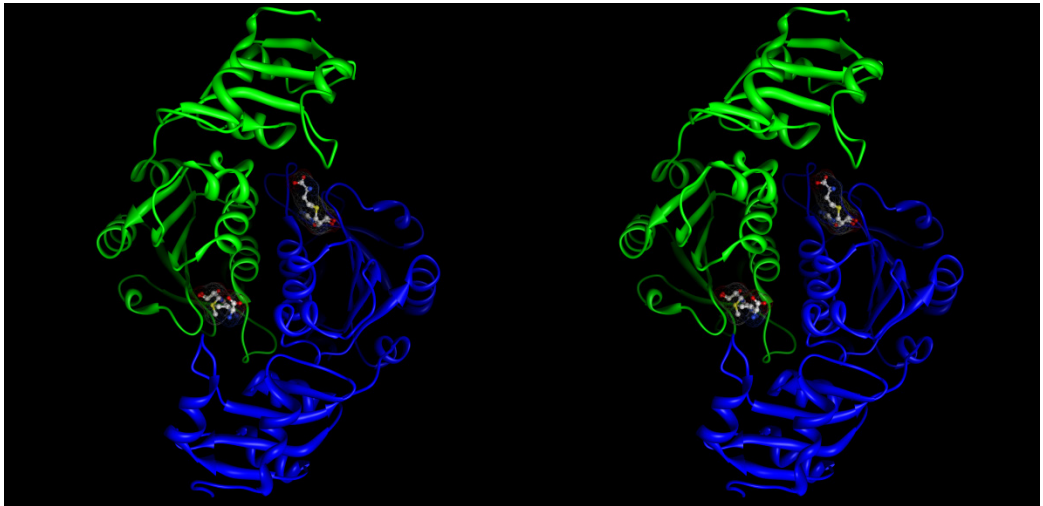
#### **1.3.1. Resistance in thiostrepton-producing organisms**

*Streptomyces* species that produce thiostrepton also possess the means to avert self-toxicity by the antibiotic. The first insights into this innate resistance came from observations of the differential abilities of reconstituted ribosomes to bind the antibiotic; ribosomes reconstituted fully or in part from components derived from *S. azureus* (the producing organism) were unable to bind the antibiotic (166). This was determined to be the result of the 2'-O-methylation of ribose on an adenine in the rRNA of *S. azureus* (167) by an enzyme present in a crude cellular protein extract prepared from *S. azureus*. Purification and characterization of the enzyme responsible for rRNA methylation revealed that this enzyme catalyzed the specific transfer of a methyl group from *S*-adenosyl-L-methionine (AdoMet) to 23S rRNA, rather than the intact ribosome, implying that this modification occurs at an early stage in ribosome assembly, prior to subunit association or the incorporation of proteins to the ribosomal complex (168). The binding site of this enzyme on the ribosomal complex overlaps with

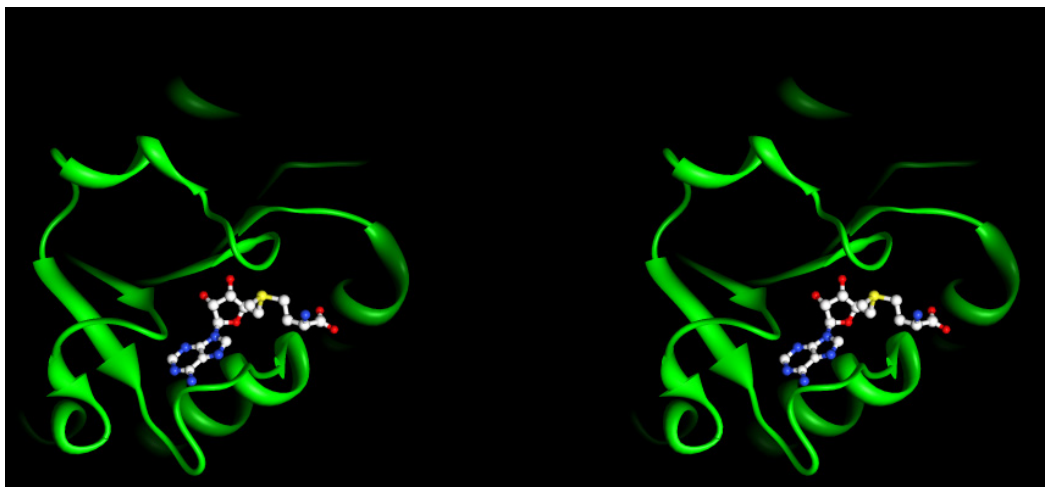
that of ribosomal protein L11/ thiostrepton and accordingly, the enzyme will not methylate RNA in the presence of either (*169*). In addition, extensive mutagenesis in combination with biochemical assays revealed the nucleotides within the L11 binding necessary for binding of this methyltransferase, with A1067 being the likely recipient of the methyl group from AdoMet (*169, 170*) (Figure 1.7).

In a recent collaborative effort by our group, the molecular structure of the resistance conferring 23S rRNA 2'-O-methyltransferase (TSR) has been solved (Figure 1.8A) (*171*). The enzyme's structure definitively placed TSR within the SPOUT family of Methyltransferases, as predicted by comparative sequence analysis and homology modeling using known members of this class (*171–174*). The enzyme was crystallized as a homodimer, with one AdoMet molecule bound to each monomer. Each monomer features an N-terminal (NTD) and C-terminal domain (CTD), the latter of which includes the AdoMet binding pocket (Figure 1.8A). The binding pocket is formed mostly from one monomer, although amino acids from the other monomer make vital contributions to its architecture. Also critical to the formation of the binding pocket is the presence of a deep trefoil knot, which keeps the AdoMet molecule entrenched within the binding pocket by maintaining close contacts with the adenosine moiety (Figure 1.8B) (*171*).

A)



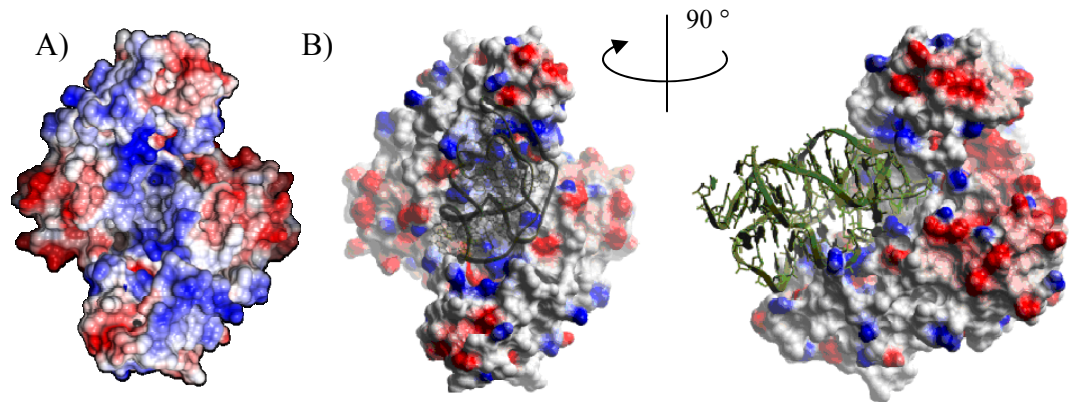
B)



**Figure 1.8. The TSR-AdoMet complex.** A) Stereoview of the TSR dimer with individual subunits colored blue and green (PDB: 3GYQ). (B) Magnified stereoview of the CTD knot as discussed in the text. Images were generated using *UCSF Chimera 1.5.2*

The binding of RNA by TSR appears to be governed by electrostatic interactions between the negatively charged RNA and a region of positive charge that is wedged between the NTD from each monomer (Figure 1.9). Productive RNA binding is also dependent on RNA tertiary structure, particularly a stem-loop structure that comprises 29 nucleotides including the

target A1067, which was consistent with earlier work by Bechthold and Floss (169) (Figure 1.5B). In addition, the modeled binding of RNA by TSR implies that while only one monomer functions in a catalytic capacity, both are required for correct positioning of the RNA (171).



**Figure 1.9. The interaction of RNA with TSR.** A) The TSR dimer is overlaid with an electrostatic surface potential map (blue: positive, red: negative). (B) Two orthogonal views of RNA (green) interacting with the zone of positive charge from the TSR dimer (Adapted from Dunstan *et al.* (163))

#### 1.3.1.1. RNA methylation and antibiotic resistance

The 23S rRNA methylation accomplished by TSR was the first instance described in the literature where specific RNA methylation conferred antibiotic resistance but this mechanism has since been found to be responsible for resistance to a number of antibiotics. Included among these is the nosiheptide resistance methyltransferase that renders *Streptomyces actuosus*, that produces this antibiotic, resistant to the drug (175, 176). The recent solution of the crystal structure for this enzyme showed high structural similarity to TSR (in addition to high sequence similarity) and accompanying biochemical investigations

indicated a similar mode of action similar to TSR (177). *Streptomyces viridochromogenes*, the producer of the orthosomycin antibiotic avilmycin, is protected from the effects of the drug by producing the methyltransferases AviRa and AviRb, which carry out the N-methylation at G2535 and the 2'-O-methylation at U2479 that disrupts drug binding at the target site (46).

Among the clinically relevant antibiotic classes, resistance to macrolides and aminoglycosides is known to result from methylation at their respective binding sites. Erythromycin and related drugs are prevented from binding to their target site at the peptidyl transferase center on the 50S subunit of the ribosome by mono-or dimethylation at N<sup>6</sup> of the adenosine moiety from A2058 (178). This base resides on the peptidyl transferase loop in domain V of 23S rRNA, which together with hairpin 35 from domain II, forms the macrolide binding site (179).

Although direct, enzymatic modification of aminoglycosides is the primary resistance mechanism to this class of drugs, methylations inactivating aminoglycosides occur to 16S rRNA in the decoding region of the A-site from 30S ribosomal subunit, at either A1405 (Kgm and Arm families) or A 1408 (Kam and Pam families) (180–182). The former is methylated at the N<sup>7</sup> position and the latter at N<sup>1</sup>(182). The resistant phenotype depends on the site where modification occurs but in either case, resistance results from the disruption of drug binding (183, 184).



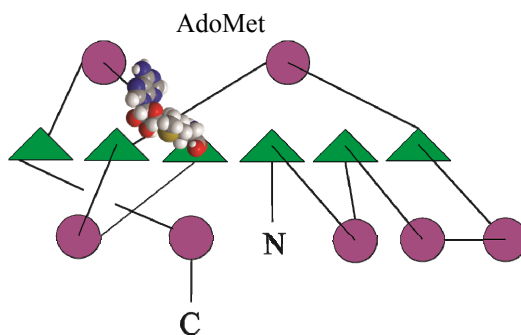
### 1.3.1.2. AdoMet-dependent methyltransferases

TSR belongs to the large family of AdoMet-dependent methyltransferases (E.C. 2.1.1.X) that catalyze the transfer of a methyl group from the ubiquitous co-factor AdoMet, to small molecule, protein, or nucleic acid targets. Along with the role in antibiotic defense described in the previous section, the transmethylation carried out by these enzymes are known to be crucial to important cellular processes including metabolite synthesis and cell signaling (*185*).

It was initially believed that methyltransferases shared the same core structure, embodied by a Rossmann-like fold that constructed the AdoMet binding pocket (*185*). The subsequent discovery and structural characterization of additional members of this family found diversities in protein tertiary structure and AdoMet binding that led to the creation of 4 additional classes, although most members of the methyltransferase family belong to Class I (Rossmann-like fold) (*186*). As well, in spite of relatively low sequence similarities, members within a given class display a high degree of structural similarity (*187*).

As earlier stated, TSR is part of the SPOUT class of methyltransferases (Class IV). This group represents the unification of the SpoU and TrmD families, which were discovered to share conserved motifs, particularly in the AdoMet binding region (*173*). Crystal structures of SPOUT methyltransferases, including the TSR and the nosiheptide-resistance methyltransferase, revealed defining structural features of this class, which include an active site located

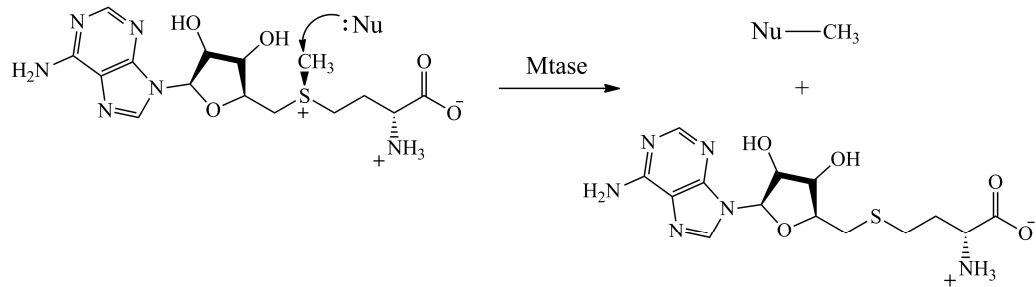
near the homodimeric interface that is formed by residues from both subunits and a deep trefoil knot in the AdoMet binding region of the CTD of the protein (Figure 1.8) (171, 174, 177, 186, 188–191).



**Figure 1.10. Topological diagram of the SPOUT Methyltransferases (Class IV).**  $\alpha$ -Helices are purple circles and  $\beta$ -sheets are green triangles.

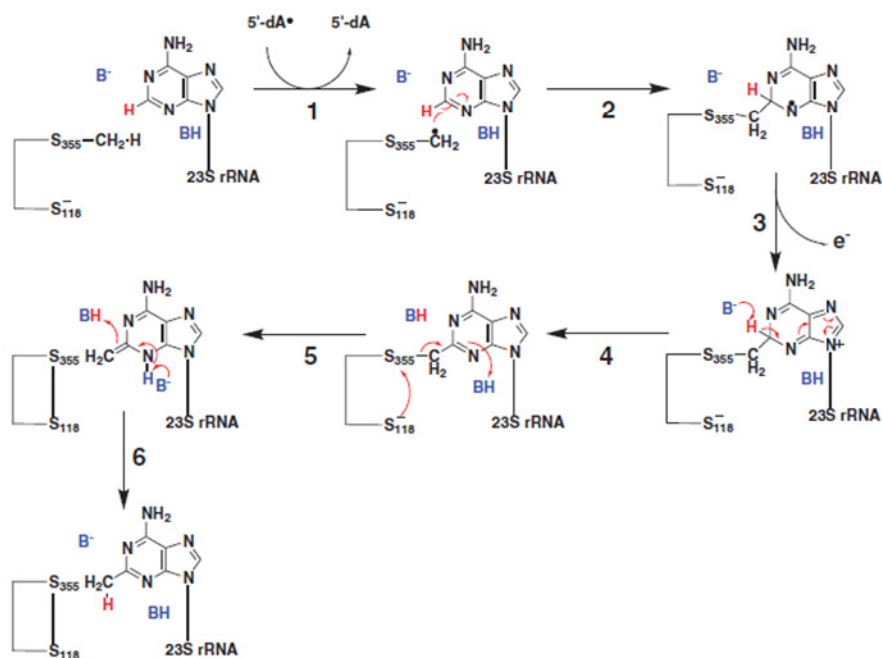
### 1.3.1.3. Mechanism of transmethylation

The acceptors of the electron deficient methyl group from AdoMet are nucleophilic atoms on targets of methyltransferases, such as oxygen (ribose hydroxyl, aromatic hydroxyl), nitrogen (exocyclic nitrogens from adenosine) or sulfur (aromatic thiols). Transmethylation proceeds via an energetically favoured  $S_N2$ -type mechanism, with an inversion of methyl group stereochemistry and the concomitant generation of S-adenosylhomocysteine (Figure 1.11) (186, 192). Invariably, the nucleophilic acceptor requires activation prior to methylation, which contributes to the observed differences in active site architecture within and between class members (193).



**Figure 1.11. General mechanism for methyltransferase catalysis.**

While the above mechanism accounts for most biological transmethylation reactions, it is believed that a significant number of methyltransferases accomplish methylation to a non-nucleophilic acceptor atom through the generation of a radical species (*194, 195*). Members of this large Radical SAM superfamily of enzymes accomplish reductive cleavage of AdoMet utilizing an iron-sulfur cluster that is coordinated by a conserved “Cys-xxx-Cys-xx-Cys” motif, generating the highly reactive 5'-deoxyadenosine radical in the process (*196, 197*). The mechanisms for two RNA methylating enzymes, RlmN and Cfr, that belong to this family, have been recently described and in each case, RNA methylation is initiated by the transfer of the methyl group to one of the cysteines that coordinates the iron cluster, followed by the reductive cleavage of a second AdoMet molecule with a concomitant generation of the 5'-deoxyadenosyl radical. This radical subsequently removes a proton from the methyl group attached to the cysteine to generate a carbon-centered radical that attacks the non-nucleophilic carbon atom on the adenine from RNA (Figure 1.12) (*198*).



**Figure 1.12. Postulated mechanism of RlmN.** BH, unidentified general acid; B<sup>-</sup>, unidentified general base. From [Poehlsaard and Douthwaite, 2011. *A Radically Different Mechanism for S-Adenosylmethionine-Dependent Methyltransferases*. *Science* 332, 604 – 607]. Reprinted with permission from AAAS.

#### 1.3.1.4. AdoMet-dependent methyltransferases as tools

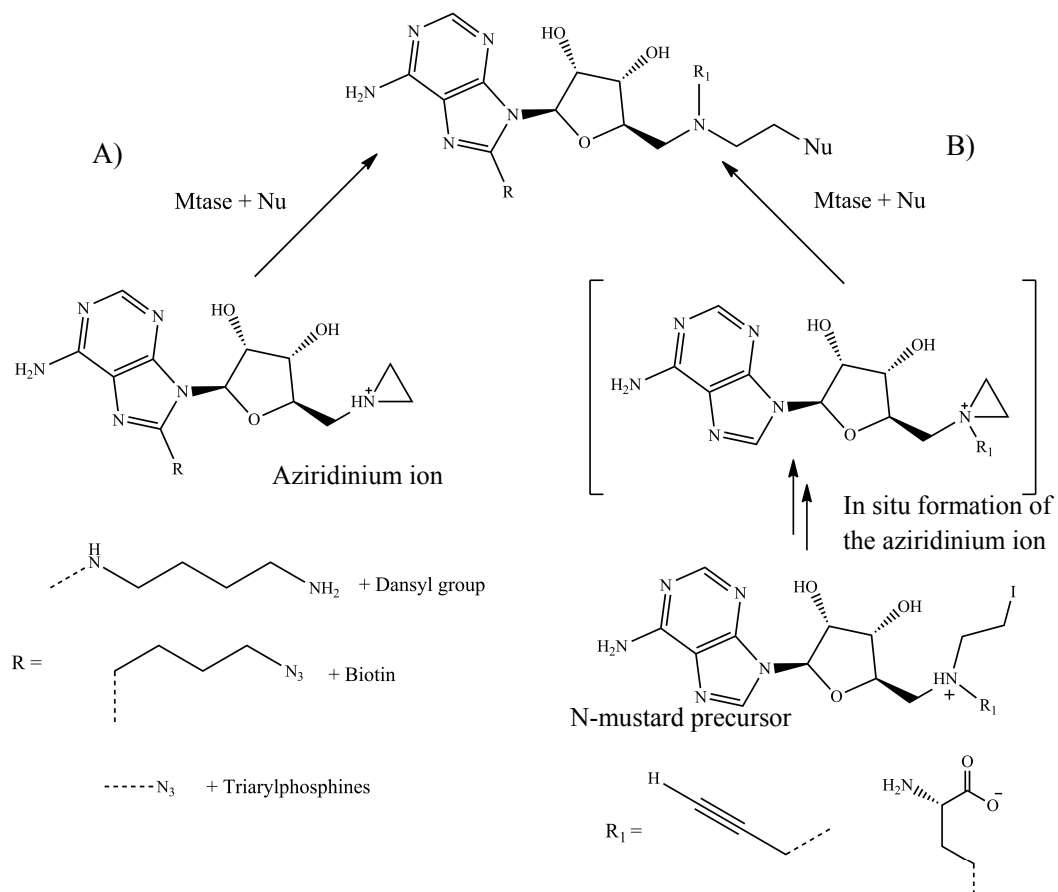
The favorable energetics for the transfer of a methyl group from AdoMet relative to other cellular sources (eg. methionine) makes this cofactor the preferred methyl donor in the cell. Accordingly, AdoMet is the second most prevalent cofactor present in the cell (199) and AdoMet-dependent methyltransferases account for a not insignificant proportion of cellular proteins. The family currently includes over 200 members (according to the nomenclature of the Enzyme Commission) and many more are predicted to exist based on bioinformatics studies. Although crystal structures for several dozen of these

have been deposited into the Protein Database (PDB), the majority of the enzymes from this family remain uncharacterized and their cellular targets, unknown. However, it is believed that the methylations carried out by these enzymes will continue to prove to be involved in important cellular processes.

Biochemical characterization of methyltransferases, particularly the identification of novel or unknown methyltransferase targets, is often difficult due to the absence of straightforward means for detection of modified substrates. The methyl group itself is devoid of conspicuous physical characteristics (fluorescence, absorbance) and physical or chemical changes that occur to the target are generally useful in cases of *a priori* knowledge of the target. As a result, much effort has been directed towards the development of AdoMet analogues from which groups that enable substrate specific labeling are transferred.

In the first reported instance of such analogues, the methionine region of AdoMet was replaced by the reactive aziridine group which enabled the addition of the ribonucleoside region of AdoMet to a DNA methyltransferase target (Figure 1.13A) (200). Further modification of these analogues at the 8 position of the ribonucleoside with an extended linker terminating in a primary amine or an azido group allowed for the attachment of reporter molecules for site-specific substrate labeling, or site specific DNA scission after coupling with triarylphosphines via Staudinger ligation (201–203). Preparation of an *N*-mustard AdoMet analogue featuring a propargyl alkyne resulted in *in situ*

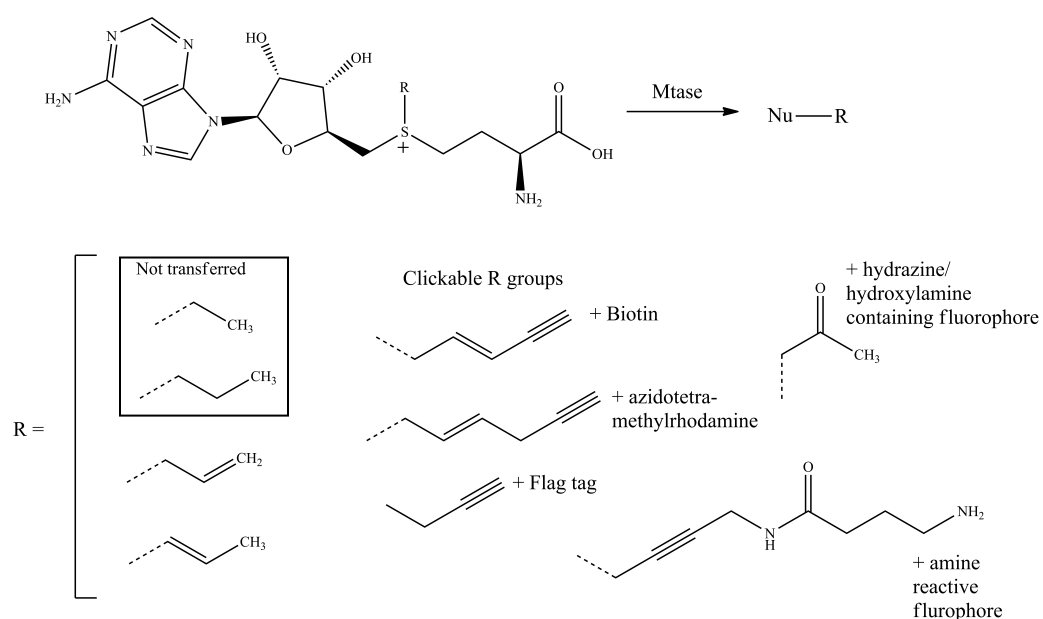
formation of an aziridinium ion and subsequent addition of a riboadenosyl moiety amenable to “click” chemistry (Figure 1.13B) (204–206).



**Figure 1.13. Riboadenosyl transfer from AdoMet analogues.** The aziridine containing AdoMet analogue is either directly synthesized (A) or forms *in situ* from an N-mustard precursor (B). Nucleophilic ring opening of the aziridine group results in the transfer of the whole cofactor molecule to the Mtase target. Additional appendages on the adenosine moiety allow for coupling to reporters.

Methyltransferases were initially thought to be unable to catalyze the transfer of extended alkyl chains to their targets, however, it was found that rates of transfer were improved by the introduction of  $\alpha$ - $\beta$ -unsaturation within the alkyl chain (207, 208). Moreover, the placement of an additional alkynyl

group at the end of the alkyl chain facilitated substrate labeling via click chemistry (209–211). Likewise, the elaboration of such alkyl chains by attachment of a terminal amine group (instead of the propargyl group) via an amide linker also allowed for attachment of reporter molecules (Figure 1.14) (212).



**Figure 1.14. Mtase catalyzed transfer of extended alkyl chains.** Substitution of the methyl group for the alkyl chains shown results in the alkylation of the Mtase target (except in the case of the ethyl or propyl group). The presence of a terminal chemical handle on the modifying group enables facile coupling to reporter molecules.

The methyltransferase targets for the transfer of alternative groups described above have included protein, DNA and small molecules, highlighting the versatility and applicability of this technology to different classes of methyltransferases. However, alternative group transfer has been mainly demonstrated when these analogues have been present in stoichiometric

amounts, a situation not likely to be conducive to the discovery of novel or unknown methyltransferase targets. One notable exception to this was the reported transfer of a methyl ketone group to small molecule substrates of the catechol-O-methyltransferase and the thiopurine-S-methyltransferase (213). The use of this keto-AdoMet analogue marks one of the few instances where an AdoMet analogue was used to successfully identify a previously unknown methyltransferase target, which was enabled by the presence of the reactive ketone group that allowed for bio-orthogonal conjugation (213).

The development of AdoMet analogues is a promising area that can be potentially be utilized for the transfer of “unnatural” groups to a variety of biomolecules. Such analogues can be further used as novel reagents for the introduction of molecular probes to biomolecules. Their widespread application may, however, be limited by the reactivity of these alternate groups, which could potentially engage in spurious reactions that either inhibit the enzyme under study or lead to misleading conclusions about substrate identity.

### **1.3.2. Resistance in organisms that do not produce thiostrepton**

#### **1.3.2.1. Thiostrepton resistant mutants**

Along with the specific methylation of A1067 (or an equivalent base), thiostrepton binding leading to the inhibition of protein biosynthesis is reliant upon the structure of the RNA region surrounding this nucleotide and the presence of ribosomal protein L11. The characterization of the 23S rRNA thiostrepton and TSR binding site necessarily involved the use of RNA



transcripts that differed in sequence from that of native 23S rRNA (119, 128, 169, 214). As could therefore be expected, nucleotides vital to thiostrepton binding were unveiled in *in vitro* experiments that utilized such transcripts or ribosomes possessing mutations to the L11 binding domain on 23S rRNA (214). As well, various thiostrepton-resistant strains were determined to possess mutations to the corresponding region in the 23S rRNA (121, 132, 215–217).

The complete absence of L11 (or its equivalent) not surprisingly results in thiostrepton resistance, as was discovered in mutant strains of *Bacillus* and *Chlamydomonas* (129, 218, 219). In addition, thiostrepton insensitivity results from alterations to the sequence of L11 protein itself. This was first observed in *Halobacterium halobarium* and subsequently shown to be due to the mutation of the conserved proline residue (132, 216) and these findings also contributed to the understanding of the role played by L11 in thiostrepton binding, as discussed in section 1.2.3.1. Sequencing and characterization of the genes encoding L11 from a series of thiostrepton sensitive *Thermus thermophilus* isolates found a correlation between the conformational flexibility of these L11 mutants and the level of thiostrepton sensitivity; decreasing sensitivity with increasing L11 flexibility (131). These findings highlighted the importance of L11 not only for thiostrepton binding, but in ribosome structure and protein synthesis and were later supported by the demonstration of the interaction of thiostrepton with the ribosome, in which the protein is essentially immobilized and thus prevented from undergoing conformational dynamics that are requisite for EF-G and EF-G-dependent activities (127, 142, 143).

### 1.3.2.2. Thiostrepton binding proteins

After its discovery, the gene encoding TSR became routinely used in the construction of *Streptomyces* cloning vectors that employed thiostrepton as a selectable marker for use in organisms that may have possessed natural sensitivity to the antibiotic (47). Such vectors also enabled the study of additional effects of thiostrepton in these species. One of these was the elevated levels in the expression of several genes in response to the presence of the drug, which correlated with increased resistance to thiostrepton and related thiopeptides (47, 220).

The expression of the two most abundant of these proteins was due to transcriptional activation of the promoter for the *tipA* gene by thiostrepton (47). In the presence of thiostrepton, this gene encodes the in-frame expression of both proteins, designated TIP-AL and TIP-AS, from independent transcription start sites on the gene. The transcription of TIP-AS commences downstream from that of TIP-AL and the expression of TIP-AS is several fold greater than that of TIP-AL (48). Both proteins were found to bind thiostrepton, indicating that TIP-AS represents the thiostrepton binding CTD of TIP-AL, however TIP-AL was found to additionally bind to the *tipA* promoter and the affinity of this interaction was increased by thiostrepton (48). Additional structural evidence suggests that thiostrepton binding at the CTD of TIP-AL, initiates conformational changes that are translated to the NTD of the protein which enables its binding to the *tipA* promoter (221). At the same time, the thiostrepton-TIPAS interaction serves as a means to prevent unbridled

overexpression of *tipA*. Therefore, by operating in tandem to regulate their expression, TIP proteins induce thiostrepton (and thiopeptide) resistance through sequestration. Moreover, *TipA* genes have been identified in several *Streptomyces* species that do not produce thiostrepton (222–224), which may not only reflect their importance in thiostrepton resistance, but an additional, unknown cellular function.

Binding between thiostrepton and the TIP proteins occurs irreversibly by covalent bonding between a cysteine residue from the protein and a DHA from the thiostrepton tail (225). The solution of the NMR structure for TIP-AS, along with NMR ligand binding studies pointed to covalent bonding between Cys 214 (TIP-AL numbering according to Holmes *et al* (48)) and the terminal DHA in the thiostrepton tail (226). This was also found to be the case for a series of related thiopeptide also possessing a DHA tail region, although the extent to which functions dependent on these protein-antibiotic interaction were executed appeared to be affected by the length of the tail as well as the structure of the thiopeptide core (220). These findings implied the significance of non-covalent interaction in the formation of stable protein-antibiotic complexes, which was in line with demonstrable activity in tail-less thiopeptide derivatives, along with earlier observations where TIP proteins non-covalently bound to thiostrepton required harsh denaturing conditions to be released (48). Moreover, the interaction between thiostrepton and TIP proteins modeled from the NMR data by Kahmann *et al.* (226) indicates extensive non-covalent associations between

the antibiotic and protein, however, this aspect of the thiostrepton-TIP interaction has not been well studied.

#### **1.4. Research Objectives**

In light of the dire problems posed by bacterial antibiotic resistance, this thesis aims to illustrate the potential of the thiopeptides as a source for novel alternative antimicrobial chemotherapies, using thiostrepton as a paradigm.

In spite of diverse biological and clinically relevant properties, the aqueous insolubility of thiostrepton has limited its use to veterinary applications and as a research tool in the study of ribosome function. The research herein will expand upon work begun in this laboratory and describes a semi-synthetic approach towards the selective and controllable modification of thiostrepton, to generate antibacterial derivatives with improved aqueous solubility. These derivatives can be used as platforms for future structure-activity studies in drug development. The mode of action of these derivatives will be evaluated using cell free and whole cell approaches, which will be further used to probe the molecular determinants of thiostrepton interactions on the bacterial ribosome.

A deepened understanding of processes conferring thiostrepton resistance will not only increase the fundamental knowledge on thiopeptide resistance, but may prove to be useful in the rational design of drugs that evade resistance mechanisms. To this end, extensive mutagenesis studies, in conjunction with biochemical and biophysical investigations will be applied towards elucidating the molecular mechanisms responsible for TSR mediated

resistance in thiostrepton-producing organisms and the TIP protein mediated resistance seen in organisms that do not produce the drug.

Finally, the synthesis of a novel AdoMet analogue from which a trifluoromethyl ketone group would be transferred was pursued. This analogue would contribute added diversity to the functional groups that are transferrable by methyltransferases and its potential applications are discussed.

## CHAPTER 2: SYNTHESIS AND BIOLOGICAL ACTIVITY OF THIOSTREPTON ANALOGUES.

---

### 2.1. Preface

In spite of their poor aqueous solubility (75), the thiopeptide family of antibiotics is an attractive source for novel antimicrobial compounds owing to their diverse biological activities and low (or non-existent) incidence of clinical observed resistance. For this reason, recent attention has been directed toward the improvement of this physical property while maintaining their antibacterial activity.

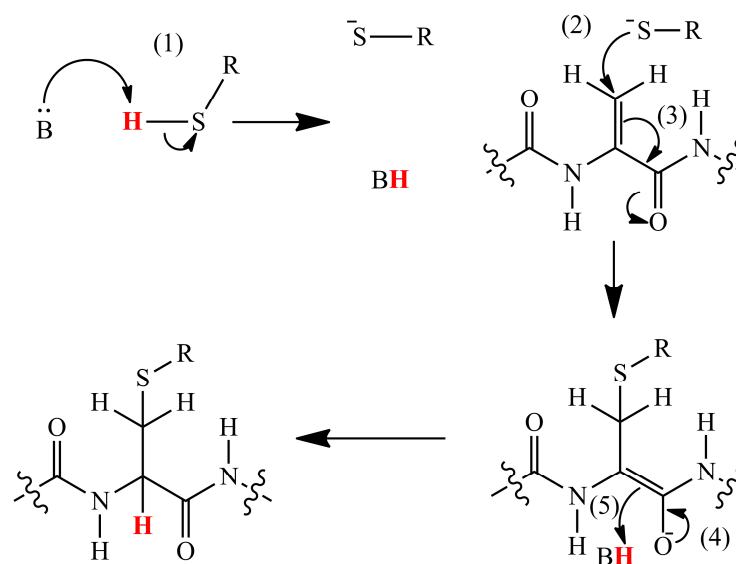
As illustrated in Chapter 1, thiopeptides have remarkably complex structures, including highly modified amino acids and multiple chiral centers, which is not atypical of natural products. More often than not, the biological activities of thiopeptides are contingent upon the presence of such moieties, which invariably present nontrivial synthetic challenges, thus making the total synthesis of these compounds an arduous undertaking (75, 76, 88–90, 227–230). This limits the practicality and feasibility of *de novo* syntheses in the generation of thiopeptide analogues with improved physicochemical properties. More recently, the biosynthetic gene clusters for thiostrepton and other thiopeptides have been discovered, highlighting the intricacy of the natural biogenesis of these compounds, in which numerous enzymes accomplish the concerted prepeptide processing, post translation modifications and cyclizations required for the formation of the active compound (Chapter 1; (106, 108, 111, 113, 231,

232)). Hence, the derivation of thiopeptide analogues through synthetic bioengineering would present different but equally formidable challenges as those presented by *de novo* synthesis. Nevertheless, the continual expansion of genomic information concerning thiopeptide biosynthesis has drawn some attention to this approach (233, 234).

In this chapter, a semi-synthetic approach towards the preparation of biologically active thiostrepton analogues will be illustrated. Among the many sites for potential elaboration on the thiostrepton molecule, the alkene groups on its three DHA residues and lone DHB residue seem most attractive as these groups should be susceptible to nucleophilic Michael addition reactions. Such reactions have been demonstrated with free DHA or its analogues, as well as with a DHA resident on another antibiotic, nocathicin (235–238). This approach was applied by our laboratory to the more complicated thiostrepton molecule, which features four potential Michael acceptors. Polar thiols were used as Michael donors to regioselectively append thiostrepton with groups that should impart aqueous solubility (Figure. 2.1). During the course of our work, Schoof and coworkers (239) employed a similar modification approach in the preparation of a fluorescent thiostrepton derivative.

The antibacterial activities of the synthesized analogues were assessed utilizing bacterial strains known to be susceptible to thiostrepton. Since thiostrepton is an inhibitor of bacterial protein synthesis, the mode of activity of these analogues was also investigated using analysis of *in vitro* translation efficiencies of a model protein. In addition, the derivatization of thiostrepton

with structurally dissimilar groups was attempted, for preliminary evaluations of the structure-activity relationship of a range of thiostrepton analogues.



**Figure 2.1. Mechanism for Michael addition of thiols to DHA.** The reaction commences with the abstraction of the thiol proton by a base to generate a nucleophilic thiolate (1). Attack on the electron deficient carbon on the DHA olefin leads to addition of the donor group (2) and rearrangement of the double bond (3). Delocalization of the negative charge from the oxyanion (4) results in attack of the earlier protonated base, completing the reaction and generating a new chiral center.

## 2.2. Materials and Methods

### 2.2.1. Chemicals and Reagents

Thiostrepton ( $\geq 90\%$  purity), 2-mercaptoethanesulfonic acid ( $\geq 98\%$  purity), captopril ( $\geq 98\%$  purity) and 1-thio-2- $\beta$ -D-glucose ( $\geq 98\%$  purity) were all purchased from Sigma (Oakville, Canada). Anhydrous dimethylformamide, dimethylsulfoxide, acetonitrile and trifluoroacetic acid were purchased from Caledon Laboratory Chemicals (Georgetown, Canada). Triethylamine was obtained from EMD Sciences (Gibbstown, USA) and deuterated chloroform and methanol were from Cambridge Isotopes (Andover, USA).



## **2.2.2. Equipment**

### **2.2.2.1 Chromatography**

High performance liquid chromatography was performed using a Waters 625 Chromatography System equipped with a 996 photodiode array detector and Millennium 3.20 software (Millford, USA). Compound purification was carried out using a Zorbax Eclipse C-8 column (5 $\mu$ M, 4.6  $\times$  150 mm) (Agilent, Mississauga, Canada), with 0.1% TFA in MilliQ grade water and acetonitrile as the polar and non-polar mobile phases, respectively, at a flow rate of 0.5 ml/minute.

### **2.2.2.2. Mass spectrometry**

High resolution ESI-mass spectrometry was performed with a Micromass<sup>TM</sup> Quadrupole-time of flight (Q-TOF) Ultima Global mass spectrometer in positive ion mode and the data analyzed using MaxEnt software (Waters, Millford, USA).

### **2.2.2.3. Luminescence**

Total luminescence (total light emitted) was recorded in white 96-well microplates (BD Biosciences, Mississauga, Canada) with a SpectraMax M5 (Molecular Devices, Downingtown, USA) that was calibrated to an internal standard.

### **2.2.2.4. Nuclear magnetic resonance**

NMR spectra were acquired on a Bruker Advance 600 MHz spectrometer. <sup>1</sup>H chemical shifts are in ppm relative to residual solvent peaks (7.24 ppm for CDCl<sub>3</sub>). Typical NMR samples were prepared by dissolving 2 – 4

mg of analyte in 0.6-0.7 mL of mixture of deuterated chloroform and deuterated methanol (4:1). TOCSY spectra were acquired using the pulse sequence for homonuclear Hartman-Hahn transfer (240), with 80 ms mixing time.

### 2.2.3. General methods

#### 2.2.3.1 Synthesis of thiostrepton analogues

In an inert (argon) atmosphere, thiostrepton (50 mg; 0.03 mmoles) was dissolved in 1 mL of anhydrous DMF. To this solution, triethylamine (10 equivalents; 42  $\mu$ L) was added, followed by 1 equivalent of aqueous thiol (2-mercaptoethanesulfonic acid, captopril or 1-thio-2- $\beta$ -D-glucose), prepared as 150 mM stock solutions. Reactions were mixed on a platform shaker for 18-24 hours at 4  $^{\circ}$ C and then dried under vacuum, leaving an orange-yellow solid. Michael adducts were isolated by RP-HPLC utilizing different elution conditions: *Method 1; purification of 1.2*. The solid reaction product obtained after vacuum drying was dissolved in deionized H<sub>2</sub>O (1.5 mg/mL), filtered using a 0.2 micron syringe filter, then separated over a linear increasing gradient of acetonitrile (0.5 %/min), with flow rates of 0.5 or 1 ml/ minute. *Method 2; purification of 1.3 & 1.4*. Vacuum dried reaction product was dissolved in 50% DMSO (1.4 mg/ml) and then separated over a linear increasing acetonitrile gradient of 0.25 %/minute, at a flow rate of 0.5 mL/ minute.

**2-Mercaptoethanesulfonic acid adduct (1.2):** HPLC (Method 1):  $t_R = 31$  minutes.  $^1\text{H NMR}$  (600MHz,  $\text{CDCl}_3$ :  $\text{CD}_3\text{OD}$  (4:1)):  $\delta$  8.15, (s, 1H), 8.12 (s, 1H), 8.04 (s, 1H), 7.43 (d,  $J = 9.65$  Hz, 1H), 7.40 (s, 1H), 7.18 (s, 1H), 7.06 (s, 1H), 6.77 (d,  $J = 9.84$  Hz, 1H), 6.27, (dd,  $J = 5.92, 10.02$  Hz, 1H), 6.23 (m, 1H), 6.21 (s, 1H), 6.10 (q,  $J = 6.562$  Hz, 1H), 5.71 (s, 1H), 5.64 (d,  $J = 3.45$  Hz, 1H), 5.60 (s, 1H), 5.52 (s, 1H), 5.20 (s, 1H), 5.19 (s, 1H), 5.17 (s, 1H), 4.86 (dd,  $J = 9.19, 12.74$  Hz, 1H), 4.82-4.78 (m, 1H), 4.60 (m, 1H), 4.29 (m, 1H), 4.09-4.03 (m, 4H), 3.95 (m, 1H), 3.68 (dq,  $J = 6.20, 12.47$  Hz, 1H), 3.53 (m, 1H), 2.84 (d,  $J = 3.98$  Hz, 1H), 2.50 (s, 1H), 2.19-2.15 (m, 1H), 1.78 (s, 1H), 1.59 (d,  $J = 6.57$  Hz, 3H), 1.48 (d,  $J = 7.08$  Hz, 3H), 1.43 (m, 1H), 1.32 (dd,  $J = 3.65, 6.21$  Hz, 3H), 1.26 (d,  $J = 6.61$  Hz, 3H), 1.16 (d,  $J = 6.30$  Hz, 3H), 1.10 (s, 1H), 1.04 (d,  $J = 6.67$  Hz, 3H), 1.02 (s, 3H), 0.99 (m, 2H), 0.88, (d,  $J = 6.88$  Hz, 3H), 0.79 (m, 1H), 0.67 (d,  $J = 6.21$  Hz, 3H). HRMS (ESI) calculated for  $\text{C}_{74}\text{H}_{91}\text{N}_{19}\text{O}_{21}\text{S}_7$  (M +  $\text{H}^+$ )  $m/z$  1807.4682; found: 1807.4820.

**Captopril adduct (1.3):** HPLC (Method 2):  $t_R = 37.2$  minutes.  $^1\text{H NMR}$  (600MHz,  $\text{CDCl}_3$ :  $\text{CD}_3\text{OD}$  (4:1)):  $\delta$  9.76 (s, 1H), 8.67 (d,  $J = 8.90$  Hz, 1H), 8.50 (s, 1H), 8.15 (s, 1H), 8.13 (d, 1.21 Hz, 1H), 8.03 (s, 1H), 7.86 (s, 1H), 7.66 (s, 1H), 7.46 (d,  $J = 10.05$  Hz, 1H), 7.43 (s, 1H), 7.41 (d,  $J = 1.23$  Hz, 1H), 7.17 (s, 1H), 7.06 (d,  $J = 1.23$  Hz, 1H), 7.01 (d,  $J = 7.93$  Hz, 1H), 6.94 (d,  $J = 7.07$  Hz, 1H), 6.77 (d,  $J = 10.17$  Hz, 1H), 6.26 (dd, obscure), 6.25 (s, 1H), 6.23-6.18 (m, 1H), 6.11 (q,  $J = 7.01$  Hz), 5.70 (s, 1H), 5.65 (d,  $J = 8.61$  Hz, 1H), 5.62 (d,  $J = 10.01$  Hz, 1H), 5.51 (s, 1H), 5.21 (s, 1H), 5.20 (d,  $J = 9.89$  Hz, 1H), 5.16 (s, 1H), 4.86 (dd,  $J = 9.27, 12.53$ , 1H), 4.70 - 4.62 (m, 2H), 4.38-4.36 (m, 2H), 3.94-

3.91 (m, 1H), 3.69 (dq,  $J=5.68, 6.46$  Hz, 1H), 3.54 (m, 1H), 3.51 (m, 1H), 2.95 - 2.86 (m, 1H), 2.77 - 2.74 (m, 1H), 2.51 (d,  $J=6.06, 1.38$  Hz, 1H), 2.19 (m, 1H), 2.14 (m, 2H), 2.08 (m, 2H), 1.95 - 1.90 (m, 2H), 1.60 (d,  $J=6.44$  Hz, 3H), 1.49 (d,  $J=7.03$  Hz, 3H), 1.31 (d,  $J=6.14$  Hz, 3H), 1.25 (d,  $J=6.57$  Hz, 3H), 1.18 (d,  $J=6.38$  Hz, 3H), 1.09 (d,  $J=6.73$  Hz, 3H), 1.06 (d,  $J=6.61$  Hz, 3H), 1.02 (s, 3H) 1.00 - 0.95 (m, 2H), 0.87 (d,  $J=6.81$  Hz, 3H), 0.77 (d,  $J=6.67$  Hz, 3H), 0.71 (d,  $J=6.15$  Hz, 3H). HRMS (ESI) calculated for  $C_{81}H_{100}N_{20}O_{21}S_6$  ( $M + H^+$ )  $m/z$  1881.5696; found: 1881.5864

**Captopril adduct (1.4):** HPLC (Method 2):  $t_R = 39.4$  minutes.  $^1H$  NMR (600MHz,  $CDCl_3$ :  $CD_3OD$  (4:1)):  $\delta$  9.76 (s, 1H), 8.15 (s, 1H), 8.12 (s, 1H), 8.03 (s, 1H), 7.87 (s, 1H), 7.45 (d,  $J=10.01$  Hz, 1H), 7.43 (d,  $J=10.29$  Hz, 1H), 7.41, 7.17 (s, 1H), 7.06, 6.98 (d,  $J=7.61$  Hz, 1H), 6.95 (d,  $J=7.78$  Hz, 1H), 6.77 (d,  $J=9.87$  Hz, 1H), 6.26 (dd,  $J=5.58, 9.99$  Hz, 1H), 6.23 (d,  $J=6.23$  Hz, 1H), 6.21 (s, 1H), 6.11 (q,  $J=7.03$  Hz, 1H), 5.70 (s, 1H), 5.66 (d,  $J=8.65$  Hz, 1H), 5.62 (d,  $J=10.06$  Hz, 1H), 5.55 (s, 1H), 5.21 (s, 1H), 5.19 (d,  $J=6.62$  Hz, 1H), 5.17 (d,  $J=2.73$  Hz, 1H), 4.86 (dd,  $J=8.98, 12.59$  Hz, 1H), 4.76 - 4.73 (m, 2H), 4.34 - 4.30 (m, 2H), 3.95 - 3.93 (m, 1H), 3.69 (dq,  $J=6.06, 6.42$  Hz, 1H), 3.54 (m, 1H), 3.53 - 3.48 (m, 1H), 2.95 - 2.87 (m, 1H), 2.79 - 2.75 (m, 1H), 2.51 (d,  $J=6.63$  Hz, 1H), 2.18 - 2.16 (m, 1H), 1.60 (d,  $J=6.48$  Hz, 3H), 1.49 (d,  $J=6.98$  Hz, 3H), (d,  $J=6.28$  Hz, 3H), 1.26 (d,  $J=6.44$  Hz, 3H), 1.18 (d,  $J=6.37$  Hz, 3H), 1.09 (d,  $J=6.07$  Hz, 3H), 1.05 (d,  $J=6.70$  Hz, 3H), 1.02 (s, 3H), 0.99 - 0.94 (m, 2H), 0.87 (d,  $J=6.81$  Hz, 3H), 0.77 (d,  $J=7.21$  Hz, 3H), 0.70 (d,  $J=6.12$  Hz,

3H). HRMS (ESI) calculated for C<sub>81</sub>H<sub>100</sub>N<sub>20</sub>O<sub>21</sub>S<sub>6</sub> (M + H<sup>+</sup>) *m/z* 1881.5696; found: 1881.5860 .

### **2.2.3.2. Computational determination of the solubility properties for thiostrepton and its derivatives.**

The aqueous solubility of thiostrepton and its derivatives was assessed through computational determinations of the octanol/ water partition coefficient (LogP). Predictions (miLogP) were performed using the online Molinspiration Property Engine v2007.04 after determination of physico-chemical properties using the JME molecular editor (version January 2008) (Molinspiration Cheminformatics, <http://www.molinspiration.com>). For comparative purposes, LogP was also calculated according to the methods described in (241) and (242), using the structure prediction and calculation plugins for Marvin 5.3.01, 2010, ChemAxon (<http://www.chemaxon.com>). Chemical structures for thiostrepton and its Michael adducts, as well as for tetracycline and erythromycin, were drawn in ChemBioDraw Ultra (CambridgeSoft, USA) and exported in SMILES structure format, which were then imported into the various LogP prediction software.

### **2.2.3.3. Inhibition of bacterial growth**

Antimicrobial susceptibility testing was performed by the broth microdilution technique, in sterile, 96-well microplates, in accordance with methods prescribed by the National Committee for Clinical Laboratory Standards (243). Test concentrations for compounds **1.1** – **1.4** against *S. aureus*, *B. subtilis* and for compound **1.1** against *E. coli* were 32, 16, 8, 4, 2, 1, 0.5, 0.25,

0.125 and 0.0625  $\mu\text{g}/\text{mL}$ . Compounds **1.2 – 1.4** were tested against *E. coli* at concentrations of 128, 64, 32, 16, 8, 4, 2, 1, 0.5 and 0.25  $\mu\text{g}/\text{mL}$ . The minimum inhibitory concentration of bacterial growth was the lowest compound concentration that resulted in no visible bacterial growth. All tests were performed in triplicate.

#### **2.2.3.4. *In vitro* inhibition of protein synthesis.**

Inhibition of *in vitro* prokaryotic translation was quantified using the *E. coli* S30 Extract System for Circular DNA (Promega, Madison, USA) with the pBESTluc plasmid (Promega) according to the manufacturer's protocol. Individual translation reactions (25  $\mu\text{L}$ ) contained 10  $\mu\text{L}$  of Premix without amino acids, 7.5  $\mu\text{L}$  of S30 extract, 2.5  $\mu\text{L}$  of complete amino acid mix, 2.5  $\mu\text{L}$  of pBESTluc (700 ng/  $\mu\text{L}$ ) and 2.5  $\mu\text{L}$  of test compound. Control reactions received 2.5  $\mu\text{L}$  of 50% DMSO. Test compounds were initially dissolved in DMSO and then diluted to appropriate working concentrations with deionized water. The final concentration of DMSO in the reactions was 2.5% (v/v). Control reactions received 2.5  $\mu\text{L}$  of 50% DMSO in place of test compound. Reactions were incubated for 60 minutes at 37 °C and then placed on ice for 5 minutes, after which the luciferase assay reagent was added. Luminescence was recorded 5 minutes after the addition of 25  $\mu\text{L}$  of SteadyGlo Luciferase assay reagent (Promega).

#### **2.2.3.5. Reaction of thiostrepton with ionic copper**

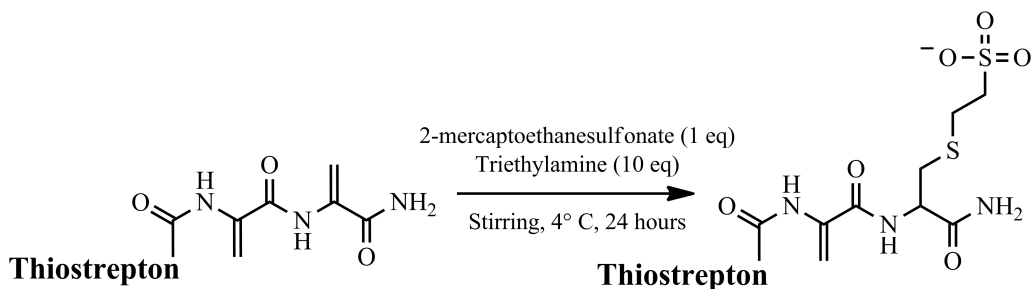
The complexation of thiostrepton with copper performed according to previously described methods (244). To a solution of thiostrepton prepared in

dioxane was added a large (5 – 10 fold) molar excess of aqueous  $\text{CuCl}_2$  and the resultant solution incubated at 37 °C for 24 hours. Dioxane was then added and the resulting light green precipitate washed successively with dioxane and ether and the residual solvent removed under vacuum. Parallel reactions performed in DMF found this solvent to be unsuitable, causing an “oiling out” effect upon vacuum drying of the reaction mixture. Crystallization of a copper-thiostrepton complex from the dried dioxane precipitate was attempted using various solvent systems, detailed in **Section 2.3.4**.

## **2.3. Results and Discussion**

### **2.3.1. Synthesis of thiostrepton derivatives**

The conditions for the preparation of the thiostrepton derivatives were established in this laboratory (172) and are shown in Scheme 2.1. Qualitative mass spectrometric analysis of the crude product mixture resulting from the reaction of thiostrepton with 2-mercaptoethanesulfonate (MENZA), indicated substantial formation of a product consistent with the single-addition of MENSA to thiostrepton. However, prior attempts at obtaining pure amounts of this compound were not successful, which prevented reliable determination of the site of addition and biological activity testing.



**Scheme 2.1. Synthesis of Michael adducts of thioestrepton**

## **2.3.2. Purification & characterization of thioestrepton derivatives**

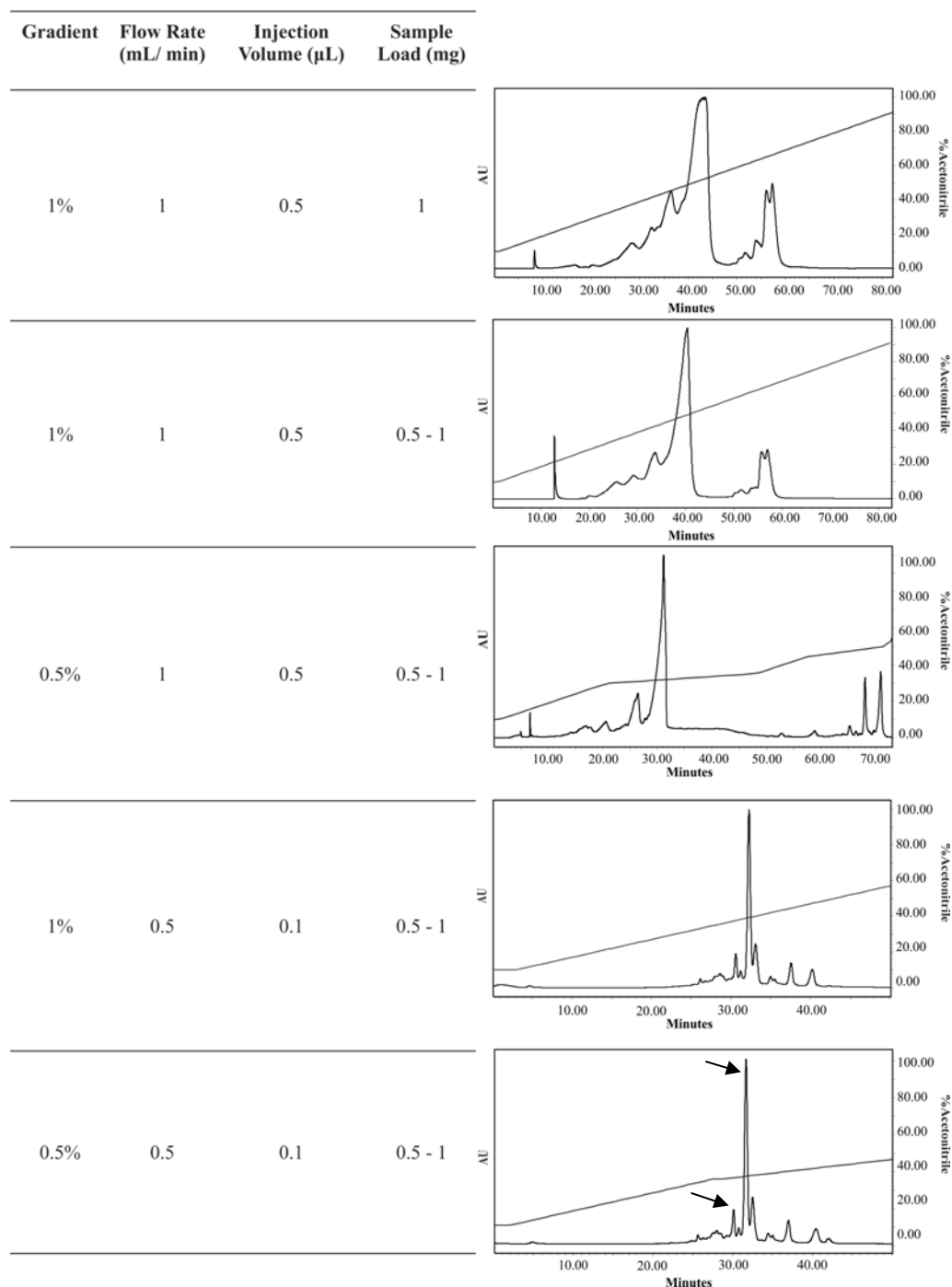
### **2.3.2.1. Optimization of purification conditions**

Previous attempts at HPLC-based purification of the thioestrepton-Michael adducts using reverse phase C-18 chromatography did not achieve adequate resolution of the composite products of the reaction mixture. This necessitated multiple rounds of purification, which when coupled with long run times, was an impractical approach for obtaining sufficient material for full physical characterization and biological testing.

Optimization of the purification scheme began with the use of a C-8 reverse phase column instead of a C-18 column. The difference in column chemistry and the shorter column length (150 mm for the C-8, versus 250 mm for the C-18) reduced the run time, while product resolution was significantly improved due to the reduced particle size of the C-8 column (5  $\mu\text{M}$  for the C8 column, versus 10  $\mu\text{M}$  for the C18). Purification conditions were then optimized with respect to the acetonitrile gradient, flow rate, injection volume and sample load (Figure. 2.2), culminating in final purification conditions that provided



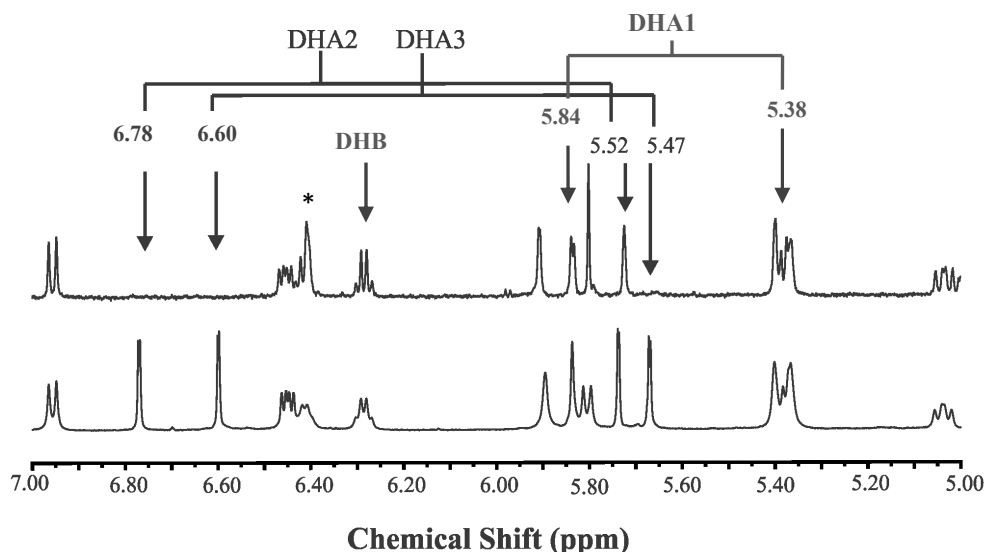
excellent resolution of the target materials, in separate fractions, eluting at 29.2 minutes and 31 minutes, which were identified by ESI-MS.



**Figure 2.2. Optimization of the HPLC purification of thiostrepton-MENSA derivatives.** The bottom panel shows the final purification conditions. Fractions containing the thiostrepton-MENSA derivatives (indicated by arrows) were identified by analysis of the ESI-mass spectra (29.2 minutes, 31 minutes).

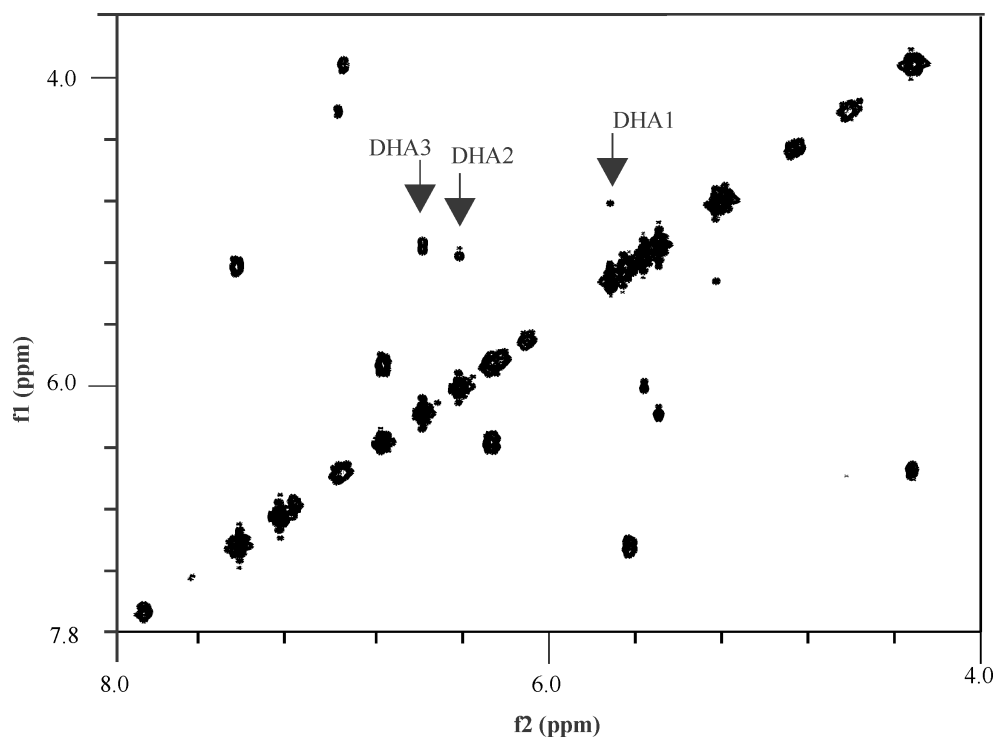
### 2.3.2.2. Physical characterization of the thiostrepton-MENSA derivative

Although the mass of the purified product indicated the single addition of MENSA to thiostrepton, the site of addition on the thiostrepton molecule remained to be deduced as there are four different potential sites for attachment. In addition, two HPLC fractions were identified which contained products consistent with the single addition of MENSA to thiostrepton. The entire proton spectrum for thiostrepton itself had been fully assigned (83, 245), hence the determination of the addition site was initially attempted using proton NMR. It was presumed that addition of MENSA would bring about the loss of the corresponding olefin chemical shifts, but as can be seen from Figure. 2.3, this was not entirely observed. While the chemical shifts from DHA3 were absent, only one of those from DHA2 was in evidence and a new peak was observed at 6.42 ppm.



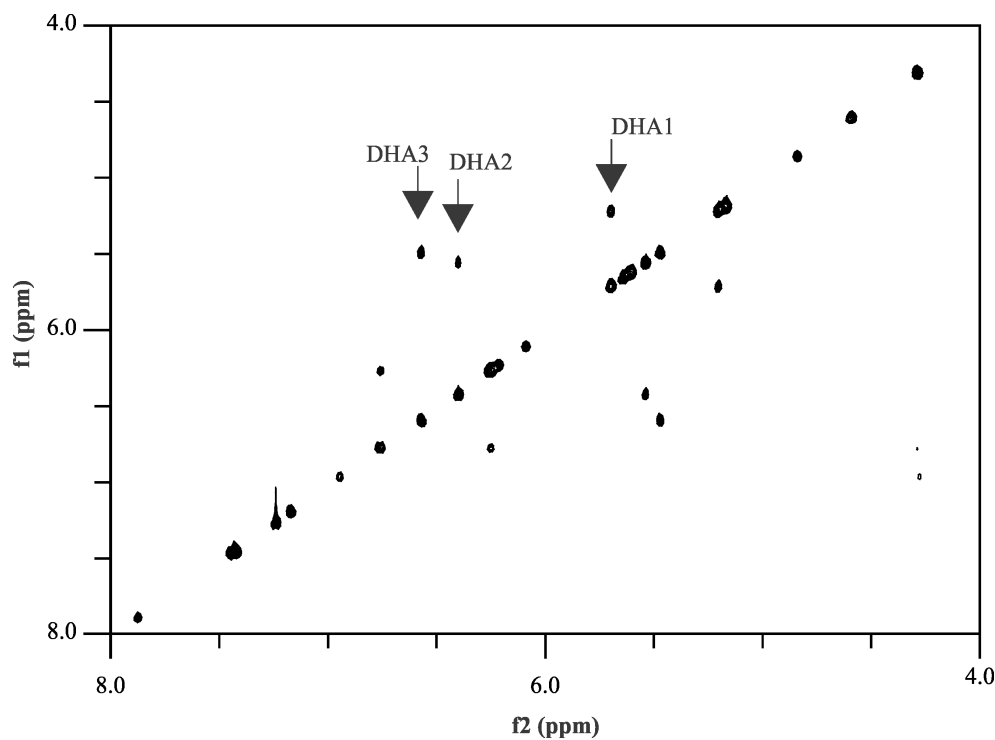
**Figure 2.3. Proton NMR of the MENSA derivative of thiostrepton.** A section of the NMR spectra encompassing the chemical shifts of the olefin protons from the DHA and DHB residues in thiostrepton (bottom trace) and the thiostrepton-MENSA adduct (top trace) are shown. A unique peak (marked by an asterisk) is apparent in the spectrum for the MENSA adduct.

Unambiguous assignment of these olefin chemical shifts was sought with 2-dimensional NMR. A proton COSY experiment was first performed with unmodified thiostrepton to verify proton coupling between the olefin protons from the DHA residues (Figure 2.4).



**Figure 2.4. Proton COSY spectrum of thiostrepton.** Cross peaks resulting from coupling between DHA olefin protons are indicated by arrows.

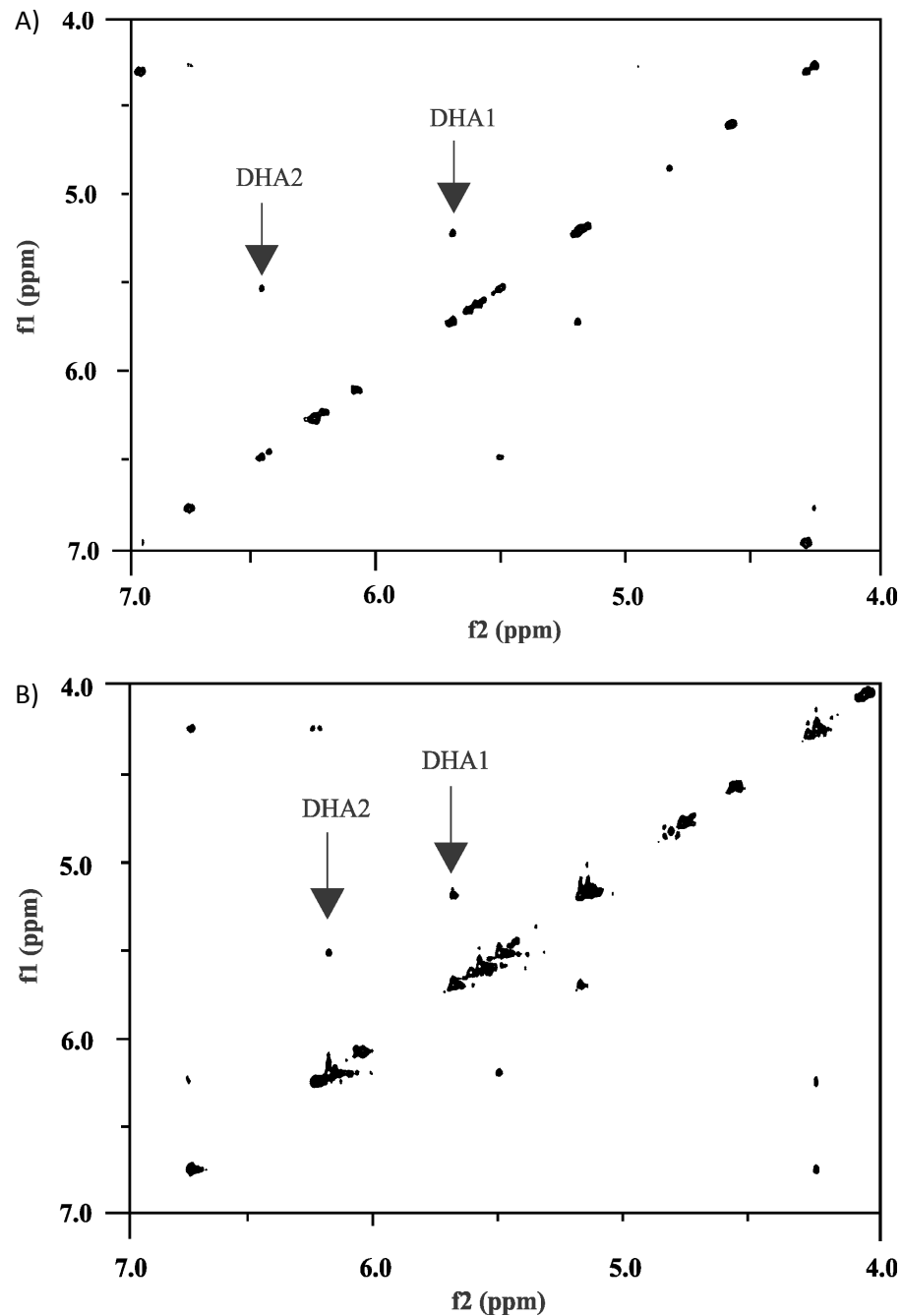
As expected, correlations were observed between the chemical shifts attributed to DHA olefin protons (DHA1: 5.38, 5.84; DHA2: 5.52, 6.54 ppm; DHA3: 5.47, 6.37 ppm). The proton TOCSY spectrum of unmodified thiostrepton confirmed that the observed COSY correlations indeed arose from the olefin protons from the respective DHA residues (Figure. 2.5).



**Figure 2.5. Proton TOCSY spectrum of thioestrepton.** The displayed region is superimposable with that observed from the COSY spectrum, indicating that the observed cross peaks arise from protons residing on the same carbon atom, thus confirming the proton assignment for the olefin protons.

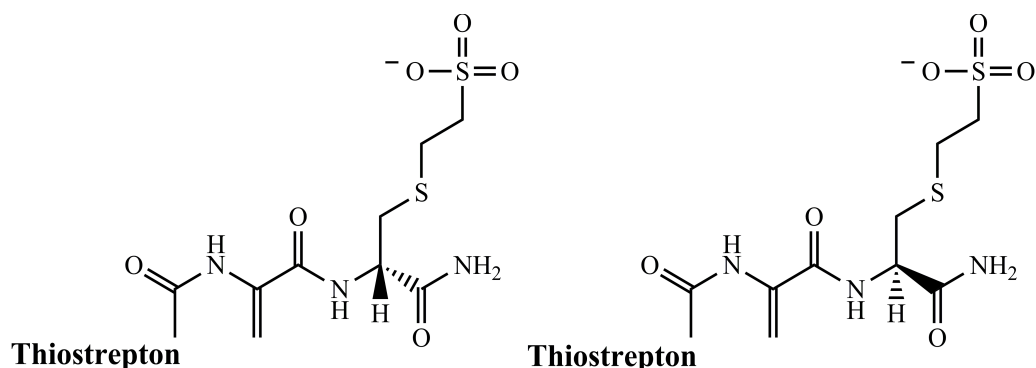
Under identical conditions, TOCSY spectra for the purified single addition products were devoid of cross-peaks corresponding to DHA3 protons, which upon analysis confirmed this residue to be the site of nucleophilic addition (Figure 2.6). In addition, the correlation between the chemical shifts at 5.52 ppm and the unique chemical shift at 6.42 ppm in the spectrum of the product eluting after 29.2 minutes (Figure. 2.6A), identifies the proton responsible for this new chemical shift as the second DHA2 olefin proton, meaning that the chemical shift for one of the DHA2 olefin protons was perturbed in response to the presence of the MENSA appendage. Likewise, the

cross peak between the chemical shifts at 5.52 ppm and 6.20 ppm in the spectrum of the single addition product eluting after 31 minutes confirms this



**Figure 2.6. TOCSY spectra of thioestrepton-MENSA derivatives.** Partial TOCSY spectra for HPLC products eluting after A) 29.2 minutes B) 31 minutes.

compound to be a single site MENSA adduct, with addition occurring at DHA3. Therefore, these two products represent a diastereomeric pair, which accounts for the discrepancy in the chemical shifts for the DHA2 protons (Figure 2.7).



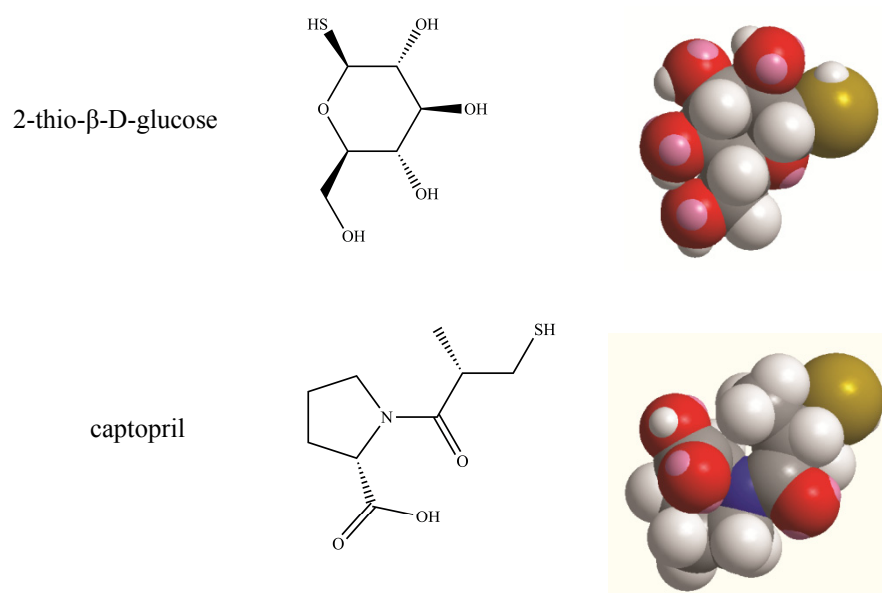
**Figure 2.7. Configurations of the MENSA appendage in the thioestrepton derivatives.** The absolute stereochemistry of each compound is unknown, however HPLC indicated that one of these conformations is favored.

### 2.3.2.3. Modification of thioestrepton by bulky, polar thiols

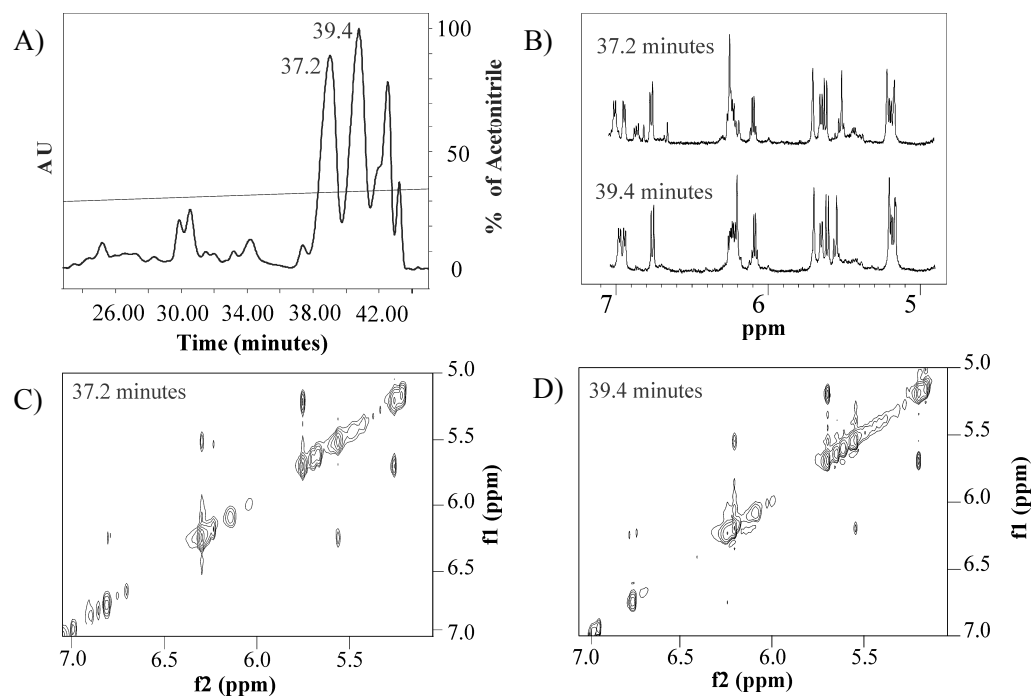
The tail region of thioestrepton appears to make important contributions to the high affinity binding of the antibiotic to the bacterial ribosome (*120, 126, 127, 142, 143*) however, the demonstrated amenability of this region to facile chemical modification potentially allows for extensive derivatization of the thioestrepton molecule. In order to more deeply assess the effect that modifications in this region may have on the physical and biological properties of thioestrepton, derivatives that featured bulky tail appendages were prepared.

Under the conditions detailed by Scheme 2.1, modification was first attempted with 2-thio- $\beta$ -D glucose, which possesses a very different structure than MENSA. Mass spectrometry and  $^1\text{H}$  NMR analyses suggested the presence of the desired thioestrepton-glucose adduct, but multiple reaction side products

were also evident and unfortunately, (diastereomerically) pure samples of this single-site Michael adduct could not be obtained. It is likely that the sugar moiety contributed to the formation of undesired products and hampered chromatography separation. Thiostrepton modification was therefore attempted with captopril, as it was thought that five-membered ring of this molecule would mimic the steric interactions brought on by 2-thio- $\beta$ -D glucose (Figure 2.8). Modifications with captopril produced a similar outcome as that with MENSA, with the desired captopril adducts being detected in two separate HPLC fractions, representing a total overall yield of 45% (Figure 2.9A)). Further characterization of these compounds by NMR confirmed them to be a diastereomeric pair (Figure 2.9C and D).



**Figure 2.8. Structures of 2-thio- $\beta$ -D glucose and captopril.** 3D structures for 2-thio- $\beta$ -D-glucose and captopril were generated from SMILES structures, using *Chem 3D Pro version 12.02.1076* (Cambridgesoft, Cambridge, USA).

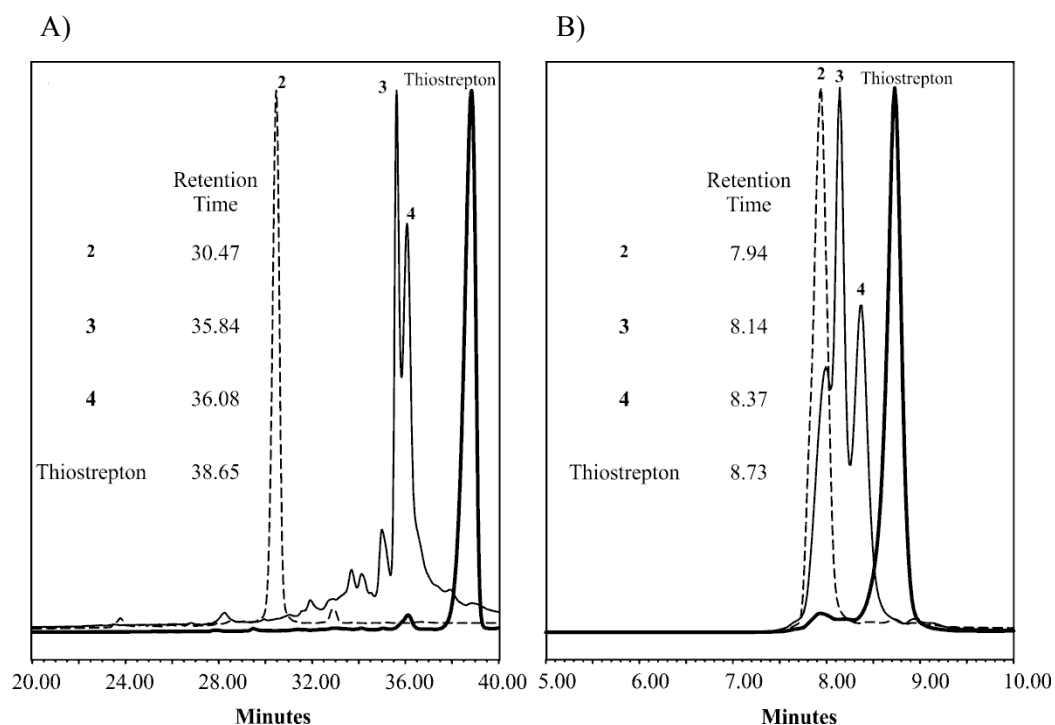


**Figure 2.9. Purification and characterization of the thiostrepton-captopril derivative.** A) HPLC chromatogram of the products from the reaction of thiostrepton with captopril. Captopril adducts were identified by ESI mass spectrometry in the fractions eluting after 37.2 minutes and 39.4 minutes. B) <sup>1</sup>H NMR showing the chemical shifts in the olefin region of the thiostrepton-captopril derivatives. C) and D), TOCSY spectra of thiostrepton-captopril derivatives showing proton correlations in the olefin region.

#### 2.3.2.4. Aqueous solubility of thiostrepton derivatives

The solubility of the thiostrepton derivatives relative to the highly hydrophobic unmodified thiostrepton was qualitatively assessed by analytical HPLC. Under identical conditions for gradient or isocratic separation, the derivatives exhibited shorter retention times than thiostrepton, indicating their greater polarity/ aqueous solubility (Figure 2.10). The order of decreasing aqueous solubility was reflected by computational determinations of compound solubility (Table 2.1.).





**Figure 2.10. Relative (aqueous) solubility of Michael adducts.** From Myers *et al.* (246). RP-HPLC chromatograms for the separation of a mixture of thioestrepton and its derivatives using a C-18 column with A) gradient elution: 0-100% acetonitrile over 100 minutes; and B) isocratic elution: 0.1% TFA/ acetonitrile (50:50). 2: MENSA derivative, 3 & 4: captopril derivatives

**Table 2.1.** Theoretical solubility of Thioestrepton and Michael adducts

Compound	miLogP*	LogP (predicted)	
		Viswanadhan <i>et al.</i> (241) <sup>†</sup>	Klopman <i>et al.</i> (242) <sup>†</sup>
Thioestrepton	-1.567	-1.01	-0.97
2 (neutral)	-4.151	-4.41	-1.91
2 (negative)	-4.796	-6.67	-4.38
3/4 (neutral)	-2.969	-3.03	-0.85
3/4 (negative)	-4.205	-6.71	-4.35
TBG adduct	-3.569	-5.89	-3.45
Erythromycin	2.281	1.22	4.20
Tetracycline	-0.978	-0.16	0.39

\*miLogP = Molinspiration predicted LogP value. † LogP calculation using the structure prediction and calculation plugins for Marvin 5.3.01, 2010, ChemAxon (<http://www.chemaxon.com>). † Electrolyte concentration: Cl<sup>-</sup> = 0.1 (mol/dm<sup>3</sup>) and Na<sup>+</sup>/K<sup>+</sup> = 0.1 (mol/dm<sup>3</sup>).

### 2.3.3. Biological activity of various thiostrepton derivatives

The inhibition of bacterial growth by the thiostrepton analogues was assessed against the Gram-positive bacteria *Staphylococcus aureus* and *Bacillus subtilis* as well as the Gram-negative *Escherichia coli*. Table 2.2 shows that the thiostrepton derivatives were less potent antibacterial agents against these organisms than unmodified thiostrepton, as seen by their higher MIC values. Encouragingly, the antibacterial activity displayed by **1.2** against *S. aureus* and *B. subtilis* compared favorably with that which has been reported for conventional antibiotics (247) and compounds **1.3** and **1.4**, though less potent than **1.2**, exhibited notable antibacterial activity. Like thiostrepton, none of its derivatives displayed any activity against *E. coli*, indicating no extension of antibacterial activity to Gram-negative bacteria.

**Table 2.2. Antibacterial activity of thiostrepton analogues.**

Compound	Minimum Inhibitory Concentration ( $\mu\text{g}/\text{mL}$ ) <sup>†</sup>		
	<i>S. aureus</i> (ATCC 6338)	<i>B. subtilis</i> (ATCC 6633)	<i>E. coli</i>
<b>Thiostrepton</b>	$\leq 0.0625$	$\leq 0.25$	$\geq 32$
<b>2</b>	$\leq 2$	$\leq 8$	$\geq 128$
<b>3</b>	$\leq 32$	$\leq 32$	$\geq 128$
<b>4</b>	$\leq 32$	$\leq 32$	$\geq 128$
TBG adduct <sup>‡</sup>	$\geq 50$	$\geq 50$	$\geq 50$

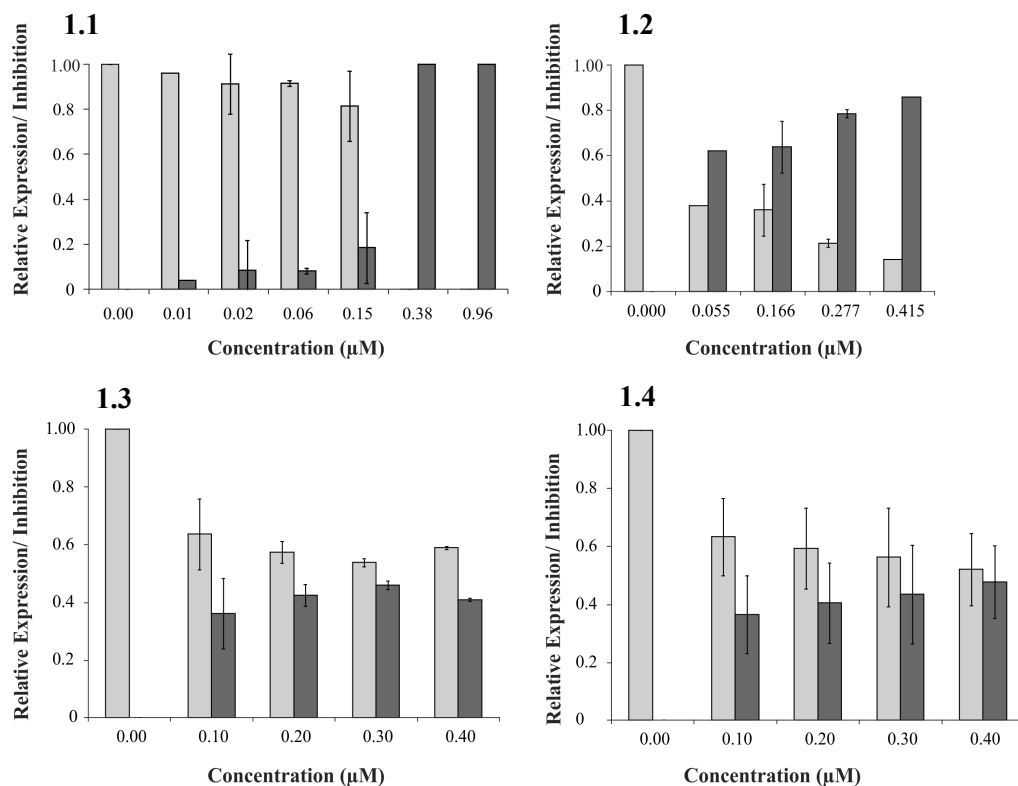
<sup>†</sup> Minimum inhibitory concentrations are reported as less than or equal to lowest compound concentration that inhibited visible bacterial growth. Antimicrobial susceptibility tests were performed in triplicate, with DMSO present at 5% (v/v).

<sup>‡</sup> Activity was assessed by disc diffusion, for a partially purified sample.

Preliminary screens for antibacterial activity by the suspected 2-thio- $\beta$ -D-glucose derivative using disc diffusion found no activity up to the highest concentration tested (50  $\mu\text{g}/\text{mL}$ ), but it should be pointed out that this assessment was performed on an impure sample of this compound.

Thiostrepton exerts its antibacterial activity through the inhibition of protein synthesis. *In vivo* antibacterial activity is restricted to Gram-positive bacteria but protein translation by the ribosomes of both Gram-positive and Gram-negative species is inhibited by the antibiotic (120, 132, 167). To establish the inhibition of protein synthesis as the mechanism of antibacterial activity for the thiostrepton derivatives, *in vitro* translation reactions using *E. coli* ribosomes were performed in the presence of the derivatives. A plasmid bearing the firefly luciferase gene was used as the template DNA in these reactions, which allowed for convenient monitoring of protein expression by measuring the luminescence of the gene product (248–251). Prior to measuring *in vitro* translation in the presence of thiostrepton or its derivatives, the linear range for light output by the luciferase was determined, as well as the linear range for the assay duration. In addition, the effect of DMSO on light output was measured. These experiments (detailed in Appendix 2) served to define the parameters of the assays for inhibition of translation with respect to duration, maximum concentration of compound, maximum proportion of DMSO and the acceptable range of luminescence.

Overall, luciferase expression was observed to decrease with increasing concentrations of thiostrepton or its derivatives, which is consistent with the inhibition of protein synthesis being responsible for the observed inhibition of bacterial growth (Figure. 2.11). This effect was more evident in the presence of **1.2**, where a marked reduction in protein expression occurred in a dose-dependent fashion similar to the effect seen with unmodified thiostrepton.



**Figure 2.11. Effect of thiostrepton and its derivatives on *in vitro* protein synthesis.** From Myers *et al.* (246). The expression or luciferase  $\square$  or the inhibition  $\blacksquare$  of luciferase synthesis was observed by the luminescence output of translation reactions containing different amounts of thiostrepton (1.1) or its derivatives and are expressed relative to control reactions containing no antibiotic. Values reflect the means of at least 2 experiments. Error bars represent one standard deviation of the mean.

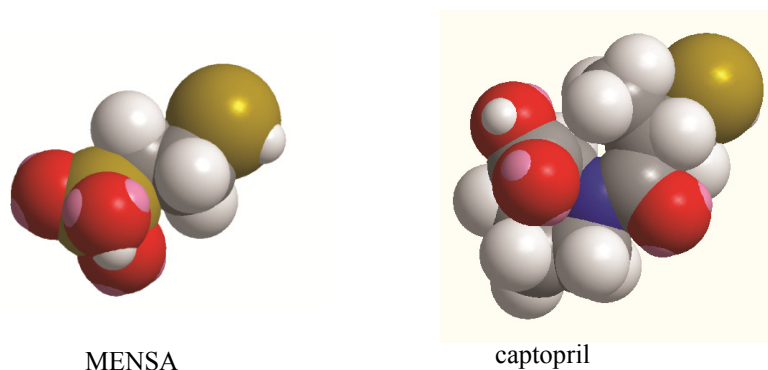
Interestingly, the results suggest a lower apparent  $IC_{50}$  for the MENSA analogue ( $\leq 0.05 \mu\text{M}$ ) as compared to unmodified thiostrepton (0.15 – 0.38  $\mu\text{M}$ ). This is likely a consequence of the increased aqueous solubility of the MENSA derivative with respect to thiostrepton, which would possibly enable its greater availability to affect its activities in the largely aqueous environment of the *in vitro* translation reactions. The decrease in luciferase expression in the

presence of the captopril derivatives **1.3** and **1.4** occurred to a lesser extent than seen with derivative **1.2** and luciferase expression/ inhibition of luciferase expression appeared to approach a constant value of approximately 50%. Since **1.3** and **1.4** are a diastereomeric pair, the finding of similar levels of *in vivo* and *in vitro* activity for these suggests that the stereochemistry at the new chiral centre generated upon thiostrepton modification does not affect compound binding or activity.

It is worth mentioning that the effect of **1.2** on protein synthesis was not directly reflected by its inhibition of bacterial growth. The results from the assays of the inhibition of protein synthesis imply that **1.2** would exhibit a lower MIC value than thiostrepton, which was contrary to what was observed experimentally. A similar discrepancy was also noted between the inhibition of protein synthesis and inhibition of bacterial growth by **1.3** and **1.4**. These observations may be indicative of another factor limiting to antibacterial activity, one of which may be the impeded uptake of the analogues by the bacterial cells. The uptake of thiostrepton by bacterial cells has not been studied in detail, however, the increased size and hydrophilicity of the analogues may hamper their ability to transverse the hydrophobic bacterial cell membrane.

As earlier stated, the thiostrepton-MENSA derivatives proved to be more potent inhibitors of bacterial growth than the thiostrepton-captopril derivatives. The results from the *in vitro* luciferase translation assays show this was due to differential abilities at inhibiting protein synthesis. The appendages of the thiostrepton derivatives present distinct structures; MENSA adopting a linear,

extended conformation compared to the globular and more voluminous structure of captopril (Figure 2.12).

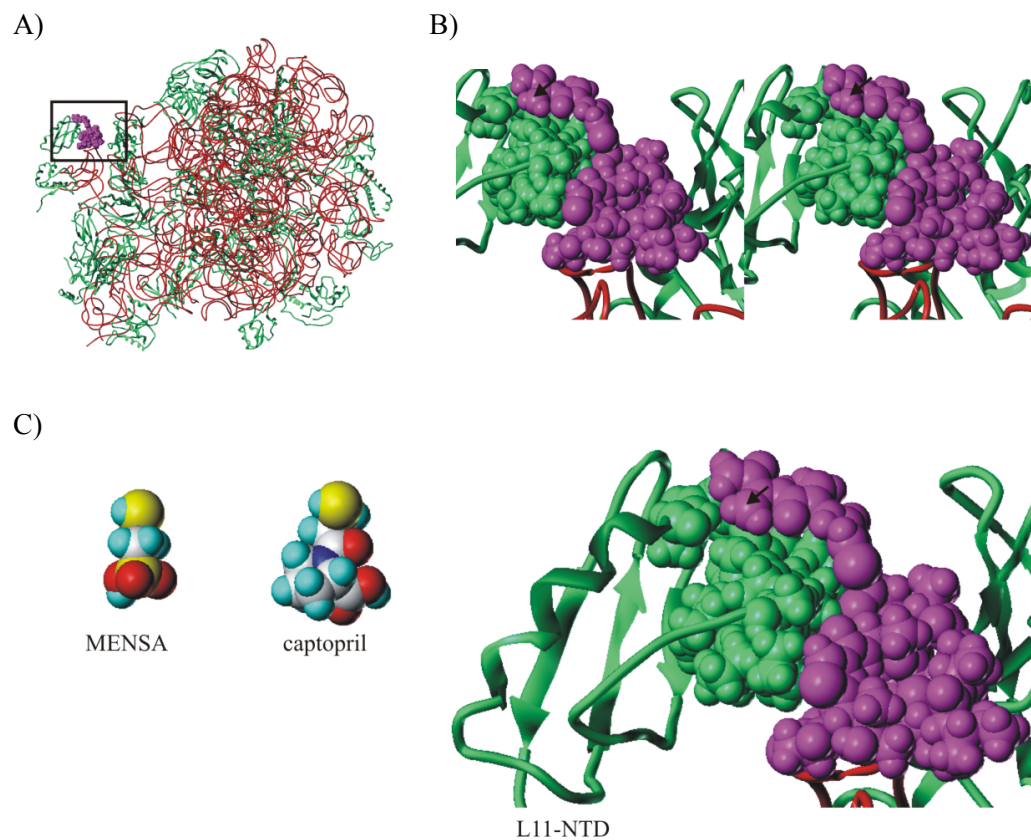


**Figure 2.12. Space-filling structures of the polar thiols used to modify thiostrepton.** Structures were generated using *Chem 3D Pro version 12.0.2.1076* (Cambridgesoft, Cambridge, USA).

The site of addition was located to the tail region of thiostrepton and the different conformations and sizes of these appendages would result in different steric and spatial interactions at this region of the thiostrepton molecule and by extension, any activities in which this region of the molecule participates.

As earlier stated, the interaction between the L11-NTD and thiostrepton is crucial for tight binding to thiostrepton to the bacterial ribosome and extensive biochemical and structural data show that the tail region of thiostrepton increases the affinity of thiostrepton for the bacterial ribosome through its non-covalent interactions with the L11-NTD (120, 126, 127, 142, 143). Therefore, the finding of a correlation between tail structure and biological abilities for the thiostrepton derivatives coincides with this important contribution by the tail region as modifications in this region affect its

interaction with the L11-NTD. This further implies there to be conformational and spatial limitations to modifications of the tail region that do not compromise activity. These limitations are not evident from the available crystal structure of the 50S ribosomal subunit from *Deinococcus radiodurans* bound with thiostrepton (143); the 50S subunit of the *D. radiodurans* ribosome being virtually identical to that of *E. coli* (252). The structure implies that the space surrounding the tail of thiostrepton can accommodate sizeable appendages in this region. At the same time, upon closer examination, this structure highlights the potential for localized disruptions to the interaction between the tail and the L11-NTD and such disruptions would be to a degree dependent on the nature of the appendage (Figure. 2.13). It should be noted that although the crystal structure shows the “bound” position for the thiostrepton tail, the inherent rotational flexibility of the tail (85) could lead to diminished, eliminated or repulsive interactions with the L11-NTD and this could be magnified by larger appendages. Therefore, given the importance of the interaction between L11-NTD and the tail region for binding and activity, captopril induces more extensive disruptions than MENSA (Figure 2.13C), which is consistent with the finding of similar inhibition of translation by thiostrepton and its MENSA analogue, compared to the reduced inhibition by the captopril analogues.



**Figure 2.13. Importance of the thiostrepton tail in ribosome binding.** (From Myers *et al.* (246)) A) Thiostrepton (magenta) bound to the 50S ribosomal subunit (rRNA in red; ribosomal proteins in green) from *D. radiodurans*. B) Magnified view of the boxed region from A); the site of Michael addition is indicated by arrow. C) MENSAs and captopril shown next to a region of the thiostrepton-50S complex. Images were generated using *Sybyl 8.1* software. The structure of the 50S subunit from the *Deinococcus radiodurans* bound with thiostrepton was imported as a PDB file (3CF5) into the software. MENSAs and captopril were drawn using the drawing component and energy minimized using the Tripos force field, with default parameters.

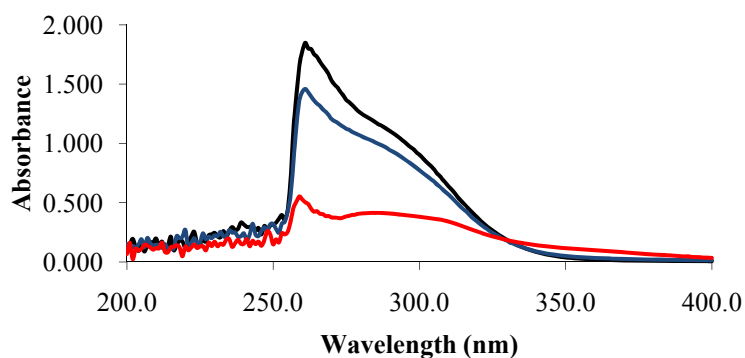
### 2.3.4. Thiostrepton-Copper Interactions

The interaction of thiostrepton with copper is unlikely to be of biological relevance, however, the antibacterial activity of thiostrepton has been shown to sigmoidally fall off in the presence of  $\text{Cu}^{2+}$ , with relative activity approaching zero at a 4:1 ratio of  $\text{Cu}^{2+}$  to thiostrepton (253). This would imply a maximum copper binding capacity for thiostrepton of 4 copper atoms per molecule of thiostrepton, which was later supported by electron spin resonance spectroscopy



studies (254). The reduction in thiostrepton activity in response to copper binding therefore suggests there to be a structural change to the thiostrepton molecule that would interfere with its interactions with the ribosome. However, spectroscopic data has thus far only allowed for tentative hypotheses of the ligand coordination at these supposed copper binding sites, with the oxygen from amide carbonyl groups and the nitrogen from thiazole groups being implicated (244, 254). Hence, with the view towards the structural characterization of the thiostrepton-copper interaction, crystallization of the purported thiostrepton-copper complex was attempted.

The complexation of thiostrepton with copper was initially attempted using previously described methods, but mass spectrometric analysis of the product precipitated by dioxane was inconclusive, yielding a spectrum dominated by thiostrepton ions.



**Figure 2.14. Effect of copper on UV absorbance of thiostrepton.** Spectra obtained in 20% DMSO for thiostrepton (black) and the filtrate (blue) and precipitate (red) after dioxane-induced precipitation of the complexation reaction are shown. The filtrate from the dioxane precipitation resembles that of thiostrepton. Note the increased absorbance in the 275 – 325 nm range for the precipitate obtained by dioxane precipitation.

However, it is likely that the conditions of mass spectrometry resulted in the loss of thioestrepton-bound copper. On the other hand, the spectrophotometric analysis of the product showed increased absorbance between 275 nm and 325 nm, which coincided with previous analyses of the thioestrepton-copper complex (244) (Figure. 2.14).

Initial attempts at crystallization of this product from ethanol and water<sup>1</sup> were unsuccessful, with poor quality crystals remaining only after total evaporation of the solvent. This was not improved by varying the ratio of thioestrepton to ionic copper, therefore different crystallization solvent systems were explored. First among these solvent systems was chloroform/ methanol. Crystallization did not result from the use of various fixed starting ratios for these solvents, but was eventually induced after the initial dissolution of the product in methanol, followed by the slow addition of chloroform<sup>2</sup>. These crystals unfortunately were determined to be CuCl<sub>2</sub> by X-ray analysis experiments. Similar results were obtained from solvent systems consisting of pyridine, pyridine/ dichloromethane, pyridine/ chloroform, pyridine/ dioxane, while solvent systems comprised of 2-propanol/ pyridine, 2-propanol/ methanol and dioxane/ methanol did not yield crystals suitable for X-ray diffraction.

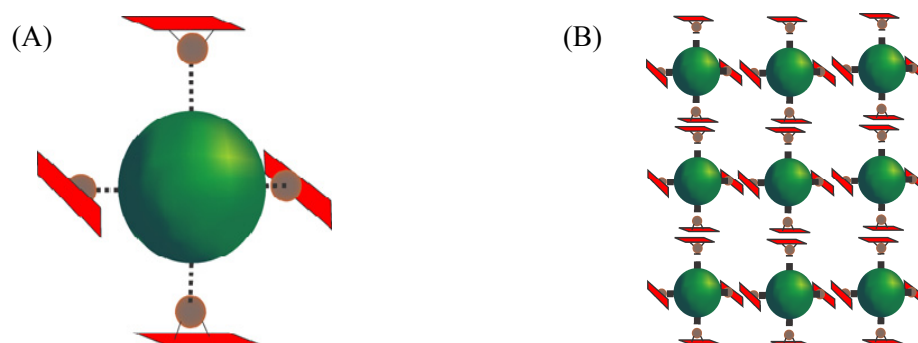
Molecular structures have been determined for copper complexes with aliphatic ketones and haloketones as well as aromatic ketones (255–258) and it

---

<sup>1</sup> The precipitate was dissolved in a minimum amount of ethanol heated to near boiling. ddH<sub>2</sub>O was added slowly until the precipitation was first observed, which was removed by the further addition of small amount of hot ethanol. Crystallization was allowed to proceed through slow evaporation.

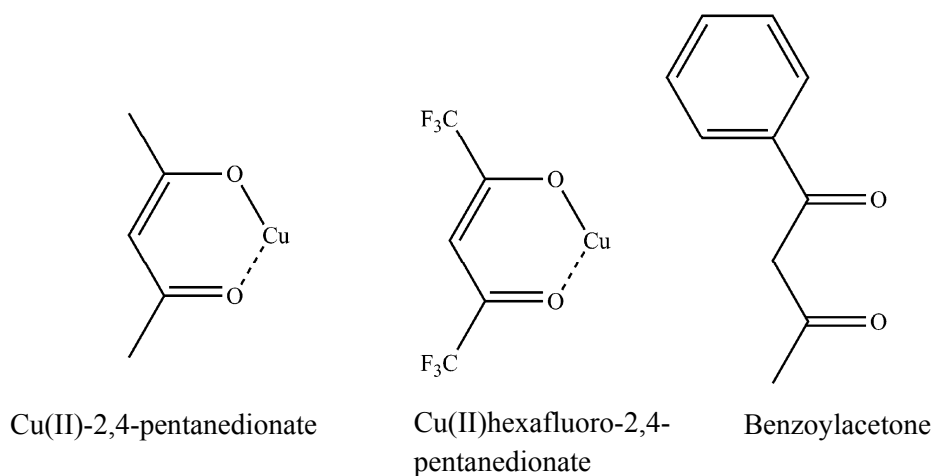
<sup>2</sup> The precipitate was dissolved in minimum methanol at ambient temperature, followed by the slow addition of chloroform. Crystallization was allowed to proceed by slow evaporation.

was thought that the inclusion of such organic molecules could aid crystallization of thiostrepton-copper complexes. Presumably, the copper in these organic complexes would coordinate with specific atoms in thiostrepton, while crystal lattice formation would be promoted by interactions between the organic complexes (Figure. 2.15).



**Figure 2.15. Interaction of thiostrepton with organic copper complexes.** (A) Depiction of the molecular structure for thiostrepton (green) in complex with copper (brown) and an organic molecule (red). (B) Possible lattice arrangement of the molecule from (A). Lattice stability (and crystallization) is promoted by interactions between the organic molecules.

Complexation reactions were therefore attempted with three different organic compounds: copper (II)-2,4-pentanedionate; copper (II) hexafluoro-2,4-pentandionate and benzoyl acetone (Figure. 2.16).



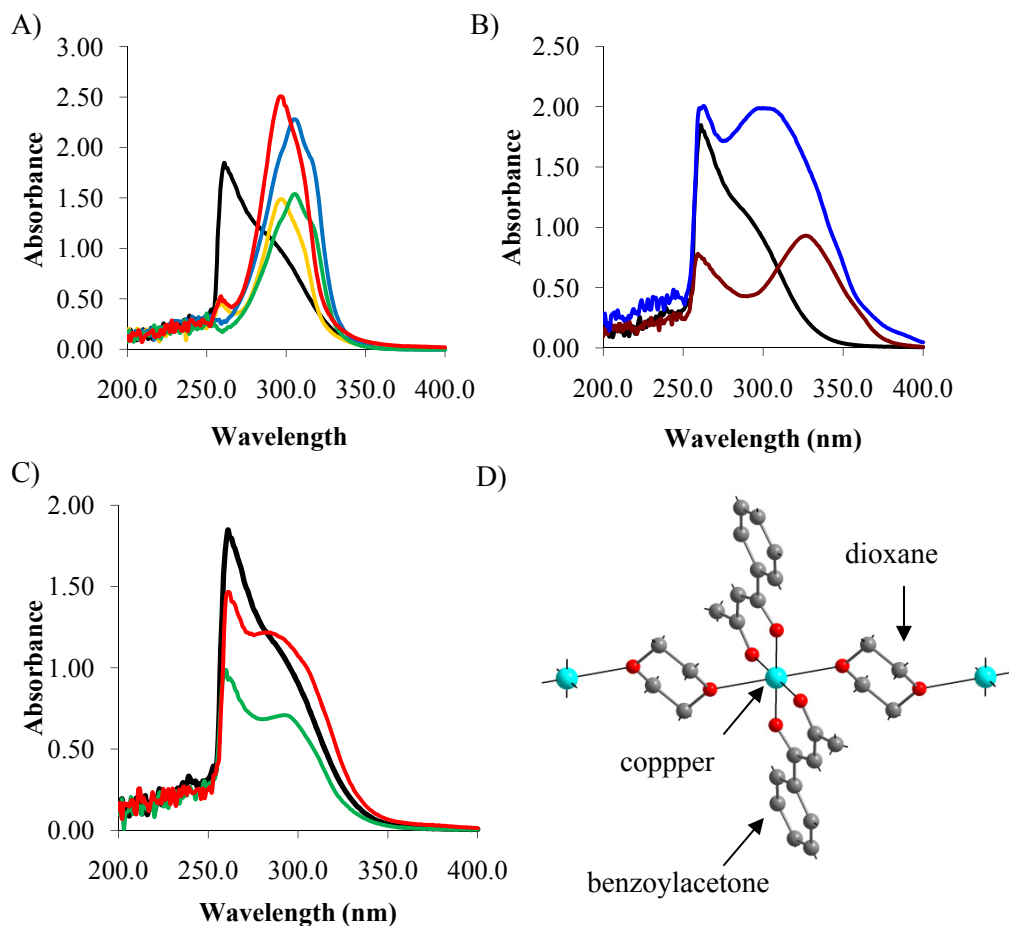
**Figure 2.16. Ketones used to aid thiostrepton-copper complexation**

UV absorbance spectra for the dioxane precipitates resulting from complexation reactions in the presence of these compounds showed dramatically increased absorbance from 275 nm – 325 nm (Figure. 2.17A). However, very little absorbance was observed in the region where maximum thiostrepton absorbance occurs (250-280 nm), suggesting that the precipitated material consisted largely of these organic ketones. Hence, the reaction conditions were modified such that thiostrepton was present in a 2-fold excess of CuCl<sub>2</sub> and the organic ketone. UV spectra for dioxane precipitates from these reactions featured two absorbance maxima, occurring between 250-275 nm and 275-325 nm, which was suggestive of complex formation. Crystals were eventually obtained from the benzoylacetone reactions, however, these were found to be a complex of benzoylacetone and copper, featuring a hexacoordinate copper with octahedral geometry (Figure. 2.17D).

The existence of a stable thiostrepton-copper complex remains unproven and its non-occurrence cannot be excluded. Yet, in spite of the inability to

obtain crystals and the corresponding molecular structure of this proposed complex, the spectrophotometric analyses of thiostrepton in the presence of ionic copper was suggestive of an interaction between this metal and thiostrepton. This would imply that the observed absorbance changes, particularly in complexation reactions performed in the absence of organic ketones, resulted from structural changes occurring in the thiostrepton molecule in response to its interaction with copper.

A broader evaluation of solvent systems may lead to the crystallization of the thiostrepton-copper complex, but it remains possible that this complex is inherently not amenable to crystallization. On the other hand, thiostrepton has proved to be well suited to study by NMR (PDB: 2L2W, 2L2Y, 2L2X, 2L2Z). Hence, further study of the thiostrepton-copper interaction might include monitoring chemical shift changes in thiostrepton in response to copper titration. From these, the ligand binding sites could be unequivocally identified and the global changes to thiostrepton structure revealed, which undoubtedly would reveal novel antibiotic-metal interactions.



**Figure 2.17. UV-absorbance spectra for thioestrepton in complex with copper and ketones.** (A) Complexation reactions performed at a 1:4 ratio of thioestrepton and copper(II) pentanedionate (yellow), copper(II) hexafluoro-2,4-pentanedionate (blue), benzoyl acetone and copper chloride (green). (B) Modified conditions for the complexation reaction with benzoyl acetone where the components were added individually (brown) or thioestrepton was added to an incubating mixture of benzoyl acetone and  $\text{CuCl}_2$ . In both cases, the components were present at a 2:1:1 ratio (thioestrepton: benzoyl acetone:  $\text{CuCl}_2$ ). (C) Reaction of thioestrepton with copper (II) pentanedionate (red), copper (II) hexafluoro-2,4-pentane dionate (green) at a 2:1 ratio (thioestrepton: ketone). (D) Molecular structure of the crystals obtained using benzoyl acetone. The carbonyl oxygens from benzoyl acetone occupy equatorial positions around copper, while the oxygen from dioxane makes axial contacts.

## 2.4. Conclusions, perspectives and future work

A facile semi-synthetic approach has been used to prepare novel, regio-specific derivatives of thiostrepton. These derivatives display improved aqueous solubility over the parent molecule and in the case of MENSA derivatives, exhibit significant antibacterial effects against Gram-positive bacteria. In addition, the importance of the tail region of thiostrepton for its antibacterial properties has been shown through the preparation and evaluation of derivatives featuring structurally contrasting modifications to this area of the molecule. These findings were consistent with previous reports of the enhancement of thiostrepton binding to the bacterial ribosome by the tail region of the molecule. Finally, the absorbance changes to thiostrepton that occur in the presence of copper may be indicative that structural changes are induced in the antibiotic by its binding of copper.

The results of this work highlight the thiostrepton tail as an attractive area for modifications, particularly with respect to improving the aqueous solubility of the molecule. However, a caveat to the generation of practically useful derivatives, with respect to antibacterial activity, has been illustrated; future derivitizations of thiostrepton in this region should take into account the consequences that potential steric and spatial interaction of the modifying group may have on antibacterial activity. Therefore, this work can serve as a platform for the development of novel thiostrepton derivatives, with improved physicochemical properties and increased potency as antibacterial agents. As well, this study assessed the susceptibility of two Gram-positive bacteria to

thiostrepton derivatives, but a broader species evaluation would likely prove to be more informative and demonstrate the applicability of these compounds.

As earlier stated, Gram-negative species are excluded from the effects of thiostrepton, presumably because of the inability of the antibiotic to penetrate the Gram-negative cell wall. Thiostrepton will, however, bind to and inhibit translation from the ribosomes of these bacteria. Hence, future studies can address the extension of the spectrum of thiostrepton activity to the Gram-negative genera by preparing derivatives that target such bacteria. While this may involve detailed studies of the mechanism of thiostrepton uptake by cells, Gram-negative uptake of thiostrepton can theoretically be achieved by appending thiostrepton with a short peptide sequence that will target it to the interior of Gram-negative cells, analogous to the utilization of cell-penetrating proteins for the cellular internalization of (macro)molecules (259–261). In addition, such a sequence can be coupled to a reporter molecule for proof-of-principle studies of the internalization of thiostrepton derivatives in Gram-negative cells. Finally, thiostrepton derivatives of the kind described here may be used in the study of the mechanism(s) by which thiostrepton exerts its antagonistic effects against causative agents for malaria and tuberculosis and certain cancers and may serve as lead compounds in the development of novel anti-malarial, anti-tuberculosis and anti-cancer drugs.



## CHAPTER 3: DETERMINANTS OF ADO MET BINDING AND METHYL GROUP TRANSFER FOR THIOSTREPTON-RESISTANCE METHYLTRANSFERASE

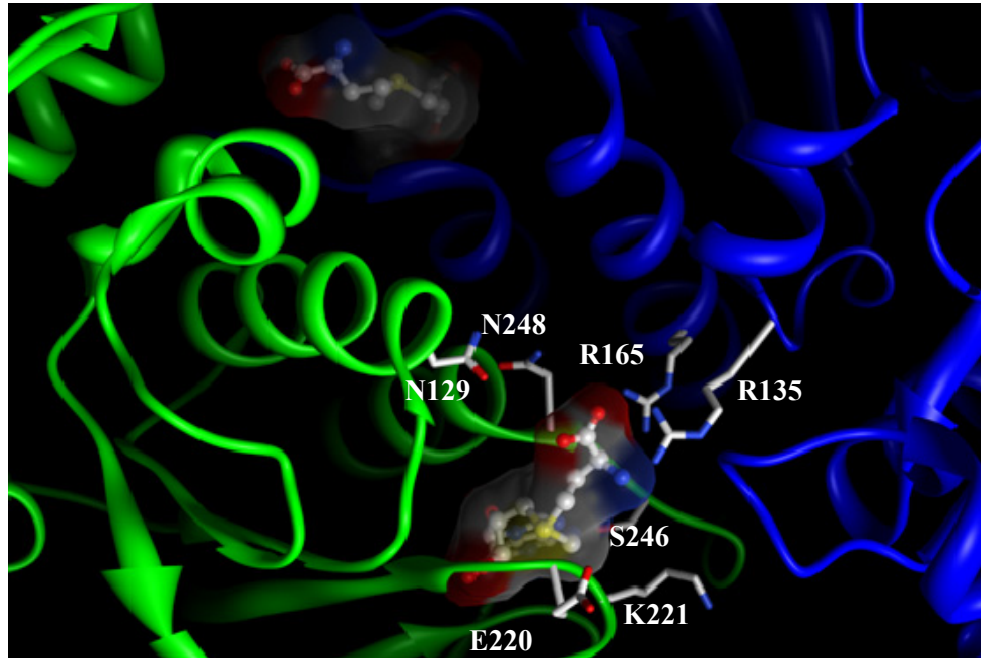
---

### 3.1. Preface

The molecular structure of the thiostrepton-resistance methyltransferase (TSR) bound with AdoMet showed several active site residues in positions that imply important functional roles in enzyme activity. A subsequent report on the molecular structure of the related nosiheptide-resistance methyltransferase (NHR) drew similar conclusions regarding the relevance of equivalent residues. For instance, the mutation of R135 or R165 (TSR numbering) in NHR to alanine resulted in drastic reductions in enzyme activity, indicating the importance of these residues and additional residues of potential significance were similarly identified (171, 262). However, the details on the specific roles of these residues in methyl group transfer were not made clear.

This chapter focuses on clarifying the specific functions of several TSR active site residues. Residues of possible importance were identified according to their proximity and side chain orientation in relation to AdoMet, which could potentially allow for binding interactions or reactions (Figure 3.1). The significance of these residues was determined from comparative enzyme activity assays between the native enzyme and variants featuring engineered point mutations which abolished, conserved or altered the possible structure of the selected amino acid side chains. In addition, the determination of the kinetic

parameters of RNA methylation by these select TSR variants, in conjunction with studies on AdoMet binding, was used to determine which residues played important roles in substrate/co-substrate binding and methyl group transfer.



**Figure 3.1. Potentially relevant amino acid residues in the TSR active site.** Point mutations generated were: N129A, N129D, R135A, R135K, R165A, R165K, E220A, E220Q, K221A, S246A, N248A and N248D. Image was generated from the PDB file 3GYQ using *UCSF Chimera software v. 1.5.2*.

## 3.2. Materials and Methods

### 3.2.1. Chemicals and Reagents

#### 3.2.1.1. PCR and DNA manipulation

DNA polymerase (*Pyrococcus furiosus*) and its buffer (200 mM Tris-HCl (pH 8.8), 100 mM  $(\text{NH}_4)_2\text{SO}_4$ , 100 mM KCl, 1 mg/mL BSA, 20 mM  $\text{MgSO}_4$ , 1% (v/v) Triton X-100), dinucleotide triphosphates (dNTPs; supplied as an aqueous mixture titrated to pH 7.0 with NaOH, containing 10 mM of each base), T4 DNA ligase and its buffer (400 mM Tris-HCl, 100 mM  $\text{MgCl}_2$ , 100 mM

DTT, 5 mM ATP (pH 7.8) and DNA ladders (1kB and 100bp) were from Fermentas (Now ThermoFisherScientific, Ottawa, Canada ). The restriction enzymes *BamHI* and *NdeI* as well as the restriction enzyme buffer NEB3 (100 mM NaCl, 50 mM Tris-HCl, 10 mM MgCl<sub>2</sub>, 1 mM Dithiothreitol, pH 7.9) were obtained from New England Biolabs (Ipswich, USA). All enzymes were used according to the manufacturer's specifications. Oligonucleotide primers for PCRs were synthesized by Sigma (Oakville, Canada).

#### **3.2.1.2 Media**

Bacto-tryptone, imidazole, isopropyl  $\beta$ -D-1-thiogalactopyranoside (IPTG) yeast extract, tris (hydroxymethyl) aminoethane (Tris), potassium chloride and dithiothreitol (DTT) were all from Bioshop (Burlington, Canada). Glycerol and kanamycin sulphate were from EMD Millipore (Toronto, Canada) and ethylenediaminetetraacetic acid (EDTA) from BioBasics Inc. (Markam, Canada).

#### **3.2.1.3. Enzyme substrates**

Ribosomal RNA (16S/23S; *E. coli* MRE600) was supplied by Roche Diagnostics (Laval, Canada) as a 2.67  $\mu$ M solution in a buffer comprised of 10 mM Tris-HCl (pH 7.5), 100 mM NaCl and 1 mM MgCl<sub>2</sub>. This solution was concentrated to prepare 7  $\mu$ M working stock solutions using a Nanosep filtration device with a 30 kDa molecular weight cut-off (Pall Life Sciences).

*S*-Adenosyl-L-methionine (chloride salt) was from Sigma (Oakville, Canada).

### **3.2.2. Equipment**

#### **3.2.2.1 Incubators**

Growth of liquid bacterial cultures was performed in a Series 25 controlled environment incubator shaker (New Brunswick Scientific Co., Inc., Edison, USA). A Precision® gravity convection incubator from Precision Scientific Inc. (Chicago, USA) was used for the growth of plated bacterial cultures.

#### **3.2.2.2. Centrifugation**

Large volume sample ( $\geq 10$  mL) centrifugation was performed with a Beckman Coulter Avanti® JE centrifuge (Fullerton, USA). A Heraeus Biofuge microcentrifuge (Sepatech GmbH, Germany) was used for samples of a volume  $\leq 1.5$  mL.

#### **3.2.2.3. Cell disruption**

Prior to cell lysis, bacterial cell suspensions were sonicated to uniformity using a Sonicator™ cell disruptor model W225 from Heat Systems-Ultrasonics Inc. (Plainview, USA) converter model #2 with a standard tapered microtip, at an output control setting at 5. The cells were lysed using an EmulsiFlex-C5 homogenizer (Avestin, Ottawa, Canada). Ice cooling was utilized to prevent protein denaturation from the heat generated during these procedures.

#### **3.2.2.4. Chromatography**

HisTrap™ HP (1 mL), HiTrap Benzamidine FF™ (1 mL), MonoQ and Supedex-75 columns were all from GE Healthcare (formerly Amersham Biosciences, Uppsala, Sweden). Protein purification was carried out using a

Waters Chromatography system (Waters 626 pump, 600s controller and 2996 photodiode array detector and Millennium 3.20 software). Buffers were prepared using Milli-Q grade water and filtered (0.2  $\mu\text{M}$  membrane filter; Pall Life Sciences, East Hills, USA) and degassed before use. Protein samples were passed through a 0.45  $\mu\text{M}$  cellulose acetate filter (Pall Life Sciences) prior to introduction on to a column.

#### **3.2.2.5. Spectrophotometry**

Absorbance measurements for protein quantification using the Bradford method (263) were performed with an Ultrospec 2100 pro UV/VIS spectrophotometer (GE Healthcare). DNA quantification was carried out using a Nanodrop 2000 spectrophotometer (Thermo Scientific, Ottawa, Canada).

Circular dichroism was performed with a Jasco J715 spectropolarimeter, in the low UV region (190 – 250 nm), with a band width of 1 nm, at a scanning speed of 100 nm/ min. Spectra from 15 scans were averaged. Samples were prepared at 0.16 mg/ mL ( $\sim 2.7 \mu\text{M}$ ) in a buffer comprised of 50 mM Tris (pH 7.5), 150 mM KCl and 10% glycerol (v/v).

#### **3.2.2.6. Fluorescence spectroscopy**

Fluorescence measurements were carried out in black 96 well microplates (Corning Life Science, Tewksbury, USA) using a SpectraMax M5 (Molecular Devices, Downingtown, USA) that was calibrated to an internal standard.

### **3.2.2.7. Isothermal Titration Calorimetry**

Isothermal titration calorimetry was performed with an ITC200 (Microcal, Piscataway, USA) calorimeter and the data analyzed with *Origin* software v. 5.0 (Microcal).

### **3.2.2.8. Mass Spectrometry**

Electrospray ionization mass spectrometry was performed in positive ion mode with a Micromass™ QTOF Ultima Global mass spectrometer (Waters, Millford, USA) and the data processed with MaxEnt software (Waters).

### **3.2.2.9. Polymerase chain reactions (PCR)**

Polymerase chain reactions were carried out with a Techne TC-512 thermal cycler (Keison Products, Chelmsford, UK).

## **3.2.3. General Methods**

### **3.2.3.1. Electrophoresis**

Sized based DNA separation was performed by agarose gel electrophoresis. Agarose gels were prepared by dissolving reagent grade agarose to a final concentration of 1% (w/v), in TAE buffer (40 mM Tris base, 20 mM glacial acetic acid and 1 mM EDTA). A microwave oven was used to completely dissolve the agarose and upon cooling, ethidium bromide was added to a final concentration of 0.5 µg/ mL. This mixture was then poured into a casting tray and allowed to solidify. DNA samples were prepared by mixing with loading buffer (10 mM Tris-HCl, pH 7.5, 50 mM EDTA, 10% glycerol, 0.25% Bromophenol Blue) at a ratio of 5:1 (DNA/ loading buffer). Sample

electrophoresis was performed at 80 volts, in parallel with a 100 bp or 1kb DNA ladder for size estimation after visualization under UV light.

Protein separations were performed by reducing SDS-polyacrylamide gel electrophoresis, using the PhastSystem™ (Pharmacia, now GE Healthcare, Uppsala, Sweden). Samples were mixed with loading buffer (150 mM Tris-OH, 2% SDS, 1%  $\beta$ -mercaptoethanol, 10% glycerol, 0.1% Bromophenol blue pH 8.0) and boiled for 10 minutes before separation. The samples were then applied to precast acrylamide gels with a 10-15% gradient of acrylamide, 112 mM acetate, 112 mM Tris, pH 6.4 and separated using buffer strips containing 0.20 M tricine, 0.20 M Tris, 0.55% SDS, 3% agarose at a pH of 8.1 (gels and buffer strips from Pharmacia). Upon completion of electrophoresis, gels were stained with 0.1% Coomassie brilliant blue G-250 in 30% methanol and 10% acetic acid and the protein bands visualized after destaining in methanol/acetic acid/ ddH<sub>2</sub>O (3:1:6).

### **3.2.3.2. Protein Mass Spectrometry**

Protein samples were prepared for mass spectrometry by exchanging the sample buffer for Milli-Q grade water (5 exchanges, each with 10 volumes of H<sub>2</sub>O) using a Nanosep® centrifugal device (Pall Life Sciences) with a 10 kDa molecular weight cutoff. These samples were then diluted into a 1:1 mixture of acetonitrile/ water with 0.2% formic acid and injected into the mass spectrometer in positive ion mode. Molecular ion spectra were deconvoluted using MaxEnt software.

### **3.2.3.3. Protein Quantification**

Protein concentration was determined by the Bradford assay. The assay dye was prepared by dissolving 100 mg of Coomassie Brilliant Blue G-250 in 50 mL of 95% ethanol, to which 100 mL of 85% phosphoric acid were added. The mixture was diluted to 0.5 L by the addition of ddH<sub>2</sub>O and filtered through Whatman 1 filter paper. Bovine serum albumin (supplied as a lyophilized powder,  $\geq 96\%$  purity; Sigma) was prepared as a 1 mg/mL solution in the assay buffer and then diluted to make standard protein solutions. Standard protein solutions were mixed with 2.5 mL of the assay dye and the absorbance measured at 595 nm to generate a standard curve correlating protein concentration with the absorbance. Sample concentration was thus determined by extrapolation of absorbance readings from the standard curve, after similar treatment as the standards. Samples falling outside the linear range of the standard curve were diluted.

### **3.2.3.4. DNA Manipulation**

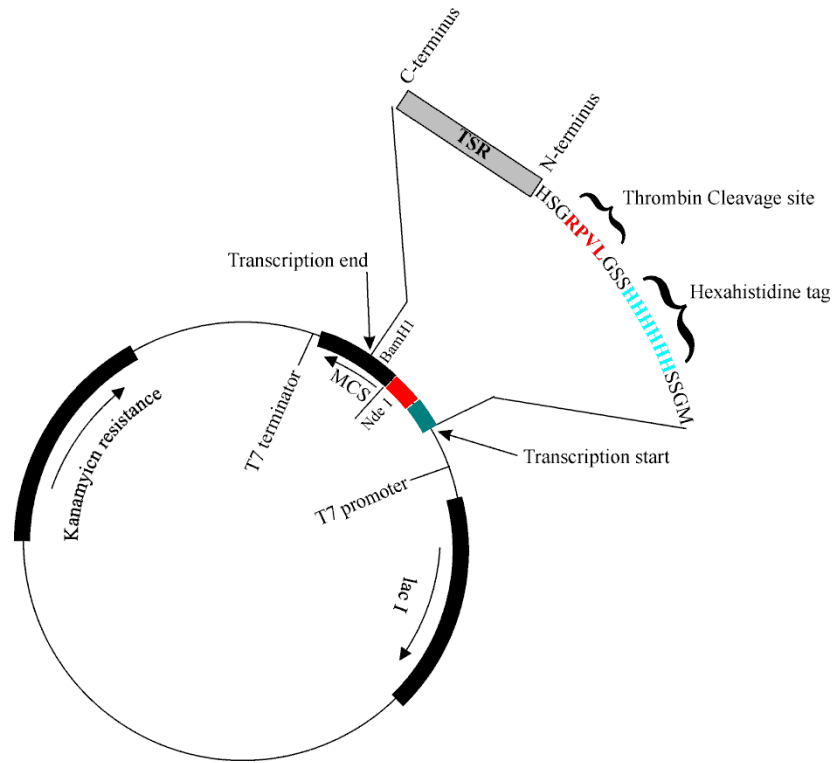
DNA manipulation and cloning were performed in accordance with standard protocols outlined by Sambrook *et al.* (264).

### **3.3.2.5. Site Directed Mutagenesis of TSR**

The TSR gene was previously cloned into the plasmid vector pET28a (172), which appends a DNA sequence encoding 6 histidines to the 5' end of the gene. The hexa-histidine encoding sequence is separated from the TSR gene by a DNA sequence encoding a thrombin protease cleavage site and the entire sequence (hexahistidine-thrombin cleavage site-TSR) is flanked by the T7



promoter and terminator, at the 5' and 3' ends respectively. The protein of interest is therefore expressed with a thrombin cleavage site and 6 histidine residues at its N-terminal end (Figure 3.2).



**Figure 3.2. Schematic of the pET28a plasmid bearing the TSR gene.** The TSR gene is inserted in the multiple cloning site (MCS) between the restriction sites for NdeI and BamHI. Transcription from the indicated starting point leads to the translation of TSR with the thrombin cleavage site and the hexahistidine tag fused to its N-terminus.

**Table 3.1: PCR primers for site directed mutagenesis of TSR**

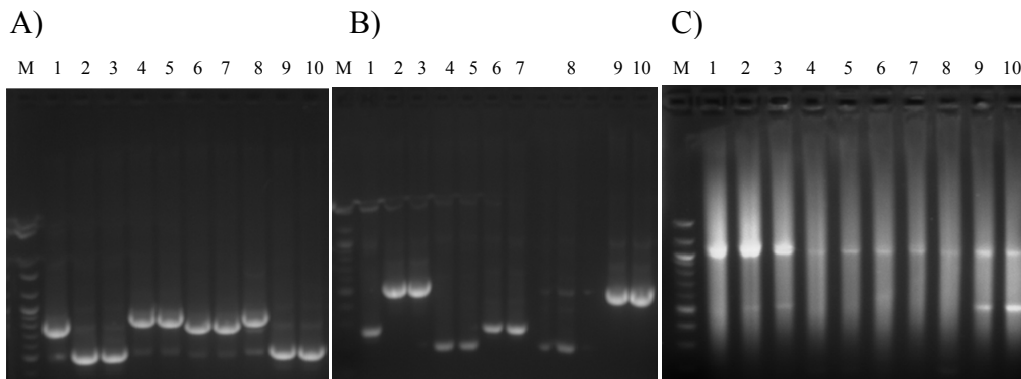
	Forward	Reverse
<b>N129A</b>	ATCGGCGCG ATA GTA CGC ACG TCG	GCG TAC TAT CGC GCC GAT CGC CCC GAC GAT CTT CAC CCC
<b>N129D</b>	ATCGGCGCG ATA GTA CGC ACG TCG	GCG TAC TAT CGC GCC GAT GTC CCC GAC GAT CTT CAC CCC
<b>R135A</b>	ACGTCGCTC GCG CTC GGA GCG TCG	TCC GAG CGC GAG CGA CGT CGC TAC TAT CGC GCC GAT GTT
<b>R135K</b>	ACGTCGCTC GCG CTC GGA GCG TCG	TCC GAG CGC GAG CGA CGT CTT TAC TAT CGC GCC GAT GTT
<b>R165A</b>	ACGTCGCTC GCG CTC GGA GCG TCG	TCC GAG CGC GAG CGA CGT CGC TAC TAT CGC GCC GAT GTT
<b>R165K</b>	ACGTCGCTC GCG CTC GGA GCG TCG	CGC TCC GAG CGC GAG CGA CGT CTT TAC TAT CGC GCC GAT GTT CCC
<b>E220A</b>	AAGGGTGGG CCT TCC GAC CTG TTC	GTC GGA AGG CCC ACC CTT CGC GCT GCC GAA CAG CAA GGC
<b>E220Q</b>	AAGGGTGGG CCT TCC GAC CTG TTC	GTC GGA AGG CCC ACC CTT CTG GCT GCC GAA CAG CAA GGC
<b>K221A</b>	AAGGGTGGG CCT TCC GAC CTG TTC	GTC GGA AGG CCC ACC CTT CGC GCT GCC GAA CAG CAA GGC
<b>S246A</b>	CTCAACGTT TCC GTT TCC CTC GGA	GGA AAC GGA AAC GTT GAG CGC CTC GGT CTG GCT CAT CAT
<b>N248A</b>	GTTTCCGTT TCC CTC GGA ATC GCG	TCC GAG GGA AAC GGA AAC CGC GAG AGA CTC GGT CTG GCT
<b>N248D</b>	GTTTCCGTT TCC CTC GGA ATC GCG	GAT TCC GAG GGA AAC GGA AAC GTC GAG AGA CTC GGT CTG GCT

Oligonucleotides are shown left – right in the 5' – 3' direction

**Table 3.2. Experimental conditions for PCR reactions to generate full length mutant TSR genes**

	Minutes	Temperature (°C)
<b>Initial denaturation</b>	5	95
<b>Hot start</b>		
<i>10 cycles</i>		
Denaturation	2	95
Annealing	1	60 – 50 (reduce by 1° every cycle)
Extension	2.5	72
<b>PAUSE – ADD T7 PRIMERS</b>	5	72
<i>25 cycles</i>		
Denaturation	2	95
Annealing	1	50
Extension	2.5	72
<b>Final Extension</b>	10	72

Reactions were carried out in a total volume of 50 µL and contained 1 unit of polymerase, 2.5 mM of dNTPs, equal concentrations of 5' and 3' gene fragments with the total of DNA not exceeding 100 ng and 10% DMSO (v/v).



**Figure 3.3. Site directed mutagenesis of TSR.** UV-imaged ethidium bromide stained agarose gels containing the products for the first (A) and second (B) PCR reactions and products from the ligation of complementary TSR gene fragments (C). M, 100 bp DNA ladder; 1, E220A; 2, N129D; 3, N129A; 4, N248A; 5, N248D; 6, E220Q; 7, E220A; 8, S246A; 9, R165K; 10, R165A.

Attempts at introducing point mutations into the TSR sequence using the QuickChange site-directed mutagenesis kit (Stratagene, La Jolla, USA) were unsuccessful, therefore the PCR overlap and extension method was employed to effect the desired mutations (265). For each mutant, two primers were designed to allow extension from a region encompassing the targeted codon on the sense and anti-sense strand, when used with the corresponding T7 primer (Table 3.1); essentially creating 5' and 3' gene fragments. Since the mutation-containing primers for the generation of each of these fragments feature a short span of complementarity with each other, the full length mutated TSR gene is produced upon the ligation of these two complementary PCR products, in a reaction utilizing only the T7 primers. High amounts of the mutagenized gene fragments were obtained with standard PCR conditions<sup>3</sup> using a hot start protocol (Figures 3.3A, 3.3B), but initial attempts at the creation of the full length gene were unsuccessful. Various trouble shooting approaches were investigated, including variation of annealing time, gradient PCR and concentration adjustments of the template(s). These alterations brought about slight improvements to the success of fragment ligation, but also revealed that the reaction was sensitive to the relative concentrations of the templates as well as the total DNA concentration. The fragments were eventually annealed by using identical amounts of the templates and adding the T7 primers after 10 cycles of PCR in the absence of the T7 primers. The annealing temperature was successively decreased with each cycle, which allowed the product to form in appreciable amounts prior to

---

<sup>3</sup> 25 cycles, Denaturation: 95°C for 2 minutes; annealing: 50°C for 1 minute; extension: 72°C for 2 minutes.

addition of the T7 primers (Table 3.2, Figure 3.3C). The full length product was excised and purified from the gel (Gel extraction Kit, Qiagen, Toronto, Canada), then doubly digested with *Bam*HI and *Nde*I. This digested product was inserted into pET28a plasmid doubly digested with the same enzymes using T4 DNA ligase (1 unit of T4 ligase per 100 ng of total DNA (vector/ insert (1:3)) to produce plasmids bearing the mutated TSR gene.

#### **3.2.2.6. Expression, Purification & Characterization of TSR Mutants**

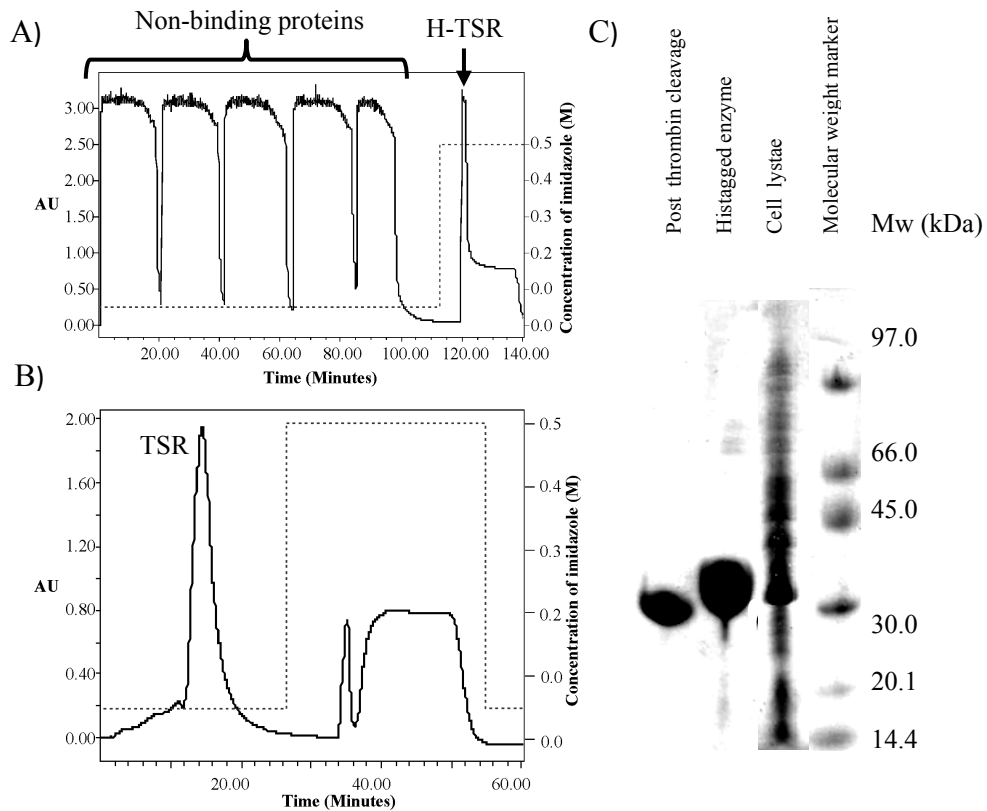
The expression and purification of TSR was performed according to previously established methods (171, 172). Plasmids bearing the TSR gene were used to transform *E. coli* XL1 Blue cells and the transformants selected by kanamycin resistance on nutrient agar plates containing kanamycin at 30 µg/ mL). Plasmids recovered from these cells (Plasmid miniprep Kit, Qiagen,) were used to transform *E. coli* BL21 cells, which were plated onto nutrient agar containing kanamycin (30 µg/ mL). A single colony of these successful transformants was cultured in 1L of Luria-Bertani broth containing kanamycin (30 µg/ mL) and protein expression was induced at the mid-log stage of bacterial growth (O.D. 0.6-0.8) by the addition of IPTG to a final concentration of 1 mM (Figure 3.3). Protein expression was continued for an additional 2 – 4 hours at 30 °C and the cells collected by centrifugation (6000 × g for 15 minutes at 4 °C). Pelleted cells were resuspended in buffer A (50 mM Tris pH 8, 500 mM KCl, 20 mM imidazole and 10% glycerol (v/v)) and sonicated to uniformity (6 cycles of 10 pulses lasting 1-2 seconds each, with cycles

interspersed by 1 minute. Performed on ice<sup>4</sup>), after which cell lysis was completed by liquid homogenization at 15000 – 18000 p.s.i. The cell debris was removed by centrifugation (48,300 × g for 20 minutes at 4 °C) and the soluble proteins injected on to a nickel affinity column attached to a Waters Chromatography System (10 mL/ injection). Non-binding proteins eluted isocratically with buffer A, after which His-tagged TSR was obtained by isocratic elution with buffer B (50 mM Tris pH 8, 500 mM KCl, 500 mM imidazole, 10% glycerol (v/v)) (Figure 3.3). EDTA was immediately added upon elution at a final concentration of 2 mM, and the protein solution dialyzed against 0.5 L of buffer C (50 mM Tris pH 7.5, 150 mM KCl, 10% glycerol (v/v)) for 6 hours, with replacement of the buffer after the first three hours and then overnight against 1L of fresh buffer.

The protein concentration was determined by the Bradford assay, with typical yields between 30 and 40 mg of protein from 5 – 6 g of pelleted cells. The hexa-histidine affinity tag was removed by incubation with thrombin protease (1 unit per 0.1 mg of protein in buffer C, with CaCl<sub>2</sub> added to a final concentration of 2.5 mM, overnight at 4 °C). TSR was obtained by isocratic elution in buffer A, after the introduction of the completed thrombin cleavage reaction mixture to nickel affinity and benzamidine columns attached in series. The purity of the protein was assessed by SDS-PAGE and ESI-mass spectrometry was used to confirm the expected protein molecular mass.

---

<sup>4</sup> Sonication was performed on ice to prevent protein denaturation as this process generates heat.



**Figure 3.4. Overexpression and purification of TSR and its variants in *E. coli*.** (A) Chromatogram showing the separation of His-tagged TSR from cellular proteins by nickel affinity chromatography. (B) Recovery of TSR after thrombin cleavage of the hexahistidine tag (C) Sample SDS-PAGE showing the various stages of TSR purification.

If necessary, an additional purification step of anion exchange chromatography was performed. The protein solution was introduced onto a Mono-Q anion exchanger (GE Healthcare, formerly Pharmacia) and non-binding proteins eluted isocratically in a buffer comprised of 50 mM Tris pH 8, 50 mM KCl and 10% glycerol (v/v). TSR was obtained over a linear increasing gradient of KCl (50 – 500 mM in 100 minutes), eluting between 250-300 mM of KCl. Point mutants were purified in an identical manner as the native protein and their identity was confirmed by ESI-mass spectrometry of the respective

purified proteins as well as by DNA sequencing of the plasmids bearing the corresponding gene.

#### *3.2.2.6.1. Size exclusion chromatography*

Size exclusion chromatography was performed in buffer C, using a Superdex-75 column attached to a Waters chromatography system. A standard solution comprised of blue dextran, bovine serum albumin, carbonic anhydrase and cytochrome c was used for the estimation of sample relative molecular weight.

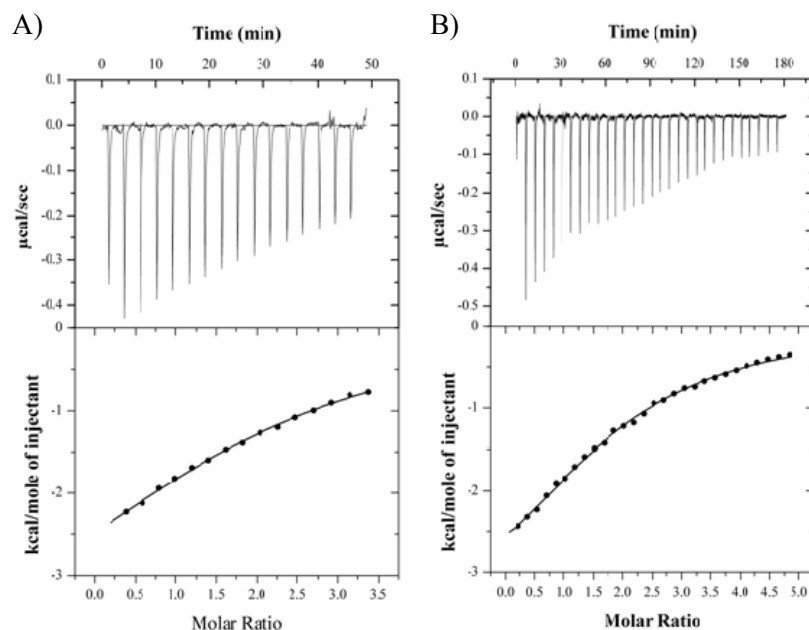
#### **3.2.2.7. RNA methylation by TSR**

The methylation of rRNA by TSR and its point mutants was monitored with a commercially available Methyltransferase Fluorometric Assay Kit (Cayman Chemical Company, Michigan USA), according to the manufacturer's specifications. Fluorescence measurements were performed using an excitation wavelength of 530 nm and emission at 584 nm, with an emission filter at 570 nm and the photomultiplier (gain) set to low. The supplied assay buffer was supplemented with 5 mM MgCl<sub>2</sub> and 25 mM NH<sub>4</sub>Cl and the pH adjusted to 7.5 to satisfy the optimum requirements for TSR activity (168, 172). Activity assays contained 0.35 μM of 16S/23S rRNA, 1mM AdoMet and various concentrations of enzyme, while kinetic assays contained 0.35 μM of 16S/23S rRNA, 0.1 μM of enzyme and concentrations of AdoMet between 0 and 0.5 μM.

### 3.2.2.8. Isothermal Titration Calorimetry

The dissociation constant for the binding of AdoMet to TSR has not been previously measured, hence the experimental parameters were optimized prior to the investigation of the effects of point mutations to TSR-AdoMet binding. Initial experiments used 16 or 20 injections of AdoMet (1mM) into TSR (0.05 mM). From these, the binding stoichiometry was estimated to be 2 from non-linear curve fitting of the integrated heats of injection utilizing the model for a one binding site per subunit model. This coincides with the crystal structure of the TSR-AdoMet complex which found two molecules of AdoMet bound per dimer of enzyme (171). However, this approach did not achieve sufficient coverage of the binding isotherm, which when combined with the inherently low quantity of heat released per injection, contributed to unreliable values for the binding constants. This was not solved by using a higher starting concentration of AdoMet as it was observed that concentrations exceeding 2.5 mM caused an erratic experimental baseline. These problems were remedied by increasing the number of injections to 30, reducing the volume of the injection to 1.25  $\mu$ l from 2.47  $\mu$ l and increasing the duration between injections from 180 to 360 seconds, to allow ample time for the system to re-equilibrate between injections. Figure 3.5 compares the results between ITC experiments utilizing the initial and optimized experimental conditions and it is evident that the latter offers increased coverage of the isotherm, which constitutes reduced errors in the non-linear regression and greater accuracy and reliability in the determined binding constants.





**Figure 3.5. Optimization of ITC experiments for investigation of the binding of AdoMet to TSR.** Titration of AdoMet into TSR using (A) the initial experimental conditions and (B) optimized experimental conditions as described in the text. The top panel shows the raw data after subtraction of the experimental baseline. Bottom panels show the binding isotherm, obtained from non-linear fitting of the integrated heats per injection, fitted to the model for one set of binding sites.

Enzyme used in ITC experiments was dialyzed overnight against 1L of a buffer comprised of 50 mM Tris (pH 7.5), 75 mM KCl and 10% glycerol (v/v). The dialysate was used to freshly prepare working solutions of protein and AdoMet. Titrations were performed at 25 °C and consisted of 30 injections of 1.25 µL of AdoMet (1.98 - 2.50 mM) into a sample cell containing protein solution (0.0822 - 0.098 mM). The heat of dilution/ mixing was obtained from injections of AdoMet into buffer lacking protein. After subtraction of the heats of dilution/ mixing obtained from injections of AdoMet into a cell containing the ITC buffer, titration curves were analyzed using Origin software and the

data fit using the model for one set of binding sites (per subunit) (Please refer to Appendix 4 for a detailed description of the data fitting)

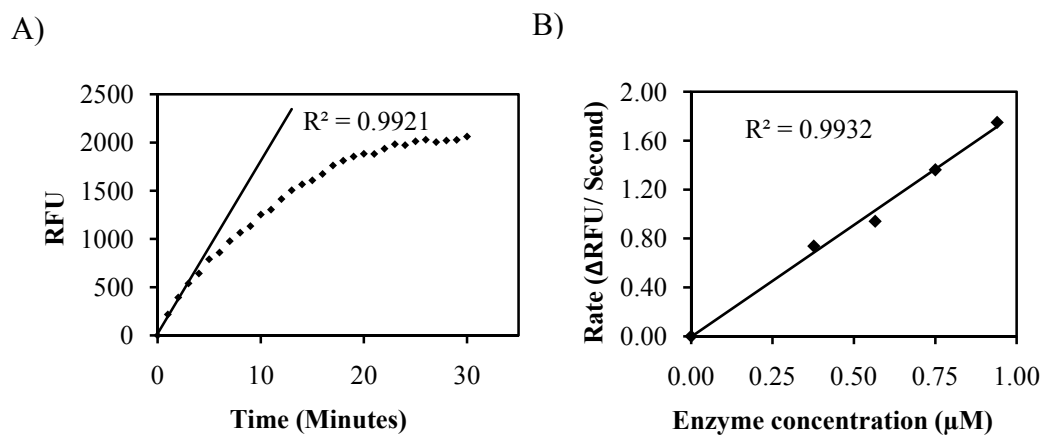
### **3.3. Results & Discussion**

#### **3.3.1. Development of the coupled fluorometric assay**

Ahead of experimental measurements, the suitability of the Methyltransferase Fluorometric Assay kit for determining TSR activity was investigated (266). Examination of an alternate commercially available assay (Assay Designs, Brockville, Canada) revealed several technical problems, particularly an unstable assay background that caused wide variability between replicates. This was attributed to incomplete quenching of the reaction by the prescribed method. A variable background would undoubtedly complicate measurements of enzyme activity where the SAH output would be expected to be low, such as in the lower substrate concentrations required for performing enzyme kinetics or with the assays of TSR variants in which enzyme activity may be reduced. In addition, an unknown AdoMet concentration was included in the reagents from the commercial supplier which prevented the determination of the kinetic constants for enzyme turnover of this substrate. These technical limitations were circumvented with the assay from the Cayman Chemical Company. In its continuous format, this assay removed the requirement for quenching of the enzyme reaction, thereby providing stable, consistent measurements of the assay background. Moreover, AdoMet could be added

exogenously which allowed for the determination of kinetic parameters for its utilization by TSR.

The conditions of the coupled fluorescence assay required additional optimization before being used to monitor the initial rate of AdoMet turnover by TSR. Previous assays of TSR had been performed using enzyme concentrations of 40 – 60 nM (130, 169), therefore exploratory assays were performed with 100 nM of enzyme and monitored continuously for 30 minutes. Fluorescence was observed to increase linearly with time during the first 3 minutes of the assay, indicating this to be the appropriate duration for the calculation of the initial rate (Figure 3.6A). As well, the initial rate of enzyme activity was found to correlate linearly with enzyme concentration up to 1  $\mu$ M (Figure 3.6B).

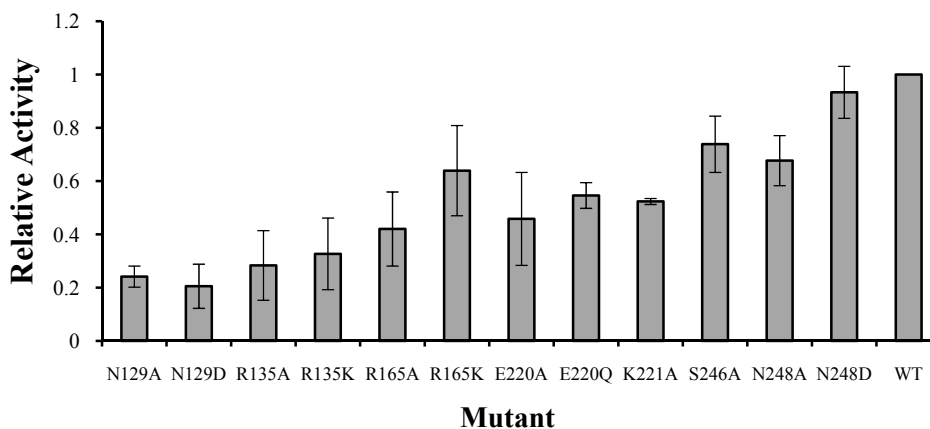


**Figure 3.6. Development of the coupled fluorometric assay for TSR.** (A). Reaction progress curve for TSR activity monitored by the coupled fluorometric assay. Background fluorescence in the absence of enzyme has been subtracted. Assays contained 100 nM of TSR, 1 mM of AdoMet and 0.35  $\mu$ M 16S/ 23S rRNA. Data points are the mean of duplicate experiments. (B). Dependence of initial rate of TSR activity on enzyme concentration in the presence of 1mM of AdoMet and 0.35  $\mu$ M 16S/ 23S rRNA.

### 3.3.2. Effect of point mutations on TSR activity

The molecular structure for TSR has the amino acid residues N129, R135, R165, E220, K221, S246 and N248 within suitable proximity to make potentially important interactions with AdoMet. Point mutations were therefore generated at these sites and the activities of these variants relative to native TSR were assessed using the optimized coupled fluorometric assay. In some cases, different point mutants of the same site were generated in order to probe the chemical significance of these residues in enzyme activity.

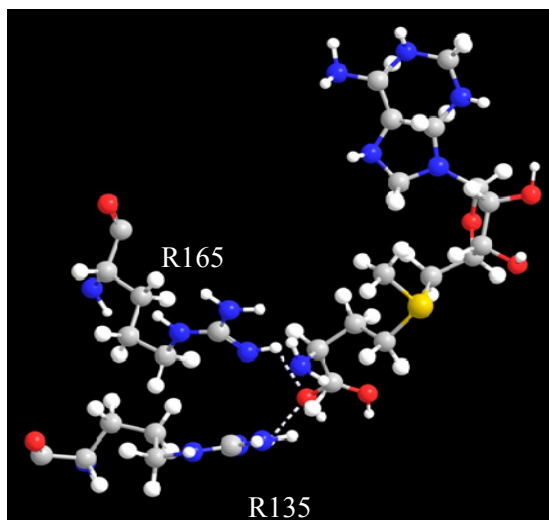
The results of these assays are presented in Figure 3.7 where it can be seen that substitution at N129 had the most deleterious effect on enzyme activity, with both variants exhibiting approximately 20% of the wild type activity. The sensitivity of this residue to mutation may not be surprising given its conserved nature among methyltransferases of this class (262).



**Figure 3.7. Relative activity of point mutants of TSR.** The initial enzymatic reaction rates (rate of SAH formation) by TSR variants relative to that of the native enzyme (WT) are shown. Assays were performed with 100 nM of enzyme, 1 mM of AdoMet and 3.5  $\mu$ M of 16S/ 23S rRNA. Error bars represent the standard deviation of duplicate experiments.

Interestingly, there was no significant difference in activity between N129 variants with alanine or an aspartic acid residue in place of asparagine, despite the contrasting properties that would be exhibited by these respective side chains.

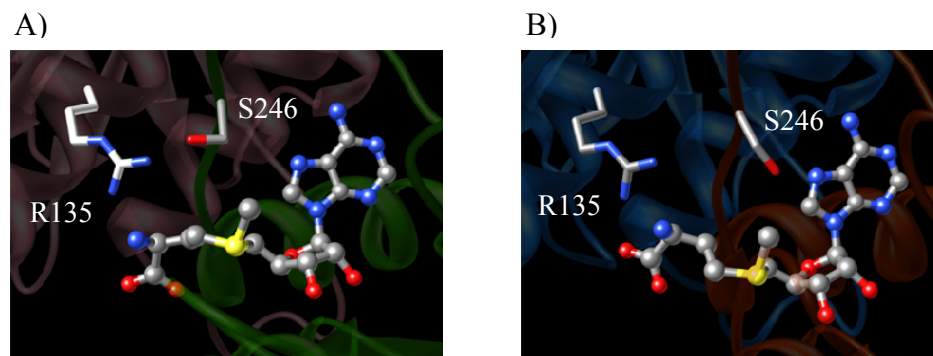
The substitution of alanine for R135 or R165 caused notable reductions in activity, with enzyme activity appearing to be more sensitive to the R135 mutations. This finding matched the reported relative activities of equivalent point mutants of the nosiheptide resistance methyltransferase (262). Unlike that study where only the alanine mutants of R135 and R165 were investigated, lysine substitutions at these sites were generated here. It was found that the R165K mutant displayed markedly higher relative activity than R165A (65% for R165K versus 40% for R165A), while a comparatively lower difference was observed between the R135 mutants (35% for R135K versus 30% for R135A). Both residues are situated in favorable positions for hydrogen bonding with AdoMet (Figure 3.8) and the loss of this capability upon replacement with the non-polar alanine could account for the reduced activity of these mutants. Even so, the lack of significant recovery of activity for the R135K mutant relative to R135A is suggestive of an additional function for this residue, although hydrogen bonding with AdoMet may be the sole function for R165.



**Figure 3.8. Hydrogen bonding between AdoMet and R135 and R165.** Possible hydrogen bonds are depicted as dashed lines between amine hydrogens from R135 and R165 and the oxygen from the carboxylate of AdoMet. The figure was generated using *UCSF Chimera v.1.5.2*.

The catalytic mechanism proposed for the nosiheptide resistance methyltransferase implicates S246 as an active participant in methyl group transfer by hydrogen bonding with R135 which presumably keeps this arginine in position to withdraw a proton from the 2' hydroxyl from RNA (262). No evidence confirming the importance of this residue in TSR activity was found here, as this variant displayed near 80% of the native enzyme's activity. A comparison of the active sites of these two enzymes highlights differences with respect to the orientation of the side chain of S246 and well as AdoMet in their respective active sites. In the catalytic subunit of the nosiheptide resistance methyltransferase, S246 is within hydrogen bonding distance of R135, with the hydroxyl group of S246 pointing towards the guanidino group of R135 (Figure 3.9A). These two residues are further apart in the catalytic subunit of TSR, with

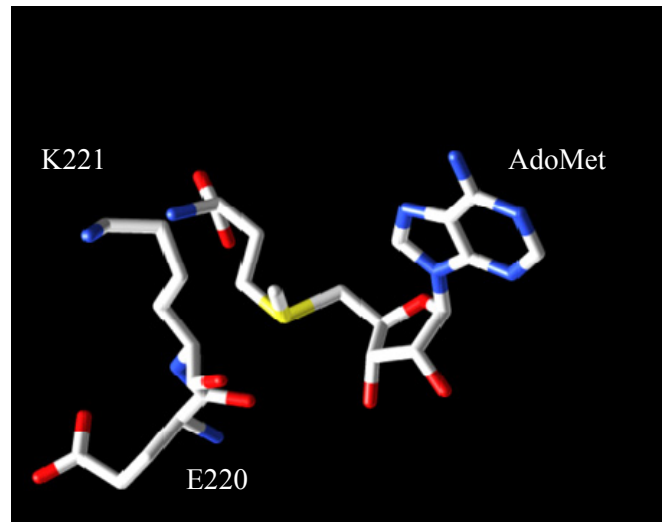
the hydroxyl from S246 pointing away from the side chain of R135 (Figure 3.9B). Such positioning of S246 in the TSR active site would not be conducive to hydrogen bonding with R135, although it is possible that the static crystal structure fails to capture rotational movement of this hydroxyl. In any case, such movement would be of negligible significance for TSR activity (as seen from the activity assays of the S246A mutant) and therefore, S246 is likely not to function in a role analogous to that suggested for NHR.



**Figure 3.9. Orientation of S246 in the active sites of (A) the nosiheptide resistance methyltransferase and (B) TSR**

Noteworthy reductions in enzyme activity were seen for the E220 and K221 variants, with relative activities of approximately half that of the native enzyme. The crystal structure of TSR positions the side chains of E220 and K221 facing away from AdoMet moieties with which they could possibly engage in an interaction (Figure 3.10). Hence, these residues may be important for polar or electrostatic interactions with RNA or secondary interactions with AdoMet that correctly position either substrate in the active site. The N248 variants exhibited 70% and 90% of the wild type activity (N248A and N248D,

respectively), indicating that these residues to be inconsequential with respect to enzyme activity.



**Figure 3.10. Orientation of K221 and E220 with respect to AdoMet in the CTD of TSR.**

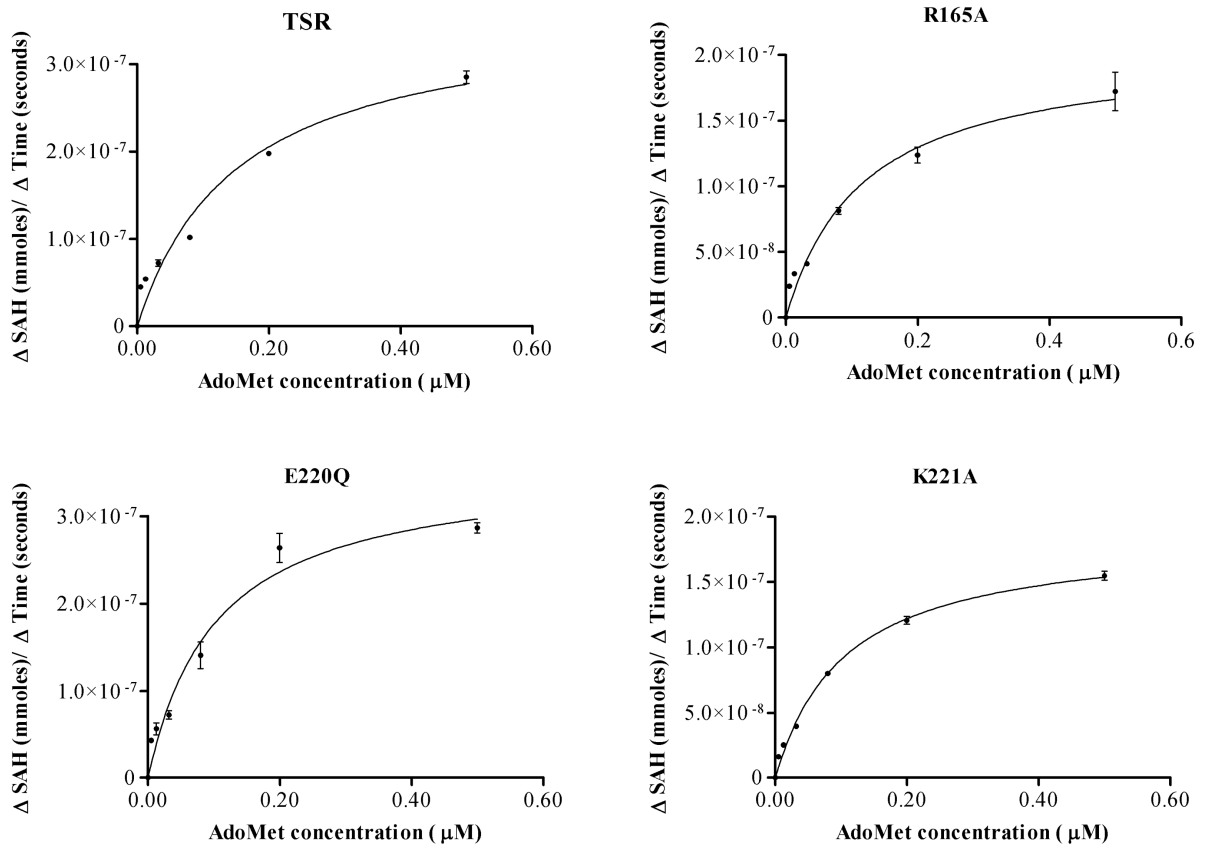
The comparative activity assays of the TSR variants highlighted the importance of N129, R135 and R165 in enzyme function. However, these results were ambiguous as the observed reduction in activity could be due to diminished capacity for AdoMet binding or the loss of the ability to catalyze methyl group transfer. In addition, the possibility of RNA interactions with these residues adds some difficulty to the interpretation of these results. The placement of the N129 side chain in the crystal structure of the native TSR does not imply a direct interaction between N129 and AdoMet, nor does the modeled binding of RNA to TSR suggest an important interaction of N129 with RNA (171). Therefore, the diminished activity of the N129 variants may reflect its importance in either methyl group transfer, or mask a more subtle, indirect



interaction with AdoMet. On the other hand, R135 and R165 are well situated to make electrostatic or hydrogen bonding interactions with the amino or carboxyl groups of AdoMet, yet these residues are also well situated to participate in methyl group transfer. Resolution of these ambiguities was sought by studying the kinetic parameters for AdoMet utilization by a select group of TSR variants, along with parallel AdoMet binding studies.

### **3.3.3. Enzyme Kinetics of AdoMet for TSR Mutants**

Kinetic constants for AdoMet-dependent TSR catalyzed rRNA methylation determined using the coupled fluorometric assay were in agreement with previously reported values for these constants that were obtained using radiometric assays, which validated this assay (differences in the RNA substrate notwithstanding). Michaelis-Menten plots for AdoMet dependent activity of TSR and variants R165A, E220Q and K221A are shown in Figure 3.11 and the kinetic parameters derived from non-linear curve fitting to the Michaelis-Menten equation are presented in Table 3.3 (curve fitting methodologies are described in Appendix 5).



**Figure 3.11. Michaelis-Menten plots for TSR and its variants.** Error bars represent the standard error of the mean from triplicate experiments.

With the exception of N129A and R135A for which kinetic parameters could not be determined under the conditions of the assay, the apparent  $K_m$  for AdoMet remained largely unaffected in the variants assessed. Significant reductions in the apparent maximum velocity ( $V_{max}$ ), turnover number ( $k_{cat}$ ) and substrate specificity ( $k_{cat}/K_m$ ) were, however, noted for R165A and K221A. This pointed towards compromised AdoMet turnover in these variants, which can be taken to signify a role in AdoMet binding.

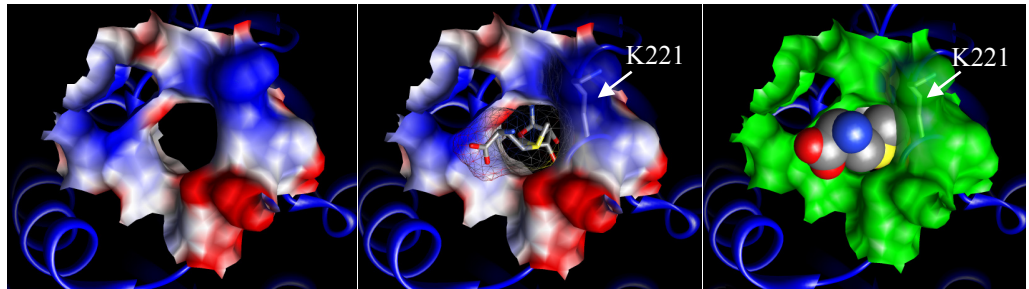
**Table 3.3 Kinetic parameters for enzyme catalyzed RNA methylation by TSR and its variants**

	$K_m$ ( $\mu\text{M}$ )	$V_{max}$ ( $\times 10^{-2}$ ) ( $\mu\text{mol}/\text{min}/\text{mg}$ )	$k_{cat}$ ( $\times 10^{-2}$ ) ( $\text{sec}^{-1}$ )	$k_{cat}/K_m$ ( $\times 10^2$ ) ( $\mu\text{M}^{-1}\text{sec}^{-1}$ )
<b>TSR</b>	155.16 $\pm$ 36	1.87 $\pm$ 0.18	1.81 $\pm$ 0.17	1.16
<i>Reference</i>				
(172)	40.0 $\pm$ 5.0	1.00 $\pm$ 0.1	ND	ND
(168) <sup>†</sup>	100 $\pm$	-	-	-
(169) <sup>‡</sup>	150 $\pm$ 30	-	-	-
<b>N129A</b>	ND	ND	ND	ND
<b>R135A</b>	ND	ND	ND	ND
<b>R165A</b>	116.60 $\pm$ 19.40	1.07 $\pm$ 0.069	1.02 $\pm$ 0.067	0.87
<b>E220Q</b>	102.70 $\pm$ 17.23	1.85 $\pm$ 0.120	1.79 $\pm$ 0.120	1.74
<b>K221A</b>	104.20 $\pm$ 7.78	0.96 $\pm$ 0.026	0.93 $\pm$ 0.025	0.89

For the determination of kinetic values, RNA concentration was kept at 0.35  $\mu\text{M}$ , while the concentration of AdoMet was varied between 0 and 0.4 mM. †: Methylation of total *E. coli* rRNA was assayed. ‡: An RNA fragment containing nucleotides 1029 – 1122 from *E. coli* rRNA was used as a substrate.

The possibility of hydrogen bonding between R165 and AdoMet has been discussed earlier and these findings are in agreement with this. On the other hand, the position of the K221 side chain suggests that this residue is relevant in the formation of the AdoMet binding pocket. As illustrated in Figure 3.12, K221 completes the enclosure of AdoMet in the binding pocket, with the alkyl chain of the lysine R-group facing the methyl group from AdoMet. This

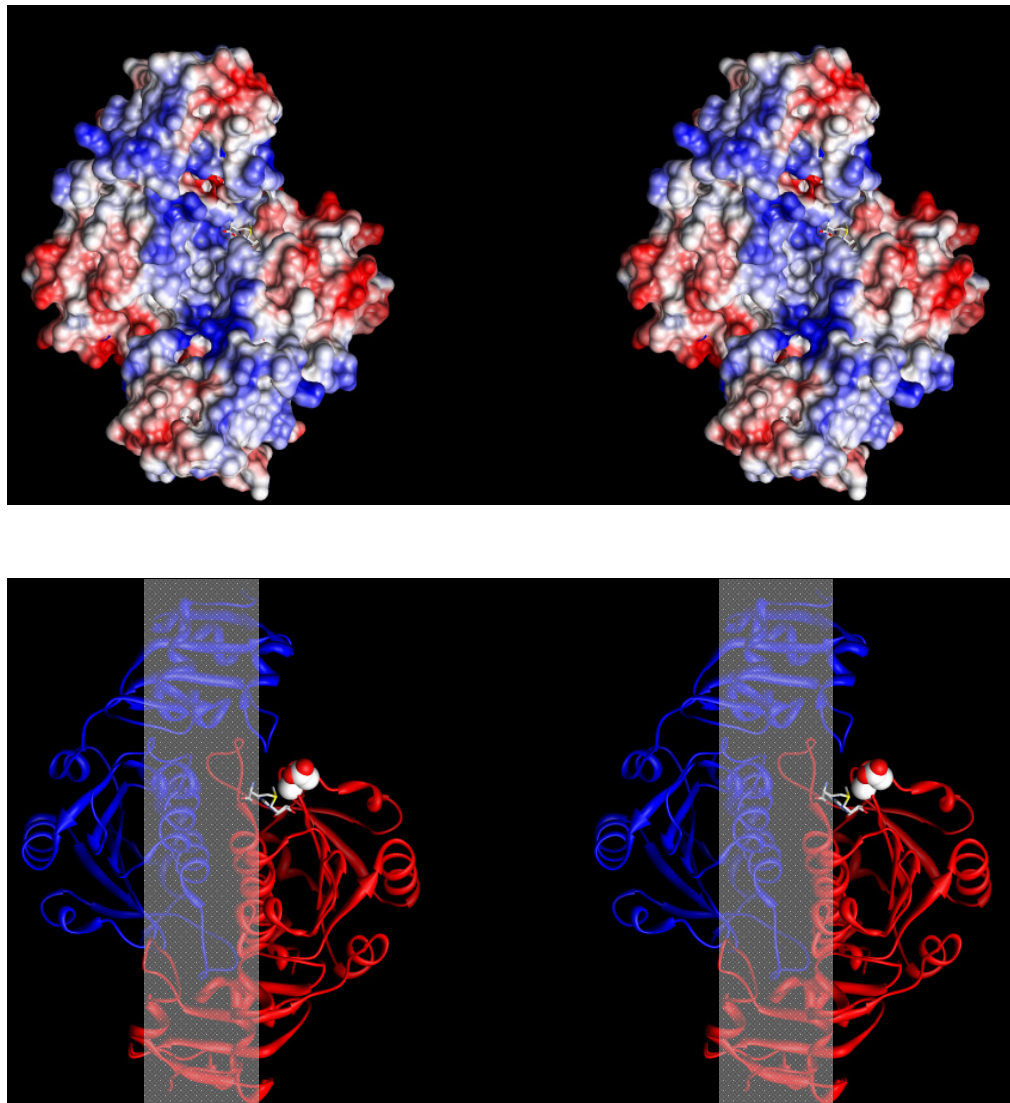
complete enclosure of AdoMet is not likely be achieved by the smaller methyl group from alanine, leading to improper orientation and binding of AdoMet and consequently, the reduced activity observed for the K221A variant.



**Figure 3.12. The importance of K221 in the AdoMet binding pocket of TSR.** (Left) Amino acid residues surrounding AdoMet have been overlaid with an electrostatic surface potential in blue (positive) and red (negative), revealing the AdoMet binding pocket. (Middle) The position of K221 is shown relative to bound AdoMet. (Right) The AdoMet binding pocket is colored in green and AdoMet is shown as a space-filling model. Surfaces were added to the PDB structure file for TSR (3GYQ) using *USCF Chimera v.1.5.2*.

Interestingly, the kinetic parameters for E220Q were unchanged with respect to the native enzyme, in spite of an approximate 50% reduction in activity relative to the native enzyme. The equivalent residue in the nosiheptide resistance methyltransferase has been proposed to stabilize the amine-terminal end of AdoMet (262) and a similar role for this residue has been suggested in TSR (171). Indeed, the carboxyl group of E220 is oriented such that H-bonding or electrostatic interactions between the E220 (side chain) carboxylate and the amine group from AdoMet is conceivable. This may account for the reduced activity of the E220A and E220Q variants, which would present uncharged side chains at the experimental pH, although glutamine may participate in H-bonding or polar interactions. Given the similar levels of reduced activity for these variants, it may be speculated that this loss of activity was due to the absence of

a negative charge at this position. Enzyme kinetic data indicates this to be of little significance with respect to AdoMet, hence, this may reflect the loss of an interaction of this residue with RNA (Figure 3.13).



**Figure 3.13. Possible role of E220 in RNA binding.** Top panel shows a stereo view of TSR dimer mapped with an electrostatic potential surface in blue (positive) and red (negative). Note the stripe of positive charge that spans the length of the molecule, which is believed to be the area of RNA contact (163). In the stereo-view shown in the bottom panel, the subunits of the TSR dimer are depicted as ribbons (catalytic subunit in red and non-catalytic in blue). AdoMet bound to the catalytic subunit has been rendered as sticks and E220 is shown as a space-fill. The proposed region of RNA interaction is shaded gray and encompasses the side chain of E220. Figures were generated from the PDB structure file for TSR (3GYQ) using *UCSF Chimera v.1.5.2*.

### 3.3.4. AdoMet binding in point mutants of TSR

Further clarification of the functional roles played by active site residues of demonstrable importance from the enzyme assays was obtained by studying the binding of AdoMet to TSR variants. The binding stoichiometry remained at 2 molecules of AdoMet per dimer of enzyme, however marked differences in binding affinity were observed (Table 3.4, Fig. 3.14).

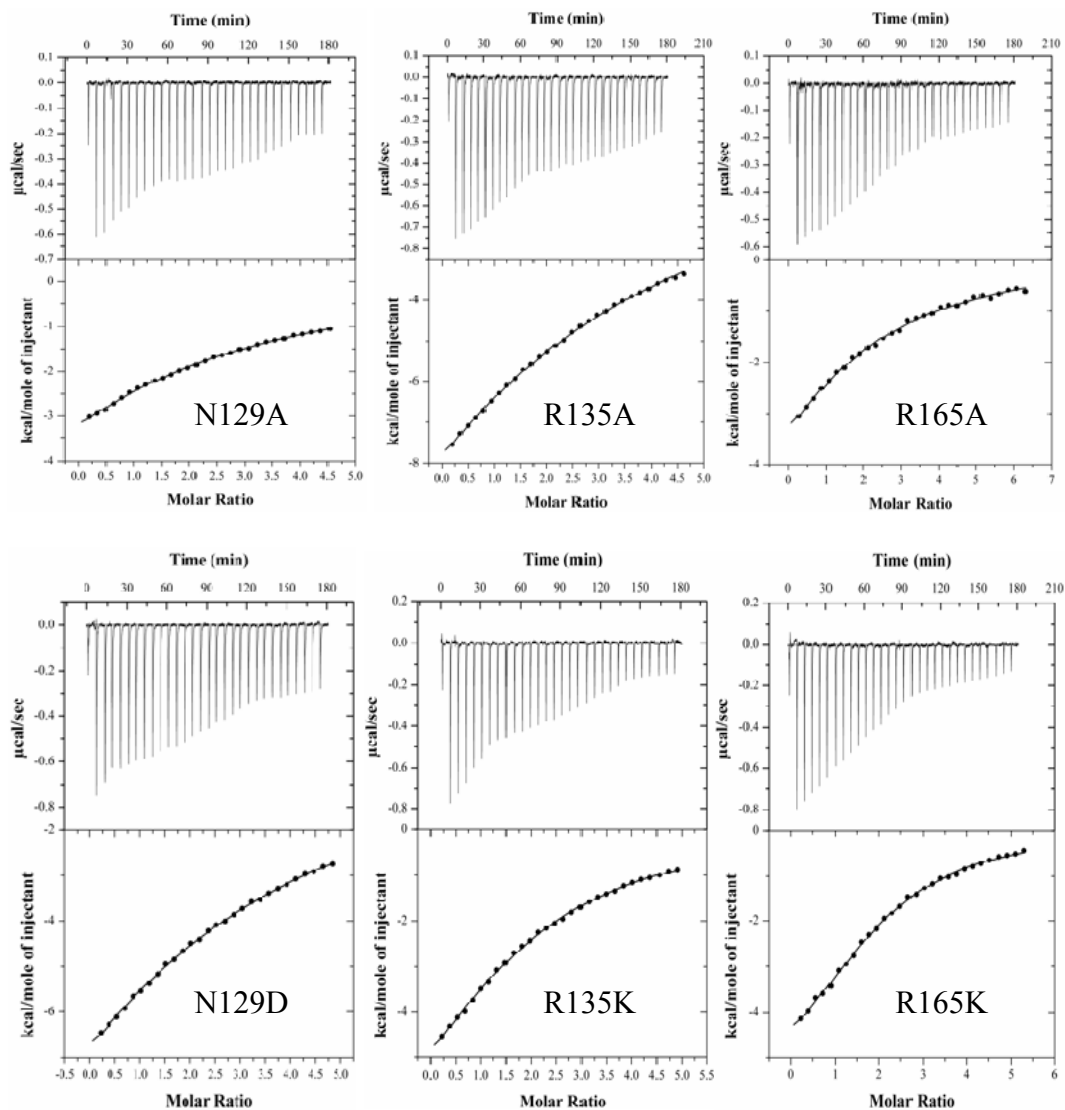
**Table 3.4. Parameters for AdoMet binding to TSR and its variants**

	<b>n</b> (stoichiometry)	<b>K<sub>d</sub> (μM)</b>	<b>ΔH (kcal/ mol)</b>	<b>ΔS (cal.mol<sup>-1</sup>.deg<sup>-1</sup>)</b>
<b>TSR</b>	2.03 ± 0.11	108.21 ± 7.32	-3.96 ± 0.26	4.64 ± 0.76
<b>N129A</b>	1.98 ± 0.30	507.34 ± 92.70	-10.16 ± 1.70	-19.55 ± 0.64
<b>N129D</b>	2.32 ± 0.37	620.00 ± 65.43	-29.75 ± 6.13	-86.75 ± 7.08
<b>R135A</b>	1.98 ± 0.52	894.39 ± 17.18	-72.52 ± 25.39	-233 ± 39.6
<b>R135K</b>	1.89 ± 0.06	147.49 ± 7.94	-9.37 ± 0.43	-14.40 ± 0.42
<b>R165A</b>	1.78 ± 0.15	150.15 ± 11.80	-7.81 ± 1.24	-10.95 ± 2.05
<b>R165K</b>	1.90 ± 0.09	94.29 ± 17.52	-6.60 ± 0.34	-4.07 ± 1.13

Binding constants were determined from non-linear curve fitting using the model for one set of sites, using concentration of enzyme dimer. Errors represent the standard deviation of three replicates, with the errors of individual replicates ≤ 15%.

AdoMet binding affinity was decreased for both N129 mutants, which indicates that the poor relative activity of these variants can be attributed, at least partially, to their diminished AdoMet binding capacity. As earlier stated, the crystal structure of the TSR-AdoMet complex does not indicate a direct interaction between AdoMet and N129, but the replacement of N129 by aspartic acid would introduce a negatively charged carboxylate group in proximity to the carboxylate group from AdoMet. It is therefore plausible that the charge

repulsion between these neighboring negatively charged groups would disrupt AdoMet binding in this variant.

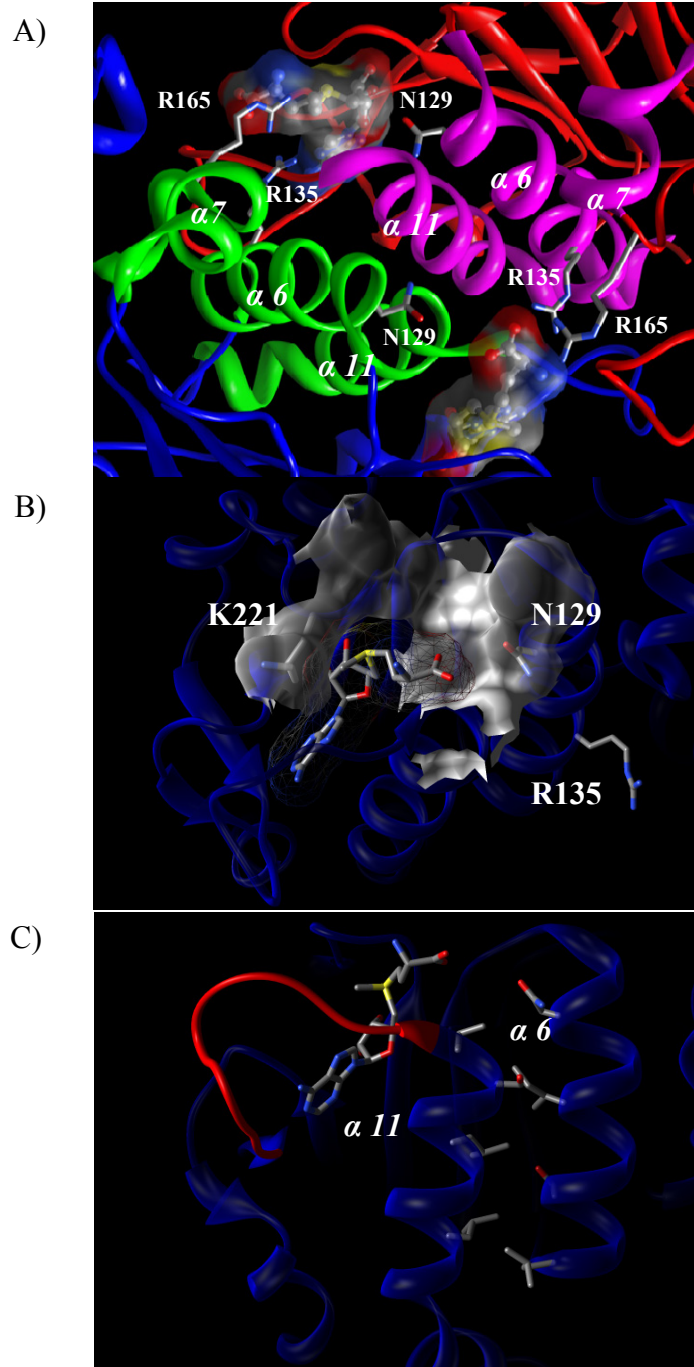


**Fig. 3.14. Measurement of AdoMet binding to point mutants of TSR by isothermal titration calorimetry.** Top panels from each figure show the heat released per injection of AdoMet into a sample cell containing TSR variant. The background heat from the injection of AdoMet into a sample cell containing buffer has been subtracted. Bottom panels show the binding isotherm for the integrated heats/ injection fitted to a model for one set of binding sites.

This explanation does not account for the poor AdoMet binding (and activity) observed for N129A variant. Closer inspection of the TSR crystal structure shows that N129 resides near the end of helix 6 (Figure 3.15A) and both N129 and helix 6 are highly conserved among AdoMet-dependent methyltransferases in this class (189, 191, 267–269). Helix 6 is a pivotal structural feature that is integral to the overall structure of TSR, particularly in the formation of the dimer interface through its interactions with helix 11 (171, 262). Yet, as illustrated in Figure 3.15B, this association between helices 6 and 11, also appears to be important in the formation of the AdoMet binding pocket. Residues at the ends of helices 6 and 11 (including N129) directly contribute a significant area to the binding pocket surrounding the carboxyl end of AdoMet and helix 11 is held in position through extensive hydrophobic contacts along its length with helix 6 (Figure 3.15C). This positioning for helix 11 allows for the formation of the binding pocket surrounding the adenine moiety of AdoMet by residues I238 – L247 (Figure 3.14C). Moreover, R135, demonstrated earlier to be crucial for AdoMet binding and enzyme activity, is also located on helix 6 with its side chain ideally oriented for interactions with AdoMet.

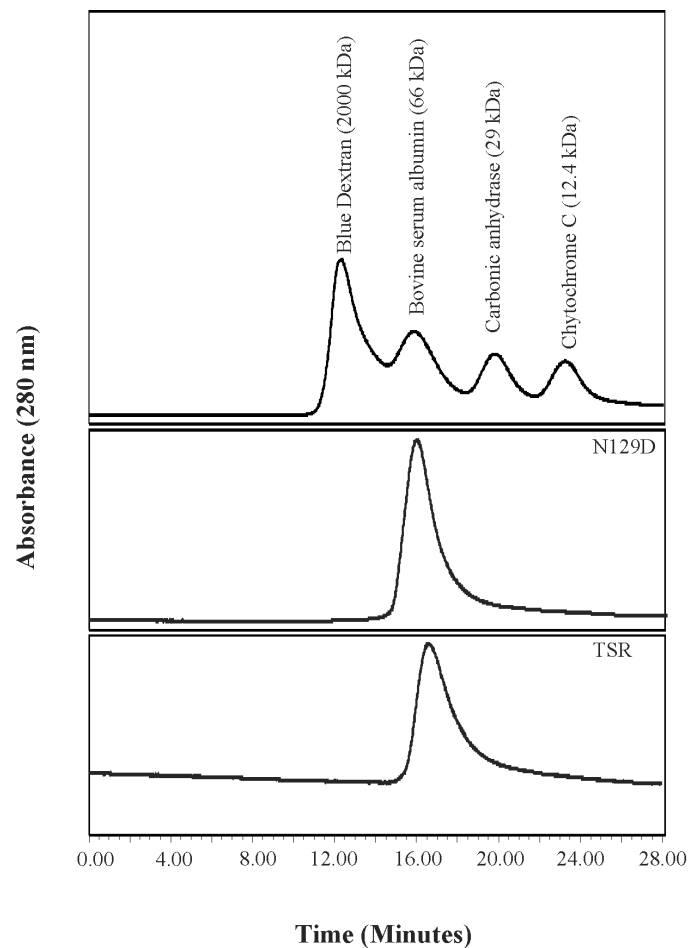
According to the above interpretation, N129 mediates key structural elements that are required for proper AdoMet binding. As such, it could be expected that the effects of an alanine or aspartic acid substitution at N129 would be manifested by observable changes to protein structure, in addition to reduced activity and AdoMet binding affinity.





**Figure 3.15. Importance of N129/ Helix 6 for the AdoMet binding site.** A) The figure centers on the TSR dimer interface, with AdoMet bound in the CTD of each monomer. The catalytic subunit is shown in blue, with helices 6, 7, and 11 in green and the non – catalytic subunit is colored red, with helices 6, 7 and 11 in magenta. Helices have been numbered according to (163). (B) AdoMet binding pocket for the catalytic subunit of TSR. The surface of the binding pocket contributed by V124, I126 ( $\alpha$  6), N129 ( $\alpha$  6), S219, E220, K221, N248 ( $\alpha$  11), V249 ( $\alpha$  11), is colored gray. (C) 90° x-axis rotation of the orientation shown in (B). The adenosine binding loop, consisting of residues 238 – 248, is shown in red. Residues likely involved in hydrophobic interactions between helices 6 and 11 are shown.

Since it has been put forth that N129 is important for the proper formation and positioning of helix 6, an integral feature in the formation of the TSR dimer interface, the mutation of N129 could be reasonably expected to disrupt TSR dimerization. Size exclusion chromatography was thus performed on the N129D variant using conditions known to maintain TSR in its native dimer form (172).

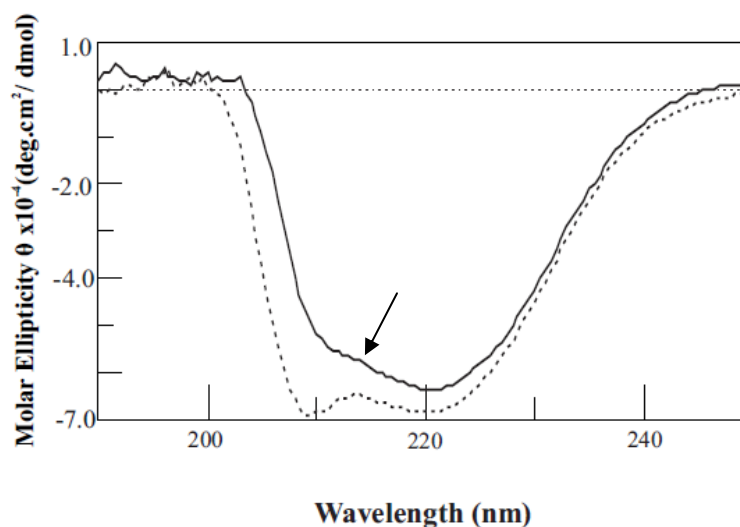


**Figure 3.16. Size exclusion chromatography of TSR and its N129D variant.** Chromatograms show that TSR and the N129D variant both elute after 16 minutes. This corresponds to a relative molecular weight of approximately 65 kDa, which is in agreement with the dimeric molecular weight of TSR (58364 Da). Top panel shows the separation of a standard protein mixture using the identical conditions.

The resultant chromatogram was identical to that obtained from native TSR, indicating subunit dissociation was not responsible for the observed properties of this variant (Figure 3.16).

The hypothesized importance of N129 towards helices 6 and 11 also implies that the effects of an N129 mutation would cause alterations in protein secondary structure. Therefore, the gross secondary structure of the N129D variant was compared to that of native TSR using circular dichroism. In contrast to the results of size exclusion chromatography, the CD spectrum for N129D diverged appreciably from that of native TSR (Figure 3.17). This was indicative of differences in the secondary structure of these two proteins, which by and large appear to be the result of reduced helical content of the N129D variant relative to TSR.

This finding is in agreement with the suggested structural role of N129 and offers some evidence supporting the notion that the formation of  $\alpha$ -helical regions that are critical to AdoMet binding is dependent on N129. Hence, the altered landscape of the binding pocket caused by perturbations to these regions of the enzyme in N129 variants, would result in diminished or eliminated AdoMet stabilizing interactions, with a simultaneous expansion of the internal cavity of the binding pocket. The net effect of these would serve to reduce AdoMet binding affinity and by extension, enzyme activity.



**Figure 3.17. Circular dichroism spectra for TSR and its N129D variant.** Near UV spectra for TSR (dashed line) and its N129D variant are shown. Both proteins are predominantly  $\alpha$ -helical, however secondary structural features differ between the two, as denoted by the shift in the N129D spectra with respect to TSR (indicated by and arrow).

As mentioned earlier, it is believed that the withdrawal of the hydrogen from the 2' hydroxyl of A1067 by a neighboring amino acid promotes the nucleophilic attack on the methyl group from AdoMet that results in RNA methylation. The positions of R135 and R165 relative to AdoMet makes one of these residues a likely candidate to act in this capacity, and indeed, a substitution of alanine at either of these sites caused a reduction in enzyme activity. The comparative effects of alanine and lysine substitutions at these sites showed that binding affinity was virtually unchanged by a substitution to lysine, but alanine mutations caused reduced affinity, particularly at R135. With respect to R165, these differential binding affinities were reflected in the enzyme activity assays, where the relative activity of R165K was greater than that of R165A. Interestingly, although the binding affinity of R135K was similar to that of the native enzyme, both R135 variants exhibited similar

activity (~ 20% activity of the native enzyme). This indicates that R135 is more critical to AdoMet binding than R165, but also offers evidence of an additional important role for this residue.

The reported pKa of the proton from the 2'hydroxyl group on adenosine is approximately 12.0 (270). Therefore, a sufficiently basic side chain, such as that of the guanidino group from arginine (pKa ~12.5(271)), would be required to effect its withdrawal. The pKa of the primary amino group from the lysine side chain is typically 2 units lower than that of arginine (271), hence the low activity of the R135K variant undoubtedly reflects the inability of the lysine side chain to accomplish sufficient proton removal/ polarization. At the same time, although methyl group transfer is impeded with this R135K variant, polar/ electrostatic interactions or hydrogen bonding with AdoMet would be maintained, which would account for an AdoMet binding affinity comparable to that of the native enzyme in this variant.

### **3.4. Conclusions, perspectives and future work**

The factors underlying AdoMet binding and AdoMet dependent RNA methylation by TSR have been investigated. AdoMet binding was also shown to be heavily dependent on an active site asparagine (N129), which appears to be vital for maintaining the structural integrity of the AdoMet binding pocket by facilitating the formation of important secondary structures. Direct interactions between AdoMet R135 and R165 were also shown to be important in AdoMet binding and these interactions most likely take the form of hydrogen bonding

between amine and carboxyl groups from arginine and AdoMet, respectively. As well, the kinetic parameters for AdoMet-dependent TSR catalyzed methyl group transfer have been determined using an adapted and validated fluorometric assay. By determining these kinetic parameters for TSR variants that featured point mutations at key active site residues, in conjunction with AdoMet binding studies, uncertainties in the details surrounding the mechanism of methyl group transfer by TSR have been addressed. It can be concluded that R135 from the non-catalytic subunit acts in a basic capacity, increasing the nucleophilicity of the oxygen from the 2'-hydroxyl on A1067 in rRNA, thus enabling the attack of the methyl group from AdoMet bound in the catalytic subunit of the TSR dimer.

Future work in this area can address the significance of the structurally different subunits in the TSR dimer and related Mtases. The dimeric enzyme was crystallized with AdoMet occupying the binding site of both subunits (171, 262), and the current interpretation of crystallographic data implies that one subunit functions in a catalytic capacity. This can be explored through ligand competition/ displacement experiments aimed at comparing AdoMet affinities between these two sites. Similar studies on TSR composed of sequentially different subunits (hetero-dimers) may prove to be additionally informative.

A greater understanding of the role played by the proposed non-catalytic subunit would be provided from the solution of the structure for the ternary TSR-AdoMet-rRNA complex. Such studies would supply the lacking information on TSR-RNA interactions and would highlight the consequences of

dual substrate binding, which may include cooperative effects. These endeavors may potentially reveal additional mechanistic details of TSR catalysis (sequential versus ping-pong) which may present a more accurate portrayal of *in vivo* processes. In the absence of X-ray derived structures, residue specific labels may be exploited to monitor changes that occur to enzyme secondary structure in combination with biophysical techniques such as NMR or fluorescence. This approach may also aid in the confirmation of the proposed structural importance of N129.

## CHAPTER 4: SYNTHESIS OF A NOVEL AdoMet ANALOGUE AND EVALUATION AS AN AdoMet METHYLTRANSFERASE CO-SUBSTRATE

---

### 4.1. Preface

The transmethylation carried out by AdoMet-dependent methyltransferases (MTases) is not accompanied by an easily assayable physical or chemical characteristic, making the study of the kinetics of these enzymes challenging. This is compounded by the typically low substrate turnover by these enzymes as well as the product inhibition resulting from the accompanying production *S*-adenosyl-L-homocysteine (AdoHcy). Usually, AdoMet containing a radiolabel at the methyl group is utilized in these assays (169, 171). Isolation of the methylated product of the enzyme reaction, usually by chromatography, followed by scintillation counting, yields data which can be utilized to determine Mtase enzyme kinetics. The advent of various assays that couple the degradation of AdoHcy to Mtase activity have circumvented these tedious procedures (see Appendix 6) and provide a continuous assay protocol. However, the utility of such assays to investigate new but uncharacterized Mtases (which represent the vast majority of MTases) may be limited, particularly with respect to substrate identification.

Current intense interest is also being focused in the literature (Chapter 1) on the use of various Mtases to transfer *non-methyl* groups from analogues of AdoMet. These groups have featured chemical moieties that allow subsequent facile conjugation to convenient reporter molecules, enabling substrate-specific



labeling. The development of such analogues has been reported in many recent studies (Chapter 1), however the transfer of these alternative groups has mainly been demonstrated in instances where they are present in stoichiometric amounts, a situation that is likely not conducive to the discovery of unknown substrates. One notable exception to this was the transfer of a ketone group to small molecule substrates by catechol-O-methyltransferase and thiopurine-S-methyltransferase (213). In addition, this keto-AdoMet was used to identify an unknown substrate of TPMT, marking this as one of the few instances where AdoMet analogues have been successfully used to identify a novel MTase substrate.

This chapter describes the synthesis of a novel AdoMet analogue, featuring a fluoroketone group. It was hoped that the presence of a trifluoromethyl group adjacent to the ketone functionality would allow facile chemical modification, as carbonyls adjacent to the CF<sub>3</sub>-group are known to be more electrophilic. In addition to expanding the repertoire of groups transferable by Mtases, the inclusion of fluorine would add an additional capacity for substrate labeling through <sup>19</sup>F NMR. The usability of this analogue with Mtases was assessed with commercially available recombinant human thiopurine methyltransferase, which is known to promiscuously methylate aromatic thiol substrates with a methyl group from AdoMet (272–274).

## **4.2. Material and Methods**

### **4.2.1. Chemicals and Reagents**

S-Adenosyl-L-homocysteine, silver perchlorate, silver p-toluene sulfonate, silver trifluoromethanesulfonate, 3-bromo-1,1,1-trifluoroprop-2-one, 4-nitrobenzenethiol, sodium iodide and potassium iodide were all reagent grade from Sigma (Oakville, Canada). Thiopurine-S-methyltransferase (TMPT; E.C. 2.1.1.67) and adenosylhomocysteine nucleosidase (mTAN; E.C.3.2.2.29) were obtained from G Biosciences (St. Louis, USA). Tris(2-carboxyethyl)phospine (TCEP) was from Thermo Fisher Scientific (Rockford, USA) and monobasic and dibasic potassium phosphate from BioShop (Burlington, Canada).

### **4.2.2. Equipment**

#### **4.2.2.1. Chromatography**

High performance liquid chromatography was performed using a Waters (Millford, USA) Chromatography system (Waters 626 pump, 600s controller and 2996 photodiode array detector and Millennium 3.20 software). Analytical HPLC was performed using a Waters C18 reverse phase column (4  $\mu$ M, 3.9  $\times$  150 mm) and preparative scale purifications were carried out using a Supelco C18 column (5  $\mu$ M, 10  $\times$  250 mm). In all cases, 0.1% aqueous TFA and acetonitrile were the polar and non-polar mobile phases, respectively.

#### **4.2.2.2. Spectrophotometry**

Quantification of AdoMet and the AdoMet analogue was performed spectrophotometrically, using standard curves generated using known concentrations of AdoMet and the reported extinction coefficient of 15, 400

M.cm<sup>-1</sup> at 260 nm (275). Absorbance measurements required for enzyme activity determination were carried out in clear 96-well microplates on a SpectraMax M5 microplate reader (Molecular Devices, Downingtown, USA).

#### **4.2.2.3. Mass spectrometry**

Prior to analysis, samples were diluted into a 1:1 solution of acetonitrile and water containing 0.2% formic acid. Electrospray ionization mass spectrometry was performed in positive ion mode, with a QTOF Ultima Global mass spectrometer (Micromass (Waters)) and the data processed with MaxEnt software (Waters).

#### **4.2.2.4. Gas chromatography**

Samples were prepared as solutions in acetone. Gas chromatography was performed with an Agilent 5975B Inert series Quadropole GC/MS system (Agilent Technologies). Helium was used as the carrier gas for gas chromatography with a 30m DB-1 column (Agilent Technologies) and a temperature gradient of 30°C – 250°C over 30 minutes. On-line electron impact mass spectrometry was performed with an electron energy of 70 eV.

#### **4.2.2.5. Nuclear Magnetic Resonance**

NMR spectra were acquired using either a 500 or 300 MHz spectrometer (Bruker, Milton, ON). Sweep widths were 10.5 ppm and 300 ppm for proton and fluorine nuclei, respectively. AdoMet analogues were prepared at 1-2 mg/mL in D<sub>2</sub>O, while organic samples were prepared in CDCl<sub>3</sub> (3 – 5 mg/ mL).

### 4.2.3. General Methods

#### 4.2.3.1. Synthesis of 3-iodo-1,1,1-trifluoroprop-2-one

Potassium iodide (335 mg, 2 mmoles) was dissolved in 40 mL of distilled methanol. To this solution, 3-bromo-1,1,1-trifluoroprop-2-one (200  $\mu$ L, 2 mmoles) was added and the mixture stirred at room temperature, in the dark for 8 hours, under an inert (argon) atmosphere. The solvent was then removed under vacuum, leaving yellow-brown slurry, to which 30 mL of ddH<sub>2</sub>O was added. This mixture was extracted twice with 30 mL of diethyl ether and the organic layer washed successively with ddH<sub>2</sub>O (2  $\times$  30 mL) followed by washing with 30 mL of a saturated brine solution. The organic layer was then dried over anhydrous sodium sulphate<sup>5</sup>. The solvent was removed under vacuum to leave 312 mg of an oily, yellow-brown liquid which was confirmed by GC-MS to be 3-iodo-1,1,1-trifluoroprop-2-one (75% yield). Further analysis by <sup>1</sup>H and <sup>19</sup>F NMR indicated the compound to exist predominantly as the hydrated ketone. <sup>1</sup>H-NMR (300 MHz in CDCl<sub>3</sub>):  $\delta$  4.099 (s, 2H; ketone), 3.558 (s, 2H; hydrate); <sup>19</sup>F-NMR:  $\delta$  -75.3 (CF<sub>3</sub>- ketone), -84.0 (CF<sub>3</sub>- hydrate). >90% purity by CG-MS.

#### 4.2.3.2. Synthesis of S-adenosyl-S-(1,1,1-trifluoropropan-2-one)-L-methionine (4.1).

To one equivalent of AdoHcy (50 mg, 0.13 mmoles) dissolved in 4 mL of a 1:1 mixture of formic acid/ acetic acid at 0°C under an inert atmosphere, 30

---

<sup>5</sup> Alternatively, the yellow-brown slurry was washed with diethyl ether (3  $\times$  10 mL) and the organic portion retained. The solvent was then removed under vacuum, leaving an oily yellow-brown liquid.

equivalents of 3-bromo-1, 1, 1-trifluoroprop-2-one (405  $\mu\text{L}$ , 3.9 mmol) or 10 equivalents 3-iodo-1,1,1-trifluoroprop-2-one (155  $\mu\text{L}$ , 1.3 mmol) were added in a drop-wise fashion over 5 minutes. To the resulting light brown mixture was added 100  $\mu\text{L}$  of an acetonitrile solution containing one equivalent of silver salt (silver perchlorate ( $\text{AgClO}_4$ ), silver p-toluenesulfonate ( $\text{AgOTs}$ ) or silver trifluoromethanesulfonate ( $\text{AgTf}$ )). The mixture was stirred at  $0^\circ\text{C}$  for 5 minutes, then allowed to warm to room temperature and stirred in the dark for 72 hours. The reaction was quenched by the addition of 10 mL of ddH<sub>2</sub>O and the mixture then filtered through a 0.45  $\mu\text{m}$  nylon membrane to remove the precipitated silver salt. After washing with diethyl ether ( $3 \times 15\text{ mL}$ ), the aqueous layer was retained and lyophilized, leaving a white powder. A portion of the crude reaction mixture (10 mg) was dissolved in 0.1% aqueous TFA (800  $\mu\text{L}$ ) and this solution was passed through a 0.2  $\mu\text{m}$  filter. The filtered solution was then divided into 100  $\mu\text{L}$  aliquots which were stored at  $-80^\circ\text{C}$  or kept on Dry Ice prior to fractionation by semi-preparative HPLC using a C18 resin. Directly upon thawing, a 100  $\mu\text{L}$  aliquot of the crude reaction product was injected onto a C18 column (250  $\times$  100 mm, 5 $\mu\text{m}$ ) and the desired product was obtained using a linear, increasing gradient of acetonitrile (2 – 7% acetonitrile over 10 minutes, then 7 – 15% over 8 minutes, at a flow rate of 5 mL/min). Fractions were collected in vessels that were kept on dry ice and then lyophilized. The concentration of purified analogue was determined from extinction coefficient values for AdoMet/ AdoHyc ( $\epsilon_{260} = 15,400\text{ M}^{-1}\text{ cm}^{-1}$ ).

#### 4.2.3.3. Synthesis of the thiopurine methyltransferase product standard (1,1,1-trifluoro-3-[(4-nitrophenyl)thio]propane-2-one) (4.3)

4-Nitro-benzenethiol (87 mg, 0.56 mmoles) was dissolved in 3.5 mL of anhydrous tetrahydrofuran (Sigma Aldrich) under an inert (argon) atmosphere. Triethylamine (100  $\mu$ L, 0.72 mmoles) was added and the solution stirred at ambient temperature for 10 minutes. 3-Bromo-1, 1, 1-trifluoroprop-2-one (100  $\mu$ L, 0.96 mmoles) was then added, and the mixture stirred for an additional 4 hours. The reaction was quenched by the addition of 4 ml of saturated  $\text{NH}_4\text{Cl}$  and then washed with ethyl acetate ( $3 \times 15\text{mL}$ ). The organic layer was dried over  $\text{MgSO}_4$  and then purified by silica gel chromatography (0-40% ethyl acetate in hexane). Fractions containing the desired product were identified by thin layer chromatography and these were pooled and the solvent removed under vacuum to give 60.5 mg (38%) of a yellow powder.  $^{19}\text{F}$  NMR analysis indicated the product to be predominantly the hydrated ketone. m.p.: 70 – 74  $^\circ\text{C}$ ,  $R_f$ : 0.35 (Ethyl acetate/ hexane, 2:3).  $^1\text{H}$ -NMR (300 MHz in  $\text{CDCl}_3$ ):  $\delta$  8.15 (s, 1H), 8.13 (s, 1H), 7.56 (s, 1H), 7.53 (s, 1H), 3.58 (s, 1H), 3.45 (s, 1H);  $^{13}\text{C}$ -NMR:  $\delta$  147.02, 144.03, 131.15, 126.42, 124.62, 124.43, 29.67;  $^{19}\text{F}$ -NMR:  $\delta$ : 79.5 ( $\text{CF}_3$ -ketone), -84.8 ( $\text{CF}_3$ -hydrate). HRMS calculated for [ $\text{C}_9\text{H}_8\text{F}_3\text{NO}_4\text{S} + \text{H}^+$ ]: 284.020, found 284.003.

#### 4.2.3.4. TPMT activity assay

##### *Coupled spectrophotometric assay*

Spectrophotometric assays of TPMT activity were performed by monitoring the reduction in absorbance at 411 nm, which corresponds to the

disappearance of the 4-nitrobenzenethiol substrate, according to Lee *et al.* (213). Assays were performed in clear 96-well plates (Greiner Bio-One, Monroe, USA) and each 100  $\mu$ L reaction consisted of 200 mM potassium phosphate (pH 8), 2 mM TCEP, 1  $\mu$ M mTAN, 50  $\mu$ M 4-nitrobenzenethiol and 50  $\mu$ M of AdoMet and 100  $\mu$ M of **4.2**. Reactions were initiated by the addition of the enzyme TPMT at various concentrations (0.5  $\mu$ M, 1.0  $\mu$ M, 6.0  $\mu$ M) and monitored continuously for 30 minutes. Control reactions contained no enzyme. After 30 minutes, the reaction mixtures were subjected to analytical HPLC with a Waters  $\mu$ Bondapak C18 column (4  $\mu$ m, 3.9 x 150 mm). The polar and non-polar mobile phases were 0.1% TFA in water and acetonitrile, respectively and the products were eluted with the following conditions: 40% acetonitrile for 5 minutes, then a linear increase to 60% acetonitrile over 15 minutes, a hold at 60% acetonitrile for 5 minutes and then a return to 45% acetonitrile over 5 minutes.

#### *Coupled fluorometric assay*

Fluorometric assays of TPMT activity were performed with the Methyltransferase Fluorometric Assay Kit (Cayman Chemical Company, Ann Arbor, USA), according to the manufacturer's specifications, in black 96-well microplates (Corning Life Sciences, Tewksbury, USA). Reactions (200  $\mu$ L) contained 50  $\mu$ M of AdoMet or 100  $\mu$ M of AdoMet analogue, 50  $\mu$ M of 4-nitrothiophenol and varying concentrations of TPMT.

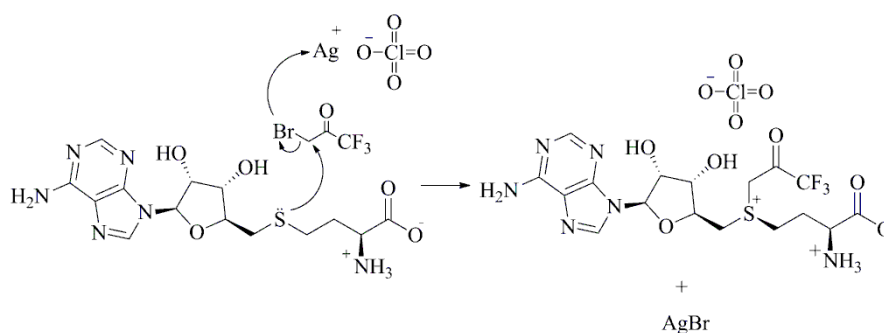
#### 4.2.3.5. Competition assays

Fluorometric assays of TPMT catalyzed methylation of 4-nitrothiobenzene were performed as previously described, each containing 50  $\mu\text{M}$  of AdoMet in the presence of varying concentrations of fluoroketo-AdoMet.

### 4.3 Results and Discussion

#### 4.3.1 Synthesis of S-adenosyl-S-(1,1,1-trifluoropropan-2-one)-L-methionine (4.1)

Attempts at obtaining **4.1** utilizing a synthetic method that was reported successful in synthesizing the non-fluorinated parent compound as described by Lee *et al.* (213) did not result in the desired novel fluorinated product. Therefore,  $\text{AgClO}_4$  was utilized to drive the alkylation of the sulfur atom of AdoHcy with the 3,3,3-trifluoromethyl-2-propanone group through the formation of silver bromide (Figure 4.1).



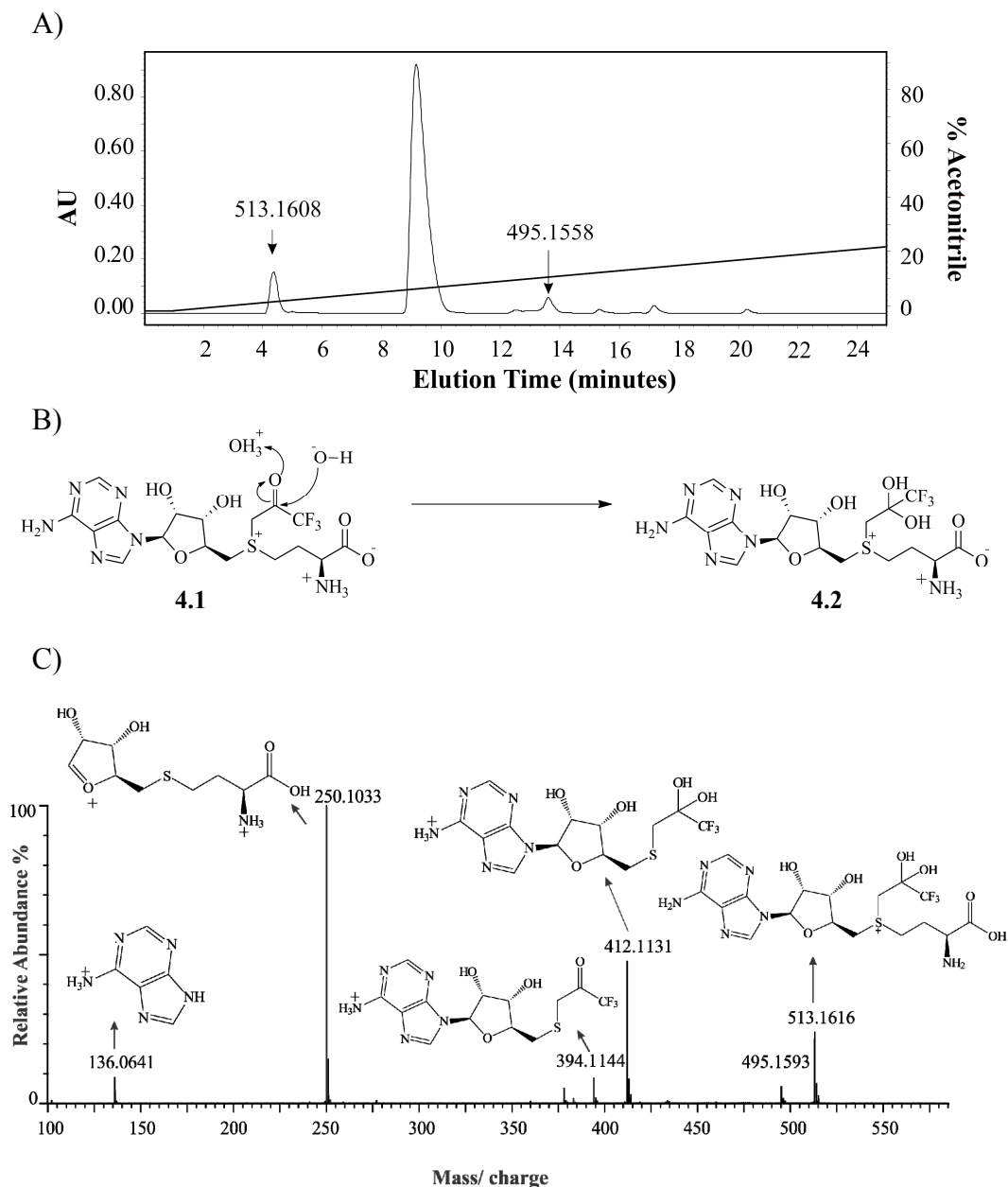
**Figure 4.1. Mechanism for the formation of S-adenosyl-L-(1,1,1-trifluoropropan-2-one)-L-methionine.**

After 24 hours, analysis of the analytical HPLC and ESI-MS data on the reaction mixture indicated the formation of two products having masses of

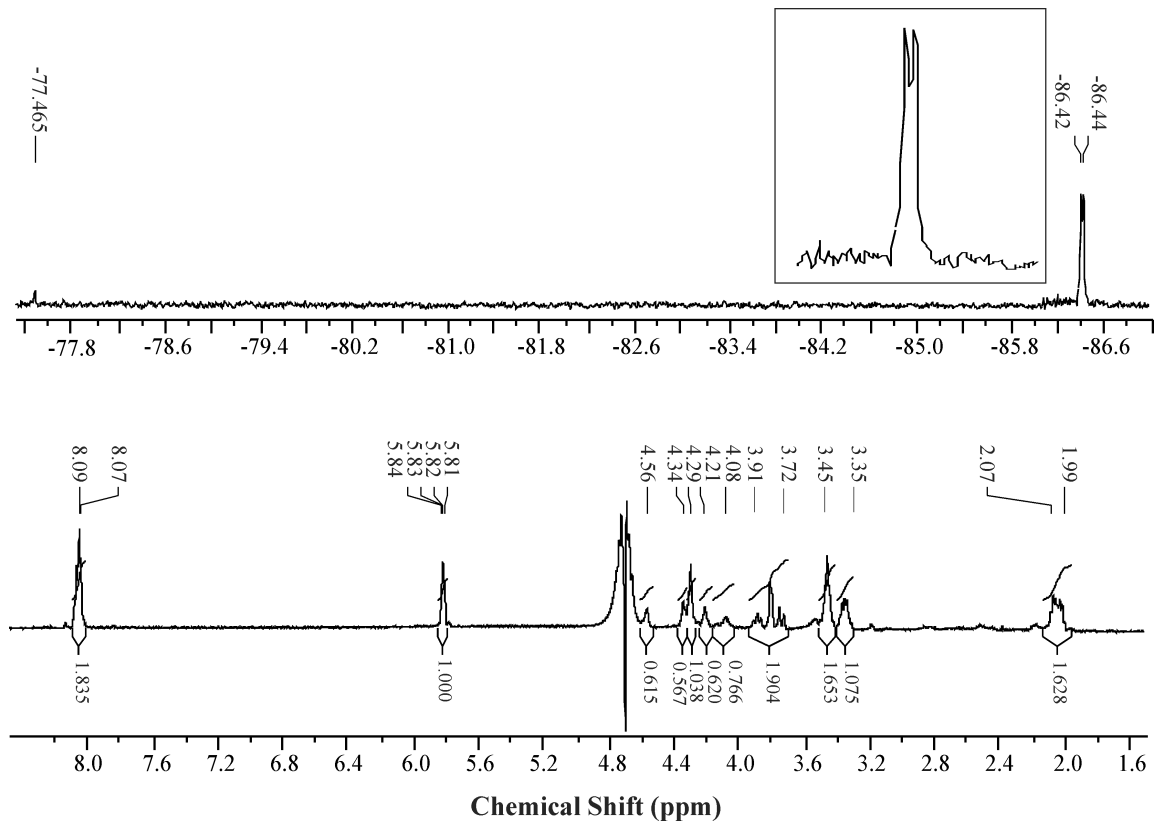


495.16 Da and 513.16 Da that eluted at 4.2 minutes and 12.5 minutes respectively. These were consistent with the addition of the trifluoroacetone group to AdoHcy; the compound of  $M_w$  513.16 being the hydrated ketone form (**4.2**) of the desired analogue (Fig. 4.2B). Together, these products represented ~10% of the total reaction products, with the suspected hydrated ketone form predominating (Fig. 4.2A). Comparison of fragment ion mass spectra for this product with spectra reported for a methyl-ketone AdoMet (213) derivative revealed a similar ion fragmentation pattern (Fig. 4.2C) and final confirmation of product identity and structure was obtained with NMR analyses.

The  $^{19}\text{F}$  NMR spectrum for **4.2** (Fig. 4.3A) showed two peaks of roughly equal intensity at -86.42 and -86.44 ppm and a minor peak at -77.46 ppm. These were in agreement with predicted  $^{19}\text{F}$  chemical shifts of the fluorines from the hydrated ketone (-80.68) and ketone (-77.47) forms of the desired derivative (ACD/ I-Lab NMR predictor). The addition of 1,1,1-trifluoroprop-2-diol to the sulfide of SAH generates a chiral sulfonium centre, therefore the peaks at -86.42 and -86.44 ppm correspond to the  $-\text{CF}_3$  fluorines from each of the diastereomers. This was analogous to  $^1\text{H}$  spectra for the methylketone AdoMet analogue prepared by Lee and coworkers (213), where two methyl group chemical shifts were in evidence, corresponding to the stereo-isomers at the chiral sulfonium centre. These researchers did not report the presence of a hydrated ketone form of their derivative, however, the trifluoromethyl group in the derivative described here increases the electrophilicity of the carbonyl carbon, which shifts the equilibrium in favor of the hydrate formation (276–278).



**Figure 4.2. Purification of the fluoroketo-AdoMet analogue.** A) HPLC chromatogram showing the products from the reaction of 3-bromo-1,1,1-trifluoroacetone with AdoHcy, in the presence of  $\text{AgClO}_4$ . The product eluting after 4.2 minutes was found to have a mass of 513.1608, which corresponds to the hydrated ketone form of the desired derivative. (B) Formation of S-adenosyl-S-(1,1,1-trifluoropropan-2-diol)-L-methionine (**4.2**) in aqueous conditions. (C) Tandem mass spectra for the product eluting after 4.2 minutes. The structure of observed fragment ions are shown. The fragmentation pattern is similar to that of the propan-2-one AdoMet derivative obtained by Lee and coworkers and is consistent with the proposed compound of mass 513.16.



**Figure 4.3. NMR characterization of the fluoroketo-AdoMet analogue.** Top trace:  $^{19}\text{F}$  spectrum of the product eluting after 4.2 minutes. The inset zooms in on the peaks at -86.42 and -86.44, which correspond to  $-\text{CF}_3$  fluorines from the two stereo-isomers of the hydrated ketone form of the derivative. The peak at -77.465 is attributed to  $-\text{CF}_3$  fluorines from the ketone form of the derivative; the stereo-isomers were unresolved due to the low intensity of these signals. Bottom trace:  $^1\text{H}$  spectrum of the fluoroketo-AdoMet analogue.

$^1\text{H-NMR}$  (500 MHz,  $\text{D}_2\text{O}$ ):  $\delta$  8.09-8.06 (m, 2H, aromatic), 5.82 (q, 1H, H1'), 4.56 (m, 1H, H1'), 4.34 (t, 1H, H3'), 4.29 (m, 1H, H4'), 4.21 (m, 1H), 4.08 (m, 1H), 3.91-3.72 (m, 2H, H5'), 3.45 (t, 2H, H $\lambda$ ), 3.35 (t, 1H, H $\alpha$ ), 2.07-1.99 (m, 2H, H $\beta$ ).  $^{19}\text{F-NMR}$ :  $\delta$  -77.46 (ketone), -86.42, -86.44 (hydrate). ESI- HRMS (calculated):  $\text{C}_{17}\text{H}_{24}\text{N}_6\text{O}_7\text{F}_3\text{S}$  (s-adenosyl-S-(1,1,1-trifluoropropan-2-diol)-L-methionine); 513.1359 (513.1379),  $\text{C}_{17}\text{H}_{22}\text{N}_6\text{O}_6\text{F}_3\text{S}$  (s-adenosyl-S-(1,1,1-trifluoropropan-2-one)-L-methionine); 495.1290 (495.1274). MSMS: adenine +  $\text{H}^+$ ; 136.0641 (136.0618), s-ribosylhomocysteine +  $\text{H}^+$ ; 250.1033 (250.0744), 5'-(1,1,1-trifluoropropan-2-one)-thio-5'deoxyadenosine +  $\text{H}^+$ ; 394.1144 (394.0791), 5'(1,1,1-trifluoropropan-2-diol)-thio-5'deoxyadenosine +  $\text{H}^+$ ; 412.1131 (412.0897), s-adenosyl-S-(1,1,1-trifluoropropan-2-one)-L-methionine; 495.1593 (495.1268).

### 4.3.2 Optimization of reaction conditions for the synthesis of 4.1

Obtaining preparative amounts of the desired AdoMet analogue presented several challenges. The poor synthetic yield was compounded by the apparent decomposition of the desired product, which occurred in a manner similar to that described for AdoMet (279–283). As a result, attempts were made to improve the overall product yield and alternative routes to the synthesis of the AdoMet analogue were explored.

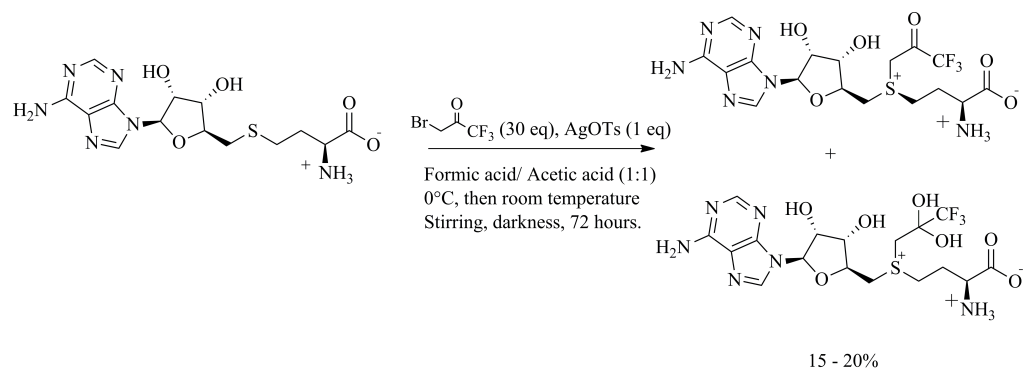
#### 4.3.2.1. General conditions

In the initial reactions conditions, solid granules of  $\text{AgClO}_4$  were added to a stirring solution of AdoHcy and 3-bromo-1,1,1-trifluoroactone in a mixture

of formic acid and acetic acid. It was observed that the silver salt did not readily dissolve in this solvent, hence  $\text{AgClO}_4$  was subsequently added as a solution prepared in a minimum volume of acetonitrile. This, in addition to extending the reaction time to 72 hours improved the yield to 15-20%. Reactions allowed to progress beyond this time suffered from extensive decomposition of both the starting material and product (determined by HPLC/ MS analyses).

#### **4.3.2.2 . Silver salts**

AdoMet stability is improved by the presence of halide or tosylate counterions to the sulfonium centre (284, 285). The reaction was therefore performed with silver tosylate ( $\text{AgOTs}$ ) or silver triflate ( $\text{AgOTf}$ ), with a view towards improving product stability and consequently, the net yield of viable product. The use of  $\text{AgOTs}$  improved the combined yield of **4.1** and **4.2** to ~ 20%, with **4.2** as the major product. This reagent also appeared to improve product stability prior to HPLC purification. Silver triflate was found to be an unsuitable reagent, resulting in a product of molecular weight 527.13 Da, consistent with the addition of the fluoroketone group to the sulfone of AdoHcy. Increasing the proportionate amount of silver salt did not cause a noticeable improvement to product yield, but further complicated product purification due to the formation of acetonitrile-silver complexes as well as SAH-silver complexes that co-eluted with the desired product. These optimizations culminated in Scheme 4.1.



**Scheme 4.1. Optimized conditions for the synthesis of trifluoromethyl ketone derivatives of AdoMet.**

#### 4.3.2.3. Synthesis of 3-iodo-1,1,1-trifluoroprop-2-one (4.3) and its reaction with AdoHcy.

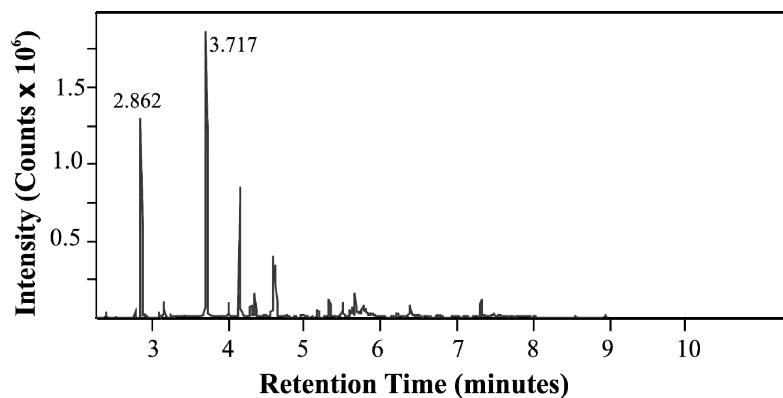
The susceptibility of  $\alpha$ -haloketones to nucleophilic attack at the  $\alpha$  position proceeds in the direction  $I > Br > Cl > F$ , with iodine containing compounds being most susceptible (286). It therefore follows that the use of 3-iodo-1,1,1-trifluoroprop-2-one would achieve a greater extent of addition of the trifluoro-propanone/ propan-2-diol group to AdoHcy, than 3-bromo-1,1,1-trifluoroprop-2-one. Similar approaches have been used by Coward and others to obtain fair to moderate yields of sulfonium salts of 5' substituted adenosines as well as AdoMet derived sulfonium salts through methylation of the corresponding sulfide with methyl iodide (287–289).

The conversion of 3-bromo-1,1,1-trifluoroprop-2-one was initially attempted using conventional Finkelstein reaction conditions<sup>6</sup>, but conversion into 3-iodo-1,1,1-trifluoro propan-2-one by this method did not exceed 35% (Figure 4.4). This was not improved by extending the reaction duration, increasing temperature or reflux conditions. On the contrary, these alterations served to increase the production of undesired side products, which complicated chromatographic purification of the target compound.

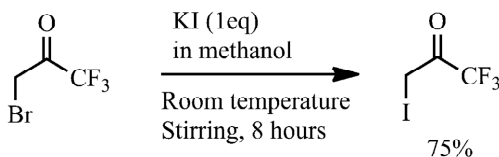
Although the Finkelstein reaction is widely believed to be an equilibrium process and driven by the formation of insoluble NaBr, high yielding halogen transfers have been accomplished using potassium iodide without the precipitation of KBr. Hence, the replacement of bromine with iodine was attempted with KI in acetonitrile, ethanol or methanol (Scheme 4.2). It was found that KI in methanol resulted in > 90% conversion (by GC/ MS) of the bromoketone, with negligible side products, giving the desired iodoketone in 60-75% yield (Fig. 4.5). The high purity of the obtained 3-iodo-trifluoro-1,1,1-prop-2-one removed the requirement for purification and the addition of the trifluoropropan-2-diol group to AdoHcy using this reagent was attempted according to Scheme 4.1.

---

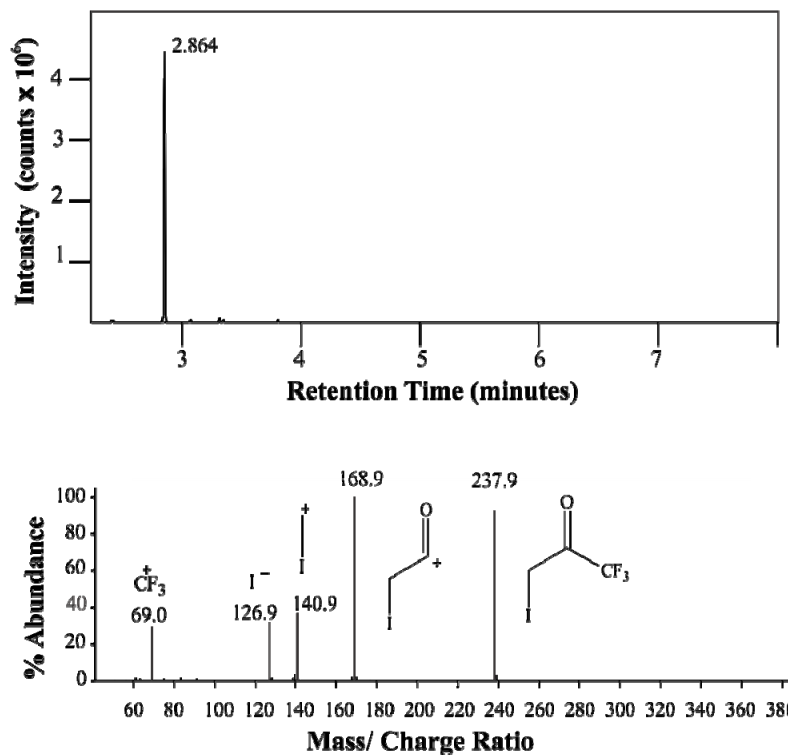
<sup>6</sup> To 335 mg of NaI dissolved in acetone were added 200  $\mu$ L of 3-bromo-1,1,1-trifluoroacetone. This mixture was stirred in the dark for a maximum of 24 hours. Precipitated NaBr was removed by filtration and the solvent evaporated. Diethyl ether (30 mL) was added to the residual yellow-brown liquid and this mixture was washed successively with ddH<sub>2</sub>O and brine then dried over sodium sulfate. The solvent was removed under vacuum to leave a yellow-brown oily liquid.



**Figure 4.4. Attempted synthesis of 3-iodo-1,1,1-trifluoroprop-2-one using conventional Finkelstein conditions.** The gas chromatogram of the crude reaction product mixture is shown. Products of retention time of 2.862 and 3.717 minutes correspond to 3-iodo-1,1,1-trifluoroprop-2-one and the starting material 3-bromo-1,1,1-trifluoroprop-2-one, respectively (EI-MS).



**Scheme 4.2. Synthesis of 3-iodo-1,1,1-trifluoropropan-2-one**



**Figure 4.5. Analysis of the products from the reaction of 3-bromo-1,1,1-trifluoroprop-2-one with KI in methanol.** Gas chromatogram of the crude reaction products, which shows greater than 95% conversion into 3-iodo-1,1,1-trifluoroprop-2-one (top panel). EI-mass spectrum of 3-iodo-1,1,1-trifluoroprop-2-one (retention time of 2.864 minutes); the structures of the resultant fragment ions are shown (bottom panel).



The reaction progress was qualitatively monitored by ESI-MS which indicated maximum AdoHcy modification occurring after 3 days. Analytical HPLC of the crude reaction products suggested a small improvement in yield, with 20 – 25 % conversion of AdoHcy mainly into the hydrated ketone, but it should be stated that this yield was achieved using proportionately less amounts of the iodoketone.

#### **4.3.2.4. Attempted synthesis of activated trifluoromethyl ketones**

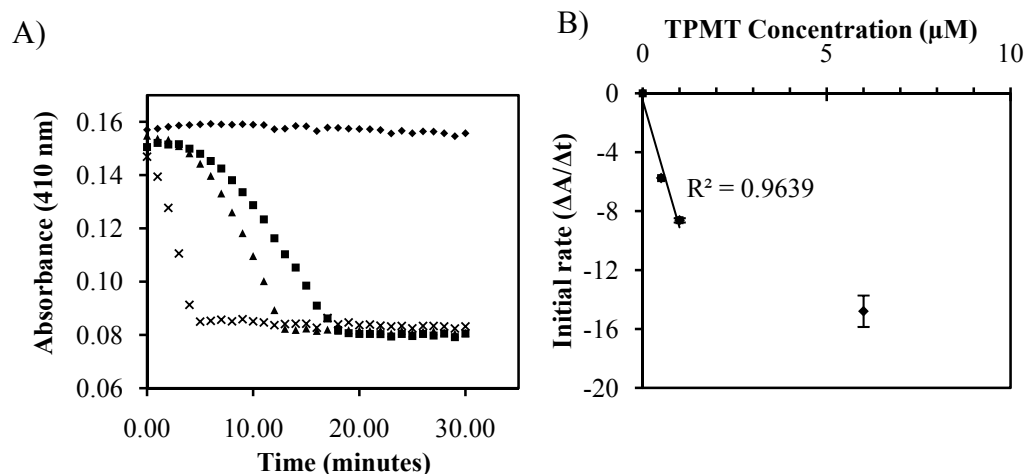
Activated alkylating agents have been successfully employed in the generation of AdoMet analogues in moderate to fair yields ranging between 20 and 60% (208, 210, 211). In these syntheses, alkyl chains were added to AdoHcy after being made more electrophilic by their coupling to mesyl or tosyl groups, which have the added benefit of serving as good leaving groups. Hence, it was thought that the use of the analogous activated trifluoromethyl propanone would result in greater yields of the desired AdoMet analogue.

Syntheses of triflated or tosylated trifluoromethyl ketones were attempted by heating an excess of silver salt (AgOTs or AgTf) with 3-bromo-1,1,1-trifluoro-prop-2-one to reflux in acetonitrile over 24 hours. Unfortunately, although ESI-MS of the crude reaction product mixture suggested the presence of the desired compounds, a complex mixture of crude reaction products was also evident, which prevented the purification of the target compounds. It is likely that the enhanced reactivity of the ketone group due to the neighboring trifluoromethyl group hampered the success of these reactions.

### 4.3.3. Evaluation of the trifluoropropane-2,2-diol AdoMet derivative (4.2) as a potential Mtase co-substrate

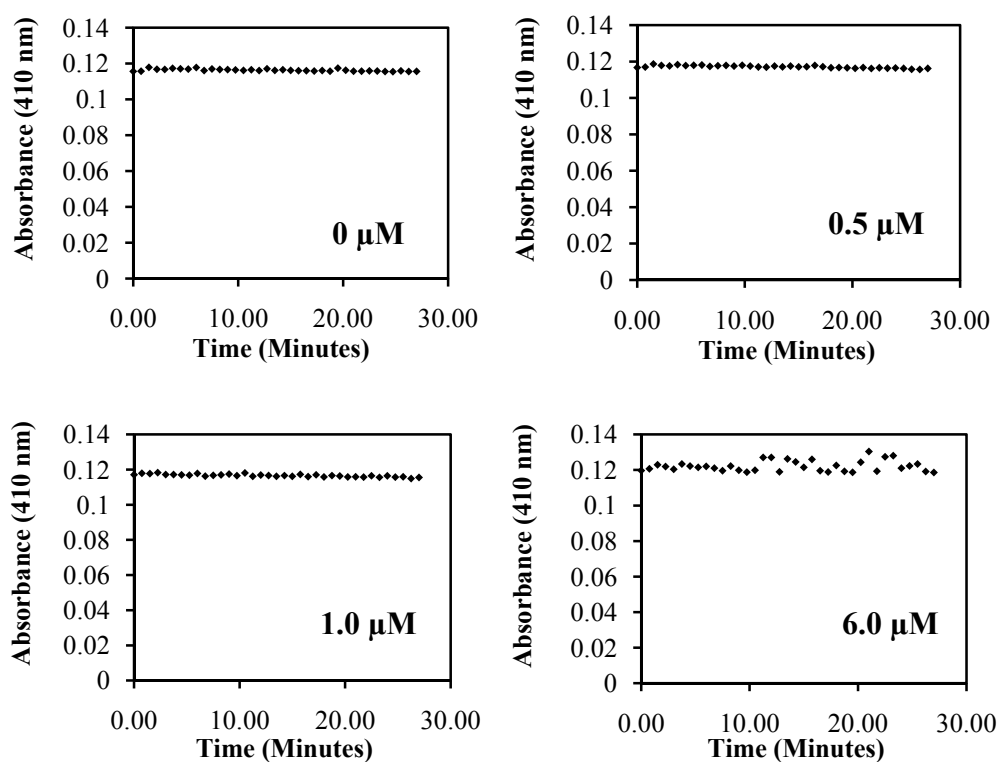
#### 4.3.3.1. Thiopurine methyltransferase activity with 4.2.

As earlier stated, thiopurine methyltransferase promiscuously methylates aromatic thiol substrates, which together with its demonstrated transfer of a methylketone group to 4-nitrobenzenethiol (213), made it an appropriate candidate to assess the potential of 4.2 as a methyltransferase co-substrate. The coupled spectrophometric assay for TPMT activity was previously performed in a volume of 1 mL (213, 290). However, using the same concentrations of the assay components, enzyme catalyzed methylation of 4-nitrothiophenol could be detected from assay volumes of 100  $\mu$ L, making this assay amenable to a 96-well format (Figure 4.6).



**Figure 4.6. Adaptation of the TPMT activity assay to 96-well microplate format.** Assays were performed in 96-well microplates to a total volume of 100  $\mu$ L. Data points reflect the mean of duplicate experiments. (A) Reaction progress curves at different TPMT concentrations (  $\blacklozenge$ : 0  $\mu$ M,  $\blacksquare$ : 0.5  $\mu$ M,  $\blacktriangle$ : 1.0  $\mu$ M,  $\times$ : 6.0  $\mu$ M). (B) Dependence of the initial rate 4-nitrobenzenethiol methylation on TPMT concentration.

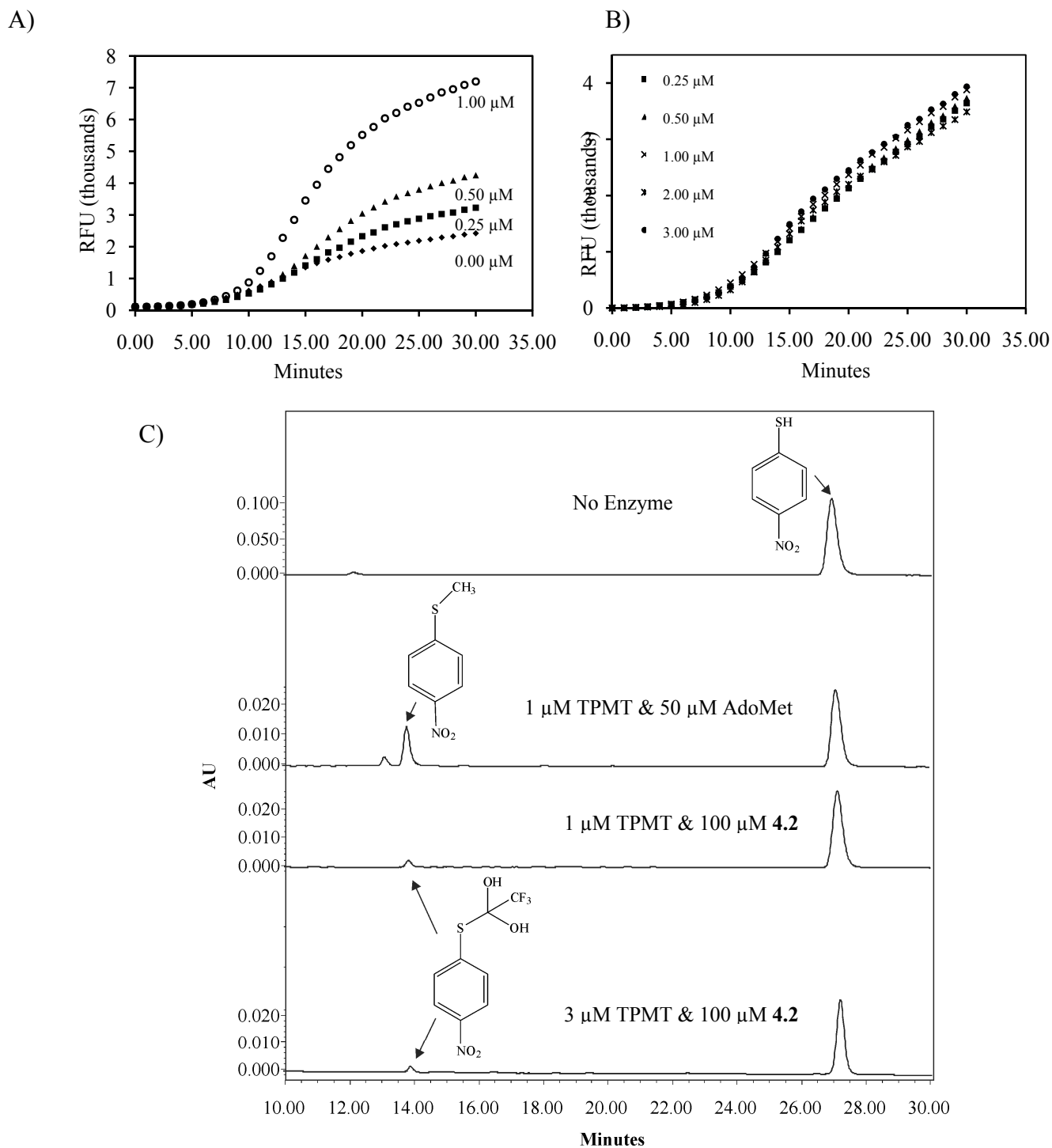
Under assay conditions identical to those used with AdoMet as the co-substrate, it appeared that the rate of reduction in absorbance in the presence of the **4.2** derivative did not exceed that was occurring in the absence of the enzyme (Figure 4.7). This could have signified that the trifluoroketone group was not transferred to 4-nitrothiophenol, however, the possibility remained that a low level of transfer of the fluoroketone group by TPMT was masked by the background reaction rate and was going undetected by the coupled spectrophotometric assay.



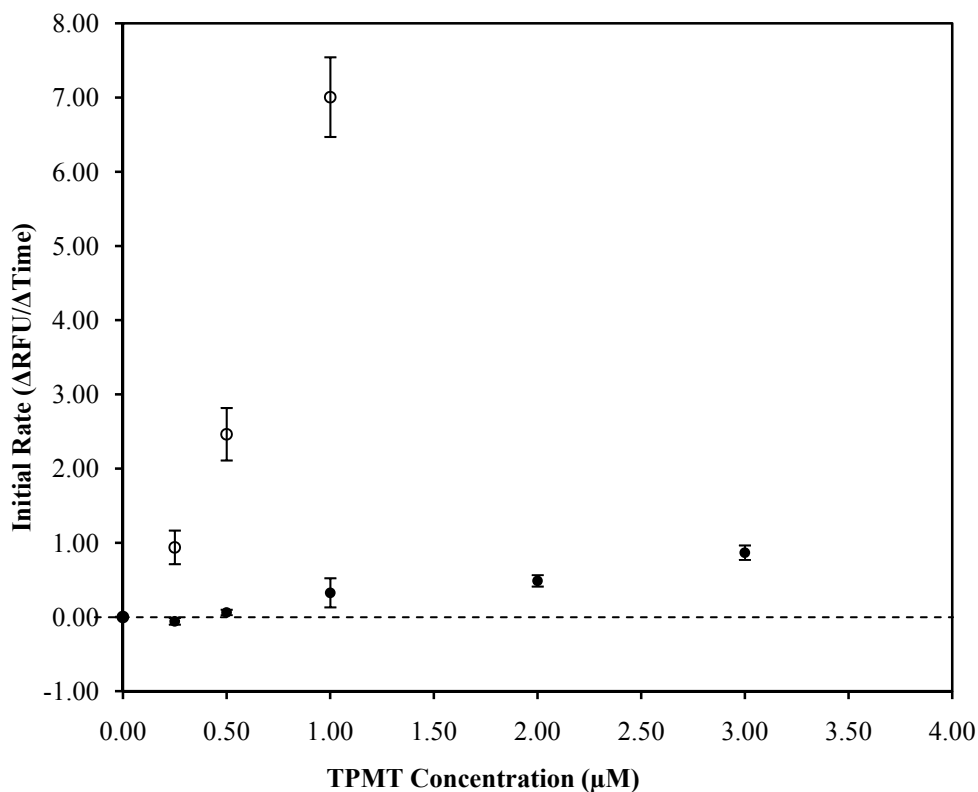
**Figure 4.7. TPMT catalyzed transfer of the trifluoroketone group to 4-nitrobenzene thiol.** Reaction progress curves for fluoroketo-AdoMet utilization by TPMT. Assays were performed as earlier described and contained 50 μM of fluoroketo-AdoMet and the indicated concentration of TPMT.

As well, since the fluoroketo-AdoMet was obtained as a mixture of stereoisomers, an inherently low rate of trifluoromethyl ketone transfer would be exaggerated by the stereo-selectivity of TPMT, which would reduce the effective **4.2** concentration. This effective concentration would also be reduced by degradation of the AdoMet analogue (although the stability of the derivative in the assay was not directly examined). With this in mind, observation of the turnover of **4.2** by TPMT was attempted with the coupled fluorometric assay as the increased sensitivity of the fluorescent reporter would enable detection of low-level TPMT activity.

Time-dependent TPMT catalyzed methylation of 4-nitrothiophenol utilizing AdoMet itself as the co-substrate, measured by the coupled fluorometric assay, mirrored the results obtained using the spectrophotometric assays (Figure 4.8A), indicating a linear correlation between the initial rate and TPMT concentrations up to 0.5  $\mu\text{M}$  (Figure 4.9). Reaction progress curves for parallel reactions carried out with the **4.2** were virtually indistinguishable below enzyme concentrations of 1.0  $\mu\text{M}$ , with no noticeable increase in fluorescence occurring above the background rate (Figure 4.8B). However, TPMT activity with **4.2** was detected by the fluorometric assay at enzyme concentrations of 1.0  $\mu\text{M}$  and greater and the transfer of the trifluoropropane-diol group was confirmed by HPLC analysis of the assay reaction products (Figure 4.8C). In addition, the initial rate of the reaction with **4.2** appeared to increase with TPMT concentrations exceeding 1  $\mu\text{M}$  (Figure 4.9).



**Figure 4.8. Modification of 4-nitrobenzenethiol by TPMT monitored by the coupled fluorometric assay.** Reaction progress curves for TPMT activity at various concentrations in the presence of A) 50  $\mu$ M AdoMet and B) 100  $\mu$ M **4.2**. Data points reflect the mean of duplicate experiments. C) HPLC chromatograms of the reaction products from TPMT reactions with AdoMet and **4.2**. The spectrophotometric properties of synthetic standards were used to identify the respective modified 4-



**Figure 4.9. Dependence of TPMT activity on enzyme concentration.** The initial rate of TPMT activity was measured in the presence of 50  $\mu\text{M}$  AdoMet (open circles) and 100  $\mu\text{M}$  **4.2** (closed circles). Error bars represent the standard deviation of the mean from duplicate experiments.

As mentioned earlier, **4.2** was obtained as a mixture of stereoisomers (approximately 50:50 according to  $^{19}\text{F}$  NMR). Therefore, the observed activity of TPMT actually represents turnover of the viable stereoisomer, effectively reducing the experimentally relevant analogue concentration by half. This would mean that TPMT activity in the presence of 100% of the appropriate isomer is likely to exceed what was observed here. Even so, in spite of the diminished TPMT activity with **4.2** relative to AdoMet, it was still gratifying to observe transfer of the trifluoropropane-diol group under the conditions used here. Invariably, the transfer of the alternative groups such as extended alkyl chains or conjugated adenoyl moieties from AdoMet analogues required

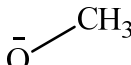
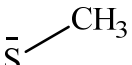
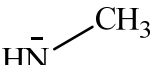

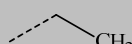
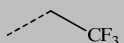
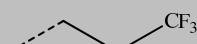
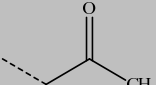
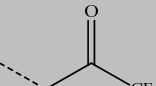
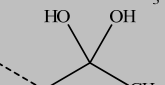
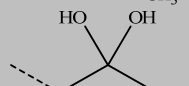
extended reaction times (2 – 24 hours) as well as enzyme and analogue concentrations in great excess of what was used in this study (1 – 20  $\mu\text{M}$  and 10 – 300  $\mu\text{M}$ , respectively) (201–205, 207, 210–212, 291). Quantitative transfer has only been demonstrated in the instance of the methylketone AdoMet analogue (213). Therefore, while the reduced rate of transfer of the trifluoropropane-diol group relative to AdoMet may not be unusual, its transfer from the AdoMet analogue synthesized here compares favorably with that shown with other AdoMet analogues.

The physical properties of the trifluoropropan-one/diol, such as its larger size and increased hydrophobicity relative to a methyl group, may contribute to its reduced rate of transfer by TPMT. These properties may be envisioned to bring about steric conflicts or unfavorable interactions within the enzyme active site that result in diminished or abolished binding of the AdoMet analogue. This is perhaps unlikely, given the wide variety in structures that are transferrable by Mtases (Chapter 1), several of which would present, similar if not greater steric problems.

A more fitting explanation seems to be that while the enzyme is able to bind the AdoMet derivative, it is unable to efficiently effect the transfer of the trifluoromethyl ketone group to the thiol substrate. AdoMet-dependent methyltransferases typically accomplish substrate methylation (or other modifications) via an  $\text{S}_{\text{N}}2$  type mechanism (Chapter 1 and (292–294)). In the case of the **4.2**, the highly electronegative trifluoromethyl group would presumably pull electron density away from the  $\alpha$ -carbon, thus increasing its

susceptibility to nucleophilic attack and this effect that would be augmented by the presence of the 2 hydroxyl groups. This was reflected by computational calculations of the thermodynamics associated with the alkylation of nucleophilic acceptors (Table 4.1).

**Table 4.1. Energy of transfer (kJ/ mol) for various groups to nucleophilic acceptors (295–297).**

Group Transferred	Nucleophilic Acceptor		
			
	-567.05	-586.89	-739.15
	-671.70	-586.89	-763.67
	-716.43	-634.41	-819.72
	-702.60	-619.21	-797.06
	-671.79	-587.32	-771.90
	-704.06	-626.89	-808.52
	-522.16	-505.98	-681.79
	-1258.60	-1181.07	-1368.13

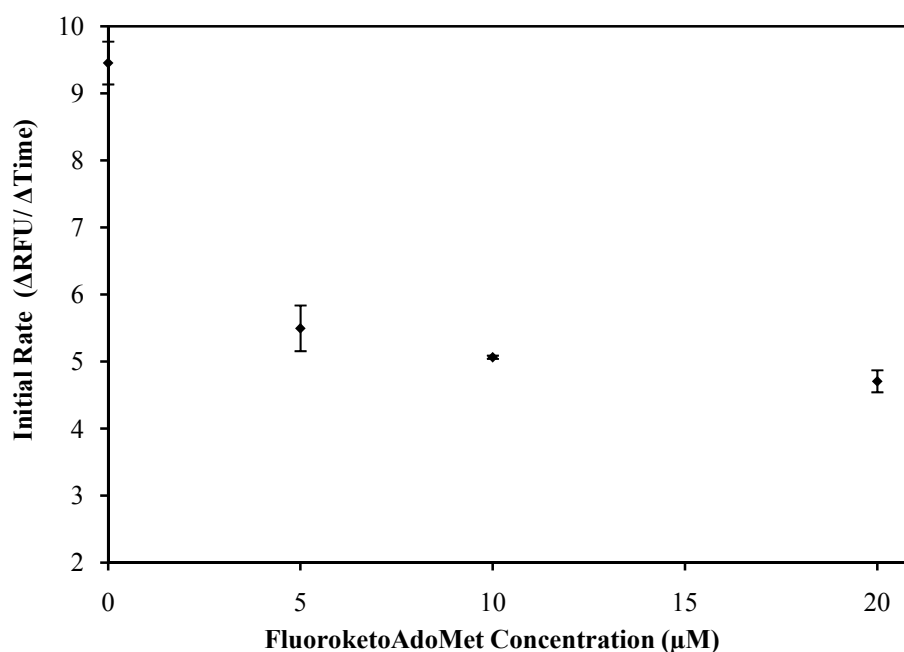
Nucleophilic acceptors represent Mtase substrates. Structure drawing and thermochemical calculations were performed in Spartan 10 software (Waveform Inc.), using the default protocol for the G3(MP2) thermochemical recipe (288–290). This recipe has been reported to reproduce experimental heats of formation for a wide variety of small molecules to within 6 kJ/mol (mean absolute error). Briefly, the heat of formation for a molecule is calculated from two equilibrium geometry calculations (at HF/6-31G\* and MP2/6-31G\*), a HF/6-31G\* frequency calculation, a MP2/6-311++G (2df, 2p) energy calculation and a QCISD(T)/6-31G\* energy calculation. The overall reaction energies for a chemical equation are then calculated using the equation:  $\Delta E = (E_{\text{product1}} + E_{\text{product2}}) - (E_{\text{reactant1}} + E_{\text{reactant2}})$



Surprisingly, these calculations predict the transfer of trifluoromethyl containing ketones or geminal diols to be more thermodynamically favored than their methyl group counterparts. Although this seemingly contradicts experimental observations, these calculations did not include the kinetic aspects of the reaction, which would contribute significantly to the overall favorability of the reaction.

By the above reasoning, substrate methylation with AdoMet would be reduced in the presence of **4.2** as the two compounds would compete for TPMT active sites, resulting in fewer available active sites being available for productive AdoMet binding due to their occupation by **4.2**. Preliminary assessments of this hypothesized effect by **4.2** were performed by monitoring time-dependent TPMT catalyzed methylation of 4-nitrobenzenethiol in the presence of **4.2**. As depicted in Figure 4.10, there is a clear reduction in AdoMet dependent TPMT activity in the presence of increasing concentrations of **4.2**, indicating competition between **4.2** and AdoMet for the TPMT active site. This finding may also be indicative of the reduced susceptibility of the  $\alpha$ -carbon from the trifluoroprop-2-one/ diol group to nucleophilic attack by the sulfur from 4-nitrothiophenol. It is worth mentioning that irreversible inhibition by **4.2** cannot be excluded in explaining these observations. Trifluoromethyl ketone (TFMK) compounds and their corresponding geminal diols are known inhibitors of proteases, phospholipases and esterases, due to the nucleophilic attack by an amino acid residue at the TFMK carbonyl carbon, whose electronegativity is enhanced by the trifluoromethyl group (277, 278). Although

the derivative obtained here was predominantly as a geminal diol, this would be in equilibrium with the corresponding ketone that could then be prone to nucleophilic attack from a basic active site residue. Conversely, the geminal diol product may cause inhibition by hydrogen bonding to key acidic/ basic residues in the enzyme active site.



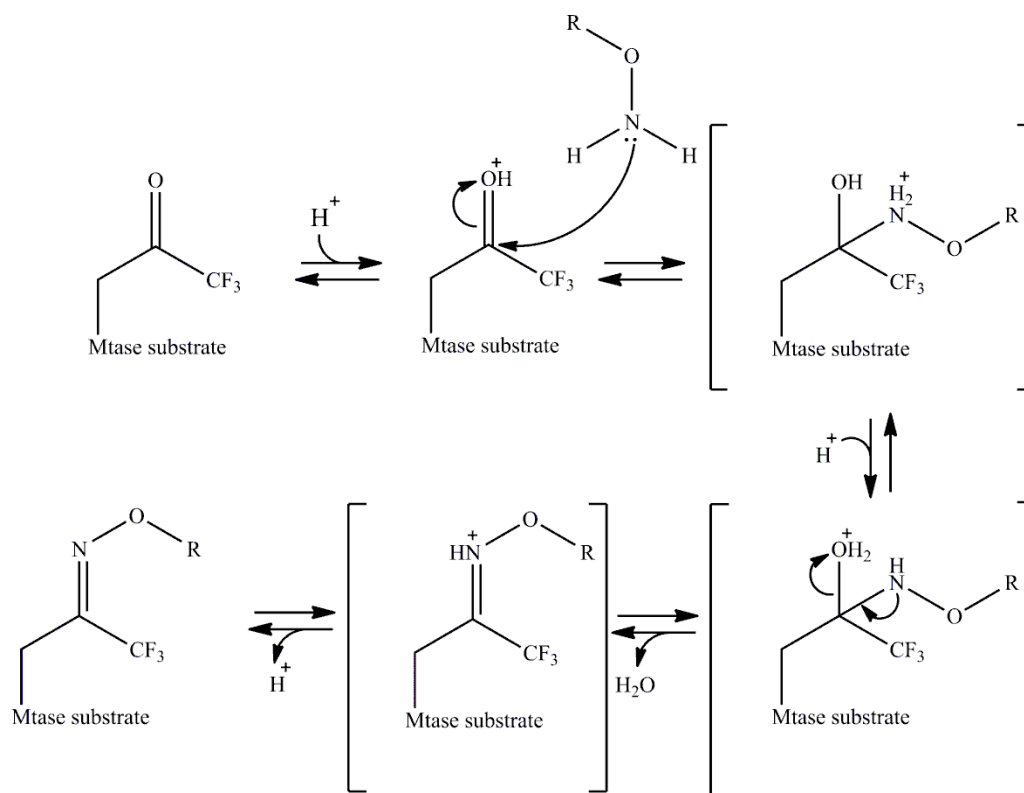
**Figure 4.10. Effect of 4.2 on TPMT-catalyzed methylation of 4-nitrothiophenol.** TPMT activity was monitored with the coupled fluorometric assay. Individual reactions included 50 μM AdoMet and varying concentrations of 4.2. Error bars represent the standard deviation of the mean of duplicate experiments.

#### 4.4. Conclusions, perspectives and future work

A novel analogue of AdoMet featuring a trifluoromethyl group has been synthesized. Using the thiopurine methyltransferase as a representative Mtase, enzyme catalyzed transfer of this group to a small molecule acceptor was demonstrated, which extends the collection of chemical moieties that can be transferred by some methyltransferase enzymes. Evidence suggested that the

analogue competes with AdoMet for the enzyme, but transfer from the analogue occurred to a lesser degree than AdoMet, which was likely the result of chemical barriers hindering the transfer of the trifluoropropane diol group to the acceptor.

The transfer of the trifluoroketone group may be promoted in the presence of increased concentrations of the MTase and/or the trifluoromethylketone-AdoMet. This could be particularly useful for further studies of the amenability of the modified product to coupling with ketone reactive molecules for purposes of substrate labeling. Lee and co-workers made use of the reaction between ketones and hydroxylamines to generate an oxime from methylketone-modified Mtase substrates and a fluorescent reporter that featured a hydroxylamine group (213). As illustrated in Figure 4.11, a similar approach could be employed for trifluoroketone modified substrates, however, in this instance, the highly electronegative trifluoromethyl group would make the carbonyl carbon more prone to nucleophilic attack.



**Figure 4.11. Attachment of reporter molecules to trifluoroketone modified Mtase substrates.** The mechanism of oxime formation from the reaction between the ketone group on a modified Mtase substrate and the hydroxylamine group from a hydroxylamine derivatized reporter molecule (represented by R; Alexa Fluor 647 for example) is shown. The electronegative trifluoromethyl group draws electron density away from the carbonyl carbon, making it more susceptible to nucleophilic attack from the nitrogen.

The increased susceptibility towards conjugative chemistry that is imparted by the trifluoromethyl ketone moiety (along with the potential for additional substrate labeling through  $^{19}F$  NMR) makes the development of AdoMet analogues featuring this group a promising area for continued research. The application of a combinatorial-type approach to structure-activity studies could prove useful in improving the turnover rate of fluoroketo groups. As alluded to earlier, the low rate of transfer of the trifluoromethyl ketone group

may derive from the proximity of the trifluoromethyl and ketone functions. Mitigation of this effect may be achieved by extending the distance between the carbonyl carbon and the sulfonium centre. This could be coupled with  $\alpha$ ,  $\beta$ - or  $\beta$ ,  $\gamma$ - unsaturation, which has been shown to aid the transfer of non-native groups (207). Alternatively, increasing the number of carbons between the carbonyl group and the point of attachment to the thioether may alleviate the negative impact on transfer caused by the increased electrophilicity that is caused by the trifluoromethyl group while preserving the reactivity of the ketone group for substrate labeling.

The generation of such libraries of AdoMet analogues is presently limited by the low synthetic yield as well as product instability. Although the use of iodinated alkylating agents was shown here to positively affect yield, further improvements may be achieved by revisiting the syntheses of the activated alkylating agents. Preliminary attempts at obtaining these agents were largely unsuccessful and the harsh conditions of extended reflux may have been a causative factor in these failures. However, the advantages afforded by a better post-alkylation leaving group that can simultaneously serve as a stabilizing counter-ion to the sulfonium ion, in addition to improving synthetic yields make this an attractive route towards the synthesis of AdoMet analogues.

The inherent instability of the AdoMet analogue (in conjunction with Mtase stereo-selectivity) limits the apparent rate of transfer of the trifluoroketo group by the enzyme. Sulfonium salts are notoriously unstable but their decomposition can be greatly slowed by their isolation as a halide or tosylate

salt. In this work, the presence of the tosylate anion likely achieves this stabilizing effect during synthesis, but since this anion is lost during HPLC purification, the analogue becomes vulnerable to decomposition. However, this counterion can be reintroduced through ion exchange chromatography. Separation of the stereo-isomers would prove to be a difficult undertaking and would require additional optimizations of the purification method utilizing HPLC columns with reduced particle size or ultra performance liquid chromatography (UPLC).

Future efforts in the development of fluorine and ketone containing AdoMet analogues will aid the continued study of Mtases, particularly with respect to the identification of novel substrates and functional probing. With regards to TSR, the demonstration of the transfer of a fluoroketo-AdoMet would be significant as this could eventually lead to TSR mediated RNA and ribosome labeling. Such modified ribosomes could be used in the examination of ribosome fine structure or the identification of new ribosomal Mtase targets. Furthermore, studies of the functional capabilities of these modified ribosomes during protein synthesis could prove to be mechanistically informative.

## CHAPTER 5: MOLECULAR INTERACTIONS BETWEEN THIOSTREPTON AND THE TIPAS RESISTANCE PROTEIN FROM *STREPTOMYCES LIVIDANS*

---

### 5.1. Preface

The reaction between thiostrepton and a cysteine residue from TIPAS or TIPAL is known to result in irreversible antibiotic binding that results in some *Streptomyces* strains exhibiting thiostrepton resistance. However, evidence also suggests the importance of a significant reversible protein-antibiotic interaction for biological activity. Several thiopeptides possessing DHA tails of varying length are able to covalently bind TIPAL/ TIPAS, while a subset of tailless analogues of these thiopeptides (including those of thiostrepton), were able to accomplish *ptipA* induction *in vivo* (220). It would be expected that the TIP protein-thiopeptide interaction is not solely dependent on covalent binding and that thiopeptide recognition by TIP proteins would be essential to the eventual irreversible protein-antibiotic interaction that leads to thiopeptide resistance. Our goal was to explore this type of interaction between thiostrepton and these proteins.

This chapter discusses the direct examination of the non-covalent TIP protein-thiopeptide interaction using the TIPAS protein and thiostrepton as the model system. In the absence of a structure of the TIPAS-thiostrepton complex, molecular modeling was used as a cursory tool for the assessment of this binding interaction, based on available NMR data (226). Recombinant techniques were used to engineer protein variants of TIPAS lacking the reactive residue, and qualitative and quantitative investigations of their binding to

thiostrepton and synthesized thiostrepton derivatives lacking the reactive molecular component were performed. Additional thiostrepton derivatives were synthesized to probe the structural features of thiostrepton important for recognition and non-covalent binding by TIPAS.

## **5.2. Materials and Methods**

### **5.2.1. Chemicals and reagents**

Dimethyl sulfoxide, dimethyl formamide, acetonitrile and trifluoroacetic acid were from Caledon Laboratory Chemicals (Caledon, Canada) and triethylamine was from EMD Chemicals (Gibbstown, USA). Thiostrepton (*Streptomyces azureus*;  $\geq 90\%$  purity) and MENSA were from Sigma (Oakville, Canada). Sodium cyanoborohydride, cyanogen bromide and diethylamine were from Sigma-Aldrich. Reagents for PCR and DNA manipulation were as listed in Chapter 3 (Section 3.2.1.1.).

### **5.2.2. Equipment**

#### **5.2.2.1. Protein chromatography**

Protein purifications were carried out with a Waters Chromatography system (Waters 626 pump, 600s controller and 2996 photodiode array detector and Millennium 3.2 software). Nickel affinity and anion exchange chromatography were performed using HisTrap™ HP (1 mL), HiTrap Benzamidine FF™ (1 mL) and MonoQ columns; all from GE Healthcare (formerly Amersham Biosciences, Uppsala, Sweden).



#### **5.2.2.2. Flash chromatography**

Thiostrepton derivatives were purified by Flash chromatography using an Isolera Flash Chromatography System (Biotage, Uppsala, Sweden) using pre-packed silica columns (Biotage).

#### **5.2.2.3. Fractionation of peptide digests using high performance liquid chromatography**

HPLC purification was performed using a Waters Chromatography system (Waters 626 pump, 600s controller and 2996 photodiode array detector and Millennium 3.2 software) with a Waters C18 column (5  $\mu$ M, 3.9 mm  $\times$  300 mm). The polar and non-polar mobile phases were 0.1% aqueous TFA and acetonitrile, respectively.

#### **5.2.2.4. Mass spectrometry**

Protein samples were prepared by first exchanging the buffer for doubly distilled water (ddH<sub>2</sub>O) using a Nanosep centrifugation device (molecular weight cut-off of 3000 Da) and the resulting solution was diluted with a mixture of acetonitrile and water (1:1) containing 0.2% formic acid. Thiostrepton derivatives were initially dissolved in acetonitrile, then diluted with a mixture of acetonitrile and water (1:1) containing 0.2% formic acid. Mass spectrometry was performed utilizing a Micromass Q-TOF Ultima Global mass spectrometer in positive ion mode. Spectra were analyzed using MaxEnt software (Waters, Millford, USA).

#### **5.2.2.5. Circular dichroism**

Spectra were acquired with a Jasco J715 spectropolarimeter, in the low UV region (190 – 250 nm), with a band width of 1 nm, at a scanning speed of 100 nm/ min. Spectra from 15 scans were averaged. Samples were prepared at 0.1 mg/ mL in a buffer comprised of 20 mM Tris pH 7.5, 5 mM DTT, 50 mM NaCl, 5 mM MgCl<sub>2</sub>, 1 mM EDTA and 10% glycerol (v/v).

#### **5.2.2.6. Fluorescence spectroscopy**

Fluorescence measurements were carried out in black 96 well microplates (Corning Life Sciences, Tewksbury, USA) using a SpectraMax M5 (Molecular Devices, Dowington, USA) calibrated to an internal standard.

#### **5.2.2.7. Nuclear magnetic resonance**

Thiostrepton derivatives (2 – 4 mg) were dissolved in 600 – 700  $\mu$ L of a mixture of deuterated chloroform and methanol (4:1). NMR spectra were acquired using either Bruker 300 MHz or 500 MHz spectrometers and chemical shifts are reported in ppm, relative to the solvent peaks (CDCl<sub>3</sub>; 7.24 ppm).

#### **5.2.2.8. Isothermal titration calorimetry**

ITC was performed using an ITC<sub>200</sub> (Microcal, now GE Healthcare, Piscataway, USA) and the data analyzed using Origin (5.0) software.

#### **5.2.2.9. Polymerase chain reactions**

PCR reactions were performed with a Techne TC-512 thermal cycler (Keison Products, Chelmsford, UK).

### **5.2.3. General methods**

#### **5.2.3.1. DNA manipulation**

DNA manipulation and cloning were performed in accordance with standard protocols provided by Sambrook *et al.* (264).

#### **5.2.3.2. Electrophoresis**

Protein and DNA electrophoresis were performed as described in Chapter 3 (Section 3.2.3.1.).

#### **5.2.3.3. Protein characterization**

Protein mass spectrometry was performed as described in Section 3.2.3.2. Protein quantification was performed as described in Section 3.2.3.3.

#### **5.2.3.4. Expression, purification and characterization of TIP proteins**

The DNA sequence encoding TIPAS as well as a sequence encoding the C-terminal 90 amino acids of TIPAS were amplified from *Streptomyces lividans* 2K4 genomic DNA (generously supplied by Professor Gerard Wright, McMaster University) using PCR techniques (Table 1). Primers were designed to introduce restriction sites for *NdeI* and *BamHI* at the 5' and 3' end of these sequences, respectively. After visualization of the ethidium bromide stained agarose gels, the desired amplicons were purified, and then doubly digested with *NdeI* and *BamHI*. The digested DNA was then inserted into the pET28a plasmid doubly digested with the same restriction enzymes, using T4 DNA ligase (Fermentas), generating plasmids bearing the coding region for TIPAS or TIPAS<sub>t</sub>. Ligation reactions were typically conducted in a volume of 20 µL with a 3:1 ratio of vector to insert DNA and 1 unit of ligase at 10-12°C, overnight. A

10  $\mu$ L portion of this ligation reaction was then used to transform chemically competent *E. coli* DH5 $\alpha$  cells, which were then spread (100  $\mu$ L) on to nutrient agar plates containing kanamycin (30  $\mu$ g/ mL) and incubated overnight at 37 °C. Single colonies were then selected and cultured overnight at 37 °C in 2 mL of Luria Bertani broth containing kanamycin (30  $\mu$ g/ mL) and the plasmid harvested using the Plasmid Miniprep Kit (Qiagen, Toronto, Canada). The presence of the TIPAS gene/ coding region for TIPAS $\alpha$  was confirmed by DNA sequencing at the Mobix Lab (McMaster University, Hamilton, Canada) (or protein analysis using SDS-PAGE after induction by addition of 1 mM IPTG), after which these plasmids were used to transform *E. coli* BL21 cells.

*E. coli* BL21 transformed with plasmids bearing the coding region for TIPAS or TIPAS $\alpha$  were grown in 1 L of Luria-Bertani broth containing kanamycin (30  $\mu$ g/ ml) at 37 °C to an optical density of 0.6-0.8 (600 nm). Protein expression was induced by the addition of 1 mM IPTG and the culture incubated at 37 °C for an additional 3-5 hours with shaking. Cells were then pelleted by centrifugation (8000  $\times$  g for 20 minutes at 4 °C) and then resuspended in lysis/ loading buffer comprised of 50 mM Tris pH 7.5, 500 mM NaCl, 5 mM MgCl<sub>2</sub>, 20 mM imidazole and 10% glycerol (v/v). Cell disruption was performed as described in Chapter 3 and cellular debris were removed by centrifugation (48,300  $\times$  g for 20 minutes at 4 °C) and the crude lysate containing the soluble proteins was directly introduced onto a 1 mL nickel affinity column (GE Healthcare), pre-equilibrated with lysis/ loading buffer. Non-binding proteins were eluted with lysis/ loading buffer and the

hexahistidine-tagged TIP proteins were eluted with a buffer containing 50 mM Tris pH 7.5, 1 M NaCl, 5 mM MgCl<sub>2</sub>, 500 mM imidazole and 10% glycerol (v/v), upon which EDTA was immediately added to the collected fractions at final concentration of 2 mM. The protein solution was then dialyzed twice, for 3 hours against 500 mL of fresh storage buffer (20 mM Tris pH 7.5, 5 mM DTT, 50 mM NaCl, 5 mM MgCl<sub>2</sub>, 1 mM EDTA and 10% glycerol (v/v)) and then overnight against 1L of fresh storage buffer. To remove the N-terminal hexahistidine tag, CaCl<sub>2</sub> was added to protein solutions at a final concentration of 2.5 mM and solutions were incubated with thrombin (GE Healthcare; 1U/100 µg of protein) overnight at 4 °C. Tag-free proteins were obtained after injection onto a nickel affinity column attached in series to a benzamidine column (GE Healthcare) and elution with loading/ lysis buffer. EDTA was immediately added to a final concentration of 2 mM to the collected fractions and the protein solution was dialyzed against storage buffer overnight. The solution was divided into aliquoted into 200 µL fractions, frozen with liquid nitrogen and stored at -80°C for future use. Protein yields were typically 30-50 mg from 3 – 5 g of pelleted cells. Point mutations (C207A, C214A, and C214S) were introduced into TIPAS by PCR driven overlap and extension (Table 5.1) and the mutants purified under the same conditions as the native protein.

Amino acid sequence of recombinant TIPAS; C207 and C214 are underlined.

G S H M G I N L T P E E K F E V F G D F D P D Q Y E E E  
V R E R W G N T D A Y R Q S K E K T A S Y T K E D W Q  
R I Q D E A D E L T R R F V A L M D A G E P A D S E G A  
M D A A E D H R Q G I A R N H Y D C G Y E M H T C L G  
E M Y V S D E R F T R N I D A A K P G L A A Y M R D A I  
L A N A V R H T P

Amino acid sequence of TIPAS<sub>t</sub>

G S H M Q D E A D E L T R R F V A L M D A G E P A D S  
E G A M D A A E D H R Q G I A R N H Y D C G Y E M H T  
C L G E M Y V S D E R F T R N I D A A K P G L A A Y M  
R D A I L A N A V R H T P

**Table 5.1. PCR primers used for TIP protein expression and point mutant generation**

	Forward	Reverse
TIPAS	GCCATATGGGAATCAACCTCACCCGGAGG	GCGGGATCCTTATCAGGGGGTGTGCC
TIPAS <sub>t</sub>	GCCATATGCAGGACGAGGCCGACGAGCTC	GCGGGATCCTTATCAGGGGGTGTGCC
Point Mutants		
C207A	CACTACGACGCGGGGTACGAGATGCACACCTGCCT	TCGTACCCCGCGTCGTAGTGGTTGCGGGCGATGCC
C214A	CACACCGCGCTGGGCGAGATG	CTCGCCCAGCGCGGTGTGCATC
C214S	GATGCACACCAGCCTGGGCGAGATGTACGTGTCCGAC	CTCGCCCAGGCTGGTGTGCATCTCGTACCCGCAGTCG

**Table 5.2. PCR conditions for amplification of the coding sequence for TIPAS and TIPAS<sub>t</sub> from *S. lividans* genomic DNA**

	Minutes	Temperature (°C)
<b>Initial denaturation</b>	5	95
Hot start		
<i>10 cycles</i>		
Denaturation	1	95
Annealing	1	60
Extension	1.5	72
<b>Final Extension</b>	10	72

Reactions were carried out in a total volume of 50 µL and contained 1 unit of *pfu* polymerase, 2.5 mM of dNTPs, 20 ng of genomic DNA and 10% DMSO (v/v).

**Table 5.3. PCR conditions to generate full length TIPAS mutant genes.**

	Minutes	Temperature ( °C)
<b>Initial denaturation</b>	5	95
<b>Hot start</b>		
<i>10 cycles</i>		
Denaturation	2	95
Annealing	1	60 – 50 (reduce by 1° every cycle)
Extension	2.5	72
<b>PAUSE – ADD T7 PRIMERS</b>	5	72
<i>25 cycles</i>		
Denaturation	2	95
Annealing	1	50
Extension	2.5	72
<b>Final Extension</b>	10	72

Reactions were carried out in a total volume of 50  $\mu$ L and contained 1 unit of *pfu* polymerase, 2.5 mM of dNTPs, equal concentrations of 5' and 3' gene fragments with the total of DNA not exceeding 100 ng and 10% DMSO (v/v). 5' and 3' fragments were generated from the TIPAS gene using standard PCR conditions: 25 cycles, Denaturation: 95°C for 2 minutes; annealing: 50°C for 1 minute; extension: 72°C for 1.5 minutes

### 5.2.3.5. Ion exchange chromatography

Protein samples were dialyzed overnight against a buffer containing 50 mM Tris (pH 7.5) and 5 mM DTT (for small volume samples, the buffer was replaced using a NanoSep centrifugation device). The protein solutions were then applied to a MonoQ anion exchange column, equilibrated with the same buffer and eluted over a linear increasing gradient of NaCl (0 – 1 M over 100 minutes).

### **5.2.3.6. Reaction of TIP proteins with thiostrepton**

TIPAS or its variants were reacted with thiostrepton according to the method described in Chiu *et al.* (225). Sodium cyanoborohydride was added to protein solutions (3.5 equivalents) and this mixture was left standing for 5 -10 minutes at room temperature. After the deactivation of excess sodium cyanoborohydride by the addition of 2 volumes of acetone, thiostrepton (prepared as a solution in DMSO) was added (5 equivalents) and this mixture was placed in a sealed vessel on a platform shaker for 60 minutes at room temperature. After incubation, the reaction mixture was passed through a 0.2 micron cellulose acetate filter to remove precipitated thiostrepton and washed (and the buffer exchanged to ddH<sub>2</sub>O for purposed of ESI-MS analysis) using a NanoSep centrifugal device (molecular weight cut-off: 3000 Da; Pall Life Sciences) to remove excess DMSO and unreacted antibiotic.

### **5.2.3.7. Cyanogen bromide digestion of TIP proteins & protein-thiostrepton complexes**

Approximately 1-2 mg of unbound protein or protein-thiostrepton complex was precipitated using trichloroacetic acid<sup>7</sup>. The dried precipitate was dissolved in 800 µl of degassed<sup>8</sup> 87.5 % formic acid. Cyanogen bromide,

---

<sup>7</sup>One volume of TCA was added to 4 volumes of protein, and this solution was incubated at 4°C for 10 minutes. Precipitated protein was then pelleted by centrifugation and washed 3 times with cold acetone. After the final wash, the supernatant was decanted and the pellet heat-dried.

<sup>8</sup> Cleavage efficiency was considerably reduced without degassing.



prepared as a 1 mL solution in degassed acetonitrile<sup>9</sup>, was added to a final concentration that was 200 M in excess of that of methionine (298) and the mixture incubated in the dark, at room temperature for 24 hours. The reaction was quenched by the addition of 5 volumes of ddH<sub>2</sub>O, and then lyophilized.

### 5.2.3.8. Synthesis of thiostrepton derivatives

#### 5.2.3.8.1. Truncated derivatives.

Truncated thiostrepton derivatives were prepared according to previous methodologies (90, 239).

**5.1.** Diethylamine (5 ml) was added to a solution of thiostrepton (0.3 mmoles/ 500 mg in 25 ml of chloroform), which was stirring at 0°C. The mixture was allowed to warm to room temperature, and stirred for an additional 4 hours. The volatiles were coevaporated with toluene and the residue purified by silica gel chromatography (2-5% CH<sub>3</sub>OH in CHCl<sub>3</sub>).

70% yield, white powder, m.p.: 230 – 245 °C, R<sub>f</sub>: 0.34 (CH<sub>3</sub>Cl/MeOH 9:1). <sup>1</sup>H NMR (300 MHz, CDCl<sub>3</sub>/ CD<sub>3</sub>OD 4:1) 9.7 (s, 1H), 8.64 (d, *J* = 9.0, 1H), 8.14 (s, 1H), 8.13 (s, 1H), 8.03 (s, 1H), 7.86 (s, 1H), 7.42 (s, 1H), 7.16 (s, 1H), 6.95 (d, *J* = 8.2, 1H), 6.92 (d, *J* = 8.2, 1H), 6.73 (d, *J* = 9.9, 1H), 6.49 (d, *J* = 1.5, 1H), 6.32 - 6.16 (m, 2H), 6.07 (q, *J* = 7, 1H), 5.69 (d, *J* = 1.6, 1H), 5.67-5.56 (m, 2H), 5.49 (m, 1H), 5.27-5.13 (m, 3H), 4.83 (dd, *J* = 9.3, 12.9, 1H), 4.68 - 4.51 (m, 1H), 4.37 - 4.22 (m, 2H), 3.72 - 3.61 (m, 2H), 3.56 - 3.44 (m, 2H), 3.02 (dd, *J* = 11.71, 12.78, 1H), 2.15 (t, *J* = 12.9, 1H), 1.85 - 1.72 (m, 1H), 1.56 (d, *J* = 6.5, 3H), 1.46 (d, *J* = 7.0, 3H), 1.28 (d, *J* = 6.5, 3H), 1.23 (d, *J* = 6.5, 3H),

---

<sup>9</sup> This was performed in the fumehood as CNBr is a highly toxic carcinogen.

1.15 (d,  $J = 6.4$ , 4H), 1.12 - 0.98 (m, 8H), 0.85 (d,  $J = 6.5$ , 3H), 0.74 (t,  $J = 7.1$ , 4H), 0.66 (d,  $J = 6.0$ , 3H). HRMS calculated for [  $C_{69}H_{82}N_{18}O_{17}S_5+2H^+$  ] 1596.4865, found (ESI) 1596.4883.

**5.2.** Diethylamine (4.5 ml) was added to a stirring mixture of **1** in chloroform (0.062 mmoles /100 mg in 5 ml  $CHCl_3$ ), at 0°C. The mixture was allowed to warm to room temperature and stirred for an additional 18 hours. After coevaporation of the volatiles with toluene, the crude mixture was purified by silica gel chromatography (2-5 %  $CH_3OH$  in  $CHCl_3$ ).

40% yield, white powder, m.p.: 230 – 245 °C,  $R_f$ : 0.29 ( $CH_3Cl/MeOH$  9:1).  $^1H$  NMR (300 MHz,  $CDCl_3/CD_3OD$  4:1) 9.73 (s, 1H), 8.64 (d,  $J = 7.6$ , 1H), 8.14 (s, 1H), 8.11 (s, 1H), 8.02 (s, 1H), 7.87 (s, 1H), 7.42 (s, 1H), 7.16 (s, 1H), 7.03 – 6.89 (m, 2H), 6.73 (d,  $J = 9.1$ , 1H), 6.40 – 6.17 (m, 2H), 6.15 – 6.02 (m, 1H), 5.77 – 5.67 (m, 1H), 5.67-5.59 (m, 2H), 5.31-5.10 (m, 3H), 4.95-4.75 (m, 1H), 4.68 – 4.51 (m, 1H), 4.41 – 4.17 (m, 3H), 3.72 – 3.63 (m, 2H), 3.55 – 3.45 (m, 2H), 3.08 – 2.96 (m, 1H), 2.93 – 2.67 (m, 2H), 2.16 (t,  $J = 12.8$ , 1H), 1.86 – 1.73 (m, 1H), 1.57 (d,  $J = 5.3$ , 3H), 1.46 (d,  $J = 5.7$ , 3H), 1.35 – 1.20 (m, 7H), 1.20 – 1.12 (m, 5H), 1.11 – 1.00 (m, 8H), 0.85 (d,  $J = 6.4$ , 3H), 0.74 (t,  $J = 6.4$ , 4H), 0.70 – 0.60 (m, 3H). HRMS calculated for [  $C_{66}H_{79}N_{17}O_{16}S_5+2H^+$  ] 1527.4651, found (ESI) 1527.4644

The spectroscopic and physical properties of synthesized **5.1** and **5.2** were identical in all respects to that reported in previous syntheses of these compounds (239).

#### 5.2.3.8.2. Michael adducts

Michael adducts of thiostrepton were prepared according to the procedures described in Chapter 2 (246). To a stirring mixture of thiostrepton or **5.1** under an inert atmosphere at room temperature (0.03 mmoles/ 50 mg in 1.5 ml of dimethylformamide), were added triethylamine (0.3 mmoles; 42  $\mu$ l), followed by MENSA (0.03 mmoles; prepared as a 150 mM stock solution in ddH<sub>2</sub>O). The mixture was cooled to 4 °C and stirred for an additional 18 hours. The solvent was removed under vacuum and the residual orange powder purified by silica gel chromatography (7 – 60 % CH<sub>3</sub>OH in CHCl<sub>3</sub>).

**5.3**: 50% yield, white powder, m.p.: 240 – 250 °C, R<sub>f</sub>: 0.54 (CH<sub>3</sub>Cl/MeOH 7:3).

<sup>1</sup>H NMR (300 MHz, CDCl<sub>3</sub>/ CD<sub>3</sub>OD 4:1) <sup>1</sup>H NMR (300 MHz, CDCl<sub>3</sub>/ CD<sub>3</sub>OD 4:1) 9.74 (s, 1H), 8.64 (d, *J* = 9.1, 1H), 8.22 – 8.09 (m, 2H), 8.03 (s, 1H), 7.87 (s, 1H), 7.42 (s, 1H), 7.17 (s, 1H), 7.05 – 6.89 (m, 2H), 6.73 (d, *J* = 10.1, 1H), 6.33 – 6.15 (m, 2H), 6.07 (q, *J* = 7.0, 1H), 5.76 – 5.67 (m, 1H), 5.61 – 5.57 (m, 2H), 5.57 – 5.47 (m, 1H), 5.29 – 5.09 (m, 3H), 4.82 (dd, *J* = 9.2, 12.72, 1H), 4.68 – 4.51 (m, 1H), 4.32 – 4.23 (m, 2H), 3.71 – 3.62 (m, 2H), 3.52 – 3.45 (m, 2H), 3.07 – 3.00 (m, 1H), 2.82 (d, *J* = 4.4, 1H), 2.81 – 2.71 (m, 1H), 2.15 (t, *J* = 13.0, 1H), 1.89 – 1.84 (m, 1H), 1.83 – 1.72 (m, 1H), 1.57 (d, *J* = 6.5, 3H), 1.46 (d, *J* = 7.0, 3H), 1.29 (d, *J* = 5.7, 3H), 1.23 (d, *J* = 6.7, 3H), 1.14 (d, *J* = 6.4, 4H), 1.10 (s, 3H), 1.06 – 0.99 (m, 6H), 0.85 (d, *J* = 6.9, 3H), 0.74 (t, *J* = 7.0, 4H), 0.66 (d, *J* = 6.6, 3H). HRMS calculated for [ C<sub>74</sub>H<sub>92</sub>N<sub>19</sub>O<sub>21</sub>S<sub>7</sub>+2H<sup>+</sup> ] 1807.4832, found (ESI) 1807.4838

**5.4.** 20% yield, white powder, m.p.: 240 – 250 °C, R<sub>f</sub>: 0.61 (CH<sub>3</sub>Cl/MeOH 7:3).  
<sup>1</sup>H NMR (300 MHz, CDCl<sub>3</sub>/ CD<sub>3</sub>OD 4:1) 9.73 (s, 1H), 8.65 (d, *J* = 8.0, 1H),  
8.22 – 8.08 (m, 2H), 8.02 (s, 1H), 7.84 (s, 1H), 7.42 (s, 1H), 7.16 (s, 1H), 7.02 –  
6.91 (m, 2H), 6.73 (d, *J* = 9.99, 1H), 6.47 (d, *J* = 4.2, 1H), 6.31 – 6.15 (m, 2H),  
6.08 (q, *J* = 7.0, 1H), 5.73 – 5.57 (m, 2H), 5.53 – 5.47 (m, 1H), 5.25 – 5.11 (m,  
2H), 4.90 – 4.77 (m, 1H), 4.67 – 4.54 (m, 1H), 4.37 – 4.21 (m, 2H), 3.70 – 3.62  
(m, 2H), 3.53 – 3.46 (m, 2H), 2.83 (d, *J* = 4.4, 2H), 2.78 – 2.72 (m, 2H), 2.25 –  
2.10 (m, 1H), 1.93 – 1.83 (m, 1H), 1.81 – 1.74 (m, 1H), 1.57 (d, *J* = 6.52, 3H),  
1.46 (d, *J* = 7.0, 3H), 1.29 (d, *J* = 5.7, 3H), 1.23 (d, *J* = 6.7, 4H), 1.17 (d, *J* = 5.8,  
4H), 1.14 – 1.10 (s, 4H), 1.09 – 1.01 (m, 10H), 0.92 – 0.82 (m, 5H), 0.81 – 0.66  
(m, 7H). HRMS calculated for [ C<sub>71</sub>H<sub>88</sub>N<sub>18</sub>O<sub>20</sub>S<sub>7</sub> + H<sup>+</sup> ] 1737.4600, found (ESI)  
1737.4546.

#### **5.2.3.9. Fluorescence quenching of TIPAS**

Protein-antibiotic reactions were performed as described in Section 5.2.3.2, with 10 μM of protein and varying amounts of thiostrepton or its truncated derivatives. Fluorescence measurements were carried out on 200 μl of the filtered and washed reaction using an excitation wavelength of 278 nm and emission at 346 nm.

#### **5.2.3.10. Isothermal titration calorimetry**

Prior to ITC experiments, protein to be used was first dialyzed overnight against a buffer comprised of 20 mM Tris pH 7.5, 10% glycerol (v/v) and 5 mM 2-mercaptoethanol. The dialysate was used to prepare working solutions of protein and the buffer was used to prepare thiostrepton analogues at 7 μM and

100  $\mu\text{M}$ , both containing DMSO at a final concentration of 15% (v/v). Titrations were performed at 25°C and consisted of 16 or 17 injections of 2.0  $\mu\text{L}$  or 2.2  $\mu\text{L}$  of antibiotic solution into a sample cell containing protein solution. The heat of dilution/ mixing was obtained from injections of the respective antibiotic solutions into buffer containing no protein (with DMSO present at 15% v/v)). After subtraction of the heats of dilution, titration curves were analyzed using Origin software and the data fitted using the model for one set of binding sites (Please refer to Appendix 4 for curve fitting methodologies)

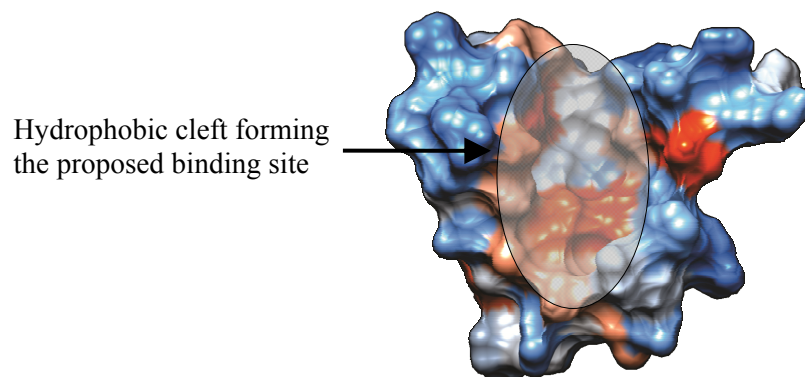
#### **5.2.3.11. Molecular modeling**

Protein Data Bank (PDB) files of TIPAS and thioestrepton were individually imported into *Molegro Virtual Docker* v. 5.0 (Molegro, Aarhus, Denmark). TIPAS was designated as the protein/ receptor and thioestrepton as the ligand. Both structures were edited to include bonds missing from the PDB file, correct improper bonds, add explicit hydrogen atoms and assign missing charges. As well, the flexible bonds in thioestrepton were allowed their full range of rotation. The thioestrepton binding site (cavity) was defined as a 16Å region that encompassed the binding site proposed by Kahmann *et al.*(226). Docking was constrained to the designated cavity and the entire simulation consisted of 15 runs of 1500 iterations each, using the MolDock SE heuristic search algorithm and MolDock scoring function (299). The poses exhibiting the 20 lowest energies were kept for analysis.

### 5.3. Results and Discussion

#### 5.3.1. Modeling the TIPAS-thiostrepton interaction

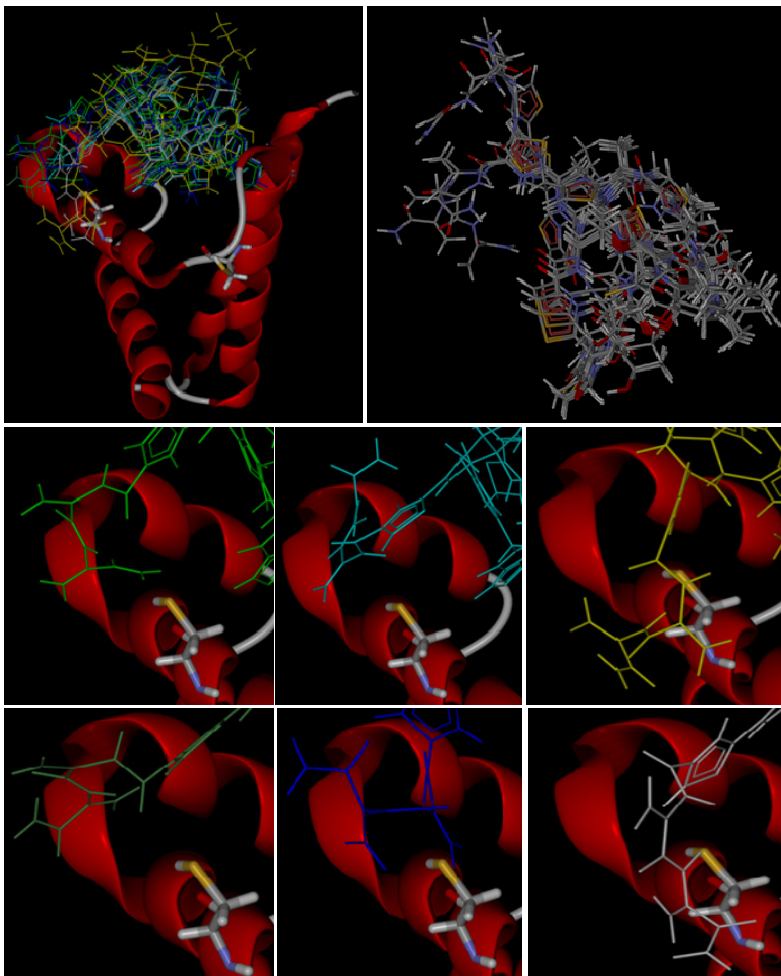
The binding of thiostrepton to its proposed TIPAS binding site was initially examined *in silico* to ascertain the possibility that such binding would allow for positions of the thiostrepton tail that would facilitate Michael addition with C214, the reactive cysteine found in the TIP proteins. Binding simulations were carefully designed so as not to introduce bias into the results; structural editing was limited to bond corrections and inclusion of hydrogen atoms and the rotatable bonds in thiostrepton were allowed their full degree of freedom. Also, the area defined as the binding cavity was exaggerated (Figure 5.1).



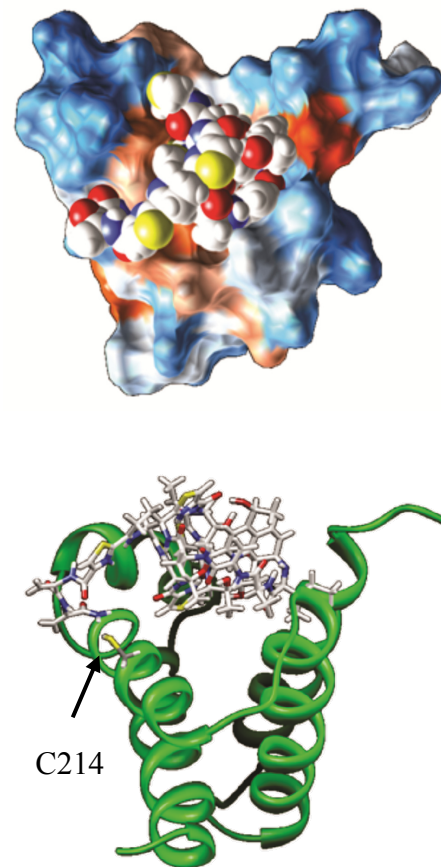
**Figure 5.1. Proposed thiostrepton binding site.** The NMR derived structure for TIPAS (PDB: 1N9Y) was imported into *UCSF Chimera v.1.5.2* and mapped with a hydrophobic surface; orange indicates greater hydrophobicity.

A sample of the docking results is presented in Figure 5.2. Of the top 20 poses returned by the docking simulation, six of these depicted the core of the thiostrepton molecule embedded in the hydrophobic cleft and the DHA tail in proximity to the C214 protein residue (Figure. 5.2A). Little deviation of the position of the thiostrepton core was seen among these poses, an observation

that was consistent across the full set of results (Figure. 5.2A). However, variation was seen in the position of the thiostrepton tail among these top poses (Figure. 5.2B), which could be expected due to the inherent flexibility of the tail (85). Nevertheless, in all cases at least one of the tail DHA residues was positioned such that Michael addition between the DHA olefin and C214 was possible, offering some theoretical support for the experimentally determined covalent antibiotic-protein interaction (Figure. 5.3).



**Figure 5.2. Modeling TIPAS-thiostrepton binding.** (A) The top left panel shows 6 outcomes of the docking of thiostrepton on TIPAS (red ribbons) that resulted in the DHA tail positioned within bonding distance of C214. Top Right panel shows an overlay of the 6 thiostrepton confirmations. (B) Orientations of the bis-DHA thiostrepton relative to C214.



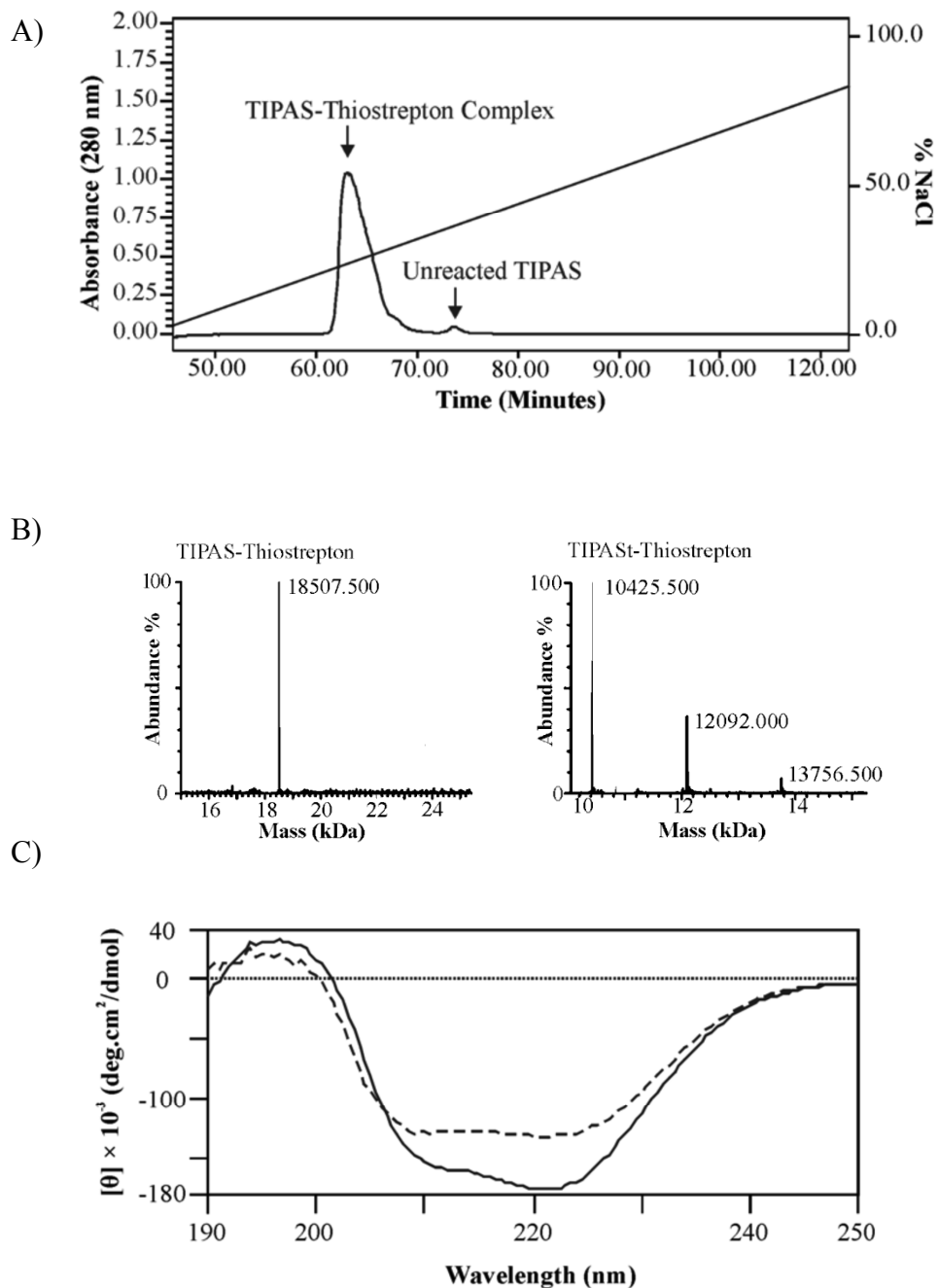
**Figure 5.3. The binding of thiostrepton to TIPAS.** (Top) Thiostrepton (space-filling) was docked into the hydrophobic cleft on TIPAS (pose 1); (Bottom) 90° x-axis rotation of pose 1 with TIPAS rendered as green ribbons. Images were generated using *UCSF Chimera*, after creating a PDB file of TIPAS bound with thiostrepton in *Molegro Virtual Docker*.



### 5.3.2. Interaction of TIPAS and its variants with thiostrepton

The available NMR structure for TIPAS excludes the N-terminal 54 amino acids of the protein, which could not be positioned by the authors of the study due to flexibility of this region of the protein (226). With the view towards future endeavors at obtaining the crystal structure of TIPAS or its complex suitable for X-ray diffraction, a truncated variant of the protein lacking these N-terminal amino acids (TIPAS<sub>t</sub>) was generated. It was found that while the native protein became virtually 100% covalently bound to thiostrepton at a 1:1 stoichiometry, TIPAS<sub>t</sub> was unreactive by comparison, with the majority of this protein remaining unbound (Figure 5.4A). Mass spectrometric analysis of the reaction products of the TIPAS<sub>t</sub>-thiostrepton reaction also indicated the formation of complexes with a 2:1 stoichiometry of antibiotic to protein in addition to 1:1 complexes (Figure 5.4B). These bis-thiostrepton protein complexes did not occur with the native TIPAS and their occurrence with TIPAS<sub>t</sub> was immediately suggestive of a conformational difference in this protein that resulted in the exposure of a second site for covalent attachment to thiostrepton. The likely candidate for this second site of attachment would be C207, although, the addition of thiostrepton to this site has not been reported in the literature.

Evidence for the suspected structural divergence of TIPAS<sub>t</sub> from TIPAS was obtained from comparative CD spectra for these proteins, shown in Figure 5.4C. The spectrum for TIPAS<sub>t</sub> indicates the loss of gross secondary and tertiary structural features for TIPAS<sub>t</sub> with respect to TIPAS which may signify that this protein is somewhat unfolded.



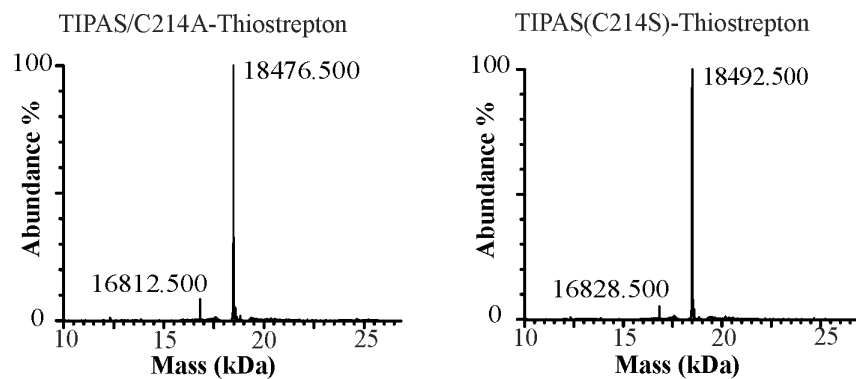
**Figure 5.4. Purification and characterization of TIP-thiostrepton complexes.** (A) Anion exchange chromatography of the TIPAS-thiostrepton reaction. The chromatograph indicates greater than 95% complex formation. (B) Deconvoluted mass spectra of the complexes formed between thiostrepton and TIPAS (the molecular weight of TIPAS is 16844 Da) and TIPAS<sup>t</sup>. The spectrum of the TIPAS<sup>t</sup> reaction shows the presence of mono- (12092.000 Da) and di- (13756.500) thiostrepton-protein complexes. (C) Far UV circular dichroism spectra for TIPAS (solid line) and TIPAS<sup>t</sup> (dashed line). Measurements were performed on 0.75 mM protein in a buffer comprised of 20 mM Tris pH 7.5, 5 mM 2-mercaptoethanol and 10% glycerol (v/v).

Such a structural change could lead to the exposure of a second potential site for covalent antibiotic attachment. Due to these structural divergences, subsequent studies of the protein-antibiotic interaction were carried out using only the full length TIPAS or its point mutants.

The TIPAS<sub>t</sub> variant encompasses the region of TIPAS proposed to construct the thiostrepton binding site and the poor (covalent) reactivity of this synthetic construct with thiostrepton was attributed to its adoption of a structure different to that in the native, full length protein. This is in agreement with the hypothesis that a significant non-covalent interaction between protein and antibiotic must precede covalent bond formation; the structural elements facilitating this non-covalent interaction are lost in the altered structure of TIPAS<sub>t</sub>, hence covalent bond formation is reduced. In order to examine this non-covalent component to antibiotic binding, the elimination of covalent protein-antibiotic binding was attempted through the generation of mutants of TIPAS in which the reactive cysteine (C214) was replaced with an alanine or a serine. At the same time, a C207A point mutant was made in order to rule out covalent binding at this site in the native protein. As expected, the formation of covalent complexes with the C207A mutant was unperturbed, but unexpectedly, the C214A and C214S were virtually 100% covalently bound by thiostrepton under the same reaction conditions as the native protein (Figure.5.5).

Covalent complex formation between thiostrepton and C214S could be explained by a Michael addition occurring with the oxygen from the serine hydroxyl, but this does not account for covalent complex formation with the

C214A mutant, where no Michael acceptor is presented at the 214 position. This implies that these complexes resulted from the covalent attachment of thiostrepton to an alternate amino acid residue. Furthermore, the occurrence of these complexes lends credence to the notion of a significant non-covalent interaction occurring between antibiotic and protein that sufficiently immobilizes the antibiotic, thereby allowing for the reorientation of the tail of thiostrepton into a position amenable to a Michael addition with a different residue.

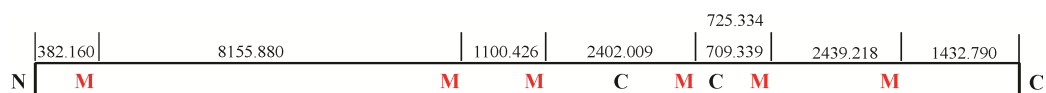


**Figure 5.5. Deconvoluted mass spectra of thiostrepton complexes with TIPAS mutants.** Masses at 16812.500 Da and 16828.500 Da correspond to the unbound C214A and C214S variants, respectively.

### 5.3.3. Mapping the site of covalent addition of thiostrepton by point mutation studies on TIPAS

The second cysteine residue (C207) in TIPAS is the most likely point of covalent attachment in the thiostrepton complexes with TIPAS mutants. Support for this was sought by peptide mapping studies on peptide fragments generated by digestion of the covalent complexes of these mutants with thiostrepton.

TIPAS features cleavage sites for several proteases and chemicals, but cyanogen bromide, which cleaves at methionines, was chosen as the cleavage agent since one of the 6 methionine residues in the TIPAS primary sequence is conveniently located between the two cysteines (Figure. 5.6).



**Figure 5.6. Cyanogen bromide cleavage sites in TIPAS.** The schematic depicts the TIPAS sequence in the N to C-terminus direction. The masses of the peptides expected from cleavage are shown (after conversion of methionine to homoserine lactone). C207 is found in the peptide of mass 2402.009; while the 214 position falls within the peptide of mass 725.334 (C214S) 709.339(C214A).

HPLC analysis of the products from cyanogen bromide cleavage of unbound TIPAS mutants yielded 7 products as predicted (Figure. 5.7) and ensuing mass spectrometry for each of these identified them individually as the expected peptide fragments, with the exception of the product of mass 2450.124 Da (designated D). The mass of this product is approximately 48 Da higher than what was expected for this peptide (Table 5.4). The increased molecular weight is attributed to the reaction of cyanogen bromide with cysteine (300, 301). In this case C207 is oxidized to cysteic acid, which was confirmed by tandem mass spectrometry (Figure 5.8). This peptide D was absent from the chromatograms of digests of TIPAS mutant complexes, while a new product eluting in a higher percentage of acetonitrile was detected (peptide D1). The mass determined for this product was consistent with the addition of thioestrepton to peptide D. The 14.811 Da difference between the observed and predicted molecular weight of peptide D bound with thioestrepton is due to a reaction between CNBr and thioestrepton that increases the mass of thioestrepton by this amount. Cyanogen

bromide is also known to engage reactions with amines (302) and its reaction with thiostrepton probably involves a primary or secondary amine from thiostrepton, or the amine from the dehydropiperidine core of the molecule. In addition, the peptide containing C214 (peptide C) was present in chromatograms of digests from both variants and no other product with a mass corresponding to the addition of thiostrepton to any of the remaining peptides was observed.

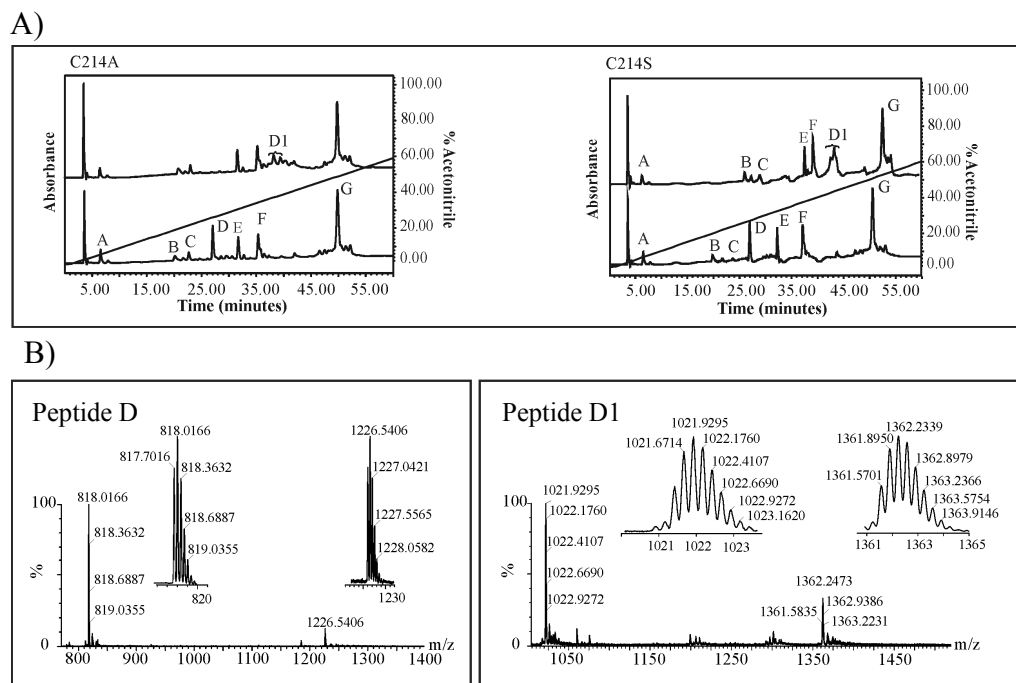
These results show that thiostrepton addition occurs to a residue within peptide D. The serendipitous oxidation of cysteine to cysteic acid by CNBr that occurred during digests of unbound TIPAS variants enabled the conformation of C207 as the reactive residue. Thiostrepton binding to a different residue would have resulted in a mass for peptide D1 48 Da higher than what was observed, due to the formation of cysteic acid. Hence, in the complexes with TIPAS variants, the Michael addition between with thiostrepton with C207 renders the thiol unavailable for reaction with CNBr.

A review of the interaction between TIPAS and thiostrepton modeled in Figure 5.3 shows C207 to be in a less favorable position for a Michael addition with the tail DHA from thiostrepton. Therefore, the unprecedented finding of covalent addition to C207 is indicative of a significant non-covalent interaction occurring between the protein and antibiotic, supporting the hypothesis that this interaction sufficiently immobilizes the core of the thiostrepton molecule on the protein, allowing for the repositioning of the flexible tail region that enables Michael addition to the less preferred C207.

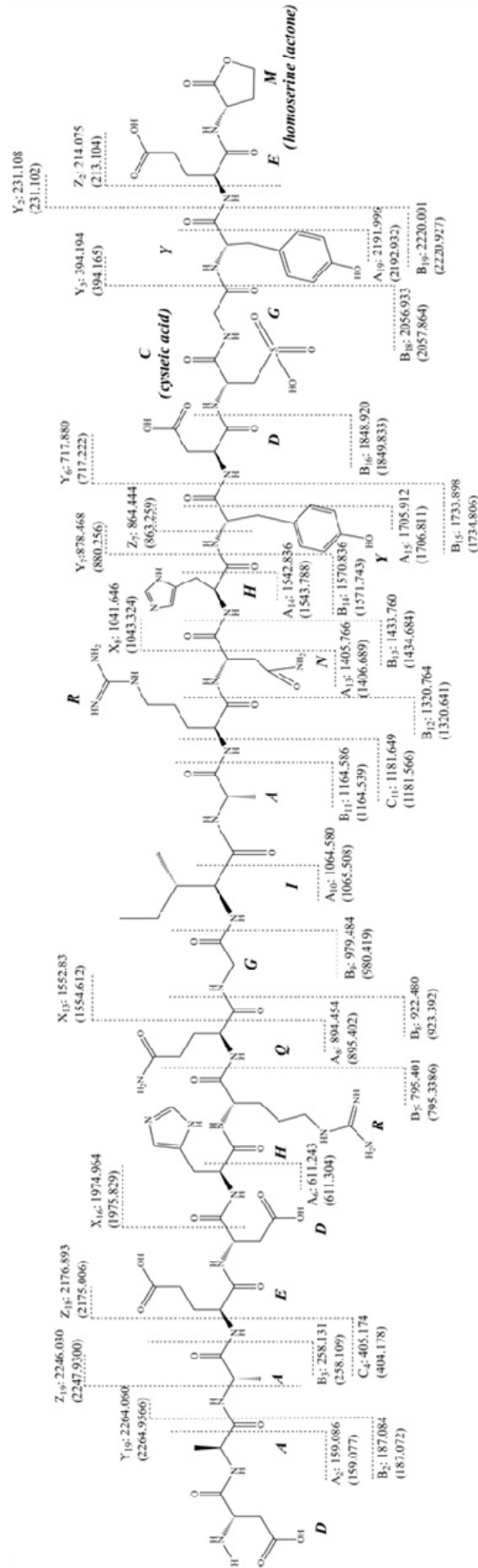
**Table 5.4. ESI-MS characterization of CNBr digestion products**

Peptide	$M_r$ (predicted <sup>†</sup> )	$M_r$ (observed <sup>†</sup> )			
		Unbound		Thiostrepton complex	
		C214A	C214S	C214A	C214S
A: 1-4	382.160	382.196	382.198	382.203	382.191
B: 73-84	1100.426	1100.543	1100.484	1100.494	1100.461
C: 106 - 112	709.339/725.334	709.391	725.402	709.410	725.390
C + Thiostrepton	2374.219/2390.214	-	-	-	-
	(C214A)/(C214S)				
D <sup>‡</sup> : 85-105	2402.009	2450.124	2450.109	-	-
D + Thiostrepton	4066.889	-	-	4081.700	4081.784
E: 135-147	1432.790	1432.836	1432.854	1432.884	1432.888
F: 113-134	2439.218	2439.388	2439.356	2439.382	2439.388
G: 5-72	8155.880	8160.500	8160.500	8160.500	8160.500

<sup>†</sup>Predicted peptide mass was calculated with methionines as homoserine lactone. Observed  $M_r$  values were deconvoluted from the multiply charged molecular ions detected by ESI-MS.



**Figure 5.7. Analysis of the cleavage products from cyanogen bromide digestion of thiostrepton complexes with TIPAS mutants.** (A) HPLC chromatograms of the products from CNBr digestion of thiostrepton complexes with the C214A variant (left panel) and the C214S variant (right panel). The bottom trace of each panel shows the products from the digestion of the unbound protein. B) ESI-mass spectra of peptide D and peptide D1. Spectra for peptide D show doubly and triply charged molecular ions of the peptide, with cysteine oxidized to cysteic acid ( $M_w$ : 2450.103 Da). Quadruply and triply charged molecular ions in the spectra from peptide D1 derive from a  $M_w$  of 4080.71 Da, which coincides with the addition of thiostrepton to C207 in peptide D (before cysteine oxidation by cyanogen bromide).

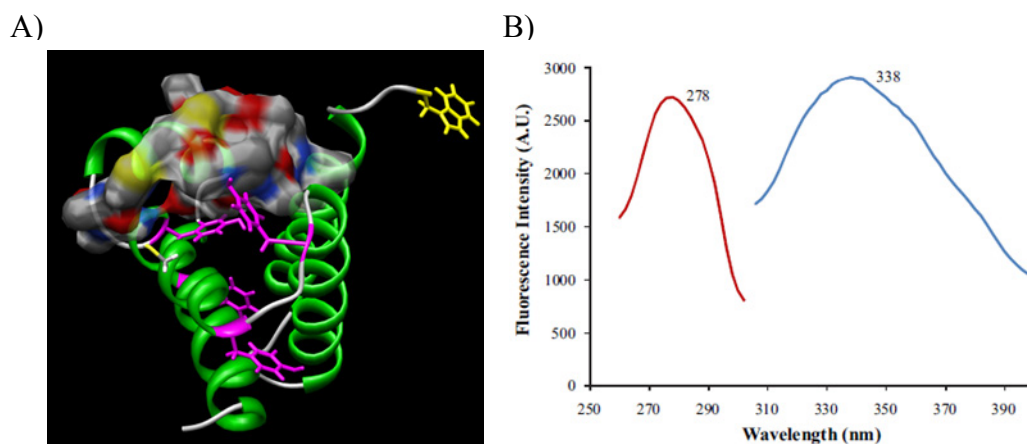


**Figure 5.8. Confirmation of conversion of cysteine to cysteic acid during CNBr digestion.** The CNBr digestion product from the unbound protein suspected to contain C207 (Mw = 2450.124 Da) is depicted. Methionine has been replaced by homoserine lactone and cysteine with cysteic acid. Ions observed in tandem mass spectrometry are shown and are in agreement with their predicted values (shown in brackets). The presence of cysteic acid is verified by the observation of A<sub>19</sub>, B<sub>18</sub>, B<sub>19</sub>, X<sub>8</sub>, X<sub>13</sub>, X<sub>16</sub>, Y<sub>6</sub>, Y<sub>7</sub>, Z<sub>7</sub>, Z<sub>18</sub> and Z<sub>19</sub>.



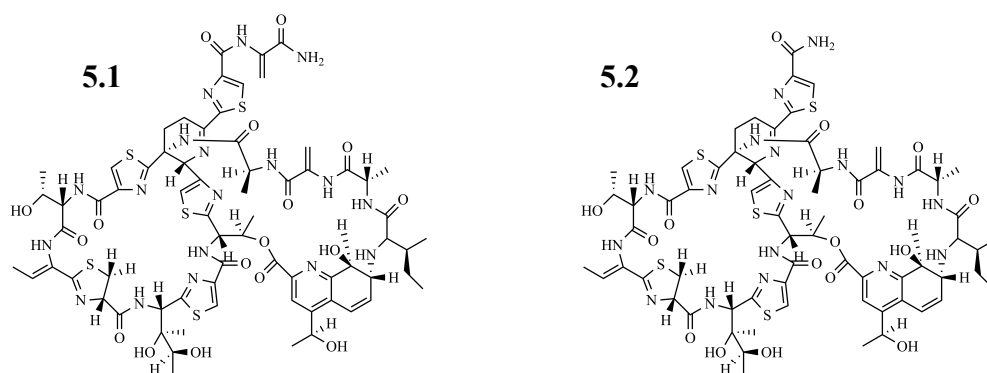
### 5.3.4. Qualitative evaluation of the non-covalent binding of thiostrepton to TIPAS

Several amino acid residues present in the primary sequence of TIPAS contribute to the intrinsic fluorescence of the protein, many of which line the proposed thiostrepton binding site (Figure. 5.9A). During NMR analyses of TIPAS (226) chemical shift changes in response to antibiotic binding were observed that were consistent with significant conformational changes in the protein structure. Since the fluorescent properties of amino acids in a protein are known to be sensitive to local environmental changes that accompany global conformational changes, it was thought that the changes in intrinsic TIPAS fluorescence that would presumably occur upon antibiotic binding would provide an expedient, qualitative, dual monitor of the general location of the antibiotic binding site as well as noncovalent protein-antibiotic binding.



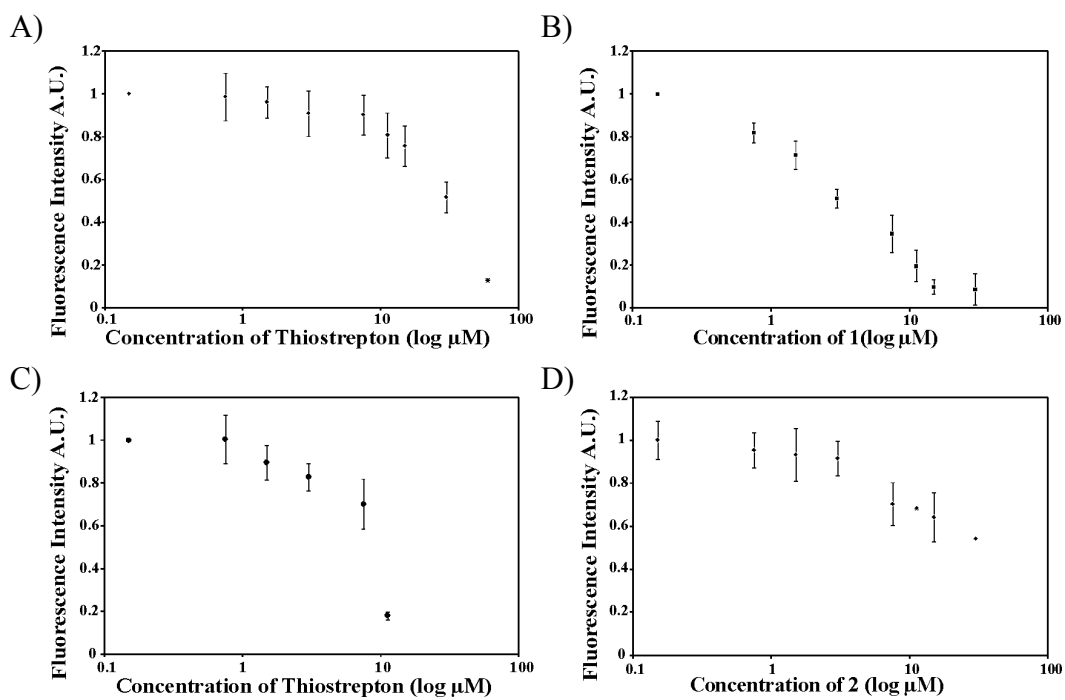
**Figure 5.9. Fluorescent residues in TIPAS.** (A) TIPAS docked with thiostrepton. Tyrosines are shown in magenta and tryptophans in yellow. The reported TIPAS crystal structure only shows the position of one tryptophan. (B) Excitation (red) and emission (blue) fluorescence maxima for TIPAS.

In order to properly investigate the non-covalent interaction of thiostrepton with TIPAS, the covalent interaction had to first be removed or prevented. The intrinsic protein fluorescence of TIPAS was therefore measured in the presence of thiostrepton derivatives **5.1** and **5.2** (Figure. 5.10). These derivatives, particularly **5.2**, lacked the reactive tail DHA and would thus be unable to form a covalent bond with TIPAS. In addition, the intrinsic fluorescence of TIPAS and its C214S mutant were measured in the presence of thiostrepton to verify a similar binding site for thiostrepton on the TIPAS mutants.



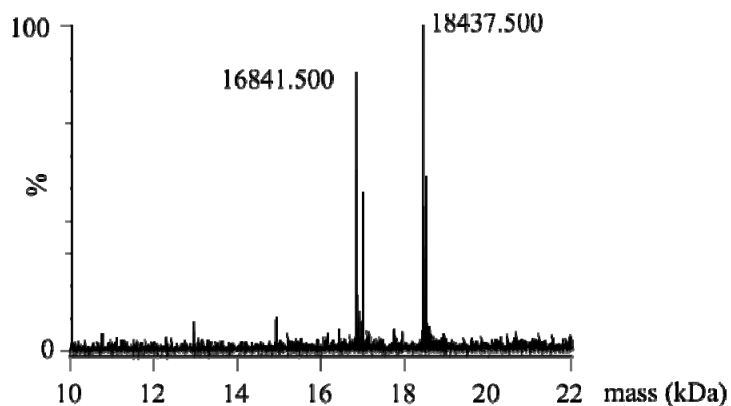
**Figure 5.10. Structures of truncated thiostrepton derivatives.**

The results of these experiments are presented in Figure. 5.11. As expected, the intrinsic fluorescence of TIPAS or its C214S mutant decreased in the presence of increasing concentrations of thiostrepton, with fluorescence approaching zero at the highest concentrations of antibiotic. These observations are consistent with the proposed antibiotic binding site on the protein, since the occupation of this site by thiostrepton would bring about decreased fluorescence.



**Figure 5.11. Effect of thiostrepton binding on TIPAS fluorescence.** A) TIPAS & thiostrepton; B) TIPAS & **5.1**; (C) TIPAS (C214S) & thiostrepton; D) TIPAS and **5.2**. Reactions of TIPAS proteins were performed as described using 10 μM of protein and varying concentrations of thiostrepton derivatives. Fluorescence readings were normalized and the mean is reported, with bars representing the standard deviation of three experiments.

This trend was also evident in the presence of the thiostrepton derivatives. The reduction of intrinsic TIPAS fluorescence caused by **5.1** mirrored that caused by thiostrepton, but it was subsequently found that **5.1** does indeed form a covalent complex with TIPAS (Figure 5.12). While this complexation occurs to a lesser extent than with thiostrepton, its formation likely contributed to the observed reductions in fluorescence. Unlike thiostrepton and derivative **5.1**, derivative **5.2** did not form a covalent complex with thiostrepton. The observed reduction in TIPAS fluorescence in the presence of this compound is therefore solely attributed to the non-covalent interaction with the protein.



**Figure 5.12. TIPAS reaction with 5.1.** Deconvoluted ESI mass spectrum of the crude product mixture from the reaction of TIPAS with 5.1, which indicates substantial covalent complexation (unbound TIPAS at 16841.500 and TIPAS covalently bound with 5.1 at 18437.500).

These observations reinforce the proposition of a significant protein-antibiotic non-covalent interaction. In the case of 5.1, the DHA in its truncated tail is likely not to be initially presented in a position that would be favorable towards Michael addition with C214. However, as with the TIPAS mutants, the non-covalent binding allows for reorientation of the tail in this derivative to a more amenable position.

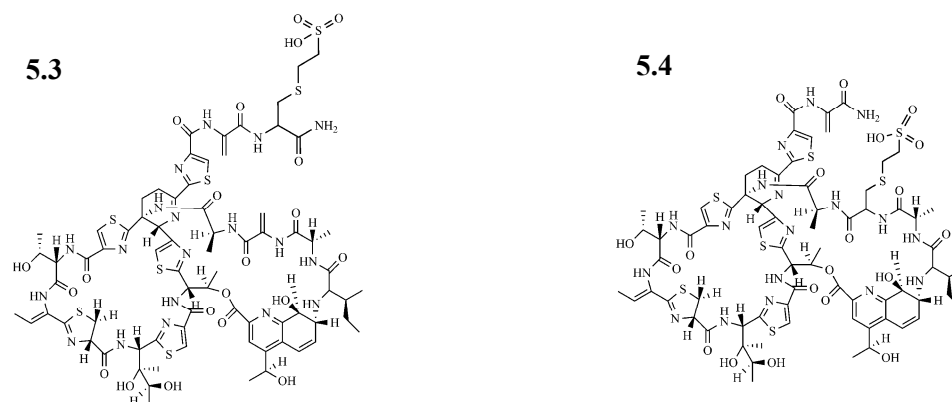
### 5.3.5. Non-covalent binding affinity of thiostrepton to TIPAS

The non-covalent binding of thiostrepton to TIPAS was quantified using isothermal titration calorimetry. In this approach, the absence of any covalent bond formation was absolutely crucial. Heat evolved from the formation of such bonds would interfere with that of the non-covalent interaction, which would ultimately result in incorrect values for the binding constants. This precluded titrations of thiostrepton into TIPAS. Although titrations of thiostrepton into a TIPAS variant (a double mutant with C207 and C214 replaced) could have

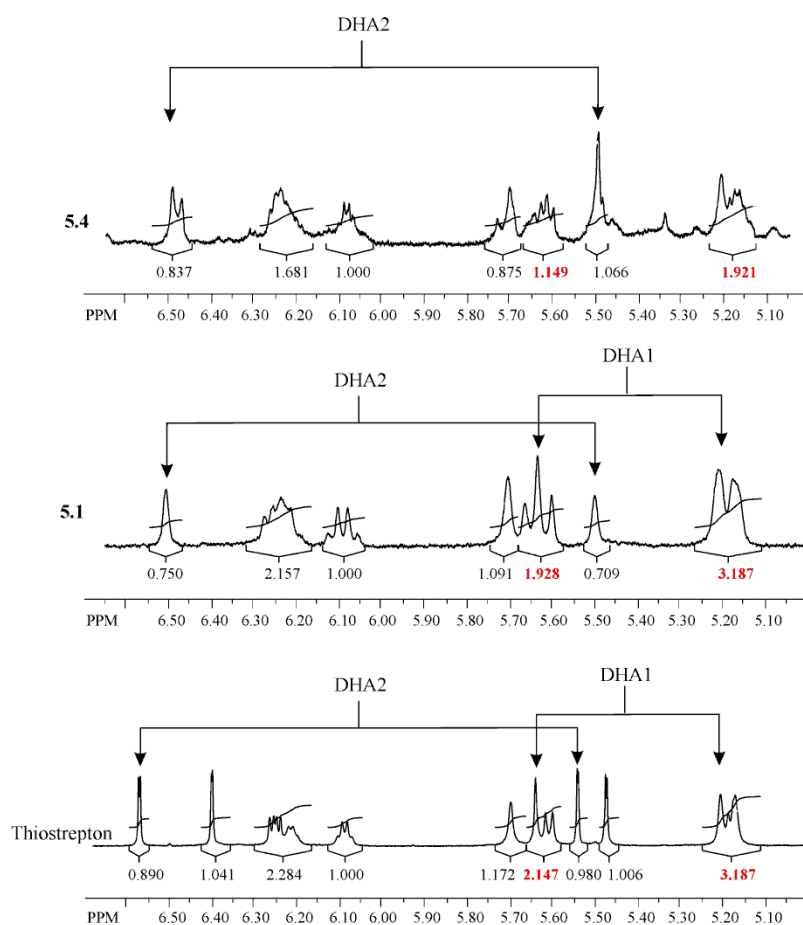
circumvented this problem of unwanted covalent bond formation, the aqueous insolubility of thiostrepton made such experiments impractical. Proportions of DMSO in excess of 25% (v/v) would be required to achieve concentrations of thiostrepton that would produce measurable results with acceptable signal to noise ratios. However, at these proportions of DMSO, the accompanying heats from dilution and mixing would eclipse those from the interaction under study.

Thiostrepton derivatives were turned to once again, in the quantification of the affinity of the non-covalent protein-antibiotic interaction. The truncated derivatives **5.1** and **5.2** exhibited better aqueous solubility than thiostrepton, making them suitable for ITC experiments. As earlier mentioned, derivative **5.1** was found to covalently bind TIPAS, hence, titrations with this derivative were performed using the C214A variant of TIPAS. Unlike native thiostrepton, this derivative did not covalently bind to this TIPAS variant, most likely because its Michael acceptor is outside the distance range for bonding with C207.

Additional derivatives, **5.3** and **5.4**, were prepared to probe the structural determinants of the non-covalent interaction (Figure 5.13). Derivative **5.3** (also featured in Chapter 2) was used to determine the contribution of the tail region of thiostrepton to non-covalent binding. The MENSA appendage would also block the reactive olefin, thus preventing covalent binding to this analogue. The synthesis of derivative **5.4** was unexpected as a Michael adduct of **5.1** with the appendage on the tail DHA was initially sought. Here, however, a novel derivative featuring a modification to the DHA on a thiostrepton macrocycle was obtained (Figure 5.14).



**Figure 5.13. Structures of Michael derivatives of thiostrepton.**

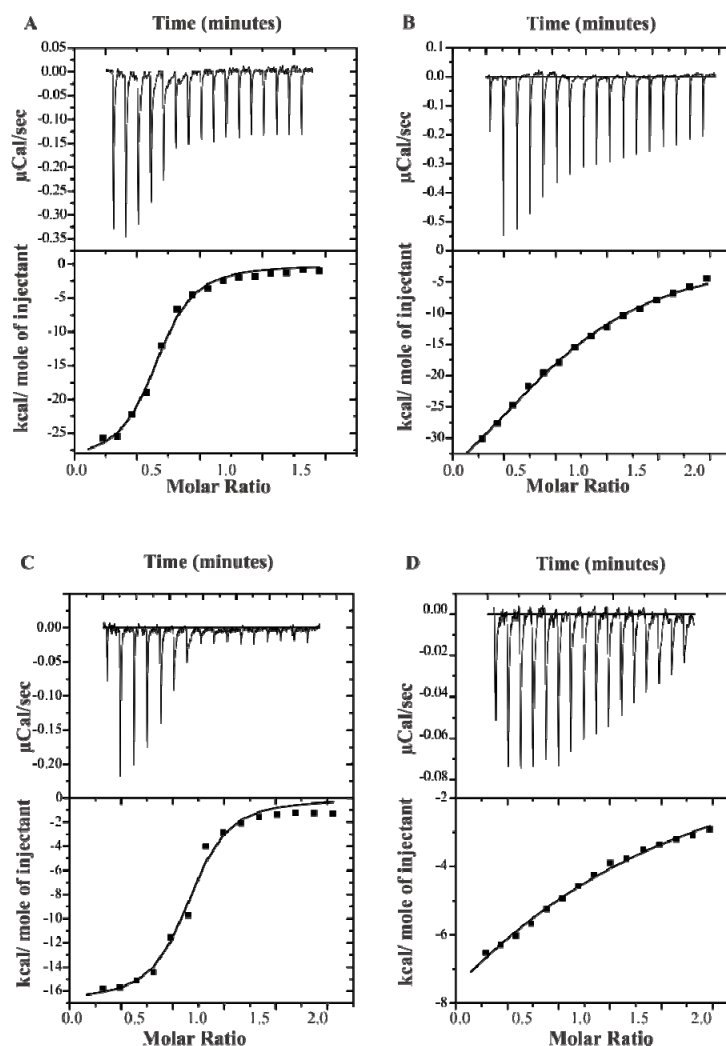


**Figure 5.14. Site of thiol Michael Addition in 5.4.** The olefin region of proton spectra for thiostrepton, **5.1** and **5.4**. is shown, with integrals indicated below spectra. Chemical shifts for DHA2 protons are present in the spectra for **5.4**, which indicates that this was not the site of thiol addition. Although the individual peaks for the DHA1 protons are obscured, integration of the region where they would be located indicates the absence of the DHA1 protons that are present in thiostrepton (and **5.1**).

A similar derivative of **5.1** has been prepared by Schoof *et al.* (239), however, in their synthesis, these researchers employed buffered conditions and used less basic conditions than were used here. Therefore, the higher pH used here likely increases the indiscriminate reactivity of MENSA hence producing isolatable yields of internally modified olefin. In any case, the opportune generation of this derivative enabled probing of the contribution from the thiostrepton macrocycles to non-covalent binding. None of the derivatives used in the ITC experiments formed covalent complexes with TIPAS during the time span of the ITC experiment (confirmed by ESI-MS immediately after completion of the titration).

The results of ITC titrations are presented in Figure 5.15. All derivatives were determined to bind TIPAS proteins at a 1:1 stoichiometry. Derivatives **5.2**, **5.3** and **5.4** bound TIPAS with dissociation constants of  $5.38 \pm 0.03 \mu\text{M}$ ,  $0.19 \pm 0.01 \mu\text{M}$  and  $12.95 \pm 0.01 \mu\text{M}$ , respectively and **5.1** bound the C214A mutant with a dissociation constant of  $0.21 \pm 0.002 \mu\text{M}$ , confirming a significant non-covalent interaction between thiostrepton and TIPAS. The finding of a low micromolar binding affinity for derivative **5.2** indicates that the thiostrepton macrocycles are the major contributors to this interaction. Fittingly, derivative **5.4** displayed the weakest affinity for TIPAS, in spite of possessing a tail region. This is explained by the added presence of the MENSA appendage on the core of the thiostrepton molecule disrupting the predominantly hydrophobic, non-covalent interactions between the thiostrepton and TIPAS, resulting in its diminished binding affinity, particularly in comparison to **5.2**. Meanwhile, the

dissociation constants for derivatives **5.1** and **5.3** were approximately 30-fold less than that of **5.2**. Since both these derivatives possess DHA tails, these results indicate that the affinity of this non-covalent interaction is enhanced by the tail region of thiostrepton.

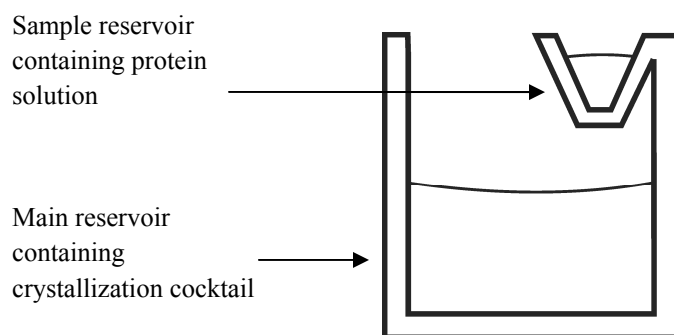


**Figure 5.15. Isothermal titration calorimetry of TIPAS with thiostrepton derivatives.** Top panels show heats of injection and bottom panels show the binding isotherm for sequential injections of **5.1** (A); **5.3** (C) and **5.4** (D) into TIPAS and **5.2** into the C214A variant of TIPAS (B).



### 5.3.6. X-ray crystallography of TIPAS & the TIPAS-thiostrepton complex

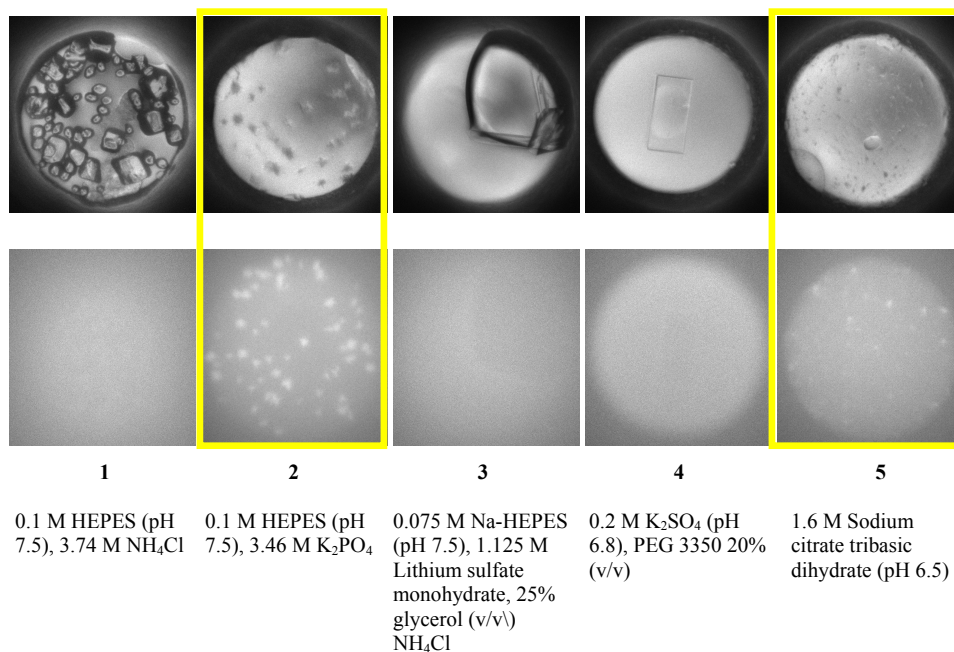
Prior to performing crystallography experiments, samples of TIPAS or the TIPAS-thiostrepton complex were first subjected to an additional level of purification by anion exchange chromatography to ensure a sample purity greater than 95% and then concentrated to 8-10 mg/mL. Suitable conditions for crystal growth were first sought with the Hampton Crystal Screen Cryo, using the sitting drop method. To the main reservoir of individual wells of a 96-well sitting drop plate was added 100  $\mu$ L of crystallization cocktail, while 1  $\mu$ L of protein solution and 1  $\mu$ L of the same crystallization cocktail were added to the sample reservoir and mixed. The wells were sealed, and left undisturbed at ambient temperature. The progress of crystal growth was monitored weekly. This initial screen proved to be largely unsuccessful, resulting mainly in protein precipitation or aggregation.



**Figure 5.16. Schematic of an individual well from a 96-well sitting drop plate.**

Continual screening for suitable conditions by this approach would have been laborious and time intensive, therefore a sample of TIPAS (10 mg/ mL)

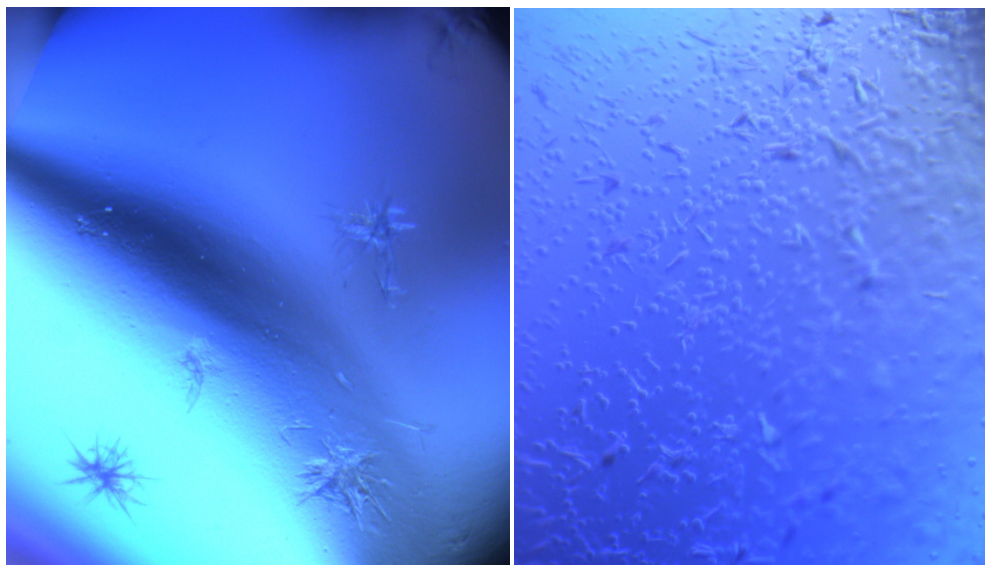
was supplied to the Hauptman Woodward Research Institute for the simultaneous screening of 1536 different conditions, by the vapor diffusion under oil technique (303). This high-throughput approach was used to identify conditions that could be further optimized, from a large collection of cocktails that simultaneously screened the effects of salts, pH, buffers and aids such as PEG. Crystal growth was tracked on a weekly basis and by week 3, several potential “hits” (wells containing observable crystalline material) were identified, along with several wells containing precipitated protein. After an additional two weeks, the corresponding wells were imaged under UV light to confirm the presence of proteinaceous crystals (Figure. 5.17).



**Figure 5.17. High throughput screening of crystal growth conditions for TIPAS.** Images of 5 wells containing suspected protein crystals are shown viewed under polarized (top panels) and UV light (bottom panels) after 5 weeks of growth. Wells exhibiting fluorescence under UV light (boxed in yellow) contain protein (micro)crystals.

The UV absorbance by the several tyrosines and tryptophans in TIPAS enabled quick confirmation of the presence of protein crystals produced by the cocktails indicated in Figure 5.17 and additional optimization of cocktail 2 was performed.

The conditions of cocktail 2 were varied with respect to  $K_2PO_4$  concentration (2.0 M, 2.5 M and 3.0 M) and pH (7.5, 8.0, 8.3), generating 9 unique conditions that were used in sitting drop crystallization trials for TIPAS and the TIPAS-thiostrepton complex. After 4 weeks, crystal growth was seen in the cocktails containing 0.1M HEPES at pH 8 with 2.0 M  $K_2PO_4$  for TIPAS and 0.1 M HEPES at pH 8.3 with 2.0 M  $K_2PO_4$  for the TIPAS-thiostrepton complex (Figure. 5.18) but this growth largely took the form of needles or needle clusters.



**Figure 5.18. Optimized conditions for crystal growth of TIPAS and the TIPAS-thiostrepton complex.** Images for TIPAS (left) and the TIPAS-thiostrepton complex (right) were taken under polarized light.

While this was an improvement with respect to the clumped micro-crystals obtained from the high throughput screen, these crystals were not of a sufficient size or quality suitable for X-ray diffraction experiments, hence an additive screen was next attempted to improve crystal quality. In this approach, minute amounts of a small molecule were added to the crystallization cocktail in an effort to aid the crystallization process. Thirty-one such additives (Appendix 8) were tested for each of the optimized conditions that yielded needles, but, unfortunately, crystal quality was not improved.

#### **5.4. Conclusions, Perspectives and Future work**

A high affinity non-covalent interaction between TIPAS and thiostrepton has been demonstrated and the underlying molecular and structural determinants for this interaction have been determined. The results are in support of the thiostrepton binding site on TIPAS that has been previously proposed and they further show that the interaction is governed predominantly by the hydrophobic interactions that occur between the thiostrepton macrocycles and the amino acid residues that form the binding site. Although the bis-DHA tail primarily serves to supply the olefin that participates in a Michael addition with the thiol from C214, the results presented here show it also enhances the non-covalent binding affinity of TIPAS for thiostrepton. Together, these findings are consistent with a binding mechanism in which the non-covalent interaction necessarily precedes the covalent binding of thiostrepton, which allows for the presentation of the tail region in the proper orientation that leads to covalent binding with the protein.

Although the results of this study provide a model for TIP mediated thiopeptide resistance, a broader understanding could be gained from the detailed study of the structural determinants for the binding of additional thiopeptides antibiotics that are susceptible to TIP mediated resistance. This would be aided by the solution of structures for the TIPAS-thiostrepton/thiopeptide complex, possibly in future by NMR studies.

Complete structures for the complex remain elusive and the attempts at crystallization of the TIPAS or the TIPAS-thiostrepton complex in this work were unsuccessful. However, many potential areas for modification remain. A higher initial protein concentration can be used since the final protein concentration was reduced to half by the addition of an equal volume of crystallization cocktail. Alternatively, the ratio of protein to crystallization cocktail in the drop can be increased. As well, additional additives such as PEG or ionic salts may be more rigorously investigated for their effects on protein crystallization and initial trials using these approaches have offered promising results. Finally, an alternative method of crystallization such as hanging drop can be attempted, which will allow for the use of a larger sample volume that can positively affect the outcome. On the other hand, structures of the complex may be sought through NMR spectroscopy.

As earlier mentioned, TIP mediated resistance occurs against a broad range of thiopeptides and it is likely that the mechanism of antibiotic binding described above extends across this group. TIP genes and their products have been identified in several *Streptomyces*, which importantly are not

manufacturers of thiopeptides or their corresponding resistance enzymes. Therefore, the findings presented have contributed to the understanding of drug resistance in this microbial class and may have implications in the design of novel thiopeptide-based antimicrobial compounds that evade resistance mechanisms.

## REFERENCES

---

1. Cundliffe, E. (2000) in *The Ribosome: Structure, Function, Antibiotics, and Cellular Interactions* (Garett, R. A., Douthwaite, S. R., Liljas, A., Matheson, A. T., Moore, P. B., and Noller, H. F., eds.) pp. 409–417, ASM Press, Washington DC
2. Davies, J. (1990) What are antibiotics? Archaic functions for modern activities. *Molecular Microbiology* **4**, 1227–32
3. Hawkey, P. M. (2008) Molecular epidemiology of clinically significant antibiotic resistance genes. *British Journal of Pharmacology* **153 Suppl**, S406–13
4. Clatworthy, A. E., Pierson, E., and Hung, D. T. (2007) Targeting virulence: a new paradigm for antimicrobial therapy. *Nature Chemical Biology* **3**, 541–8
5. Waxman, D. J., and Strominger, J. L. (1983) Penicillin-binding proteins and the mechanism of action of beta-lactam antibiotics. *Annual Review of Biochemistry* **52**, 825–69
6. Reynolds, P. E. (1989) Structure, biochemistry and mechanism of action of glycopeptide antibiotics. *European Journal of Clinical Microbiology & Infectious Diseases* **8**, 943–50
7. Ge, M. (1999) Vancomycin Derivatives That Inhibit Peptidoglycan Biosynthesis Without Binding D-Ala-D-Ala. *Science* **284**, 507–511
8. Kahne, D., Leimkuhler, C., Lu, W., and Walsh, C. (2005) Glycopeptide and lipoglycopeptide antibiotics. *Chemical Reviews* **105**, 425–48
9. Singh, M. P., Petersen, P. J., Weiss, W. J., Janso, J. E., Luckman, S. W., Lenoy, E. B., Bradford, P. A., Testa, R. T., and Greensteins, M. (2003) Mannopeptimycins , New Cyclic Glycopeptide Antibiotics Produced by *Streptomyces hygroscopicus* LL-AC98 : Antibacterial and Mechanistic Activities. *Antimicrobial Agents and Chemotherapy* **47**, 62–69
10. Breukink, E., and De Kruijff, B. (2006) Lipid II as a target for antibiotics. *Nature Reviews. Drug Discovery* **5**, 321–32
11. Chatterjee, C., Paul, M., Xie, L., and Van der Donk, W. a (2005) Biosynthesis and mode of action of lantibiotics. *Chemical Reviews* **105**, 633–84

12. Hancock, R. E., and Chapple, D. S. (1999) Peptide antibiotics. *Antimicrobial Agents and Chemotherapy* **43**, 1317–23
13. Hale, J. D. F., and Hancock, R. E. W. (2007) Alternative mechanisms of action of cationic antimicrobial peptides on bacteria. *Expert Review of Antiinfective Therapy* **5**, 951–959
14. McAuliffe, O., Ross, R. P., and Hill, C. (2001) Lantibiotics: structure, biosynthesis and mode of action. *FEMS Microbiology Reviews* **25**, 285–308
15. Melnikov, S., Ben-Shem, A., Garreau de Loubresse, N., Jenner, L., Yusupova, G., and Yusupov, M. (2012) One core, two shells: bacterial and eukaryotic ribosomes. *Nature Structural & Molecular biology* **19**, 560–7
16. Nierhaus, K. H. (2004) in *Protein Synthesis and Ribosome Structure* (Nierhaus, K. H., and Wilson, D. N., eds.) pp. 323–366, Wiley-VCH, Weinheim
17. Wilson, D. (2004) in *Protein Synthesis and Ribosome Structure* (Nierhaus, K. H., and Wilson, D. N., eds.) pp. 449–527, Wiley-VCH, Weinheim
18. Rodnina, M. V, Pape, T., Savelsbergh, A., Mohr, D., Matassova, N., and Wintermeyer, W. (2000) in *The Ribosome: Structure, Function, Antibiotics, and Cellular Interactions* (Garrett, R. A., Douthwaite, S. R., Liljas, A., Matheson, A. T., Moore, P. B., and Noller, H. F., eds.) pp. 301–317, ASM Press, Washington DC
19. Shakil, S., Khan, R., Zarrilli, R., and Khan, A. U. (2008) Aminoglycosides versus bacteria—a description of the action, resistance mechanism, and nosocomial battleground. *Journal of Biomedical Science* **15**, 5–14
20. Puglisi, J. D., Blanchard, S. C., Dahlquist, K. D., Eason, R. G., Fourmy, D., Lynch, S. R., Recht, M. I., and Yoshizawa, S. (2000) in *The Ribosome: Structure, Function, Antibiotics, and Cellular Interactions* (Garrett, R. A., Douthwaite, S. R., Liljas, A., Matheson, A. T., Moore, P. B., and Noller, H. F., eds.) pp. 419–429, ASM Press, Washington DC
21. Jana, S., and Deb, J. K. (2006) Molecular understanding of aminoglycoside action and resistance. *Applied Microbiology and Biotechnology* **70**, 140–150



22. Nissen, P., Hansen, J., Ban, N., Moore, P. B., and Steitz, T. a (2000) The structural basis of ribosome activity in peptide bond synthesis. *Science* **289**, 920–30
23. Trobro, S., and Aqvist, J. (2005) Mechanism of peptide bond synthesis on the ribosome. *Proceedings of the National Academy of Sciences of the United States of America* **102**, 12395–400
24. Wilson, D. N., and Nierhaus, K. H. (2003) The ribosome through the looking glass. *Angewandte Chemie International Edition* **42**, 3464–86
25. Schlünzen, F., Zarivach, R., Harms, J., Bashan, A., Tocilj, A., Albrecht, R., Yonath, A., and Franceschi, F. (2001) Structural basis for the interaction of antibiotics with the peptidyl transferase centre in eubacteria. *Nature* **413**, 814–21
26. Tenson, T., Lovmar, M., and Ehrenberg, M. (2003) The Mechanism of Action of Macrolides, Lincosamides and Streptogramin B Reveals the Nascent Peptide Exit Path in the Ribosome. *Journal of Molecular Biology* **330**, 1005–1014
27. Mukhtar, T. a, and Wright, G. D. (2005) Streptogramins, oxazolidinones, and other inhibitors of bacterial protein synthesis. *Chemical Reviews* **105**, 529–42
28. Bozdogan, B., and Appelbaum, P. C. (2004) Oxazolidinones: activity, mode of action, and mechanism of resistance. *International Journal of Antimicrobial Agents* **23**, 113–119
29. Gaynor, M., and Mankin, A. S. (2003) Macrolide antibiotics: binding site, mechanism of action, resistance. *Current Topics in Medicinal Chemistry* **3**, 949–961
30. Yonath, A. (2005) Antibiotics targeting ribosomes: resistance, selectivity, synergism and cellular regulation. *Annual Review of Biochemistry* **74**, 649–79
31. Savelsbergh, A., Katunin, V. I., Mohr, D., Peske, F., Rodnina, M. V, and Wintermeyer, W. (2003) An elongation factor G-induced ribosome rearrangement precedes tRNA-mRNA translocation. *Molecular Cell* **11**, 1517–23
32. Noller, H. F., Yusupov, M. M., Yusupova, G. Z., Baucom, A., and Cate, J. H. D. (2002) Translocation of tRNA during protein synthesis. *FEBS Letters* **514**, 11–6

33. Ball, P. (2000) in *The Quinolones* (Andriole, V. T., ed.) 3rd Ed., pp. 2–32, Academic Press, San Diego, CA
34. Emmerson, A. M., and Jones, A. M. (2003) The quinolones: decades of development and use. *The Journal of Antimicrobial Chemotherapy* **51 Suppl 1**, 13–20
35. Ginsburg, A. S., Grosset, J. H., and Bishai, W. R. (2003) Fluoroquinolones, tuberculosis and resistance. *The Lancet* **3**, 432–442
36. Drlica, K. (1999) Mechanism of fluoroquinolone action. *Current Opinion in Microbiology* **2**, 504–8
37. Walker, R. C. (1999) The Fluoroquinolones. *Mayo Clinic Proceedings* **74**, 1030–1037
38. Poole, K. (2005) Efflux-mediated antimicrobial resistance. *The Journal of Antimicrobial Chemotherapy* **56**, 20–51
39. Wright, G. D. (2011) Molecular mechanisms of antibiotic resistance. *Chemical Communications* **47**, 4055–61
40. Blair, J. M. a, and Piddock, L. J. V (2009) Structure, function and inhibition of RND efflux pumps in Gram-negative bacteria: an update. *Current Opinion in Microbiology* **12**, 512–9
41. Poole, K. (2012) in *Antibiotic Discovery and Development* (Dougherty, T. J., and Pucci, M. J., eds.) pp. 349–395, Springer US, Boston, MA
42. Walsh, C. (2000) Molecular mechanisms that confer antibacterial drug resistance. *Nature* **406**, 775–81
43. Babic, M., Hujer, A. M., and Bonomo, R. a (2006) What's new in antibiotic resistance? Focus on beta-lactamases. *Drug resistance updates : reviews and commentaries in antimicrobial and anticancer chemotherapy* **9**, 142–56
44. Kumarasamy, K. K., Toleman, M. a, Walsh, T. R., Bagaria, J., Butt, F., Balakrishnan, R., Chaudhary, U., Doumith, M., Giske, C. G., and Irfan, S. (2010) Emergence of a new antibiotic resistance mechanism in India, Pakistan, and the UK: a molecular, biological, and epidemiological study. *The Lancet Infectious Diseases* **10**, 597–602
45. Vester, B., and Douthwaite, S. (2001) Macrolide Resistance Conferred by Base Substitutions in 23S rRNA. *Antimicrobial Agents and Chemotherapy* **45**, 1–12

46. Treede, I., Jakobsen, L., Kirpekar, F., Vester, B., Weitnauer, G., Bechthold, A., and Douthwaite, S. (2003) The avilamycin resistance determinants AviRa and AviRb methylate 23S rRNA at the guanosine 2535 base and the uridine 2479 ribose. *Molecular Microbiology* **49**, 309–318
47. Murakami, T., Holt, T. G., and Thompson, C. J. (1989) Thiostrepton-induced gene expression in *Streptomyces lividans*. *Journal of Bacteriology* **171**, 1459–66
48. Holmes, D. J., Caso, J. L., and Thompson, C. J. (1993) Autogenous transcriptional activation of induced gene in *Streptomyces lividans*. *The EMBO Journal* **12**, 3183–3191
49. Dumas, P., Bergdoll, M., Cagnon, C., and Masson, J. M. (1994) Crystal structure and site-directed mutagenesis of a bleomycin resistance protein and their significance for drug sequestering. *The European Molecular Biology Organization Journal* **13**, 2483–2492
50. Gatignol, A., Durand, H., and Tiraby, G. (1988) Bleomycin resistance conferred by a drug-binding protein. *FEBS Letters* **230**, 171–175
51. Sheldon, P. J., Mao, Y., He, M., and Sherman, D. H. (1999) Mitomycin Resistance in *Streptomyces lavendulae* Includes a Novel Drug-Binding-Protein-Dependent Export System. *Journal Of Bacteriology* **181**, 2507–2512
52. Sheldon, P. J., Johnson, D. A., August, P. R., Liu, H. W., and Sherman, D. H. (1997) Characterization of a mitomycin-binding drug resistance mechanism from the producing organism, *Streptomyces lavendulae*. *Journal of Bacteriology* **179**, 1796–1804
53. Wright, G. D. (2010) Antibiotic resistance in the environment: a link to the clinic? *Current Opinion in Microbiology* **13**, 589–94
54. Gillespie, S. H. (2002) Evolution of Drug Resistance in *Mycobacterium tuberculosis* : Clinical and Molecular Perspective. *Antimicrobial Agents and Chemotherapy* **46**, 267–274
55. Matteelli, A., Migliori, G. B., Cirillo, D., Centis, R., Girard, E., and Raviglion, M. (2007) Multidrug-resistant and extensively drug-resistant *Mycobacterium tuberculosis*: epidemiology and control. *Expert Review of Antiinfective Therapy* **5**, 857–871

56. Wilson, P., Andrews, J., Charlesworth, R., Walesby, R., Singer, M., Farrell, D., and Robbins, M. (2003) Linezolid resistance in clinical isolates of *Staphylococcus aureus*. *Lancet* **358**, 186–188
57. Jalal, S., Ciofu, O., Høiby, N., and Gotoh, N. (2000) Molecular Mechanisms of Fluoroquinolone Resistance in *Pseudomonas aeruginosa* Isolates from Cystic Fibrosis Patients Molecular Mechanisms of Fluoroquinolone Resistance in *Pseudomonas aeruginosa* Isolates from Cystic Fibrosis Patients. *Antimicrobial Agents and Chemotherapy* **44**, 710–712
58. Alekshun, M. N., and Levy, S. B. (2007) Molecular mechanisms of antibacterial multidrug resistance. *Cell* **128**, 1037–50
59. Woodford, N., and Ellington, M. J. (2007) The emergence of antibiotic resistance by mutation. *Clinical Microbiology and Infection* **13**, 5–18
60. Bennett, P. M. (2008) Plasmid encoded antibiotic resistance: acquisition and transfer of antibiotic resistance genes in bacteria. *British Journal of Pharmacology* **153 Suppl**, S347–S357
61. Davies, J. (1994) Inactivation of Antibiotics and the Dissemination of Resistance Genes. *Science* **264**, 375–382
62. Holmes, A. J., Gillings, M. R., Nield, B. S., Mabbutt, B. C., Helena, K. M., and Stokes, H. W. (2003) The gene cassette metagenome is a basic resource for bacterial genome evolution. *Environmental Microbiology* **5**, 383–394
63. Acott, K. A., Labuza, T. P., Minra, A., Drake, J. W., Aguyagi, S. Y., Furkawa, F., Zawadska, H., Bhanet, O. S., Dufuy, D., Erismann, K. H., Grant, M. E., Hall, R. H., Biolo, S., Mccann, J., Yamasaki, E., Veron, V. J., Groot, A. P. De, Strong, F., Collins, E., Benazet, F., Cartier, M., Florent, J., Godard, C., Jung, G., Lunel, J., Mancy, D., Pascal, C., Renaut, J., Tarridec, P., Theilleux, J., Tissier, R., Dubost, M., and Ninet, L. (1980) Nosiheptide, a sulfur-containing peptide antibiotic isolated from *Streptomyces actuosus* 40037. *Experientia* **36**, 414–416
64. Depardieu, F., Podglajen, I., Leclercq, R., Collatz, E., and Courvalin, P. (2007) Modes and Modulations of Antibiotic Resistance Gene Expression. *Clinical Microbiology Reviews* **20**, 79–114
65. Hall, R. M., and Collis, C. M. (1998) Antibiotic resistance in gram-negative bacteria: the role of gene cassettes and integrons. *Drug resistance Updates : Reviews and Commentaries in Antimicrobial and Anticancer Chemotherapy* **1**, 109–119

66. Gillings, M., Boucher, Y., Labbate, M., Holmes, A., Krishnan, S., Holley, M., and Stokes, H. W. (2008) The evolution of class 1 integrons and the rise of antibiotic resistance. *Journal of Bacteriology* **190**, 5095–100
67. Davies, J., and Davies, D. (2010) Origins and evolution of antibiotic resistance. *Microbiology and Molecular Biology Reviews* **74**, 417–33
68. Wright, G. D. (2007) The antibiotic resistome: the nexus of chemical and genetic diversity. *Nature Reviews. Microbiology* **5**, 175–86
69. Andersson, D. I., and Hughes, D. (2010) Antibiotic resistance and its cost: is it possible to reverse resistance? *Nature Reviews. Microbiology* **8**, 260–71
70. Aminov, R. I., and Mackie, R. I. (2007) Evolution and ecology of antibiotic resistance genes. *FEMS Microbiology Letters* **271**, 147–61
71. McKenzie, N. L., Thaker, M., Koteva, K., Hughes, D. W., Wright, G. D., and Nodwell, J. R. (2010) Induction of antimicrobial activities in heterologous streptomycetes using alleles of the *Streptomyces coelicolor* gene *absA1*. *The Journal of Antibiotics* **63**, 177–82
72. Nodwell, J. R., and Cuthbertson, L. (2011) Better chemistry through regulation. *Chemistry & Biology* **18**, 1515–6
73. Rokem, J. S., Lantz, A. E., and Nielsen, J. (2007) Systems biology of antibiotic production by microorganisms. *Natural Product Reports* **24**, 1262–87
74. Nguyen, K. T., He, X., Alexander, D. C., Li, C., Gu, J.-Q., Mascio, C., Van Praagh, A., Mortin, L., Chu, M., Silverman, J. a, Brian, P., and Baltz, R. H. (2010) Genetically engineered lipopeptide antibiotics related to A54145 and daptomycin with improved properties. *Antimicrobial Agents and Chemotherapy* **54**, 1404–13
75. Bagley, M. C., Dale, J. W., Merritt, E. a, and Xiong, X. (2005) Thiopeptide antibiotics. *Chemical Reviews* **105**, 685–714
76. Hughes, R. A., and Moody, C. J. (2007) From amino acids to heteroaromatics-thiopeptide antibiotics, nature's heterocyclic peptides. *Angewandte Chemie International Edition* **46**, 7930–7954
77. Li, J., Qu, X., He, X., Duan, L., Wu, G., Bi, D., Deng, Z., Liu, W., and Ou, H.-Y. (2012) ThioFinder: A Web-Based Tool for the Identification of Thiopeptide Gene Clusters in DNA Sequences. *PloS One* **7**, e45878

78. Dutcher, J. D., and Vandeputte, J. (1955) Thiostrepton, a new antibiotic. II. Isolation and chemical characterization. *Antibiotics Annual* **3**, 560–561
79. Donovick, R., Parango, J. F., Stout, H. A., and Weinstein, M. J. (1955) Thiostrepton, a new antibiotic. I. In vitro studies. *Antibiotics Annual* **3**, 554–559
80. Trejo, H., Dean, D., Pluscec, J., and Brown, E. (1977) *Streptomyces Laurentii*, a new species producing thiostrepton. *The Journal of Antibiotics* **30**, 639–643
81. Bodanszky, M., Fried, J., Sheehan, J. T., Williams, N. J., Alicino, J., Cohen, A. I., Keeler, B. T., and Birkhimer, C. A. (1964) Thiostrepton. Degradation Products and Structural Features. *Journal of the American Chemical Society* **86**, 2478–2490
82. Anderson, B., Crowfoot Hodgkin, D., and Viswamitra, M. A. (1970) The structure of thiostrepton. *Nature* **225**, 233–235
83. Mocek, U., Beale, J., Floss, H. (1989) Reexamination of the <sup>1</sup>H and <sup>13</sup>C NMR Spectral Assignments of thiostrepton. *The Journal of Antibiotics* **42**, 1649–1652
84. Bond, C. S., Shaw, M. P., Alphey, M. S., and Hunter, W. N. (2001) Structure of the macrocycle thiostrepton solved using the anomalous dispersion contribution of sulfur. *Acta Crystallographica Section D Biological Crystallography* **57**, 755–758
85. Hang, P. C., and Honek, J. F. (2005) Electronic structure calculations on the thiazole-containing antibiotic thiostrepton: molecular mechanics, semi-empirical and ab initio analyses. *Bioorganic & Medicinal Chemistry Letters* **15**, 1471–1474
86. Moody, C. J., and Bagley, M. C. (1998) The first synthesis of promothiocin A. *Chemical Communications* **4**, 2049–2050
87. Bagley, M. C., Bashford, K. E., Hesketh, C. L., and Moody, C. J. (2000) Total Synthesis of the Thiopeptide Promothiocin A. *Journal of the American Chemical Society* **122**, 3301–3313
88. Hughes, R. A., Thompson, S. P., Alcaraz, L., and Moody, C. J. (2005) Total synthesis of the thiopeptide antibiotic amythiamicin D. *Journal of the American Chemical Society* **127**, 15644–15651
89. Nicolaou, K. C., Safina, B. S., Zak, M., Lee, S. H., Nevalainen, M., Bella, M., Estrada, A., Funke, C., Zécri, F. J., and Bulat, S. (2005) Total

synthesis of thiostrepton. Retrosynthetic analysis and construction of key building blocks. *Journal of the American Chemical Society* **127**, 11159–75

90. Nicolaou, K. C., Zak, M., Safina, B. S., Estrada, A. a, Lee, S. H., and Nevalainen, M. (2005) Total synthesis of thiostrepton. Assembly of key building blocks and completion of the synthesis. *Journal of the American Chemical Society* **127**, 11176–83
91. Nicolaou, K. C., Zak, M., Safina, B. S., Estrada, A. a, Lee, S. H., and Nevalainen, M. (2005) Total synthesis of thiostrepton. Assembly of key building blocks and completion of the synthesis. *Journal of the American Chemical Society* **127**, 11176–83
92. Nicolaou, K. C., Nevalainen, M., Safina, B. S., Zak, M., and Bulat, S. (2002) Biomimetically Inspired Synthesis of the Dehydropiperidine Domain of Thiostrepton. *Angewandte Chemie International Edition* **41**, 1941–1945
93. Nicolaou, K. C. (2011) in *Classics in Total Synthesis III. Further targets, strategies and methods*. (Nicolaou, K. C., and Chen, J. S., eds.) pp. 127–159, Wiley-VCH, Weinheim
94. Mori, T., Higashibayashi, S., Goto, T., Kohno, M., Satouchi, Y., Shinko, K., Suzuki, K., Suzuki, S., Tohmiya, H., Hashimoto, K., and Nakata, M. (2007) Total synthesis of siomycin A. *Tetrahedron Letters* **48**, 1331–1335
95. Bagley, M. C., and Glover, C. (2006) Synthesis of methyl sulfomycinate, sulfomycinic amide and sulfomycinine, degradation products of the sulfomycin thiopeptide antibiotics. *Tetrahedron* **62**, 66–72
96. Ammer, C., and Bach, T. (2010) Total syntheses of the thiopeptides amythiamicin C and D. *Chemistry A European Journal* **16**, 14083–14093
97. Aulakh, V. S., and Ciufolini, M. a (2011) Total synthesis and complete structural assignment of thiocillin I. *Journal of the American Chemical Society* **133**, 5900–4
98. Belhadj, T., Nowicki, A., and Moody, C. (2006) Synthesis of the “Northern-Hemisphere” Fragments of the Thiopeptide Antibiotic Nosiheptide. *Synlett* **2006**, 3033–3036
99. Kimber, M. C., and Moody, C. J. (2008) Construction of macrocyclic thiopeptides: synthesis of a nosiheptide “southern hemisphere” model system. *Chemical Communications*, 591–3

100. Zhou, P., Hagan, D. O., Mocek, U., Zeng, Z., Yuen, I. L., Frenzel, T., Unkefer, C. J., and Beale, J. M. (1989) Biosynthesis of the Antibiotic Thiostrepton. Methylation of Tryptophan in the Formation of the Methylation of Tryptophan in the Formation of the Quinaldic Acid Moiety by Transfer of the Methionine Methyl Group with Net Retention of Configuration. *Journal of the American Chemical Society* **111**, 7274–7276
101. Mocek, U., Zeng, Z., O'Hagan, D., Zhou, P., Fan, L. D. G., Beale, J. M., and Floss, H. G. (1993) Biosynthesis of the modified peptide antibiotic thiostrepton in *Streptomyces azureus* and *Streptomyces laurentii*. *Journal of the American Chemical Society* **115**, 7992–8001
102. Frenzel, T. (1990) Formation of 2-Methyltryptophan in the Biosynthesis of Thiostrepton : Isolation of S-Adenosyl- methionine : Tryptophan 2-Methyltransferase. *Archives of Biochemistry and Biophysics* **278**, 35–40
103. Priestly, N. D., Smith, T. M., Shipely, P. R., and Floss, H. G. (1996) Studies on the Biosynthesis of Thiostrepton: 4-(1-Hydroxyethyl)quinoline-2-carboxylate as a Free Intermediate on the Pathway to the Quinaldic Acid Moiety. *Bioorganic and Medicinal Chemistry* **4**, 1135–1147
104. Bycroft, B. W., and Gowland, M. S. (1978) The structures of the highly modified peptide antibiotics micrococcin P1 and P2. *Journal of the Chemical Society, Chemical Communications*, 256–257
105. Nicolaou, K. C., Safina, B. S., Funke, C., Zak, M., and Zécari, F. J. (2002) Stereocontrolled synthesis of the quinaldic acid macrocyclic system of thiostrepton. *Angewandte Chemie (International ed. in English)* **41**, 1937–40
106. Kelly, W. L., Pan, L., and Li, C. (2009) Thiostrepton biosynthesis: prototype for a new family of bacteriocins. *Journal of the American Chemical Society* **131**, 4327–34
107. Liao, R., and Liu, W. (2011) Thiostrepton maturation involving a deesterification-amidation way to process the C-terminally methylated peptide backbone. *Journal of the American Chemical Society* **133**, 2852–5
108. Liao, R., Duan, L., Lei, C., Pan, H., Ding, Y., Zhang, Q., Chen, D., Shen, B., Yu, Y., and Liu, W. (2009) Thiopeptide biosynthesis featuring ribosomally synthesized precursor peptides and conserved posttranslational modifications. *Chemistry & Biology* **16**, 141–147



109. Duan, L., Wang, S., Liao, R., and Liu, W. (2012) Insights into quinaldic acid moiety formation in thiostrepton biosynthesis facilitating fluorinated thiopeptide generation. *Chemistry & Biology* **19**, 443–8
110. Ding, Y., Yu, Y., Pan, H., Guo, H., Li, Y., and Liu, W. (2010) Moving posttranslational modifications forward to biosynthesize the glycosylated thiopeptide nocathiacin I in *Nocardia* sp. ATCC202099. *Molecular Biosystems* **6**, 1180–5
111. Morris, R. P., Leeds, J. A., Naegeli, H. U., Oberer, L., Memmert, K., Weber, E., LaMarche, M. J., Parker, C. N., Burrer, N., Esterow, S., Hein, A. E., Schmitt, E. K., and Krastel, P. (2009) Ribosomally Synthesized Thiopeptide Antibiotics Targeting Elongation Factor Tu. *Journal of the American Chemical Society* **131**, 5946–5955
112. Wieland Brown, L. C., Acker, M. G., Clardy, J., Walsh, C. T., and Fischbach, M. a (2009) Thirteen posttranslational modifications convert a 14-residue peptide into the antibiotic thiocillin. *Proceedings of the National Academy of Sciences of the United States of America* **106**, 2549–53
113. Wang, J., Yu, Y., Tang, K., Liu, W., He, X., Huang, X., and Deng, Z. (2010) Identification and analysis of the biosynthetic gene cluster encoding the thiopeptide antibiotic cyclothiazomycin in *Streptomyces hygroscopicus* 10-22. *Applied and Environmental Microbiology* **76**, 2335–44
114. Young, T. S., and Walsh, C. T. (2011) Identification of the thiazolyl peptide GE37468 gene cluster from *Streptomyces* ATCC 55365 and heterologous expression in *Streptomyces lividans*. *Proceedings of the National Academy of Sciences of the United States of America* **108**, 13053–8
115. Yu, Y., Duan, L., Zhang, Q., Liao, R., Ding, Y., Pan, H., Wendt-Pienkowski, E., Tang, G., Shen, B., and Liu, W. (2009) Nosiheptide biosynthesis featuring a unique indole side ring formation on the characteristic thiopeptide framework. *ACS Chemical Biology* **4**, 855–864
116. Kelly, J., Kutscher, A. H., and Tuoti, F. (1959) Thiostrepton, a new antibiotic: Tube dilution sensitivity studies. *Oral Surgery, Oral Medicine, Oral Pathology* **12**, 1334–1339
117. Weisblum, B., and Demohn, V. (1970) Inhibitor of 50S Ribosome Subunit Function. *Journal of Bacteriology* **101**, 1073–1075

118. Thompson, J., Cundliffe, E., and Stark, M. (1979) Binding of thiostrepton to a complex of 23-S rRNA with ribosomal protein L11. *European Journal of Biochemistry / FEBS* **98**, 261–5
119. Ryan, P. C., Lu, M., and Draper, D. E. (1991) Recognition of the highly conserved GTPase center of 23 S ribosomal RNA by ribosomal protein L11 and the antibiotic thiostrepton. *Journal of Molecular Biology* **221**, 1257–68
120. Thompson, J., and Cundliffe, E. (1991) The binding of thiostrepton to 23S ribosomal RNA. *Nature* **73**, 1131–1135
121. Rosendahl, G., and Douthwaite, S. (1994) The antibiotics micrococцин and thiostrepton interact directly with 23S rRNA nucleotides 1067A and 1095A. *Nucleic Acids Research* **22**, 357–63
122. Xing, Y., and Draper, D. E. (1995) Stabilization of a Ribosomal RNA Tertiary Structure. *Journal of Molecular Biology* **249**, 319–331
123. Conn, G. L. (1999) Crystal Structure of a Conserved Ribosomal Protein-RNA Complex. *Science* **284**, 1171–1174
124. Schmidt, F. J., Thompson, J., Lee, K., Dijk, J., and Cundliffe, E. (1981) The binding site for ribosomal protein L11 within 23 S ribosomal RNA of *Escherichia coli*. *The Journal of Biological Chemistry* **256**, 12301–5
125. Xing, Y., and Draper, D. E. (1996) Cooperative Interactions of RNA and Thiostrepton Antibiotic with Two Domains of Ribosomal Protein L11. *Biochemistry* **35**, 1581–1588
126. Lee, D., Walsh, J. D., Yu, P., Markus, M. A., Choli-Papadopoulou, T., Schwieters, C. D., Krueger, S., Draper, D. E., and Wang, Y.-X. (2007) The structure of free L11 and functional dynamics of L11 in free, L11-rRNA(58 nt) binary and L11-rRNA(58 nt)-thiostrepton ternary complexes. *Journal of Molecular Biology* **367**, 1007–22
127. Bausch, S. L., Poliakova, E., and Draper, D. E. (2005) Interactions of the N-terminal domain of ribosomal protein L11 with thiostrepton and rRNA. *The Journal of Biological Chemistry* **280**, 29956–63
128. Egebjerg, J., Douthwaite, S., and Garrett, R. a (1989) Antibiotic interactions at the GTPase-associated centre within *Escherichia coli* 23S rRNA. *The EMBO Journal* **8**, 607–11
129. Cundliffe, E., Dixon, P., Stark, M., Stöffler, G., Ehrlich, R., Stöffler-Meilicke, M., and Cannon, M. (1979) Ribosomes in thiostrepton-resistant

mutants of *Bacillus megaterium* lacking a single 50 S subunit protein. *Journal of Molecular Biology* **132**, 235–52

130. Lentzen, G., Klinck, R., Matassova, N., Aboul-ela, F., and Murchie, A. I. H. (2003) Structural Basis for Contrasting Activities of Ribosome Binding Thiazole Antibiotics. *Science* **10**, 769–778
131. Cameron, D. M., Thompson, J., Gregory, S. T., March, P. E., and Dahlberg, A. E. (2004) Thiostrepton-resistant mutants of *Thermus thermophilus*. *Nucleic Acids Research* **32**, 3220–7
132. Porse, B. T., Leviev, I., Mankin, A. S., and Garrett, R. A. (1998) The antibiotic thiostrepton inhibits a functional transition within protein L11 at the ribosomal GTPase centre. *Journal of Molecular Biology* **276**, 391–404
133. Uchiumi, T., Wada, a, and Kominami, R. (1995) A base substitution within the GTPase-associated domain of mammalian 28 S ribosomal RNA causes high thiostrepton accessibility. *The Journal of biological chemistry* **270**, 29889–93
134. Gonzalez, R. L., Chu, S., and Puglisi, J. D. (2007) Thiostrepton inhibition of tRNA delivery to the ribosome. *RNA* **13**, 2091–7
135. Kiel, M. C., Raj, V. S., Kaji, H., and Kaji, A. (2003) Release of ribosome-bound ribosome recycling factor by elongation factor G. *The Journal of Biological Chemistry* **278**, 48041–50
136. Rodnina, M. V, Savelsbergh, A., Matassova, N. B., Katunin, V. I., Semenov, Y. P., and Wintermeyer, W. (1999) Thiostrepton inhibits the turnover but not the GTPase of elongation factor G on the ribosome. *Proceedings of the National Academy of Sciences of the United States of America* **96**, 9586–90
137. Cameron, D. M., Thompson, J., March, P. E., and Dahlberg, A. E. (2002) Initiation factor IF2, thiostrepton and micrococin prevent the binding of elongation factor G to the *Escherichia coli* ribosome. *Journal of Molecular Biology* **319**, 27–35
138. Agrawal, R. K., Penczek, P., Grassucci, R. a, and Frank, J. (1998) Visualization of elongation factor G on the *Escherichia coli* 70S ribosome: the mechanism of translocation. *Proceedings of the National Academy of Sciences of the United States of America* **95**, 6134–8
139. Agrawal, R. K., Heagle, A. B., Grassucci, R. A., and Frank, J. (1999) EF-G-dependent hydrolysis induces translocation accompanied by large

conformational changes in the 70S ribosome. *Nature Structural Biology* **6**, 643–647

140. Agrawal, R. K., Linde, J., Sengupta, J., Nierhaus, K. H., and Frank, J. (2001) Localization of L11 protein on the ribosome and elucidation of its involvement in EF-G-dependent translocation. *Journal of Molecular Biology* **311**, 777–87
141. Seo, H.-S., Abedin, S., Kamp, D., Wilson, D. N., Nierhaus, K. H., and Cooperman, B. S. (2006) EF-G-dependent GTPase on the ribosome. conformational change and fusidic acid inhibition. *Biochemistry* **45**, 2504–14
142. Bowen, W. S., Van Dyke, N., Murgola, E. J., Lodmell, J. S., and Hill, W. E. (2005) Interaction of thiostrepton and elongation factor-G with the ribosomal protein L11-binding domain. *The Journal of Biological Chemistry* **280**, 2934–43
143. Harms, J. M., Wilson, D. N., Schluenzen, F., Connell, S. R., Stachelhaus, T., Zaborowska, Z., Spahn, C. M. T., and Fucini, P. (2008) Translational regulation via L11: molecular switches on the ribosome turned on and off by thiostrepton and micrococin. *Molecular Cell* **30**, 26–38
144. Walter, J. D., Hunter, M., Cobb, M., Traeger, G., and Spiegel, P. C. (2012) Thiostrepton inhibits stable 70S ribosome binding and ribosome-dependent GTPase activation of elongation factor G and elongation factor 4. *Nucleic Acids Research* **40**, 360–70
145. Blyn, L. B., Risen, L. M., Griffey, R. H., and Draper, D. E. (2000) The RNA-binding domain of ribosomal protein L11 recognizes an rRNA tertiary structure stabilized by both thiostrepton and magnesium ion. *Nucleic Acids Research* **28**, 1778–84
146. Mcconkey, G. A., Rogers, M. J., and Mccutchan, T. F. (1997) Inhibition of Plasmodium falciparum Protein Synthesis. *The Journal of Biological Chemistry* **272**, 2046–2049
147. Rogers, J. M., Bukhman, Y. V, McCutchan, T. F., and Draper, D. (1997) Interaction of thiostrepton with an RNA fragment derived from the plastid-encoded ribosomal RNA of the malaria papasite. *RNA* **3**, 815–820
148. Rogers, M. J., Cundliffe, E., and Mccutchan, T. F. (1998) The Antibiotic Micrococin Is a Potent Inhibitor of Growth and Protein Synthesis in the Malaria Parasite The Antibiotic Micrococin Is a Potent Inhibitor of Growth and Protein Synthesis in the Malaria Parasite. *Antimicrobial Agents and Chemotherapy* **42**, 715–717

149. Clough, B., Strath, M., Preiser, P., Denny, P., and Wilson, I. (R. J. M. . (1997) Thiostrepton binds to malarial plastid rRNA. *FEBS Letters* **406**, 123–125
150. Chaubey, S., Kumar, A., Singh, D., and Habib, S. (2005) The apicoplast of *Plasmodium falciparum* is translationally active. *Molecular Microbiology* **56**, 81–9
151. Goodman, C. D., Su, V., and McFadden, G. I. (2007) The effects of anti-bacterials on the malaria parasite *Plasmodium falciparum*. *Molecular and Biochemical Parasitology* **152**, 181–91
152. Clough, B., and Wilson, R. J. M. (2001) in *Antimalarial Chemotherapy* (Rosenthal, P. J., ed.) pp. 265–286, Humana Press
153. Schoof, S., Pradel, G., Aminake, M. N., Ellinger, B., Baumann, S., Potowski, M., Najajreh, Y., Kirschner, M., and Arndt, H.-D. (2010) Antiplasmodial thiostrepton derivatives: proteasome inhibitors with a dual mode of action. *Angewandte Chemie (International ed. in English)* **49**, 3317–21
154. Aminake, M. N., Schoof, S., Sologub, L., Leubner, M., Kirschner, M., Arndt, H.-D., and Pradel, G. (2011) Thiostrepton and derivatives exhibit antimalarial and gametocytocidal activity by dually targeting parasite proteasome and apicoplast. *Antimicrobial Agents and Chemotherapy* **55**, 1338–48
155. Tarr, S. J., Nisbet, R. E. R., and Howe, C. J. (2011) Transcript-level responses of *Plasmodium falciparum* to thiostrepton. *Molecular and Biochemical Parasitology* **179**, 37–41
156. Nicolaou, K. C., Zak, M., Rahimpour, S., Estrada, A. a, Lee, S. H., O’Brate, A., Giannakakou, P., and Ghadiri, M. R. (2005) Discovery of a biologically active thiostrepton fragment. *Journal of the American Chemical Society* **127**, 15042–4
157. Bhat, U. G., Zipfel, P. a, Tyler, D. S., and Gartel, A. L. (2008) Novel anticancer compounds induce apoptosis in melanoma cells. *Cell Cycle* **7**, 1851–5
158. Kwok, J. M.-M., Myatt, S. S., Marson, C. M., Coombes, R. C., Constantinidou, D., and Lam, E. W.-F. (2008) Thiostrepton selectively targets breast cancer cells through inhibition of forkhead box M1 expression. *Molecular Cancer Therapeutics* **7**, 2022–32

159. Pandit, B., and Gartel, A. L. (2011) Thiazole antibiotic thiostrepton synergize with bortezomib to induce apoptosis in cancer cells. *PLoS One* **6**, e17110
160. Qiao, S., Lamore, S. D., Cabello, C. M., Lesson, J. L., Muñoz-Rodríguez, J. L., and Wondrak, G. T. (2012) Thiostrepton is an inducer of oxidative and proteotoxic stress that impairs viability of human melanoma cells but not primary melanocytes. *Biochemical Pharmacology* **83**, 1229–40
161. Wang, M., and Gartel, A. L. (2011) Micelle-encapsulated thiostrepton as an effective nanomedicine for inhibiting tumor growth and for suppressing FOXM1 in human xenografts. *Molecular Cancer Therapeutics* **10**, 2287–97
162. Bhat, U. G., Halasi, M., and Gartel, A. L. (2009) Thiazole antibiotics target FoxM1 and induce apoptosis in human cancer cells. *PLoS One* **4**, e5592
163. Hegde, N. S., Sanders, D. a, Rodriguez, R., and Balasubramanian, S. (2011) The transcription factor FOXM1 is a cellular target of the natural product thiostrepton. *Nature Chemistry* **3**, 725–31
164. Vermeulen, M. W., and Wu, J. (2004) Use of thiostrepton as an anti-mycobacterial agent. U.S. Patent; 2004/ 00254100A1.
165. Lougheed, K. E. a, Taylor, D. L., Osborne, S. a, Bryans, J. S., and Buxton, R. S. (2009) New anti-tuberculosis agents amongst known drugs. *Tuberculosis* **89**, 364–70
166. Cundliffe, E. (1978) Mechanism of resistance to thiostrepton in the producing-organism *Streptomyces azureus*. *Nature* **272**, 792–795
167. Cundliffe, E. Thompson, J. (1979) Ribose methylation and resistance to thiostrepton. *Nature* **278**, 859–861
168. Thompson, J., and Cundliffe, E. (1981) Purification and Properties of an RNA Methylase Produced by *Streptomyces azureus* and Involved in Resistance to Thiostrepton. *Microbiology* **124**, 291–297
169. Bechthold, a, and Floss, H. G. (1994) Overexpression of the thiostrepton-resistance gene from *Streptomyces azureus* in *Escherichia coli* and characterization of recognition sites of the 23S rRNA A1067 2'-methyltransferase in the guanosine triphosphatase center of 23S ribosomal RNA. *European Journal of Biochemistry* **224**, 431–7

170. Thompson, J., Schmidt, F., and Cundliffe, E. (1982) Site of action of a ribosomal RNA methylase conferring resistance to thiostrepton. *The Journal of Biological Chemistry* **257**, 7915–7
171. Dunstan, M. S., Hang, P. C., Zelinskaya, N. V, Honek, J. F., and Conn, G. L. (2009) Structure of the thiostrepton resistance methyltransferase.S-adenosyl-L-methionine complex and its interaction with ribosomal RNA. *The Journal of Biological Chemistry* **284**, 17013–20
172. Hang, P. C. (2008) Investigations into *Streptomyces azureus* Thiostrepton-resistance rRNA Methyltransferase and its Cognate Antibiotic.
173. Anantharaman, V., Koonin, E. V, and Aravind, L. (2002) JMMB Communication SPOUT : a Class of Methyltransferases that Includes spoU and trmD RNA Methylase Superfamilies , and Novel Superfamilies of Predicted Prokaryotic RNA Methylases. *Nucleic Acids Research* **4**, 71–75
174. Tkaczuk, K. L., Dunin-Horkawicz, S., Purta, E., and Bujnicki, J. M. (2007) Structural and evolutionary bioinformatics of the SPOUT superfamily of methyltransferases. *BMC Bioinformatics* **8**, 73
175. Dosch, D., C., Strohl, W., R., and Floss, H. G. (1988) Molecular cloning of the nosiheptide resistance gene from *Streptomyces actuosus* ATCC 25421. *Biochemical and Biophysical Research Communications* **156**, 517–523
176. Li, Y., Dosch, D. C., Strohl, W. R., and Floss, H. G. (1990) Nucleotide sequence and transcriptional analysis of the nosiheptide-resistance gene from *Streptomyces actuosus*. *Gene* **91**, 9–17
177. Yang, H., Wang, Z., Shen, Y., Wang, P., Jia, X., Zhao, L., Zhou, P., Gong, R., Li, Z., Yang, Y., Chen, D., Murchie, A., and Xu, Y. (2010) Crystal Structure of the Nosiheptide Resistance Methyltransferase of *Streptomyces actuosus*. *Biochemistry*
178. Weisblum, B. (1995) Erythromycin Resistance by Ribosome Modification. *Antimicrobial Agents and Chemotherapy* **39**, 577–585
179. Hansen, L. H., Mauvais, P., and Douthwaite, S. (1999) The macrolide-ketolide antibiotic binding site is formed by structures in domains II and V of 23S ribosomal RNA. *Molecular Microbiology* **31**, 623–31

180. Beauclerk, a a, and Cundliffe, E. (1987) Sites of action of two ribosomal RNA methylases responsible for resistance to aminoglycosides. *Journal of Molecular Biology* **193**, 661–71
181. Cundliffe, E. (1992) Resistance to macrolides and lincosamides in *Streptomyces lividans* and to aminoglycosides in *Micromonospora purpurea*. *Gene* **115**, 75–84
182. Savic, M., Lovric, J., Tomic, T. I., Vasiljevic, B., and Conn, G. L. (2009) Determination of the target nucleosides for members of two families of 16S rRNA methyltransferases that confer resistance to partially overlapping groups of aminoglycoside antibiotics. *Nucleic Acids Research* **37**, 5420–31
183. Doi, Y., and Arakawa, Y. (2007) 16S ribosomal RNA methylation: emerging resistance mechanism against aminoglycosides. *Clinical Infectious Diseases* **45**, 88–94
184. Liou, G. F., Yoshizawa, S., Courvalin, P., and Galimand, M. (2006) Aminoglycoside resistance by ArmA-mediated ribosomal 16S methylation in human bacterial pathogens. *Journal of Molecular Biology* **359**, 358–64
185. Cheng, X., and Blumenthal, R. M. (eds.) (1999) *S-Adenosyl-Dependent Methyltransferases: Structures and Functions*, World Scientific, New Jersey
186. Schubert, H. L., Blumenthal, R. M., and Cheng, X. (2003) Many paths to methyltransfer: a chronicle of convergence. *Trends in Biochemical Sciences* **28**, 329–35
187. Martin, J. L., and McMillan, F. M. (2002) SAM (dependent) I AM: the S-adenosylmethionine-dependent methyltransferase fold. *Current Opinion in Structural Biology* **12**, 783–93
188. Nureki, O., Shirouzu, M., Hashimoto, K., Ishitani, R., Terada, T., Tamakoshi, M., Oshima, T., Chijimatsu, M., Takio, K., Vassylyev, D. G., Shibata, T., Inoue, Y., Kuramitsu, S., and Yokoyama, S. (2002) An enzyme with a deep trefoil knot for the active-site architecture. *Pharmacia* **58**, 1129–1137
189. Watanabe, K., Nureki, O., Fukai, S., Ishii, R., Okamoto, H., Yokoyama, S., Endo, Y., and Hori, H. (2005) Roles of conserved amino acid sequence motifs in the SpoU (TrmH) RNA methyltransferase family. *The Journal of Biological Chemistry* **280**, 10368–77



190. Michel, G., Sauvé, V., Larocque, R., Li, Y., Matte, A., and Cygler, M. (2002) The structure of the RlmB 23S rRNA methyltransferase reveals a new methyltransferase fold with a unique knot. *Structure* **10**, 1303–15
191. Mosbacher, T. G., Bechthold, A., and Schulz, G. E. (2005) Structure and function of the antibiotic resistance-mediating methyltransferase AviRb from *Streptomyces viridochromogenes*. *Journal of Molecular Biology* **345**, 27–42
192. Woodard, R. W., Tsai, M. D., Floss, H. G., Crooks, P. a, and Coward, J. K. (1980) Stereochemical course of the transmethylation catalyzed by catechol O-methyltransferase. *The Journal of Biological Chemistry* **255**, 9124–7
193. Liscombe, D. K., Louie, G. V, and Noel, J. P. (2012) Architectures , mechanisms and molecular evolution of natural product methyltransferases. *Natural Product Reports* **29**, 1238–1250
194. Yan, F., LaMarre, J. M., Röhrich, R., Wiesner, J., Jomaa, H., Mankin, A. S., and Fujimori, D. G. (2010) RlmN and Cfr are radical SAM enzymes involved in methylation of ribosomal RNA. *Journal of the American Chemical Society* **132**, 3953–64
195. Giessing, A. M. B., Jensen, S. S., Rasmussen, A., Hansen, L. H., Gondela, A., Long, K., Vester, B., and Kirpekar, F. (2009) Identification of 8-methyladenosine as the modification catalyzed by the radical SAM methyltransferase Cfr that confers antibiotic resistance in bacteria. *RNA* **15**, 327–36
196. Frey, P. a, Hegeman, A. D., and Ruzicka, F. J. (2008) The Radical SAM Superfamily. *Critical Reviews in Biochemistry and Molecular Biology* **43**, 63–88
197. Marsh, E. N. G., Patwardhan, A., and Huhta, M. S. (2004) S-adenosylmethionine radical enzymes. *Bioorganic Chemistry* **32**, 326–40
198. Grove, T. L., Benner, J. S., Radle, M. I., Ahlum, J. H., Landgraf, B. J., Krebs, C., and Booker, S. J. (2011) A Radically Different Mechanism for S-Adenosylmethionine-Dependent Methyltransferases. *Science* **604**, 604–607
199. Fontecave, M., Atta, M., and Mulliez, E. (2004) S-adenosylmethionine: nothing goes to waste. *Trends in Biochemical Sciences* **29**, 243–9

200. Pignot, M., Siethoff, C., Linscheid, M., and Weinhold, E. (1998) Coupling of a Nucleoside with DNA by a Methyltransferase. *Angewandte Chemie (International ed. in English)* **37**, 2888–2891
201. Pljevaljic, G., Pignot, M., and Weinhold, E. (2003) Design of a new fluorescent cofactor for DNA methyltransferases and sequence-specific labeling of DNA. *Journal of the American Chemical Society* **125**, 3486–92
202. Comstock, L. R., and Rajski, S. R. (2005) Conversion of DNA methyltransferases into azidonucleosidyl transferases via synthetic cofactors. *Nucleic Acids Research* **33**, 1644–52
203. Comstock, L. R., and Rajski, S. R. (2005) Methyltransferase-directed DNA strand scission. *Journal of the American Chemical Society* **127**, 14136–7
204. Weller, R. L., and Rajski, S. R. (2005) DNA methyltransferase-moderated click chemistry. *Organic Letters* **7**, 2141–4
205. Weller, R. L., and Rajski, S. R. (2006) Design, synthesis, and preliminary biological evaluation of a DNA methyltransferase-directed alkylating agent. *Chembiochem* **7**, 243–5
206. Mai, V., and Comstock, L. R. (2011) Synthesis of an azide-bearing N-mustard analogue of S-adenosyl-L-methionine. *The Journal of Organic Chemistry* **76**, 10319–24
207. Dalhoff, C., Lukinavicius, G., Klimasauskas, S., and Weinhold, E. (2006) Direct transfer of extended groups from synthetic cofactors by DNA methyltransferases. *Nature Chemical Biology* **2**, 31–2
208. Dalhoff, C., Lukinavicius, G., Klimasauskas, S., and Weinhold, E. (2006) Synthesis of S-adenosyl-L-methionine analogs and their use for sequence-specific transalkylation of DNA by methyltransferases. *Nature Protocols* **1**, 1879–86
209. Binda, O., Boyce, M., Rush, J. S., Palaniappan, K. K., Bertozzi, C. R., and Gozani, O. (2011) A chemical method for labeling lysine methyltransferase substrates. *Chembiochem* **12**, 330–4
210. Peters, W., Willnow, S., Duisken, M., Kleine, H., Macherey, T., Duncan, K. E., Litchfield, D. W., Lüscher, B., and Weinhold, E. (2010) Enzymatic site-specific functionalization of protein methyltransferase substrates with alkynes for click labeling. *Angewandte Chemie (International ed. in English)* **49**, 5170–3

211. Islam, K., Zheng, W., Yu, H., Deng, H., and Luo, M. (2011) Expanding Cofactor Repertoire of Protein Lysine Methyltransferase for Substrate Labeling. *ACS Chemical Biology* **6**, 679–684
212. Lukinavicius, G., Lapiene, V., Stasevskij, Z., Dalhoff, C., Weinhold, E., and Klimasauskas, S. (2007) Targeted labeling of DNA by methyltransferase-directed transfer of activated groups (mTAG). *Journal of the American Chemical Society* **129**, 2758–9
213. Lee, B. W. K., Sun, H. G., Zang, T., Kim, B. J., Alfaro, J. F., and Zhou, Z. S. (2010) Enzyme-catalyzed transfer of a ketone group from an S-adenosylmethionine analogue: a tool for the functional analysis of methyltransferases. *Journal of the American Chemical Society* **132**, 3642–3
214. Thompson, J., Cundliffe, E., and Dahlberg, a E. (1988) Site-directed mutagenesis of Escherichia coli 23 S ribosomal RNA at position 1067 within the GTP hydrolysis centre. *Journal of Molecular Biology* **203**, 457–65
215. Hummel, H., and Böck, A. (1987) Thiostrepton resistance mutations in the gene for 23S ribosomal RNA of halobacteria. *Biochimie* **69**, 857–61
216. Mankin, A. S., Leviev, I., and Garrett, R. A. (1994) Cross-hypersensitivity effect of mutations in 23 S rRNA yield insight into aminoacyl-tRNA binding. *Journal of Molecular Biology* **244**, 151–157
217. Aagaard, C., Phan, H., Trevisanato, S., and Garreti, R. A. (1994) A Spontaneous Point Mutation in the Single 23S rRNA Gene of the Thermophilic Archaeon Sulfolobus acidocaldarius Confers Multiple Drug Resistance. *Journal of Bacteriology* **176**, 7744–7747
218. Wienen, B., Ehrlich, R., Stoffler-Meilicke, M., Stoffler-Meilicke, G., Smith, I., Weiss, D., Vince, R., and Pestka, S. (1979) Ribosomal Protein Alterations in Thiostrepton- and Micrococcin- resistant mutants of Bacillus subtilis. *The Journal of Biological Chemistry* **254**, 8031–8041
219. McElwain, K. B., Boynton, J. E., and Gillham, N. W. (1993) A nuclear mutation conferring thiostrepton resistance in Chlamydomonas reinhardtii affects a chloroplast ribosomal protein related to Escherichia coli ribosomal protein L11. *Molecular & General Genetics* **241**, 564–72
220. Chiu, M. L., Folcher, M., Katoh, T., Puglia, a M., Vohradsky, J., Yun, B. S., Seto, H., and Thompson, C. J. (1999) Broad spectrum thiopeptide recognition specificity of the Streptomyces lividans TipAL protein and its

role in regulating gene expression. *The Journal of Biological Chemistry* **274**, 20578–86

221. Chiu, M. L., Viollier, P. H., Katoh, T., Ramsden, J. J., and Thompson, C. J. (2001) Ligand-induced changes in the *Streptomyces lividans* TipAL protein imply an alternative mechanism of transcriptional activation for MerR-like proteins. *Biochemistry* **40**, 12950–8
222. Vasant Kumar, C. (1994) Thiostrepton induced proteins in *Streptomyces*, *Amycolatopsis* and *Nocardia* species. *FEMS Microbiology Letters* **118**, 107–111
223. Yun, B., Hidaka, T., Kuzumaya, T., and Seto, H. (2001) Thiopeptide Non-producing *Streptomyces* Species Carry the tipA Gene : A Clue to Its Function. *Journal of Antibiotics* **54**, 375–3.78
224. Dong, L., Nakashima, N., Tamura, N., and Tamura, T. (2004) Isolation and characterization of the *Rhodococcus opacus* thiostrepton-inducible genes tipAL and tipAS: application for recombinant protein expression in *Rhodococcus*. *FEMS Microbiology Letters* **237**, 35–40
225. Chiu, M. L., Folcher, M., Griffin, P., Holt, T., Klatt, T., and Thompson, C. J. (1996) Characterization of the covalent binding of thiostrepton to a thiostrepton-induced protein from *Streptomyces lividans*. *Biochemistry* **35**, 2332–41
226. Kahmann, J. D., Sass, H.-J., Allan, M. G., Seto, H., Thompson, C. J., and Grzesiek, S. (2003) Structural basis for antibiotic recognition by the TipA class of multidrug-resistance transcriptional regulators. *The EMBO Journal* **22**, 1824–34
227. Lefranc, D., and Ciufolini, M. A. (2009) Total synthesis and stereochemical assignment of micrococcin P1. *Angewandte Chemie International Edition* **48**, 4198–4201
228. Nicolaou, K. C., Dethle, D. H., Leung, G. Y. C., Zou, B., and Chen, D. Y.-K. (2008) Total synthesis of thiopeptide antibiotics GE2270A, GE2270T, and GE2270C1. *Chemistry An Asian Journal* **3**, 413–429
229. Ciufolini, M. A., and Shen, Y. C. (1999) Synthesis of the Bycroft-Gowland structure of micrococcin P1. *Organic Letters* **1**, 1843–1846
230. Mori, T., Higashibayashi, S., Goto, T., Kohno, M., Satouchi, Y., Shinko, K., Suzuki, K., Suzuki, S., Tohmiya, H., Hashimoto, K., and Nakata, M. (2008) Total synthesis of siomycin A: completion of the total synthesis. *Chemistry An Asian Journal* **3**, 1013–1025

231. Engelhardt, K., Degnes, K. F., and Zotchev, S. B. (2010) Isolation and Characterization of the Gene Cluster for Biosynthesis of the Thiopeptide Antibiotic TP-1161. *Applied and Environmental Microbiology* **76**, 7093–7101
232. Ding, Y., Yu, Y., Pan, H., Guo, H., Li, Y., and Liu, W. (2010) Moving posttranslational modifications forward to biosynthesize the glycosylated thiopeptide nocathiacin I in *Nocardia* sp. ATCC202099. *Molecular Biosystems* **6**, 1180–1185
233. Oman, T. J., and Van Der Donk, W. A. (2010) Follow the leader: the use of leader peptides to guide natural product biosynthesis. *Nature Chemical Biology* **6**, 9–18
234. Li, C., Zhang, F., and Kelly, W. L. (2011) Heterologous production of thiostrepton A and biosynthetic engineering of thiostrepton analogs. *Molecular bioSystems* **7**, 82–90
235. Naidu, B. N., Li, W., Sorenson, M. E., Connolly, T. P., Wichtowski, J. a., Zhang, Y., Kim, O. K., Matiskeella, J. D., Lam, K. S., and Bronson, J. J. (2004) Organic reactions in frozen water: Michael addition of amines and thiols to the dehydroalanine side chain of nocathiacins. *Tetrahedron Letters* **45**, 1059–1063
236. Ferreira, P. M. T., Maia, H. L. S., Monteiro, L. S., and Sacramento, J. (2001) Michael addition of thiols, carbon nucleophiles and amines to dehydroamino acid and dehydropeptide derivatives. *Journal of the Chemical Society, Perkin Transactions* **1**, 3167–3173
237. Naidu, B. N., Sorenson, M. E., Connolly, T. P., and Ueda, Y. (2003) Michael addition of amines and thiols to dehydroalanine amides: a remarkable rate acceleration in water. *The Journal of Organic Chemistry* **68**, 10098–102
238. Ferreira, P. M. T., Maia, H. L. S., Monteiro, L. S., Sacramento, J., and Sebastião, J. (2000) Synthesis of  $\beta$ -substituted alanines via Michael addition of nucleophiles to dehydroalanine derivatives. *Journal of the Chemical Society, Perkin Transactions* **1**, 3317–3324
239. Schoof, S., Baumann, S., Ellinger, B., and Arndt, H.-D. (2009) A fluorescent probe for the 70 S-ribosomal GTPase-associated center. *Chembiochem* **10**, 242–5
240. Davis, D. G., and Bax, A. (1985) Assignment of complex proton NMR spectra via two-dimensional homonuclear Hartmann-Hahn spectroscopy. *Journal of the American Chemical Society* **107**, 2820–2821

241. Viswanadhan, V. N., Ghose, A. K., Reyanekar, G. R., Robins, R. K., and Al, E. T. (1989) Atomic Physicochemical Parameters for Three Dimensional Structure Directed Quantitative Structure-Activity Relationships . 4 . Additional Parameters for Hydrophobic and Dispersive Interactions and Their Application for an Automated Superposition of Certai. *Journal of Chemical Information and Computer Sciences* **29**, 163–172
242. Klopman, G., Li, J., Wang, S., and Dimayugat, M. (1994) Computer Automated log P Calculations Based on and Extended Group Contribution Approach. *Journal of Chemical Information and Computer Sciences* **34**, 752–781
243. Bush, K., Dudley, M. N., and Hecht, D. W. (2009) Methods for Dilution Antimicrobial Susceptibility Tests for Bacteria That Grow Aerobically ; Approved Standard — Eighth Edition. *Screening* **29**, 1–10
244. Chary, C., Rambhav, S., Raju, V. (1991) Spectroscopic characterization of thioestrepton-copper (II) complex. *Proceedings of the National Academy of Sciences. India, Section A* **61**, 265–272
245. Hensens, O. D., Albers-Schönberg, G., and Anderson, B. F. (1983) The solution conformation of the peptide antibiotic thioestrepton: a <sup>1</sup>H NMR study. *The Journal of Antibiotics* **36**, 799–813
246. Myers, C. L., Hang, P. C., Ng, G., Yuen, J., and Honek, J. F. (2010) Semi-synthetic analogues of thioestrepton delimit the critical nature of tail region modifications in the control of protein biosynthesis and antibacterial activity. *Bioorganic & Medicinal Chemistry* **18**, 4231–7
247. Andrews, J. M. (2001) Determination of minimum inhibitory concentrations. *The Journal of Antimicrobial Chemotherapy* **48 Suppl 1**, 5–16
248. Jayasekera, M. M. K., Onheiber, K., Keith, J., Venkatesan, H., Santillan, A., Stocking, E. M., Tang, L., Miller, J., Gomez, L., Rhead, B., Delcamp, T., Huang, S., Wolin, R., Bobkova, E. V., and Shaw, K. J. (2005) Identification of Novel Inhibitors of Bacterial Translation Elongation Factors. *Antimicrobial Agents and Chemotherapy* **49**, 131–136
249. Kondo, J., Hainrichson, M., Nudelman, I., Shallom-Shezifi, D., Barbieri, C. M., Pilch, D. S., Westhof, E., and Baasov, T. (2007) Differential selectivity of natural and synthetic aminoglycosides towards the eukaryotic and prokaryotic decoding A sites. *Chembiochem* **8**, 1700–9

250. Brandi, L., Fabbretti, A., Di Stefano, M., Lazzarini, A., Abbondi, M., and Gualerzi, C. O. (2006) Characterization of GE82832, a peptide inhibitor of translocation interacting with bacterial 30S ribosomal subunits. *RNA* **12**, 1262–1270
251. Zhou, Y., Gregor, V. E., Sun, Z., Ayida, B. K., Winters, G. C., Murphy, D., Simonsen, K. B., Vourloumis, D., Fish, S., Froelich, J. M., Wall, D., and Hermann, T. (2005) Structure-guided discovery of novel aminoglycoside mimetics as antibacterial translation inhibitors. *Antimicrobial Agents and Chemotherapy* **49**, 4942–4949
252. Schuwirth, B. S., Borovinskaya, M. a, Hau, C. W., Zhang, W., Vila-Sanjurjo, A., Holton, J. M., and Cate, J. H. D. (2005) Structures of the bacterial ribosome at 3.5 Å resolution. *Science* **310**, 827–34
253. Chary, C., Rambhav, S., Venkateswerlu, G. (1990) Inactivation of thiostrepton by copper (II). *Biology of Metals* **3**, 48–53
254. Chary, C., Sarma, C., Rambhav, S. (1990) ESR study of Cu(II): thiostrepton complex. *Current Science* **59**, 925–929
255. Zhang, L., Xu, D., Xu, Y., and Gu, J. (1997) (Benzoylacetonato- O , O “)(2,2”-bipyridine- N , N ’)(nitrato- O )copper(II). *Acta Crystallographica Section C Crystal Structure Communications* **53**, 299–301
256. Lebrun, P. C., Lyon, W. D., and Kuska, H. a. (1986) Crystal structure of bis(2,4-pentanedionato)copper(II). *Journal of Crystallographic and Spectroscopic Research* **16**, 889–893
257. Fallon, G., Moubaraki, B., Murray, K., Bergen, A., West, B. (1993) The molecular structures and magnetic properties of  $\mu_3$ -tetranuclear  $\beta$ -diketonate copper complexes [Cu(bzac)( $\mu_3$ -OC<sub>2</sub>H<sub>4</sub>OCH<sub>3</sub>)]<sub>4</sub> and [Cu( $\mu$ -dbm)( $\mu_3$ -OC<sub>2</sub>H<sub>4</sub>OCH<sub>3</sub>)]<sub>4</sub>. *Polyhedron* **12**, 1989–2000
258. Golchoubian, H. (2008) Redetermination of crystal structure of bis(2,4-pentanedionato)copper(II). *Asian Journal of Chemistry* **20**, 5834–5838
259. Heitz, F., Morris, M. C., and Divita, G. (2009) Twenty years of cell-penetrating peptides : from molecular mechanisms to therapeutics. *British Journal of Pharmacology* **157**, 195–206
260. Lindgren, M., Hällbrink, M., Prochiantz, A., and Langel, U. (2000) Cell-penetrating peptides. *Trends in Pharmacological Sciences* **21**, 99–103

261. Richard, J. P., Melikov, K., Vives, E., Ramos, C., Verbeure, B., Gait, M. J., Chernomordik, L. V, and Lebleu, B. (2003) Cell-penetrating peptides. A reevaluation of the mechanism of cellular uptake. *The Journal of Biological Chemistry* **278**, 585–90
262. Yang, H., Wang, Z., Shen, Y., Wang, P., Jia, X., Zhao, L., and Zhou, P. (2010) Crystal Structure of the Nosiheptide-Resistance Methyltransferase of *Streptomyces actuosus*. *Biochemistry* **49**, 6440–6450
263. Bradford, M. M. (1976) A rapid and sensitive method for the quantitation of microgram quantities of protein utilizing the principle of protein-dye binding. *Analytical Biochemistry* **72**, 248–54
264. Maniatis, T., Fritsch, E. F., and Sambrook, J. (1983) *Molecular Cloning. A Laboratory Manual* (Wood, E. J., ed.), Cold Spring Harbor Laboratory, New York
265. Heckman, K. L., and Pease, L. R. (2007) Gene splicing and mutagenesis by PCR-driven overlap extension. *Nature Protocols* **2**, 924–32
266. Dorgan, K. M., Wooderchak, W. L., Wynn, D. P., Karschner, E. L., Alfaro, J. F., Cui, Y., Zhou, Z. S., and Hevel, J. M. (2006) An enzyme-coupled continuous spectrophotometric assay for S-adenosylmethionine-dependent methyltransferases. *Analytical Biochemistry* **350**, 249–55
267. Nureki, O., Watanabe, K., Fukai, S., Ishii, R., Endo, Y., Hori, H., and Yokoyama, S. (2004) Deep knot structure for construction of active site and cofactor binding site of tRNA modification enzyme. *Structure* **12**, 593–602
268. Pleshe, E., Truesdell, J., and Batey, R. T. (2005) Structure of a class II TrmH tRNA-modifying enzyme from *Aquifex aeolicus*. *Acta Crystallographica Section F Structural Biology And Crystallization Communications* **61**, 722–728
269. Pagans, S., Kauder, S. E., Kaehlcke, K., Sakane, N., Schroeder, S., Dormeyer, W., Trievel, R. C., Verdin, E., Schnolzer, M., and Ott, M. (2010) The Cellular lysine methyltransferase Set7/9-KMT7 binds HIV-1 TAR RNA, monomethylates the viral transactivator Tat, and enhances HIV transcription. *Cell Host Microbe* **7**, 234–44
270. Velikyan, I., Acharya, S., Trifonova, A., Földesi, A., and Chattopadhyaya, J. (2001) The pK(a)'s of 2'-hydroxyl group in nucleosides and nucleotides. *Journal of the American Chemical Society* **123**, 2893–4



271. André, I., Linse, S., and Mulder, F. A. A. (2007) Residue-specific pKa determination of lysine and arginine side chains by indirect <sup>15</sup>N and <sup>13</sup>C NMR spectroscopy: application to apo calmodulin. *Journal of the American Chemical Society* **129**, 15805–15813
272. Woodson, L. C., Ames, M. M., Selassie, C. D., Hansch, C., and Weinshilboum, R. M. (1983) Thiopurine methyltransferase. Aromatic thiol substrates and inhibition by benzoic acid derivatives. *Molecular Pharmacology* **24**, 471–478
273. Ames, M. M., Selassie, C. D., Woodson, L. C., Van Loon, J. A., Hansch, C., and Weinshilboum, R. M. (1986) Thiopurine methyltransferase: structure-activity relationships for benzoic acid inhibitors and thiophenol substrates. *Journal of Medicinal Chemistry* **29**, 354–358
274. Deininger, M., Szumlanski, C. L., Otterness, D. M., Van Loon, J., Ferber, W., and Weinshilboum, R. M. (1994) Purine substrates for human thiopurine methyltransferase. *Biochemical Pharmacology* **48**, 2135–2138
275. Shapiro, S. K., and Ehninger, D. J. (1966) Methods for the analysis and preparation of adenosylmethionine and adenosylhomocysteine. *Analytical Biochemistry* **15**, 323–333
276. Parisi, M. F., and Abeles, R. H. (1992) Inhibition of chymotrypsin by fluorinated alpha-keto acid derivatives. *Biochemistry* **31**, 9429–9435
277. Shao, Y.-M., Yang, W.-B., Kuo, T.-H., Tsai, K.-C., Lin, C.-H., Yang, A.-S., Liang, P.-H., and Wong, C.-H. (2008) Design, synthesis, and evaluation of trifluoromethyl ketones as inhibitors of SARS-CoV 3CL protease. *Bioorganic & Medicinal Chemistry* **16**, 4652–4660
278. Wheelock, C. E., Nishi, K., Ying, A., Jones, P. D., Colvin, M. E., Olmstead, M. M., and Hammock, B. D. (2008) Influence of sulfur oxidation state and steric bulk upon trifluoromethyl ketone (TFK) binding kinetics to carboxylesterases and fatty acid amide hydrolase (FAAH). *Bioorganic & Medicinal Chemistry* **16**, 2114–2130
279. Borchardt, R. T. (1979) Mechanism of alkaline hydrolysis of S-adenosyl-L-methionine and related sulfonium nucleosides. *Journal of the American Chemical Society* **101**, 458–463
280. Eloranta, T. O., and Kajander, E. O. (1984) Catabolism and lability of S-adenosyl-L-methionine in rat liver extracts. *The Biochemical Journal* **224**, 137–44

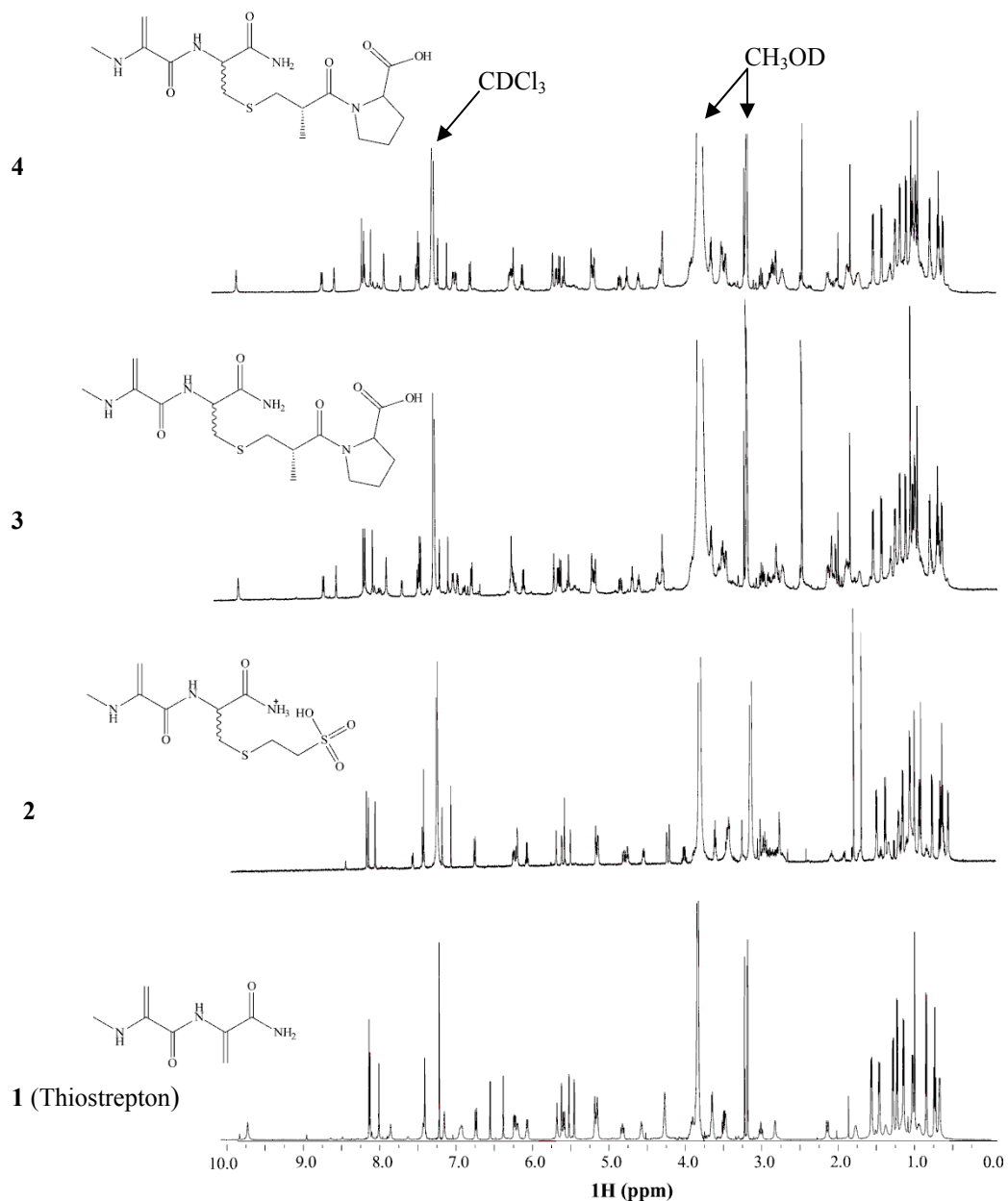
281. Hoffman, J. L. (1986) Chromatographic Analysis of the Chiral and Covalent Instability of. *Biochemistry* **25**, 4444–4449
282. Stolowitz, M. L., and Minch, M. J. (1981) S-Adenosyl-L-methionine and S-Adenosyl-L-homocysteine, an NMR Study. *Journal of the Chemical Society* **103**, 4–8
283. Wu, S. E., Huskey, W. P., Borchardt, R. T., and Schowen, R. L. (1983) Chiral instability at sulfur of S-adenosylmethionine. *Biochemistry* **22**, 2828–32
284. Matos, J. R., and Wong, C.-H. (1987) S-Adenosylmethionine : Stability and Stabilization. *Bioorganic Chemistry* **15**, 71–80
285. Park, J., Tal, J., Roessner, C. A., and Scott, A. I. (1995) Overcoming Product Inhibition of S-Adenosyl-L-methionine (SAM) Synthetase: Preparation of SAM on the 30 mM Scale. *Bioorganic and Medicinal Chemistry Letters* **5**, 2203–2206
286. Fox, M. A., and Whitesell, J. K. (2004) *Organic Chemistry*, 3rd Ed., Jones and Barlett Publishers, Mississauga
287. Tang, K. C., Mariuza, R., Coward, J. K., and Tang, K C, Mariuzza, R, Coward, J. (1981) Synthesis and evaluation of some stable multisubstrate adducts as specific inhibitors of spermidine synthase. *Journal of Medicinal Chemistry* **24**, 1277–1284
288. Anderson, Gary L, Bussolotti, Donald L, Coward, J. K. (1981) Synthesis and Evaluation of Some Stable Multisubstrate Adducts ad Inhibitors of Catechol O-Methyltransferase. *Journal of Medicinal Chemistry* **24**, 1271–1277
289. Pegg, A. E., Coward, J. K., Talekar, R. R., and Secrist, J. A. (1986) Effects of certain 5'-substituted adenosines on polyamine synthesis: selective inhibitors of spermine synthase. *Biochemistry* **25**, 4091–4097
290. Cannon, L. M., Butler, F. N., Wan, W., and Zhou, Z. S. (2002) A stereospecific colorimetric assay for (S,S)-adenosylmethionine quantification based on thiopurine methyltransferase-catalyzed thiol methylation. *Analytical Biochemistry* **308**, 358–63
291. Wang, R., Zheng, W., Yu, H., Deng, H., and Luo, M. (2011) Labeling Substrates of Protein Arginine Methyltransferase with Engineered Enzymes and Matched S-Adenosyl-L-methionine Analogues. *Journal of the American Chemical Society* **133**, 7648–7651

292. Borchardt, R. T. (1980) S-Adenosyl-L-Methionine-Dependent Macromolecule Methyltransferases: Potential Targets for the Design of Chemotherapeutic Agents. *Journal of Medicinal Chemistry* **23**, 347–357
293. Vidgren, J. Svensson, L., Liljas, A. (1994) Crystal structure of catechol O-methyltransferase. *Nature* **368**, 354–358
294. Cheng, X., Kumar, S., Posfai, J., Pflugrath, J. W., and Roberts, R. J. (1993) Crystal structure of the HhaI DNA methyltransferase complexed with S-adenosyl-L-methionine. *Cell* **74**, 299–307
295. Shao, Y., Molnar, L. F., Jung, Y., Kussmann, J., Ochsenfeld, C., Brown, S. T., Gilbert, A. T. B., Slipchenko, L. V., Levchenko, S. V., O'Neill, D. P., DiStasio, R. A., Lochan, R. C., Wang, T., Beran, G. J. O., Besley, N. A., Herbert, J. M., Lin, C. Y., Van Voorhis, T., Chien, S. H., Sodt, A., Steele, R. P., Rassolov, V. A., Maslen, P. E., Korambath, P. P., Adamson, R. D., Austin, B., Baker, J., Byrd, E. F. C., Dachsel, H., Doerksen, R. J., Dreuw, A., Dunietz, B. D., Dutoi, A. D., Furlani, T. R., Gwaltney, S. R., Heyden, A., Hirata, S., Hsu, C.-P., Kedziora, G., Khalliulin, R. Z., Klunzinger, P., Lee, A. M., Lee, M. S., Liang, W., Lotan, I., Nair, N., Peters, B., Proynov, E. I., Pieniazek, P. A., Rhee, Y. M., Ritchie, J., Rosta, E., Sherrill, C. D., Simmonett, A. C., Subotnik, J. E., Woodcock, H. L., Zhang, W., Bell, A. T., Chakraborty, A. K., Chipman, D. M., Keil, F. J., Warshel, A., Hehre, W. J., Schaefer, H. F., Kong, J., Krylov, A. I., Gill, P. M. W., and Head-Gordon, M. (2006) Advances in methods and algorithms in a modern quantum chemistry program package. *Physical Chemistry Chemical Physics* **8**, 3172–91
296. Curtiss, L. A., Redfern, P. C., Raghavachari, K., Rassolov, V., and Pople, J. A. (1999) Gaussian-3 theory using reduced Møller-Plesset order. *Journal of Chemical Physics* **110**, 4703–4709
297. Ohlinger, W. S., Klunzinger, P. E., Deppmeier, B. J., and Hehre, W. J. (2009) Efficient calculation of heats of formation. *The Journal of Physical Chemistry A* **113**, 2165–2175
298. Simpson, R. J. (2003) *Proteins and Proteomics: A Laboratory Manual* (Simpson, R. J., ed.), Cold Spring Harbor Laboratory Press
299. Thomsen, R., and Christensen, M. H. (2006) MolDock: a new technique for high-accuracy molecular docking. *Journal of Medicinal Chemistry* **49**, 3315–3321
300. Gross, E., and Witkop, B. (1962) Nonenzymatic cleavage of peptide bonds: the methionine residues in bovine pancreatic ribonuclease. *The Journal of Biological Chemistry* **237**, 1856–60

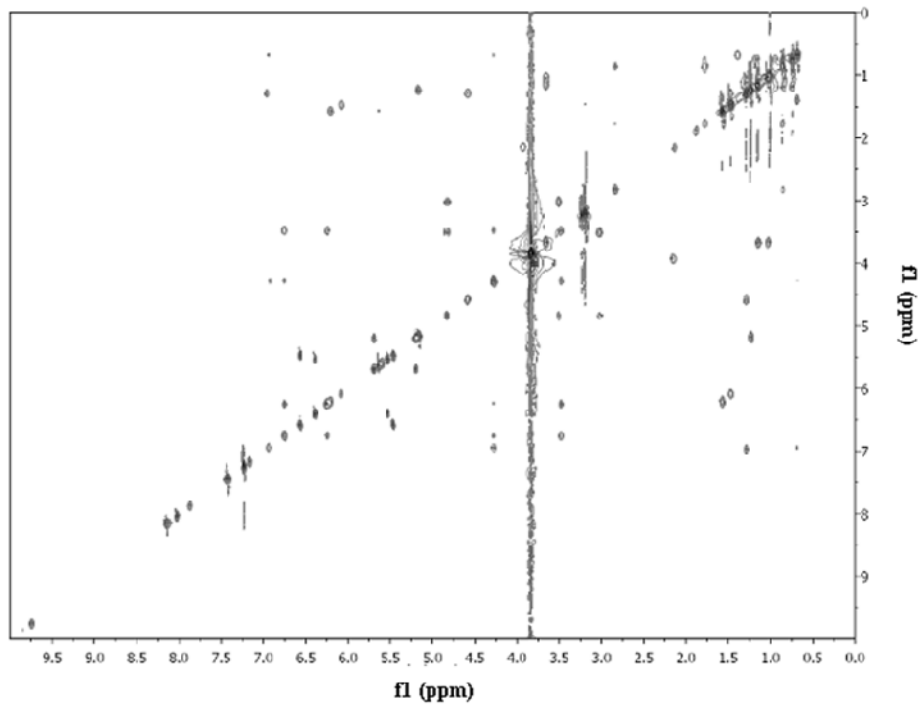
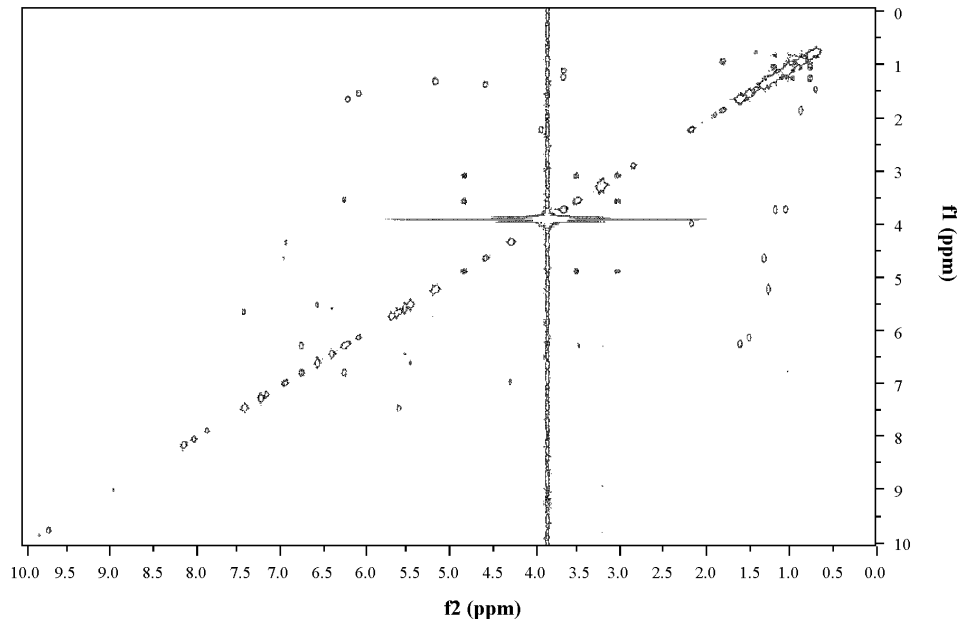
301. Smith, B. J. (1996) in *The Protein Protocols Handbook* (Walker, J. M., ed.) pp. 369–373, Humana Press
302. Mundy, B. P., Ellerd, M. G., and Favaloro, G. G. (2005) *Name Reactions and Reagents in Organic Syntheses*, 2nd Ed., John Wiley & Sons Ltd, New Jersey
303. Luft, J. R., Collins, R. J., Fehrman, N. A., Lauricella, A. M., Veatch, C. K., and DeTitta, G. T. (2003) A deliberate approach to screening for initial crystallization conditions of biological macromolecules. *Journal of Structural Biology* **142**, 170–179
304. Collazo, E., Couture, J.-F., Bulfer, S., and Trievel, R. C. (2005) A coupled fluorescent assay for histone methyltransferases. *Analytical Biochemistry* **342**, 86–92
305. Capdevila, A., Burk, R. F., Freedman, J., and Wagner, C. (2008) A Simple Rapid Immunoassay for S-adenosylhomocysteine In Plasma. *Journal of Nutritional Biochemistry* **18**, 827–831
306. Graves, T. L., Zhang, Y., and Scott, J. E. (2008) A universal competitive fluorescence polarization activity assay for S-adenosylmethionine utilizing methyltransferases. *Analytical Biochemistry* **373**, 296–306
307. Hemon, I., Gutierrez, J. A., Ho, M., and Schramm, V. L. (2011) Characterizing DNA Methyltransferases With An Ultrasensitive Luciferase-Linked Continuous Assay. *Analytical Chemistry* **83**, 4996–5004

## APPENDIX 1: NMR Spectra for thiostrepton derivatives

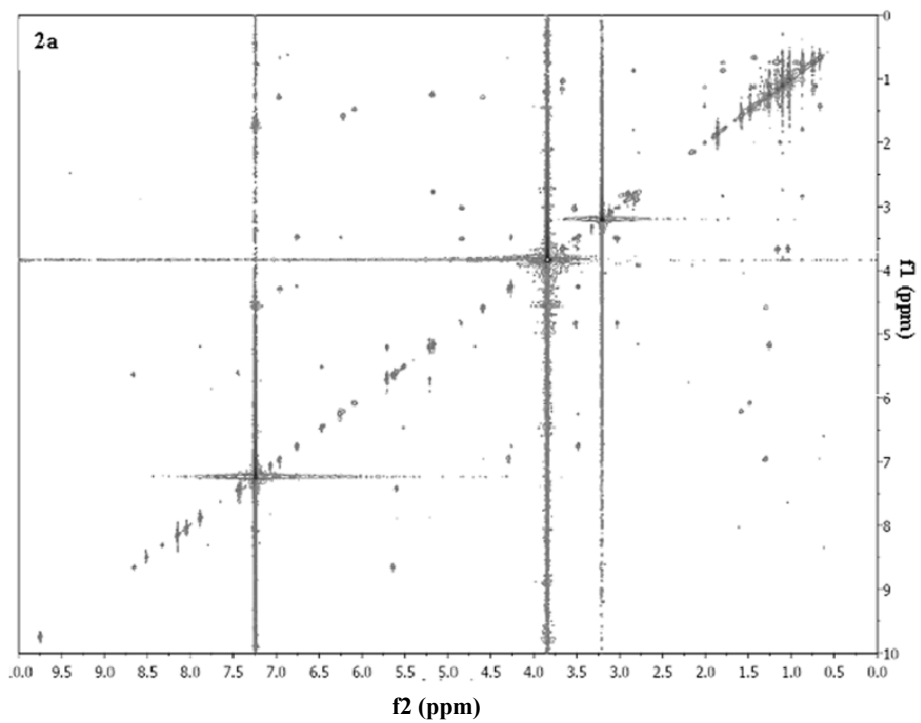
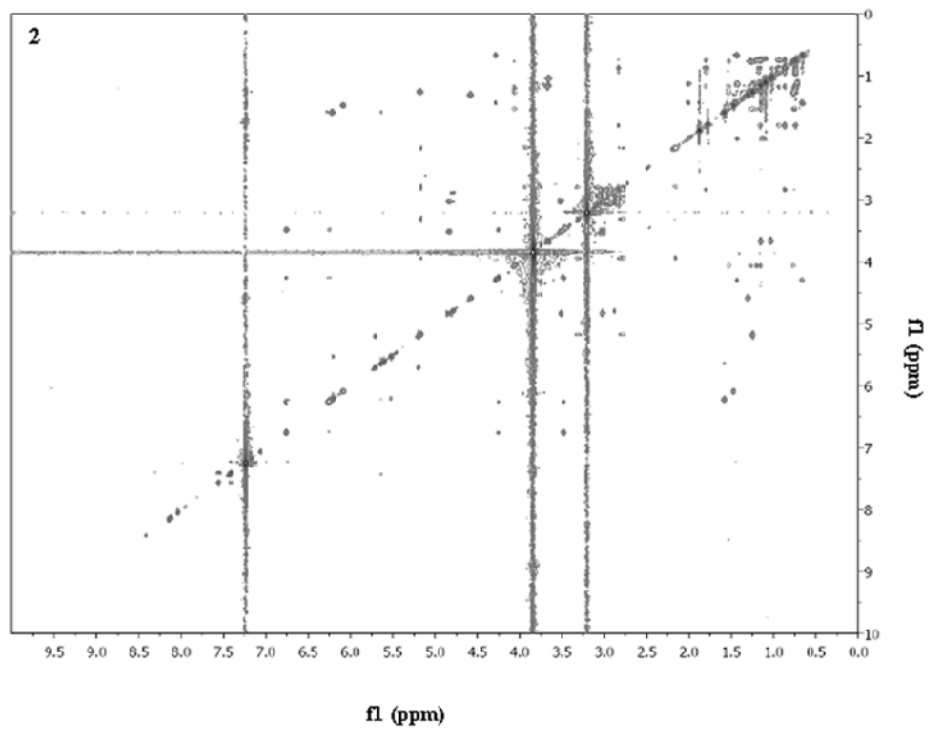
### A1.1. Michael adducts used for antibacterial activity testing



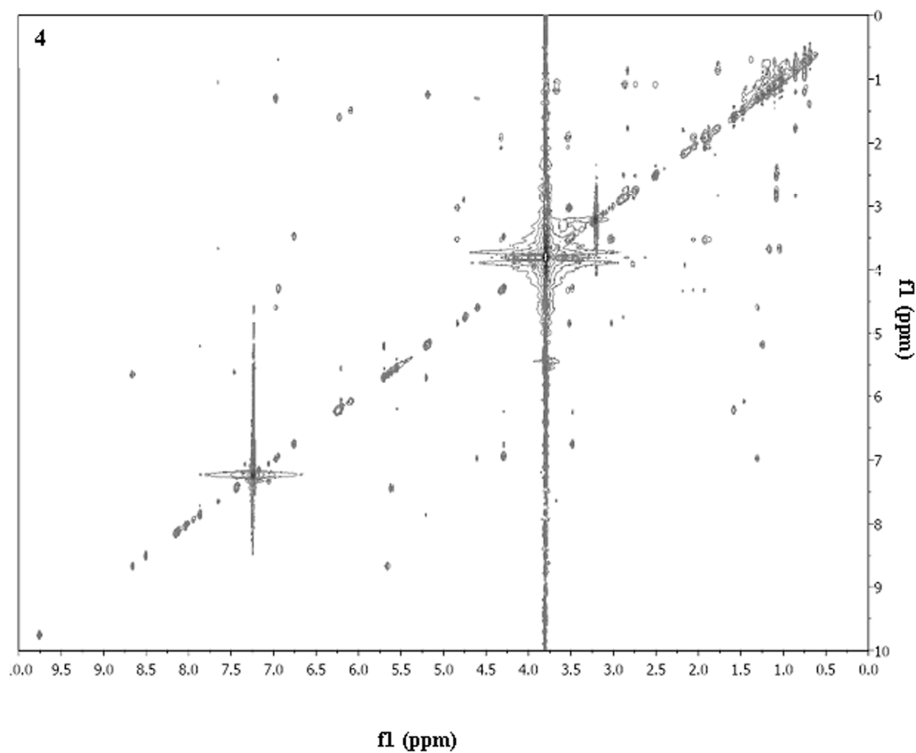
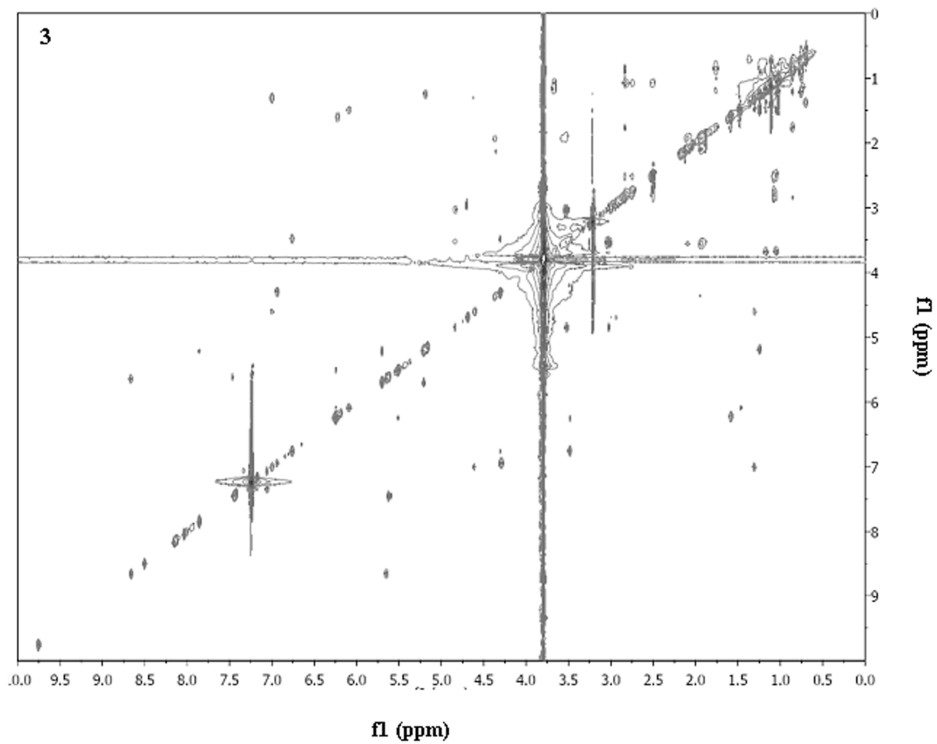
**Figure A1.1. Full proton spectra for thiostrepton and the Michael adducts used in antibacterial activity testing.** The structure of the tail region is shown. As discussed in Chapter 2, compounds **3** and **4** were obtained as separate HPLC fractions, however, the stereochemistry at the chiral center that is created by Michael addition is unknown (this is also the case with compound **2**). Compound **3** and **4** were confirmed to be diastereomers by 2-dimensional NMR (below).



**Figure A1.2 Full COSY (top panel) and TOCSY (bottom panel) spectra for thiostrepton**

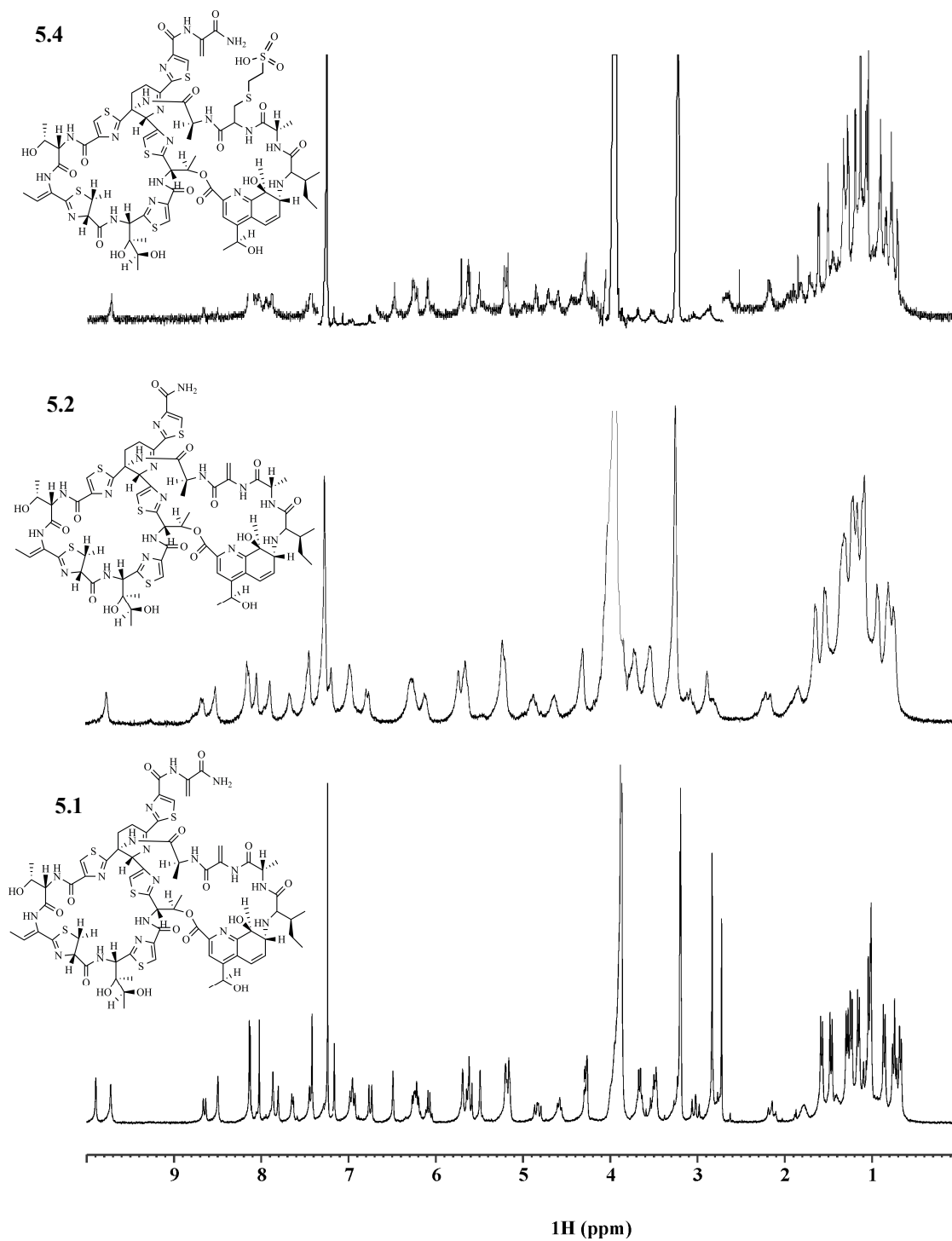


**Figure A1.3.** Full TOCSY spectra for Michael adducts of thiostrepton with MENSA. The compounds were resolved during HPLC purification, but represent a diastereomeric pair. The absolute stereochemistry for each could not be determined.



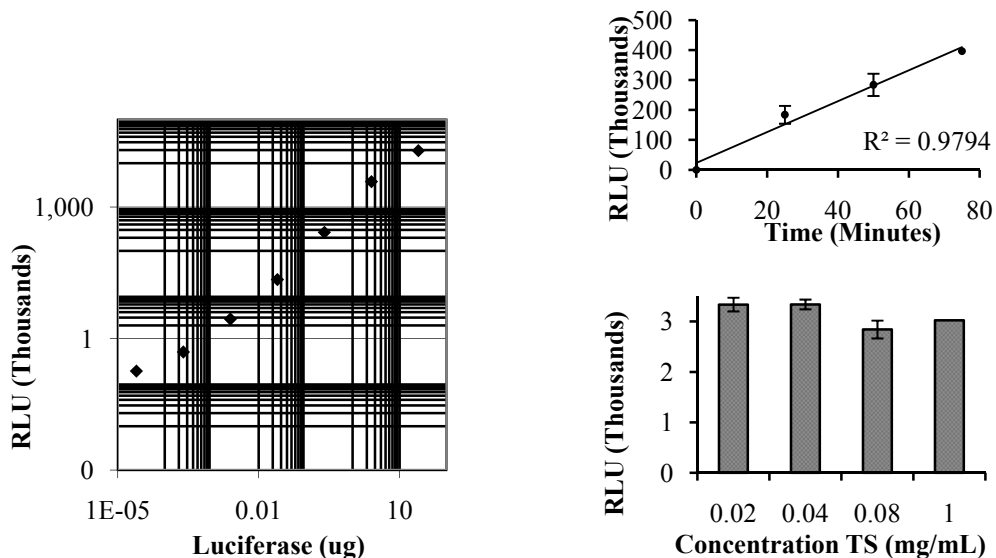
**Figure A1.4. Full TOCSY spectra for Michael adducts of thiostrepton with captopril.** As with the 2-mercaptoethanesulfonic acid adducts, the compounds are a diastereomeric pair (undetermined stereochemistry), resolved by HPLC purification.





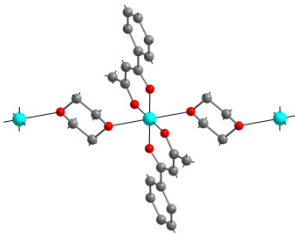
**Figure A1.5. Full proton spectra for thiostrepton derivatives used in binding studies with TIP-AS.**

## APPENDIX 2: Cell free assays of inhibition of protein translation by thiostrepton and its Michael adducts.



**Figure A2.1. Optimization of the assay for the inhibition of *in vitro* translation.** (A) Dynamic range of light output by luciferase. Luminescence was recorded for 50  $\mu\text{L}$  samples of luciferase at various concentrations in phosphate buffer. The plot indicates a linear relationship for luminescence values between  $1.0 \times 10^3$  and  $1.5 \times 10^6$  RLU, with luciferase concentration. (B) Time course for luciferase production/ light output from *in vitro* translation. Translation reactions were performed using 700-800 ng of pBESTluc. DMSO was included to a final concentration of 1% (assay volume of 25  $\mu\text{l}$ ). Uninhibited luciferase production/ light output increases linearly with time, up to 75 minutes. After this maximum time interval, RLU remains within the linear range. (C) Luciferase (20 ng in phosphate buffer) was incubated with various concentrations of thiostrepton and the light output measured. The final DMSO concentration was 50% v/v (50  $\mu\text{L}$  assay volume). Noticeable reductions in light output were observed at thiostrepton concentrations exceeding 0.04 mg/ mL (24.02  $\mu\text{M}$ ). In all cases, error bars represent the standard deviation of the mean from three replicates.

## APPENDIX 3: Crystal data and structure refinement for the thiostrepton-copper complex

Empirical formula	C <sub>24</sub> H <sub>26</sub> O <sub>6</sub> Cu	
Formula weight	473.99 g/mol	
Temperature	200(2) K	
Wavelength	0.71073 Å	
Crystal system, space group	Monoclinic, P21/n	
Unit cell dimensions	a = 8.0504(4) Å, b = 7.4273(4) Å, c = 18.4665(10) Å α = 90°, β = 100.3470(10)°, γ = 90°	
Volume	1086.21(10) Å <sup>3</sup>	
Z, Calculated density	2, 1.449 g/cm <sup>3</sup>	
Absorption coefficient	1.043 mm <sup>-1</sup>	
F(000)	494	
Crystal size	0.54 x 0.13 x 0.05 mm	
Theta range for data collection	2.96 to 27.99°	
Limiting indices	-10 ≤ h ≤ 10, -9 ≤ k ≤ 9, -24 ≤ l ≤ 24	
Reflections collected / unique	12425 / 2626 [R(int) = 0.0210]	
Completeness to theta = 27.99	99.8 %	
Absorption correction	Empirical	
Max. and min. transmission	0.9497 and 0.6027	
Refinement method	Full-matrix least-squares on F <sup>2</sup>	
Data / restraints / parameters	2626 / 0 / 142	
Goodness-of-fit on F <sup>2</sup>	1.256	
Final R indices [I > 2 σ (I)]	R1 = 0.0320, wR2 = 0.0827	
R indices (all data)	R1 = 0.0372, wR2 = 0.0854	
Largest diff. peak and hole	0.572 and -0.450 e.Å <sup>-3</sup>	

**Table A3.1. Atomic coordinates ( x 104) and equivalent isotropic displacement parameters (Å<sup>2</sup> x 103) for C<sub>24</sub>H<sub>26</sub>O<sub>6</sub>Cu.**

	x	y	z	U(eq)
Cu(1)	5000	5000	5000	26(1)
O(1)	7359(2)	5734(2)	5174(1)	30(1)
O(2)	4850(2)	5208(2)	6022(1)	32(1)
O(3)	5674(2)	1740(2)	5154(1)	35(1)
C(1)	3032(3)	6019(4)	7919(1)	53(1)
C(2)	4030(3)	6769(4)	8528(1)	45(1)
C(3)	5675(3)	7228(3)	8504(1)	42(1)
C(4)	6318(3)	6977(3)	7862(1)	37(1)
C(5)	5318(2)	6246(3)	7236(1)	28(1)
C(6)	3671(3)	5753(4)	7278(1)	41(1)
C(7)	5906(2)	5998(3)	6518(1)	27(1)
C(8)	7491(2)	6614(3)	6420(1)	31(1)
C(9)	8137(2)	6412(3)	5770(1)	28(1)
C(10)	9918(3)	7030(3)	5753(1)	39(1)
C(11)	6338(3)	563(3)	4668(1)	36(1)
C(12)	4991(3)	741(3)	5694(1)	36(1)

U(eq) is defined as one third of the trace of the orthogonalized U<sub>ij</sub> tensor.

**Table A3.2. Hydrogen coordinates ( x 104) and equivalent isotropic displacement parameters (Å<sup>2</sup> x 103) for C<sub>24</sub>H<sub>26</sub>O<sub>6</sub>Cu**

	x	y	z	U(eq)
H(1A)	1902	5683	7938	64
H(2A)	3584	6969	8964	55
H(3A)	6373	7718	8928	50
H(4A)	7453	7306	7850	45
H(6A)	2975	5228	6862	50
H(8A)	8176	7210	6821	37
H(10A)	10181	6816	5262	58
H(10B)	10711	6357	6120	58
H(10C)	10016	8319	5867	58
H(11A)	7305	-115	4948	54
H(11B)	6755	1279	4286	54
H(12A)	4488	1582	6010	54
H(12B)	5908	71	6010	54

U(eq) is defined as one third of the trace of the orthogonalized U<sub>ij</sub> tensor.

**Table A3.3. Bond lengths [Å] and angles [°] for Copper complex**

Cu(1)-O(2)	1.9185(14)
Cu(1)-O(2)#1	1.9185(14)
Cu(1)-O(1)#1	1.9463(13)
Cu(1)-O(1)	1.9463(13)
O(1)-C(9)	1.269(2)
O(2)-C(7)	1.275(2)
O(3)-C(11)	1.424(3)
O(3)-C(12)	1.429(2)
C(1)-C(2)	1.377(4)
C(1)-C(6)	1.387(3)
C(2)-C(3)	1.376(3)
C(3)-C(4)	1.388(3)
C(4)-C(5)	1.395(3)
C(5)-C(6)	1.390(3)
C(5)-C(7)	1.499(3)
C(7)-C(8)	1.398(3)
C(8)-C(9)	1.398(3)
C(9)-C(10)	1.511(3)
C(11)-C(12)#2	1.508(3)
C(12)-C(11)#2	1.508(3)
O(2)-Cu(1)-O(2)#1	180.0
O(2)-Cu(1)-O(1)#1	87.33(6)
O(2)#1-Cu(1)-O(1)#1	92.67(6)
O(2)-Cu(1)-O(1)	92.67(6)
O(2)#1-Cu(1)-O(1)	87.33(6)
O(1)#1-Cu(1)-O(1)	179.999(1)
C(9)-O(1)-Cu(1)	124.72(13)
C(7)-O(2)-Cu(1)	126.29(13)
C(11)-O(3)-C(12)	110.82(16)
C(2)-C(1)-C(6)	120.2(2)
C(3)-C(2)-C(1)	119.9(2)
C(2)-C(3)-C(4)	120.2(2)
C(3)-C(4)-C(5)	120.8(2)
C(6)-C(5)-C(4)	118.11(19)
C(6)-C(5)-C(7)	118.20(18)
C(4)-C(5)-C(7)	123.68(18)
C(1)-C(6)-C(5)	120.9(2)
O(2)-C(7)-C(8)	124.33(18)
O(2)-C(7)-C(5)	114.63(17)
C(8)-C(7)-C(5)	121.04(17)
C(9)-C(8)-C(7)	124.38(18)
O(1)-C(9)-C(8)	125.81(18)
O(1)-C(9)-C(10)	115.14(18)
C(8)-C(9)-C(10)	119.05(18)
O(3)-C(11)-C(12)#2	110.93(17)
O(3)-C(12)-C(11)#2	110.83(18)

Symmetry transformations used to generate equivalent atoms:

#1 -x+1,-y+1,-z+1 #2 -x+1,-y,-z+1

## APPENDIX 4: ITC Supplement – Curve fitting and data processing (adapted from *ITC Data Analysis in Origin. Tutorial Guide. Version 7.0. MicroCal, LLC*)

---

### A4.1. Volume correction

Before the first injection, the macromolecule (receptor; M) will be present at an initial bulk concentration,  $M_0^t$ , while the ligand (X) will be at zero concentration within the cell. The cell volume is  $V_0$ , the size of the  $i$ th injection is  $\Delta V_i$  and the total liquid injected at any point is  $\Delta V$  (sum of all individual injections). Only changes (in heat) occurring the liquid in  $V_0$  are detected, however, liquid of a volume equal to that of  $\Delta V$ , is displaced from the cell is each injection of ligand, effectively altering the concentration of macromolecule within the cell (the same number of moles of macromolecule becomes distributed throughout a volume of  $V_0 + \Delta V$ ). The law of mass conservation will hold that:

$$M_t^0 V_0 = M_t V_0 + \frac{1}{2} (M_t + M_t^0) \Delta V$$

then

$$M_t = M_t^0 \left( \frac{1 - \frac{\Delta V}{2V_0}}{1 + \frac{\Delta V}{2V_0}} \right)$$

and similarly

$$X_t^0 V_0 = X_t V_0 + \frac{1}{2} X_t \Delta V$$

### A4.2. Model for one set of sites

Terms:

K = binding constant

N = number of sites

$V_0$  = cell volume

$M_0^t$  = Initial bulk volume

$M_t$  & [M] = bulk and free concentration of macromolecule (receptor) in  $V_0$

$X_t$  & [X] = bulk and free concentration of ligand

$\Theta$  = fraction of site occupied by ligand

$$K = \frac{\theta}{1 - \theta[X]} \quad (1)$$

$$X_t = [X] + n\Theta M_t \quad (2)$$

$$\text{Combining (1) and (2) gives } \theta^2 - \theta \left[ 1 + \frac{X_t}{nM_t} + \frac{1}{nKM_t} \right] + \frac{X_t}{nM_t} = 0 \quad (3)$$

The total heat content  $Q$ , of at cell at a given fractional saturation  $\Theta$  is described by

$$Q = n\Theta M_t \Delta V_0 \quad (4)$$

where  $\Delta H$  is the heat released per mole of ligand bound. Solving the quadratic equation (3) for  $\Theta$  and substituting the solution into equation (4) gives the following expression for  $Q$ :

$$Q = \frac{nM_t \Delta H V_0}{2} \left[ 1 + \frac{X_t}{M_t} + \frac{1}{nKM_t} - \sqrt{\left( 1 + \frac{X_t}{nM_t} + \frac{1}{nKM_t} \right)^2 - \frac{4X_t}{nM_t}} \right] \quad (5)$$

Therefore,  $Q$  can be calculated for any combination of  $n$ ,  $K$  and  $\Delta H$  at the end of the  $i^{\text{th}}$  injection and designated  $Q(i)$ . However, since the ITC experiment is concerned with the change in heat content from the  $i - 1$  injection to the  $i^{\text{th}}$  injection, equation (5) is only applicable to the volume contained in  $V_0$ . Hence, the correct expression for this change in heat ( $\Delta Q$ ), after correction for the displaced volume is:

$$\Delta Q(i) = Q(i) + \frac{dV_i}{V_0} \left[ \frac{Q(i) + Q(i-1)}{2} \right] - Q(i - 1) \quad (6)$$

Fitting of the experimental data commences with initial guesses for  $n$ ,  $K$  and  $\Delta H$  by Origin, the calculation of  $\Delta Q$  for each injection and a comparison of this with what is experimentally measured, then the improvement of the initial values by Marquardt methods and continued iteration of this procedure until the fit no longer continues to improve.

### A4.3. Sample Calculations

**Table A4.1. Parameters of AdoMet binding to TSR**

#	N	Error	*K (M)	Error (M)	$\Delta H$ (cal/mol)	Error (kcal/mol)	$\Delta S$ (cal.mol <sup>-1</sup> .deg <sup>-1</sup> )
1	2.08	0.052	9010	536	-4028	148.2	4.35
2	1.91	0.048	9560	538	-4149	150	4.06
3	2.11	0.045	9260	502	-3707	119.8	5.50
	<b>N</b>		<b>K</b>		<b><math>\Delta H</math></b>		
	High	Low	High	Low	Low	High	
1	2.13	2.03	9546	8474	-3879.80	-4176.20	
2	1.96	1.86	10098	9022	-3999.00	-4299.00	
3	2.16	2.07	9762	8758	-3587.20	-3826.80	
	<b>Mean N</b>		2.03	<b>Std Dev N</b>	0.11		
	<b>Mean (1/K)</b>		$1.08 \times 10^{-4}$	<b>Std Dev (1/K)</b>	$7.0 \times 10^{-6}$		
	<b>Mean <math>\Delta H</math></b>		$-3.96 \times 10^3$	<b>Std Dev <math>\Delta H</math></b>	255.47		
	<b>Mean <math>\Delta S</math></b>		4.64	<b>Std Dev <math>\Delta S</math></b>	0.76		

Experimental details are given in Chapter 3. Prism software defines ligand binding by the parameter “K”; the inverse of this parameter, 1/K is the dissociation constant ( $K_d$ ). The table shows the values obtained from three individual replicates, after non-linear curve fitting of the integrated heats per injection, using the model for one set of sites. The error associated with each parameter from a replicate was used to generate high (+ error) and low (-error) values. The mean and standard deviation of all high and low values were reported as the final value and associated error, respectively.

**Table A4.2. Parameters for AdoMet binding to TSR mutants**

N129A							
N	Error	K (M)	Error (M)	$\Delta H$ (cal/ mol)	Error (cal/ mol)	$\Delta S$ (cal.mol <sup>1</sup> . deg <sup>-1</sup> )	Error (cal.mol <sup>1</sup> . deg <sup>-1</sup> )
2.13	±0.25	1.75×10 <sup>3</sup>	±170	-1.02×10 <sup>4</sup>	±1.59×10 <sup>3</sup>	-20	
1.83	±0.17	2.30×10 <sup>3</sup>	±197	-1.01×10 <sup>4</sup>	±1.37×10 <sup>3</sup>	-19.1	
Mean		Mean 1/K		Mean $\Delta H$		Mean $\Delta S$	
1.98	±0.30	5.07×10 <sup>-4</sup>	±9.73×10 <sup>-5</sup>	-1.02×10 <sup>4</sup>	±1.71×10 <sup>3</sup>	-19.55	±0.64

N129D							
N	Error	K (M)	Error (M)	$\Delta H$ (cal/ mol)	Error (cal/ mol)	$\Delta S$ (cal.mol <sup>1</sup> . deg <sup>-1</sup> )	Error (cal.mol <sup>1</sup> . deg <sup>-1</sup> )
2.42	±0.30	1.66×10 <sup>3</sup>	±150	-2.83×10 <sup>4</sup>	±4.60×10 <sup>3</sup>	-81.8	
2.22	±0.31	1.59×10 <sup>3</sup>	±140	-3.12×10 <sup>4</sup>	±5.58×10 <sup>3</sup>	-91.7	
Mean		Mean 1/K		Mean $\Delta H$		Mean $\Delta S$	
2.32	±0.37	6.2×10 <sup>-5</sup>	±6.54×10 <sup>-6</sup>	-2.97×10 <sup>4</sup>	±6.13×10 <sup>3</sup>	-86.75	±7.00

R135A							
N	Error	K (M)	Error (M)	$\Delta H$ (cal/ mol)	Error (cal/ mol)	$\Delta S$ (cal.mol <sup>1</sup> . deg <sup>-1</sup> )	Error (cal.mol <sup>1</sup> . deg <sup>-1</sup> )
2.00	±0.43	1.30×10 <sup>3</sup>	144	-6.44×10 <sup>4</sup>	±1.72×10 <sup>4</sup>	-205	
1.96	±0.47	1.00×10 <sup>3</sup>	99.5	-8.07×10 <sup>4</sup>	±2.31×10 <sup>4</sup>	-261	
Mean		Mean 1/K		Mean $\Delta H$		Mean $\Delta S$	
1.98	±0.52	8.94×10 <sup>-4</sup>	±1.72×10 <sup>-4</sup>	-7.25×10 <sup>4</sup>	±2.54×10 <sup>4</sup>	-233	±39.60

R135K							
N	Error	K(M)	Error (M)	$\Delta H$ (cal/ mol)	Error (cal/ mol)	$\Delta S$ (cal.mol <sup>1</sup> . deg <sup>-1</sup> )	Error (cal.mol <sup>1</sup> . deg <sup>-1</sup> )
1.88	±0.052	6.91×10 <sup>3</sup>	±311	-9.473×10 <sup>3</sup>	±369	-14.7	
1.89	±0.050	6.68×10 <sup>3</sup>	±281	-9.258×10 <sup>3</sup>	±343.4	-14.1	
Mean		Mean 1/K		Mean $\Delta H$		Mean $\Delta S$	
1.885	±0.059	1.47×10 <sup>-4</sup>	±7.94×10 <sup>-6</sup>	-9.36×10 <sup>3</sup>	±429.88	-14.4	±0.42



R165A							
N	Error	K (M)	Error (M)	$\Delta H$ (cal/ mol)	Error (cal/mol)	$\Delta S$ (cal.mol <sup>1</sup> . deg <sup>-1</sup> )	Error (cal.mol <sup>1</sup> . deg <sup>-1</sup> )
1.77	±0.16	6.91×10 <sup>3</sup>	±311	-8.53×10 <sup>3</sup>	±989.4	-12.40	
1.78	±0.099	6.47×10 <sup>3</sup>	±444	-7.09×10 <sup>3</sup>	±563.5	-9.49	
<b>Mean</b>		<b>Mean 1/K</b>		<b>Mean <math>\Delta H</math></b>		<b>Mean <math>\Delta S</math></b>	
1.775	±0.16	1.51×10 <sup>-4</sup>	±1.18×10 <sup>-5</sup>	-7.81×10 <sup>3</sup>	±1244.89	-10.95	±2.058

R165K							
N	Error	K (M)	Error (M)	$\Delta H$ (kcal/ mol)	Error (kcal/mol)	$\Delta S$ (cal.mol <sup>1</sup> . deg <sup>-1</sup> )	Error (cal.mol <sup>1</sup> . deg <sup>-1</sup> )
1.95	±0.03	1.25×10 <sup>4</sup>	±498	-6.45×10 <sup>3</sup>	±143.6	-3.27	
1.84	±0.067	9.26×10 <sup>3</sup>	±600	-6.75×10 <sup>3</sup>	±326.7	-4.87	
<b>Mean</b>		<b>Mean 1/K</b>		<b>Mean <math>\Delta H</math></b>		<b>Mean <math>\Delta S</math></b>	
1.90	0.087	9.43×10 <sup>-5</sup>	±1.75×10 <sup>-5</sup>	-6.60×10 <sup>3</sup>	±336.64	-4.07	±1.13

**Table A4.3. Parameters for the binding of thiostrepton analogues to TIP-AS (or its C214A variant)**

C214A + 5.1							
N	Error	K (M)	Error (M)	$\Delta H$ (cal/ mol)	Error (cal/mol)	$\Delta S$ (cal.mol <sup>1</sup> . deg <sup>-1</sup> )	Error (cal.mol <sup>1</sup> . deg <sup>-1</sup> )
0.93	±0.014	4.85×10 <sup>6</sup>	±7.78×10 <sup>5</sup>	-2.78×10 <sup>4</sup>	±645.8	-62.8	
0.83	±0.019	4.76×10 <sup>6</sup>	±1.05×10 <sup>6</sup>	-2.95×10 <sup>4</sup>	±1024	-68.3	
0.77	±0.013	4.94×10 <sup>6</sup>	±8.24×10 <sup>5</sup>	-2.80×10 <sup>4</sup>	±757.7	-63.3	
<b>Mean</b>		<b>Mean 1/K</b>		<b>Mean <math>\Delta H</math></b>		<b>Mean <math>\Delta S</math></b>	
0.85	±0.045	0.21×10 <sup>-6</sup>	±0.002×10 <sup>-6</sup>	-2.84×10 <sup>4</sup>	±929.16	-64.8	±3.04

TIP-AS + 5.4							
N	Error	K(M)	Error (M)	$\Delta H$ (kcal/ mol)	Error (kcal/mol)	$\Delta S$ (cal.mol <sup>1</sup> . deg <sup>-1</sup> )	Error (cal.mol <sup>1</sup> . deg <sup>-1</sup> )
1.16	±0.02	6.36×10 <sup>6</sup>	±1.72×10 <sup>6</sup>	-1.61×10 <sup>6</sup>	±511	-22.8	
1.14	±0.019	6.05×10 <sup>6</sup>	±1.30×10 <sup>6</sup>	-1.63×10 <sup>6</sup>	±435	-23.8	
1.11	±0.027	4.60×10 <sup>6</sup>	±1.23×10 <sup>6</sup>	-1.68×10 <sup>6</sup>	±620	-26	
<b>Mean</b>		<b>Mean 1/K</b>		<b>Mean <math>\Delta H</math></b>		<b>Mean <math>\Delta S</math></b>	
1.14	0.014	0.19×10 <sup>-6</sup>	±0.018×10 <sup>-6</sup>	-1.64×10 <sup>6</sup>	±360.55	-24.2	±1.64

TIP-AS + 5.2							
N	Error	K(M)	Error (M)	$\Delta H$ (kcal/ mol)	Error (kcal/ mol)	$\Delta S$ (cal.mol <sup>1</sup> . deg <sup>-1</sup> )	Error (cal.mol <sup>1</sup> . deg <sup>-1</sup> )
0.97	±0.13	$1.90 \times 10^5$	$\pm 4.13 \times 10^4$	$-6.27 \times 10^4$	$\pm 1.18 \times 10^4$	-186	
1.01	±0.090	$1.66 \times 10^5$	$\pm 1.73 \times 10^4$	$-6.54 \times 10^4$	$\pm 6.12 \times 10^3$	-195	
0.90	±0.061	$2.06 \times 10^5$	$\pm 2.09 \times 10^4$	$-6.13 \times 10^4$	$\pm 5.59 \times 10^3$	-181	
Mean		Mean 1/K		Mean $\Delta H$		Mean $\Delta S$	
0.96	±0.033	$5.38 \times 10^{-6}$	$\pm 0.34 \times 10^{-6}$	$-6.31 \times 10^4$	$\pm 7.84 \times 10^3$	-187.3	±7.09

TIP-AS + 5.3							
N	Error	K(M)	Error (M)	$\Delta H$ (kcal/ mol)	Error (kcal/ mol)	$\Delta S$ (cal.mol <sup>1</sup> . deg <sup>-1</sup> )	Error (cal.mol <sup>1</sup> . deg <sup>-1</sup> )
1.40	±0.24	$5.53 \times 10^4$	$\pm 1.09 \times 10^5$	$-2.15 \times 10^4$	$\pm 5.42 \times 10^3$	-50.3	
1.35	±0.42	$5.46 \times 10^4$	$\pm 1.77 \times 10^4$	$-2.19 \times 10^4$	$\pm 9.56 \times 10^3$	-51.7	
1.38	±0.21	$5.25 \times 10^4$	$\pm 8.30 \times 10^4$	$-2.25 \times 10^4$	$\pm 4.79 \times 10^3$	-53.9	
Mean		Mean 1/K		Mean $\Delta H$		Mean $\Delta S$	
1.38	±0.0145	$18.48 \times 10^{-6}$	$0.29 \times 10^{-6}$	$-2.20 \times 10^4$	$\pm 6.59 \times 10^3$	-51.97	±1.85

## **APPENDIX 5: Fluorometric enzyme assay supplement & enzyme kinetics for AdoMet**

---

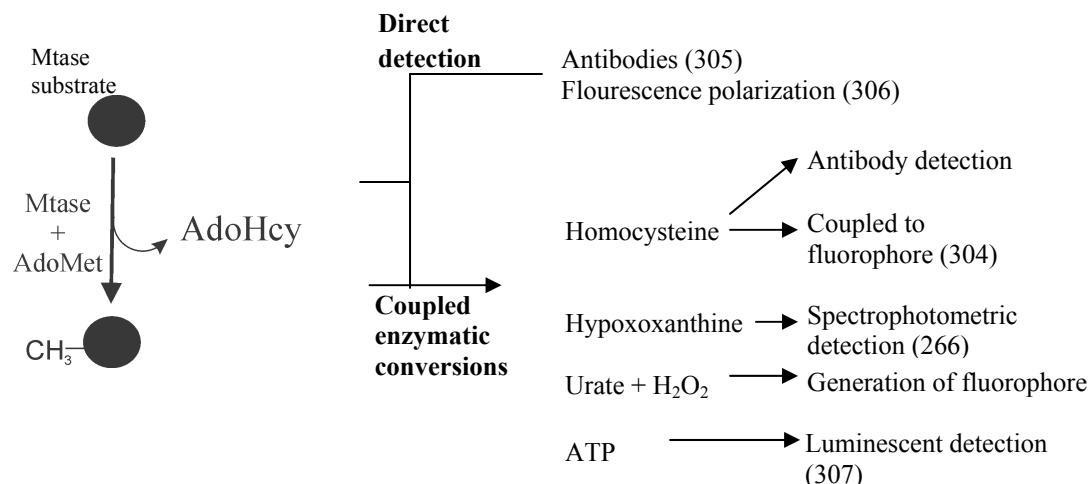
### **A5.1. General considerations.**

It was essential to maintain an RNase free environment while performing TSR assays. Therefore, RNase free (certified by the manufacturer, Corning Life Sciences, Tewksbury, USA) microfuge tubes and pipette tubes were used. 96-well microplates were supplied RNase free in sealed packages and were not re-used. When necessary, buffers or solutions were prepared using autoclaved MilliQ grade water. In addition, all working surfaces were wiped down with an RNase decontaminating solution (“RNase away”, Sigma-Aldrich).

Each fluorometric assay kit was supplied with sufficient reagents for 96 assays and these kits were quality tested by the manufacturer (Cayman Scientific Company, Ann Arbor, USA) on an individual basis. Therefore, reagents from different kits were not used together, particularly for kinetic measurements of enzyme activity otherwise introduction of an immeasurable variability and inconsistency could result. As well, assays were performed in a timely fashion and the fluorometric reagent was added last to avoid variability and minimize background due to the decomposition of this reagent.

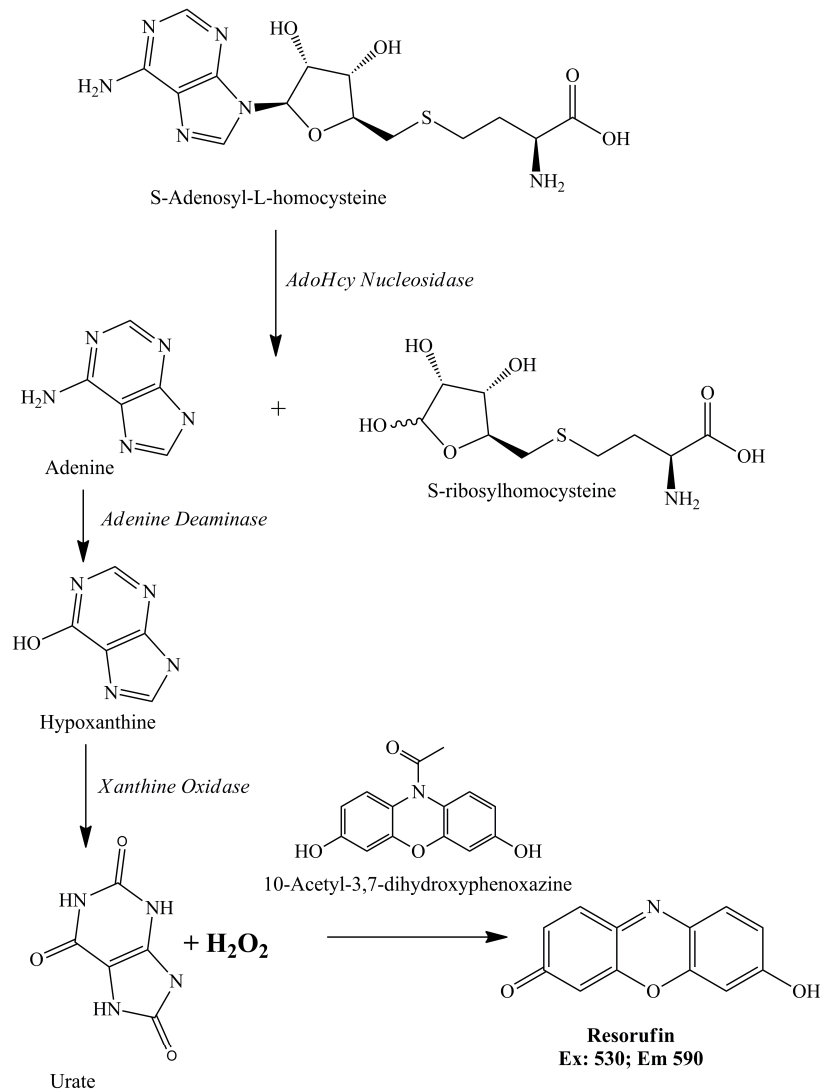
### **A5.2. Principle of the Mtase assay**

Several commercial kits that monitor methyltransferase activity through non-radiometric means are currently available. In these kits, Mtase activity is assayed by monitoring the production of S-adenosylhomocysteine (266, 304–307). AdoHcy can be directly detected through immunogenic means, or its formation during the Mtase catalyzed reaction is coupled to successive enzymatic reactions that convert the AdoHcy produced into a more easily observable or quantifiable reporter (Figure A5.1).



**Figure A5.1. General approaches to non-radiometric assays of Mtase activity.**

The kit offered by the Cayman Chemical Company was selected to monitor TSR activity and determine the kinetic parameters for AdoMet utilization by TSR, as well as for substrate utilization studies of an AdoMet analogue by TPMT. The principle of the assay is shown schematically in Figure A5.2 and it extends the spectrophotometric Mtase assay described in (266), by further converting hypoxoxanthine to urate with a concomitant production of hydrogen peroxide. Subsequent oxidation of the 10-Acetyl-3,7-dihydroxyphenoxazine by the hydrogen peroxide that is produced results in the formation of the fluorophore resorufin. Therefore, the amount of resorufin produced is directly correlated with the AdoHyc produced. Since AdoHyc production is stoichiometrically related to the amount of AdoMet initially present, fluorescence output can thus be directly correlated with (initial) AdoMet concentration. The required amounts of the individual assay reagents are predetermined and are supplied as individual vials and the assay is performed by mixing the reagents according to the manufacturer's instructions. An added benefit of the assay is its continuous format, which avoids variability from reaction quenching or washing steps that are necessary in other assays. As well, AdoMet can be added separately, which allows for the determination of the kinetic parameters of its utilization, or its substitution for an AdoMet analogue.



**Figure A5.2. Principle of the fluorometric Mtase assay from the Cayman Chemical Company.**

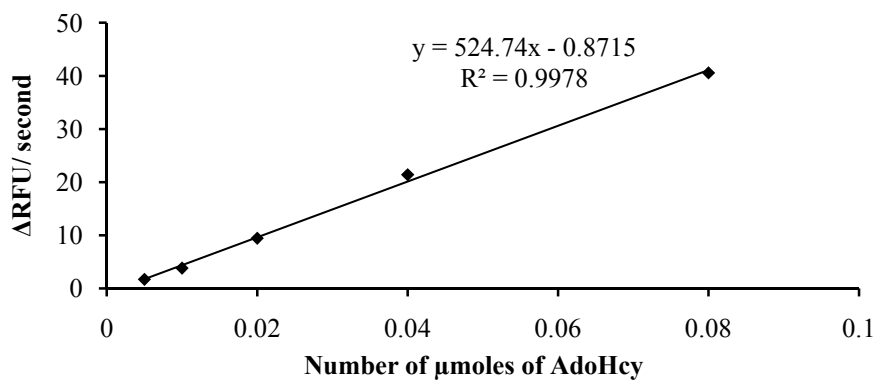
### **A5.3. Sample calculation and data processing for the determination of kinetic parameters for AdoMet turnover by TSR (and mutants).**

Quantification of AdoHcy was necessary for subsequent determinations of enzyme kinetic parameters ( $V_{\max}$ ,  $k_{\text{cat}}$ ). In order to quantify the amount of AdoHcy generated during kinetic enzyme assays, a standard curve correlating the observed change in fluorescence with the concentration of AdoHcy was generated. Reactions were set up containing known amounts of AdoHcy, but lacking enzyme (Mtase) and were performed in an identical manner to reactions where enzyme was present. Figure A5.1 shows the ranges over which the relationship is linear and the equation describing this linear correlation :

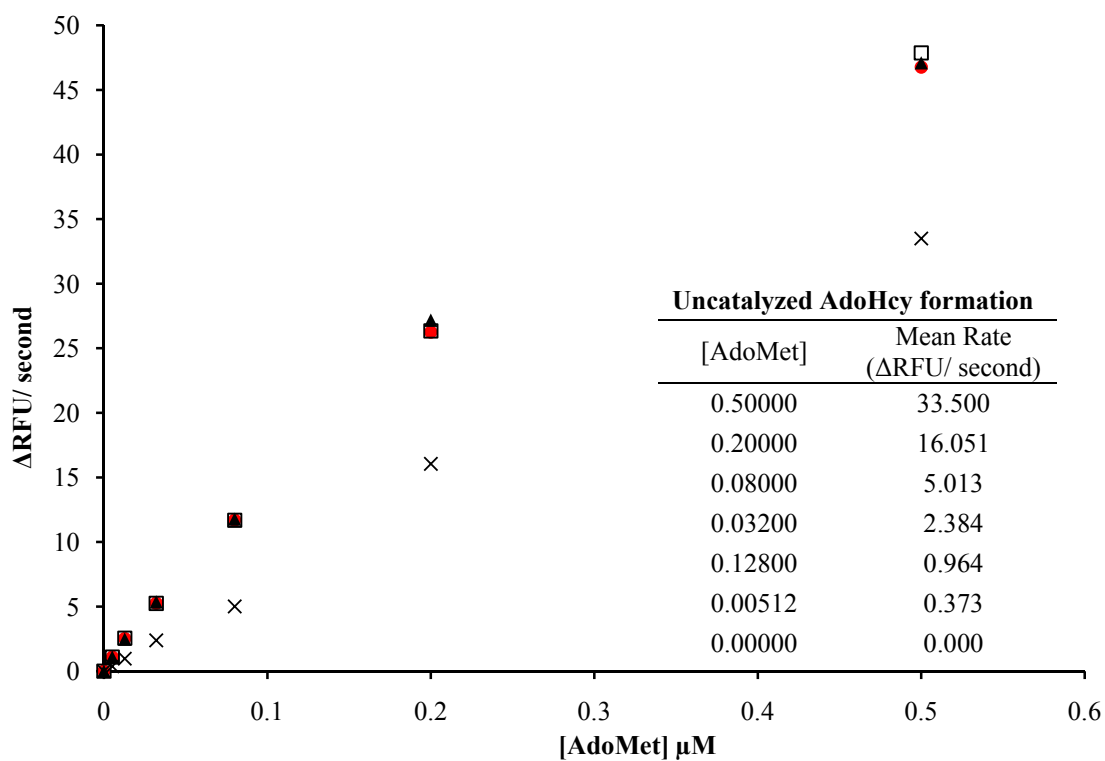
$y = 524.74x - 0.8715$ , was used to convert the observed rate ( $\Delta\text{RFU}/\text{second}$ ) from the assays containing Mtase to number of moles of AdoHcy (i.e. number of moles of AdoHcy =  $\frac{\text{observed rate} + 0.8715}{524.744}$ )

**Table A5.1. AdoHcy Standard Curve**

$\mu\text{moles of AdoHcy}$	$\Delta\text{RFU}/\text{second}$	$\Delta\text{RFU}/\text{second}$	Mean $\Delta\text{RFU}/\text{second}$
0.16	46.819	46.185	46.502
0.08	40.896	40.262	40.579
0.04	21.722	21.088	21.405
0.02	9.765	9.131	9.448
0.01	4.148	3.514	3.831
0.005	2.032	1.398	1.715
0.0025	1.178	0.544	0.861



**Figure A5.3. Linear dependence of  $\Delta\text{RFU}/\text{second}$  on  $[\text{AdoHcy}]$ .**



**Figure A5.4. Dependence of initial rate of the K221A variant of TSR on [AdoMet].** The rate of AdoHcy formation in the absence of Mtase at each AdoMet (×) concentration was obtained from assays containing no Mtase. Assays for the determination of this background rate were performed simultaneously with the assays containing Mtase (i.e. in the same 96-well plate, using the same reagent stock, at the same time).

**Table A5.2. Sample calculations for the conversion of ( $\Delta$ RFU/ second) to ( $\Delta$ [AdoHcy]/ second)**

[AdoMet] ( $\mu$ M)		0.5	0.2	0.08	0.032	0.0128	0.00512	0
<b>Observed Rate (RFU/ second)</b>	<b>1</b>	46.998	26.491	11.935	5.493	2.758	1.316	0.232
	<b>2</b>	48.123	26.6	11.943	5.507	2.809	1.348	0.258
	<b>3</b>	47.33	27.405	11.996	5.59	2.712	1.319	0.233
<b>Correction for assay background*</b>	<b>1</b>	46.766	26.259	11.703	5.261	2.526	1.084	0
	<b>2</b>	47.865	26.342	11.685	5.249	2.551	1.09	0
	<b>3</b>	47.097	27.172	11.763	5.357	2.479	1.086	0
<b>Correction for Mtase free AdoHcy formation†</b>	<b>1</b>	13.266	10.208	6.69	2.877	1.562	0.711	0
	<b>2</b>	14.365	10.291	6.672	2.865	1.587	0.717	0
	<b>3</b>	13.597	11.121	6.75	2.973	1.515	0.713	0
<b><math>\Delta</math> AdoHcy (nmoles /second)‡</b>	<b>1</b>	0.1497	0.1173	0.0801	0.0397	0.0258	0.0168	0
	<b>2</b>	0.1613	0.1182	0.0799	0.0396	0.026	0.0168	0
	<b>3</b>	0.1532	0.127	0.0807	0.0407	0.0253	0.0168	0

The raw data set for the **K221A** variant is used as an example. \* : The observed rate at 0  $\mu$ M AdoMet was subtracted from each value. †: The rate of Mtase free AdoHcy formation for each concentration of AdoMet (Figure A5.2) was subtracted from the rates corrected for assay background. ‡ After correcting for uncatalyzed AdoHcy formation, the

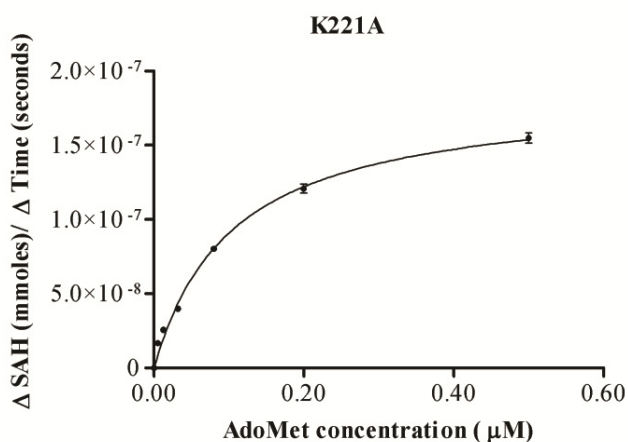
following transformation was performed to obtain  $\Delta$ AdoHcy ( $\mu$ moles) /second:  $\frac{\text{corrected rate} + 0.8715}{180(\text{seconds})}$ ; where 180 is the duration (seconds) over which the initial rate was determined



**Table A5.3. Raw data used for the generation of Michaelis-Menten plots and the determination of enzyme kinetic parameters**

[AdoMet] ( $\mu\text{M}$ )		0.5	0.2	0.08	0.032	0.0128	0.00512	0
<b>TSR</b>	1	0.334	0.199	0.1	0.067	0.053	0.045	0
	2	0.292	0.18	0.093	0.069	0.054	0.046	0
	3	0.278	0.197	0.103	0.076	0.055	0.044	0
<b>E220Q</b>	1	0.283	0.276	0.15	0.076	0.053	0.043	0
	2	0.291	0.252	0.123	0.068	0.052	0.043	0
	3	0.383	0.291	0.15	0.075	0.065	0.045	0
<b>K221A</b>	1	0.15	0.117	0.08	0.04	0.026	0.017	0
	2	0.161	0.118	0.08	0.04	0.026	0.017	0
	3	0.153	0.127	0.081	0.041	0.025	0.017	0
<b>R165A</b>	1	0.261	0.132	0.084	0.04	0.034	0.023	0
	2	0.158	0.112	0.076	0.043	0.034	0.023	0
	3	0.187	0.127	0.084	0.04	0.032	0.025	0

The rates of AdoHcy formation (nmoles/ second) at various concentrations of AdoMet are shown, after corrections for assay background and the background rate of AdoHcy formation (background rates of AdoHcy formation were determined in parallel the rate in the presence of Mtase. The background values shown in Figure A5.2 are applicable to the data sets for K221A and R165A. Separate background rates were used for TSR and E220Q). Values in red were excluded from non-linear curve fitting according to:  $\text{Rate} = V_{\max} \times [\text{AdoMet}] \div (K_m + [\text{AdoMet}])$



**$K_m(\text{AdoMet}): 104.20 \mu\text{M}$**   
 **$V_{\max}: 1.857 \times 10^{-7} \text{ (nmoles/ second)}$**

According to the Michaelis-Menten model:  $V_{\max} = E_t \times K_{\text{cat}}$ , therefore,  $K_{\text{cat}} = \frac{V_{\max}}{E_t}$

$$E_t = \frac{\text{Enzyme concentration in assay (uM)} \times \text{assay volume(ml)}}{1000 \text{ (ml)}} = \frac{0.1 \mu\text{M} \times 0.2 \text{ml}}{1000 \text{ml}}$$

$$K_{\text{cat}} (\text{sec}^{-1}) = (1.857 \times 10^{-7}) / 0.00002 = \mathbf{0.0093}$$

## APPENDIX 6: Comparison of TSR and NHR

```

NHR      MTEPAIITNASDPAVQRIIDVTKHSRASIKTTLIEDTEPLMECIRAGVQFIEVYGSSGTP
TSR      MTELDTIANPSDPAVQRIIDVTKPSRSNIKTTLIEDVEPLMHSIAAGVFEFIEVYGSDSSP
          ***      *:* ***** **:.*****.***.* **:******.:*

NHR      LDPALLDLCRQREIPVRLIDVSVINQLFKAERKAKVFGIARVPRPARLADIAERGGDVVV
TSR      FPSELLDLCGRQNIPVRLIDSSIVNQLFKGERKAKTFGIARVPRPARFGDIASRRGDVVV
          ***** :.:***** *****.***.*****:.* **.* *****

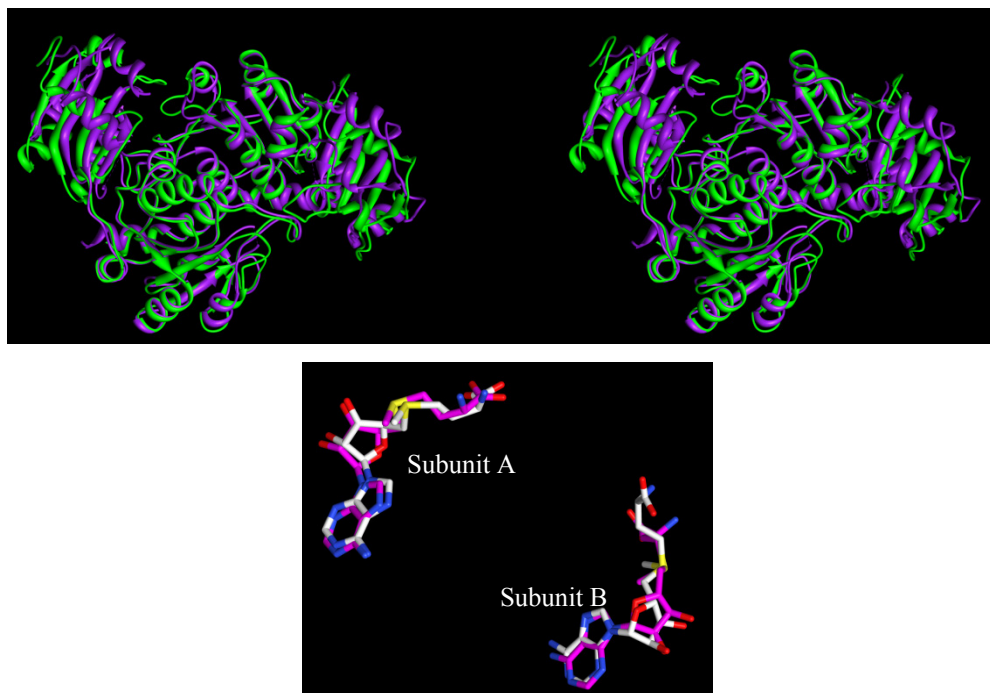
NHR      LDGVKIVGNIGAIVRTSLALGAGIVLVESDLATIADRLLRASRGYVFSLPVVLADREE
TSR      LDGVKIVGNIGAIVRTSLALGASGIILVSDITSIADRRLQASRGYVFSLPVVLSGREE
          *****:*****:*****:*****:*****:*****:*****:***

NHR      AVSFLRDNDIALMVLDTDGDLGVKDLGDRADRMALVFGSEKGGGPSGLFQEASAGTVSIPM
TSR      AIAFIRDSGMQLMTLKADGDISVKELGDNPDRLALLFGSEKGGPSDLFEEASSASVSIIPM
          *:::*:* .: **.*:***:***:***. **:*:*:***** **:*:*:*****

NHR      LSSTESLNVSVSLGIALHERSARNFAVRRAAAQA
TSR      MSQTESLNVSVSLGIALHERIDRNLAANR-----
          *.******:***** **:*..*

```

**Figure A6.1. Sequence alignment of NHR (nosiheptide resistance methyltransferase) and TSR (thiostrepton resistance methyltransferase).** Alignment was performed using CLUSTAL Omega.  $\alpha$ -helical regions are shaded purple and  $\beta$ -sheets are in blue. The two enzymes share 73% sequence identity and 82.1% sequence similarity. Accession numbers are P52391 and P18644 for NHR and TSR, respectively



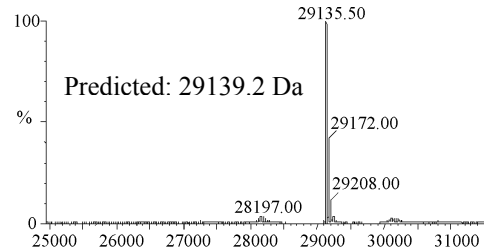
**Figure A6.2** A) Stereoview of superimposed structures for TSR (green) and the nosiheptide resistance methyltransferase (purple). (B) Superimposed structures of AdoMet, as positioned in the binding pockets of the individual subunits of TSR (white) and the nosiheptide resistance methyltransferase (magenta). Structures were generated from PDB structure files (TSR: 3GYQ; NHR 3NK6/ 3NK7) with *Chimera* software version 1.5.2.

## APPENDIX 7: Confirmation of mutant identity.

The DNA sequence of the gene encoding region from plasmids bearing mutated TSR and TIP-AS genes shown (translated sequence is shown below in upper case). Mutated codons are underlined. Deconvoluted ESI mass spectra are shown next to the sequence.

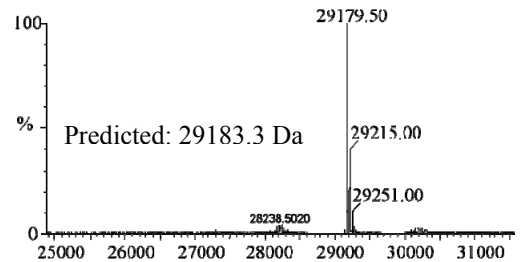
### N129A

```
atgactgagttggacaccatcgaaatccgtccgatcccgcggtgcagcggatcatcgat
M T E L D T I A N P S D P A V Q R I I D
gtcaccagccgctcgcatccaacataaagacaacgttgatcgaggacgtcgagcccctc
V T K P S R S N I K T T L I E D V E P L
atgcacagcatcgccggcgggtggagttcatcgaggtctacggcagcagcagtcct
M H S I A A G V E F I E V Y G S D S S P
tttccatctgagttgctggatctgtgctggcggcagaaacataccggctcgcctcatcgac
F P S E L L D L C G R Q N I P V R L I D
tcctcgatcgtaaccagttgttcaagggggagcgggaaggccaagacattcggcatcgcc
S S I V N Q L F K G E R K A K T F G I A
cgcgtccctcgcgccggcagggttcggcgatatcgcgagccggcgtggggacgtcgctcgtt
R V P R P A R F G D I A S R R G D V V V
ctcgacggggtgaagatcgctcggggacatcggcgcgatagtagcagcgtcgctcgcgctc
L D G V K I V G A I G A I V R T S L A L
ggagcgtcggggatcatcctggtcgacagtgacatcaccagcatcgcggaccggcgtctc
G A S G I I L V D S D I T S I A D R R L
caaagggccagcggaggttacgtcttctcccttcccgctcgttctcctcggtcgagaggag
Q R A S R G Y V F S L P V V L S G R E E
gccatcgccttcattcgggacagcgggatgcagctgatgacgctcaaggcggatggcgac
A I A F I R D S G M Q L M T L K A D G D
atttccgtgaaggaaactcgggacaatccggatcggctggccttgctgttcggcagcgaa
I S V K E L G D N P D R L A L L F G S E
aagggtgggccttcggacctgntcgaggaggcgtcttccgcctcggtttccatccccatg
K G G P S D L X E E A S S A S V S I P M
atgagccagaccgagtcctcaacgtttccggttccctcnggatcgcgctgcncgagagg
M S Q T E S L N V S V S L X I A L X E R
atcgacaggaatctcgcggccaaccga
I D R N L A A N R
```



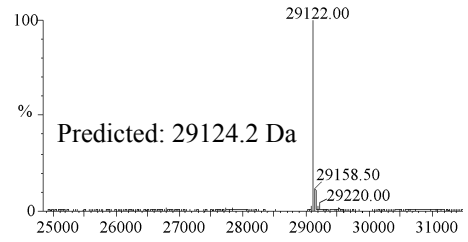
### N129D

```
atgactgagttggacaccatcgaaatccgtccgatcccgcggtgcagcggatcatcgat
M T E L D T I A N P S D P A V Q R I I D
gtcaccagccgctcgcatccaacataaagacaacgttgatcgaggacgtcgagcccctc
V T K P S R S N I K T T L I E D V E P L
atgcacagcatcgccggcgggtggagttcatcgaggtctacggcagcagcagtcct
M H S I A A G V E F I E V Y G S D S S P
tttccatctgagttgctggatctgtgctggcggcagaaacataccggctcgcctcatcgac
F P S E L L D L C G R Q N I P V R L I D
tcctcgatcgtaaccagttgttcaagggggagcgggaaggccaagacattcggcatcgcc
S S I V N Q L F K G E R K A K T F G I A
cgcgtccctcgcgccggcagggttcggcgatatcgcgagccggcgtggggacgtcgctcgtt
R V P R P A R F G D I A S R R G D V V V
ctcgacggggtgaagatcgctcggggacatcggcgcgatagtagcagcgtcgctcgcgctc
L D G V K I V G D I G A I V R T S L A L
ggagcgtcggggatcatcctggtcgacagtgacatcaccagcatcgcggaccggcgtctc
G A S G I I L V D S D I T S I A D R R L
caaagggccagcggaggttacgtcttctcccttcccgctcgttctcctcggtcgagaggag
Q R A S R G Y V F S L P V V L S G R E E
gccatcgccttcattcgggacagcgggatgcagctgatgacgctcaaggcggatggcgac
A I A F I R D S G M Q L M T L K A D G D
atttccgtgaaggaaactcgggacaatccggatcggctggccttgctgttcggcagcgaa
I S V K E L G D N P D R L A L L F G S E
aagggtgggccttcggacctgntcgaggaggcgtcttccgcctcggtttccatccccatg
K G G P S D L F E E A S S A S V S I P M
atgagccagaccgagtcctcaacgtttccggttccctcggaaatcgcgctgcacgagagg
M S Q T E S L N V S V S L G I A L H E R
atcgacaggaatctcgcggcccaaccga
I D R N L A A X R
```

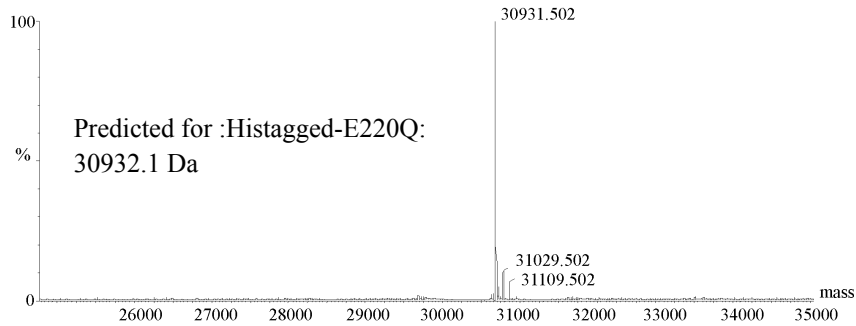


## E220A

atgactgagttggacaccatcgcaaatccgtccgatcccgcggtgcagcggatcatcgat  
M T E L D T I A N P S D P A V Q R I I D  
gtcaccaagccgtcgcgatccaacataaagacaacggtgatcgaggacgtcgagcccctc  
V T K P S R S N I K T T L I E D V E P L  
atgcacagcatcgcgccgggtggagttcatcgaggtctacggcagcgacagcagtcct  
M H S I A A G V E F I E V Y G S D S S P  
tttccatctgagttgctggatctgtgcgggcggcagaacataaccggtccgcctcatcgac  
F P S E L L D L C G R Q N I P V R L I D  
tcctcgatcgtcaaccagttgttcaagggggagcgggaaggccaagacattcggcatcgcc  
S S I V N Q L F K G E R K A K T F G I A  
cgcgtccctcgcccggccaggttcggcgatcgcgagccgcgctggggacgtcgtcgtt  
R V P R P A R F G D I A S R R G D V V V  
ctcgacgggtgaagatcgtcggaacatcggcggatagtagcacgtcgtcgtcgtc  
L D G V K I V G N I G A I V R T S L A L  
ggagcgtcgggatcatcctggtcgacagtgacatcaccagcatcgggaccggcgtctc  
G A S G I I L V D S D I T S I A D R R L  
caaagggccagccgaggttacgtcttctcccttcccgctgttctcgggtcgcgaggag  
Q R A S R G Y V F S L P V V L S G R E E  
gccatcgcttcatcgggacagcggatgcagctgatgacgctcaaggcggatggcgac  
A I A F I R D S G M Q L M T L K A D G D  
atttccgtgaaggaactcggggacaatccggatcggctggccttgcgttcggcagcggc  
I S V K E L G D N P D R L A L L F G S **A**  
aanggtgggccttccgacctgntcgaggaggcgtcttccgcctcggtttccatccccatg  
X G G P S D L X E E A S S A S V S I P M  
atgagcnnagaccgagtcctcaacgtttccnnttccctcggaatcgcgctgcacgagagg  
M S X T E S L N V S X S L G I A L H E R  
atcgacaggaatctcgcggccaaccga  
I D R N L A A N R

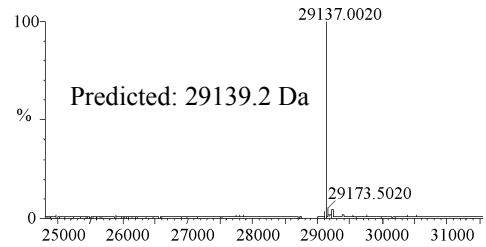


## E220Q



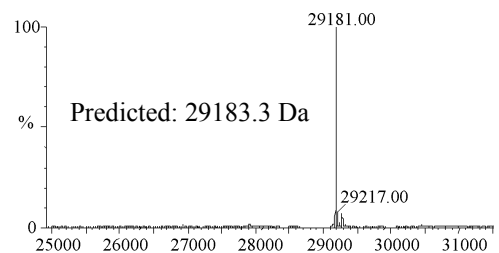
### N248A

atgactgagttggacaccatcgcaaatccgtccgatcccgcggtgcagcggatcatcgat  
M T E L D T I A N P S D P A V Q R I I D  
gtcaccaagccgtcgcgatccaacataaagacaacggtgatcgaggacgtcgagcccctc  
V T K P S R S N I K T T L I E D V E P L  
atgcacagcatcgcggccgggtggagtcatcgaggctacggcagcagcagcagtcct  
M H S I A A G V E F I E V Y G S D S S P  
ttccatctgagttgctggatctgtgccccggcagacataccgggtccgcctcatcgac  
F P S E L L D L C G R Q N I P V R L I D  
tcctcgatcgtcaaccagttgttcaagggggagcgggaaggccaagacattcggcatcgcc  
S S I V N Q L F K G E R K A K T F G I A  
cgcgtccctcgcgccggccagggtcggcgatatcgcgagccggcgtggggacgtcgtcgtt  
R V P R P A R F G D I A S R R G D V V V  
ctcgacggggtgaagatcgtcgggaacatcggcgcgatagtagcacgtcgtcgcgctc  
L D G V K I V G N I G A I V R T S L A L  
ggagcgtcggggatcatcctggtcgacagtgacatcaccagcatcgcggaccggcgtctc  
G A S G I I L V D S D I T S I A D R R L  
caaagggccagccgaggttacgtcttcccttcccgtcgttctcctcgggtcgcgaggag  
Q R A S R G Y V F S L P V V L S G R E E  
gccatcgccttattcgggacagcgggtatgcagctgatgacgctcaaggcggatggcgac  
A I A F I R D S G M Q L M T L K A D G D  
atctccgtgaaggaactcggggacaatccggatcggctggccttgcgttccggcagcga  
I S V K E L G D N P D R L A L L F G S E  
aaggggtggcctccgacctgttcgaggaggcgtcttccgctcgggttccatccccatg  
K G G P S D L F E E A S S X S V S I P M  
atgagccnagaccagtcctcgcgggttccggttccctcggaatcgcgctgcacgagagg  
M S X T E S L A V S V S L G I A L H E R  
atcgacaggaatcctcgcggccnaccgat  
I D R N L A A X R



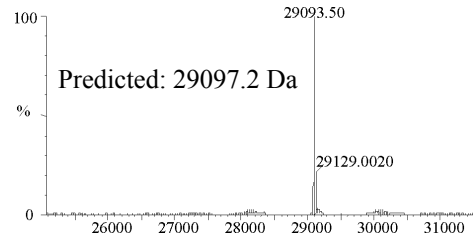
### N248D

atgactgagttggacaccatcgcaaatccgtccgatcccgcggtgcagcggatcatcgat  
M T E L D T I A N P S D P A V Q R I I D  
gtcaccaagccgtcgcgatccaacataaagacaacggtgatcgaggacgtcgagcccctc  
V T K P S R S N I K T T L I E D V E P L  
atgcacagcatcgcggccgggtggagtcatcgaggctacggcagcagcagcagtcct  
M H S I A A G V E F I E V Y G S D S S P  
ttccatctgagttgctggatctgtgccccggcagacataccgggtccgcctcatcgac  
F P S E L L D L C G R Q N I P V R L I D  
tcctcgatcgtcaaccagttgttcaagggggagcgggaaggccaagacattcggcatcgcc  
S S I V N Q L F K G E R K A K T F G I A  
cgcgtccctcgcgccggccagggtcggcgatatcgcgagccggcgtggggacgtcgtcgtt  
R V P R P A R F G D I A S R R G D V V V  
ctcgacggggtgaagatcgtcgggaacatcggcgcgatagtagcacgtcgtcgcgctc  
L D G V K I V G N I G A I V R T S L A L  
ggagcgtcggggatcatcctggtcgacagtgacatcaccagcatcgcggaccggcgtctc  
G A S G I I L V D S D I T S I A D R R L  
caaagggccagccgaggttacgtcttcccttcccgtcgttctcctcgggtcgcgaggag  
Q R A S R G Y V F S L P V V L S G R E E  
gccatcgccttattcgggacagcgggtatgcagctgatgacgctcaaggcggatggcgac  
A I A F I R D S G M Q L M T L K A D G D  
atctccgtgaaggaactcggggacaatccggatcggctggccttgcgttccggcagcga  
I S V K E L G D N P D R L A L L F G S E  
aaggggtggcctccgacctgttcgaggaggcgtcttccgctcgggttccatccccatg  
K G G P S D L F E E A S S A S V S I P M  
atgagccagaccagtcctcgcagcgttccggttccctcggaatcgcncctgcacgagagg  
M S Q T E S L D V S V S L G I X L H E R  
atcgacaggaatcctcgcggccaaccgat  
I D R N L A A N R



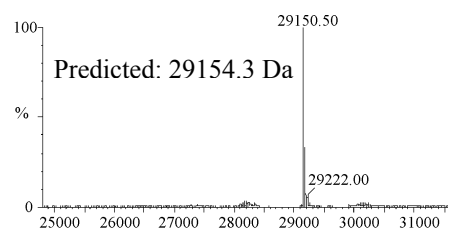
### R135A

atgactgagttggacaccatcgcaaatccgtccgatcccgcggtgcagcggatcatcgat  
M T E L D T I A N P S D P A V Q R I I D  
gtcaccaagccgtcgcgatccaacataaagacaacggtgatcgaggacgtcgagcccctc  
V T K P S R S N I K T T L I E D V E P L  
atgcacagcatcgcgccgggtggagttcatcgaggtctacggcagcagcagcagtcct  
M H S I A A G V E F I E V Y G S D S S P  
tttccatctgagttgctggatctgtgcgggcggcagaacataaccggtccgcctcatcgac  
F P S E L L D L C G R Q N I P V R L I D  
tcctcgatcgtcaaccagttgttcaagggggagcgggaaggccaagacattcggcatcgcc  
S S I V N Q L F K G E R K A K T F G I A  
cgcgtccctcgcccggccagggttcggcgatcgcgagccggcgtggggacgtcgtcgtt  
R V P R P A R F G D I A S R R G D V V V  
ctcgacgggtgtaagatcgtcgggaacatcggcggatagtagcagcgtcgtcgcgctc  
L D G V K I V G N I G A I V **A** T S L A L  
ggagcgtcggggatcactcgtcgcagagtacatcaccagcatcgcggaccggcgtctc  
G A S G I I L V D S D I T S I A D R R L  
caaagggccagccgaggttacgtcttctcccttcccgctgttctcctcggtcgagggag  
Q R A S R G Y V F S L P V V L S G R E E  
gccatcgcttcatcgggacagcggatgacagctgatgacgctcaaggcggatggcgac  
A I A F I R D S G M Q L M T L K A D G D  
atttccgtgaaggaactcggggacaatccggatcggctggccttgcgttcggcagcga  
I S V K E L G D N P D R L X L L F G S E  
aaggggtggccttccgacctgttcgagggcgtcttccgcctcggnttccatccccatg  
K G G P S D L F E E A S S A S V S I P M  
atgagcngaccgagtcctcaacgtttccgnttccctcggaaatcgcgctgcacgagagg  
M S X T E S L N V S X S L G I A L H E R  
atcgacaggaatctcgcggccnaccga  
I D R N L A A X R



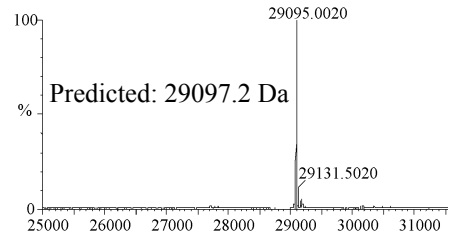
### R135K

atgactgagttggacaccatcgcaaatccgtccgatcccgcggtgcagcggatcatcgat  
M T E L D T I A N P S D P A V Q R I I D  
gtcaccaagccgtcgcgatccaacataaagacaacggtgatcgaggacgtcgagcccctc  
V T K P S R S N I K T T L I E D V E P L  
atgcacagcatcgcgccgggtggagttcatcgaggtctacggcagcagcagcagtcct  
M H S I A A G V E F I E V Y G S D S S P  
tttccatctgagttgctggatctgtgcgggcggcagaacataaccggtccgcctcatcgac  
F P S E L L D L C G R Q N I P V R L I D  
tcctcgatcgtcaaccagttgttcaagggggagcgggaaggccaagacattcggcatcgcc  
S S I V N Q L F K G E R K A K T F G I A  
cgcgtccctcgcccggccagggttcggcgatcgcgagccggcgtggggacgtcgtcgtt  
R V P R P A R F G D I A S R R G D V V V  
ctcgacgggtgtaagatcgtcgggaacatcggcggatagtagaagcagcgtcgtcgcgctc  
L D G V K I V G N I G A I V **K** T S L A L  
ggagcgtcggggatcactcgtcgcagagtacatcaccagcatcgcggaccggcgtctc  
G A S G I I L V D S D I T S I A D R R L  
caaagggccagccgaggttacgtcttctcccttcccgctgttctcctcggtcgagggag  
Q R A S R G Y V F S L P V V L S G R E E  
gccatcgcttcatcgggacagcggatgacagctgatgacgctcaangcggatggcgac  
A I A F I R D S G M Q L M T L X A D G D  
atttccgtgaaggaactcggggacaatccggatcggctggccttgcgtntcggcagcga  
I S V K E L G D N P D R L A L L X G S E  
aaggggtggccttccgacctgttcgagggcgtcttccgcctcggnttccatccccatg  
K G G P S D L F E E A S S A S X S I P M  
atgagcagaccgagtcctcaacgtttccgnttccctcggaaatcgcgctgcacgagagg  
M S Q T E S L N V S V S L G I A L H E R  
atcgacaggaatctcgcggccaaccga  
I D R N L A A N R



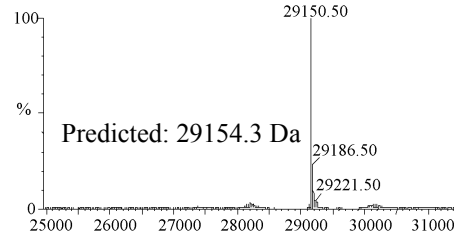
### R165A

atgactgagttggacaccatcgcaaatccgtccgatcccgcggtgcagcggatcatcgat  
M T E L D T I A N P S D P A V Q R I I D  
gtcaccaagccgtcgcgatccaacataaagacaacggtgatcgaggacgtcgagcccctc  
V T K P S R S N I K T T L I E D V E P L  
atgcacagcatcgccgggggtggagttcatcgaggtctacggcagcgacagcagtcct  
M H S I A A G V E F I E V Y G S D S S P  
tttccatctgagttgctggatctgtgcccggcagacaacataaccggtccgcctcatcgac  
F P S E L L D L C G R Q N I P V R L I D  
tcctcgatcgtcaaccagttgttcaagggggagcgggaaggccaagacattcggcatcgcc  
S S I V N Q L F K G E R K A K T F G I A  
cgcgtccctcgcccggccaggttcggcgatcgcgagccggcgtggggacgtcgtcgtt  
R V P R P A R F G D I A S R R G D V V V  
ctcgacggggtgaagatcgtcgggaacatcggcggatagtagcacgtcgtcgcgctc  
L D G V K I V G N I G A I V R T S L A L  
ggagcgtcggggatcatcctggtcgacagtgacatcaccagcatcgcggaccggcgtctc  
G A S G I I L V D S D I T S I A D R R L  
caaagggccagcgggttacgtcttccctcccgctggttctcgggtcgcgaggag  
Q R A S **A** G Y V F S L P V V L S G R E E  
gccatcgccttattcgggacagcgggatgcagctgatgacgctcaaggcggatggcgac  
A I A F I R D S G M Q L M T L K A D G D  
atttccgtgaaggaactcggggacaatccggatcggcgtggccttctggttcggcagcga  
I S V K E L G D N P D R L X L L F G S E  
aaggggtggccttccgacctgntcagaggaggcgtcttccgcctcgggttccatccccatg  
K G G P S D L F E E A S S A S V S I P M  
atgagccagancaggtctctnnaacgtttccggttccctcggaaatcgcgctgcacgagagg  
M S Q X E S X X V S V S L G I A L H E R  
atcgacaggaatctcgcggccaaccga  
I D R N L A A N R



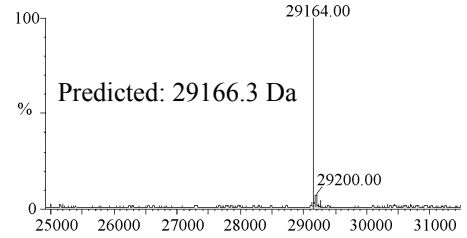
### R165K

atgactgagttggacaccatcgcaaatccgtccgatcccgcggtgcagcggatcatcgat  
M T E L D T I A N P S D P A V Q R I I D  
gtcaccaagccgtcgcgatccaacataaagacaacggtgatcgaggacgtcgagcccctc  
V T K P S R S N I K T T L I E D V E P L  
atgcacagcatcgccgggggtggagttcatcgaggtctacggcagcgacagcagtcct  
M H S I A A G V E F I E V Y G S D S S P  
tttccatctgagttgctggatctgtgcccggcagacaacataaccggtccgcctcatcgac  
F P S E L L D L C G R Q N I P V R L I D  
tcctcgatcgtcaaccagttgttcaagggggagcgggaaggccaagacattcggcatcgcc  
S S I V N Q L F K G E R K A K T F G I A  
cgcgtccctcgcccggccaggttcggcgatcgcgagccggcgtggggacgtcgtcgtt  
R V P R P A R F G D I A S R R G D V V V  
ctcgacggggtgaagatcgtcgggaacatcggcggatagtagcacgtcgtcgcgctc  
L D G V K I V G N I G A I V R T S L A L  
ggagcgtcggggatcatcctggtcgacagtgacatcaccagcatcgcggaccggcgtctc  
G A S G I I L V D S D I T S I A D R R L  
caaagggccagcaggggttacgtcttccctcccgctggttctcgggtcgcgaggag  
Q R A S **K** G Y V F S L P V V L S G R E E  
gccatcgccttattcgggacagcgggatgcagctgatgacgctcaaggcggatggcgac  
A I A F I R D S G M Q L M T L K A D G D  
atttccgtgaaggaactcggggacaatccggatcggcgtggccttctggttcggcagcga  
I S V K E L G D N P D R L A L L F G S E  
aaggggtggccttccgacctgntcagaggaggcgtcttccgcctcgggttccatccccatg  
K G G P S D L F E E A S S A S V S I P M  
atgagccngaccaggtctctcaacgtttccggttccctcggaaatcgcgctgcacgagagg  
M S X T E S L N V S V S L G I A L H E R  
atcgacaggaatctcgcggcncaaccga  
I D R N L A X N R

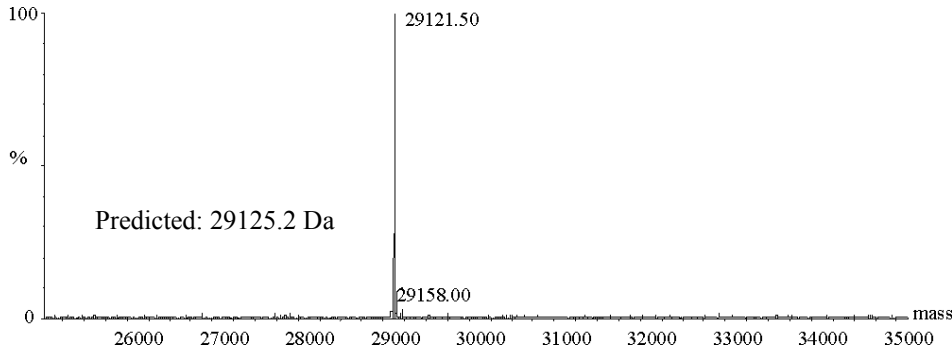


### S246A

atgactgagttggacaccatcgcaaataccgtccgatcccgcggtgcagcggatcatcgat  
M T E L D T I A N P S D P A V Q R I I D  
gtcaccaagccgtcgcgatccaacataaagacaacggtgatcgaggacgtcgagcccctc  
V T K P S R S N I K T T L I E D V E P L  
atgcacagcatcgcgccgggtggagttcatcgaggtctacggcagcgacagcagtcct  
M H S I A A G V E F I E V Y G S D S S P  
tttccatctgagttgctggatctgtgcggcgccgagaacataaccggtccgcctcatcgac  
F P S E L L D L C G R Q N I P V R L I D  
tcctcgatcgtcaaccagttggtcaaggggagcgggaaggccaagacattcggcatcgcc  
S S I V N Q L F K G E R K A K T F G I A  
cgcgtccctcgcccggccagggttcggcgatatcgcgagccggcgtgggacgtcgtcgtt  
R V P R P A R F G D I A S R R G D V V V  
ctcgacgggtgaagatcgtcggaacatcggcgatagtagcgcagtcgctcgcgctc  
L D G V K I V G N I G A I V R T S L A L  
ggagcgtcgggatcatcctggtcgacagtgacatcaccagcatcgcggaccggcgtctc  
G A S G I I L V D S D I T S I A D R R L  
caaagggccagccgaggttacgtcttctcccttcccgctgttctcctcggtcgagggag  
Q R A S R G Y V F S L P V V L S G R E E  
gccatcgcttcatcgggacagcggatgacagctgatgacgctcaaggcggatggcgac  
A I A F I R D S G M Q L M T L K A D G D  
attccgtgaaggaactcggggacaatcccggatcggctggncttgctgttcggcagcga  
I S V K E L G D N P G S A X L A V R Q R  
aanggtggccttccgacctgttcgaggangcgtcttccgcctcggnttcctccccatg  
X G G P S D L F E X A S S A S X S X P M  
atgagccagaccnaggcgctnannnnccggttncctcgggantcncgctgcacgagang  
M S Q T X A X X X P F X S G X X L H E X  
naticgacaggaatcnnngcgccnancn  
X D R N X X A X X



### K221A





C214A

atgggaatcaacctcaccocggaggagaagtctcgaggtcttcggcgacttcgaccccgac  
M G I N L T P E E K F E V F G D F D P D  
cagtacgaggaggaggtccgggaacgctgggggaacaccgacgcctaccgccagtccaag  
Q Y E E E V R E R W G N T D A Y R Q S K  
gagaagaccgcctcgtacaccaaggaggactggcagcgcatccaggacgaggccgacgag  
E K T A S Y T K E D W Q R I Q D E A D E  
ctcaccocggcgcttcgctgcocctgatggacgcgggtgagccocggactccgagggggcc  
L T R R F V A L M D A G E P A D S E G A  
atggacgcocggaggaccocggcagggcatgcoccgcaaccactacgactgcgggtac  
M D A A E D H R Q G I A R N H Y D C G Y  
gagatgcacaccocgctggggcgagatgtacgtgtccgacgaacgtttcacgcgaaacatc  
E M H T **A** L G E M Y V S D E R F T R N I  
gacgcocgcaagccggocctcggccctacatgcgcgacgcgatcctcgcgaacgcctc  
D A A K P G L A A Y M R D A I L A N A V  
cggcacaccoccc  
R H T P

C214S

atgggaatcaacctcaccocggaggagaagtctcgaggtcttcggcgacttcgaccccgac  
M G I N L T P E E K F E V F G D F D P D  
cagtacgaggaggaggtccgggaacgctgggggaacaccgacgcctaccgccagtccaag  
Q Y E E E V R E R W G N T D A Y R Q S K  
gagaagaccgcctcgtacaccaaggaggactggcagcgcatccaggacgaggccgacgag  
E K T A S Y T K E D W Q R I Q D E A D E  
ctcaccocggcgcttcgctgcocctgatggacgcgggtgagccocggactccgagggggcc  
L T R R F V A L M D A G E P A D S E G A  
atggacgcocggaggaccocggcagggcatgcoccgcaaccactacgactgcgggtac  
M D A A E D H R Q G I A R N H Y D C G Y  
gagatgcacaccagcctggggcgagatgtacgtgtccgacgaacgtttcacgcgaaacatc  
E M H T **S** L G E M Y V S D E R F T R N I  
gacgcocgcaagcccgctgcggcacaccoccc  
D A A K P V R H T P

C207A

atgggaatcaacctcaccocggaggagaagtctcgaggtcttcggcgacttcgaccccgac  
M G I N L T P E E K F E V F G D F D P D  
cagtacgaggaggaggtccgggaacgctgggggaacaccgacgcctaccgccagtccaag  
Q Y E E E V R E R W G N T D A Y R Q S K  
gagaagaccgcctcgtacaccaaggaggactggcagcgcatccaggacgaggccgacgag  
E K T A S Y T K E D W Q R I Q D E A D E  
ctcaccocggcgcttcgctgcocctgatggacgcgggtgagccocggactccgagggggcc  
L T R R F V A L M D A G E P A D S E G A  
atggacgcocggaggaccocggcagggcatgcoccgcaaccactacgacgcgggtac  
M D A A E D H R Q G I A R N H Y D **A** G Y  
gagatgcacacctgcctggggcgagatgtacgtgtccgacgaacgtttcacgcgaaacatc  
E M H T C L G E M Y V S D E R F T R N I  
gacgcocgcaagccggocctcggccctacatgcgcgacgcgatcctcgcgaacgcctc  
D A A K P G L A A Y M R D A I L A N A V  
cggcacaccocccctga  
R H T P

## APPENDIX 8: Additives used in screens for TIPAS crystallization

**Table A8.1 Additive screen reagents**

<b>Reagent #</b>	<b>Final Concentration of Additive (M)</b>	<b>Additive</b>
1	0.1	Ammonium acetate
2	0.1	Calcium acetate hydrate
3	0.1	Potassium acetate
4	0.1	Potassium hydrate
5	0.1	Potassium phosphate monobasic
6	0.1	Sodium acetate trihydrate
7	0.1	Sodium phosphate dibasic dihydrate
8	0.1	Sodium phosphate monobasic monohydrate
9	0.1	Calcium chloride dihydrate
10	0.1	Manganese chloride tetrahydrate
11	1.0	Ammonium sulfate
12	1.0	Potassium chloride
13	1.0	Lithium chloride
14	2.0	Sodium chloride
15	0.5	Sodium fluoride
16	1.0	Sodium citrate tribasic dihydrate
17	0.1	Phenol
18	30	Dimethyl sulfoxide
19	1.0	Glycine
20	1.0	Guanidine hydrochloride
21	0.1	Urea
22	10	Polyethylene glycol 3,350
23	10	Polyethylene glycol 8,000
24	30	D-(+)-Glucose monohydrate
25	30	Ethylene glycol
26	30	Glycerol
27	30	Ethanol
28	30	2-Propanol
29	30	Methanol
30	0.1	Imidazole
31	30	Tacsimate
31	0.1	sodium cacodylate trihydrate